NASA Technical Memorandum 74040

LASER VELOCIMETER SURVEY ABOUT A NACA 0012 WING AT LOW ANGLES OF ATTACK

Danny R. Hoad, James F. Meyers, Warren H. Young, Jr. and Timothy E. Hepner

January 1978

National Aeronautics and Space Administration

Langley Research Center
Hampton, Virginia 23665

LASER VELOCIMETER SURVEY ABOUT A NACA 0012 WING AT LOW ANGLES OF ATTACK

Danny R. Hoad*, James F. Meyers, Warren H. Young, Jr.*,
and Timothy E. Hepner*
Langley Research Center
Hampton, Virginia 23665

SUMMARY

An investigation has been conducted in the Langley V/STOL tunnel with a laser velocimeter to obtain measurements of airflow velocities about a wing at low angles of attack (0.6° and 4.75°). The applicability of the laser velocimeter technique for this purpose in the V/STOL tunnel was demonstrated in this investigation with measurement precision bias calculated at -1.33 percent to 0.91 percent and a random uncertainty calculated at ±0.47 percent. Free-stream measurements were obtained with this device and compared with velocity calculations from pitot-static probe data taken near the laser velocimeter measurement location. The two measurements were in agreement to within 1 percent. Velocity measurement results about the centerline at 0.6° angle of attack were typically those expected. At 4.75°, the velocity measurements indicated that a short laminar separation bubble existed near the leading edge with an oscillating shear layer.

INTRODUCTION

The laser velocimeter (LV) has a potential of measuring fluid velocities in flow conditions where traditional devices either are incapable of providing measurements or would seriously influence the measurements due to their presence. A fringe-type, two-component LV is being developed for use at the Langley V/STOL tunnel to capitalize on this potential. The most probable early use of this LV system would be the measurement of air velocities in the vicinity of a rotor system on the General Rotor Model System (GRMS) that is used extensively for aerodynamic and acoustic research in the V/STOL tunnel (ref. 1).

---

*Structures Laboratory, U.S. Army Aviation Research and Development Command

In recent years, several investigators have applied the LV to the problem of measuring helicopter rotor flow fields. (See refs. 2 to 5.) The LV has been applied to velocity measurements within turbine stages of an engine assembly (ref. 6). The examples in references 2 to 6 are indicative of applications where a conventional probe could not survive. The LV is used extensively as a research tool to determine the exhaust characteristics of jets and nozzles (refs. 7 to 9). Quite often a well-defined jet or nozzle has been used as a reference to prove the validity of the LV measurements. Characteristics of turbulent flows have been studied using the LV (refs. 10 and 11), and power-spectral data have been attempted with some success (ref. 12). These latter examples are indicative of applications where a conventional probe's presence would influence the measurement accuracy.

Recently, an LV system was temporarily installed in the 7- by 10-foot tunnel at Langley to measure the flow characteristics over a stalled three-dimensional wing (ref. 13). The system described in the present report was similar to that in reference 13. The system was operated in the backscatter mode to permit a common platform for the transmitting and receiving optics. The tunnel flow was seeded with particles of kerosene smoke with a known particle size distribution output. This was required in order to: (1) increase the number of velocity measurements per unit time to minimize tunnel run duration; and (2) control measurement precision by providing particles with proper density and size characteristics for tracking fidelity.

This investigation was designed to accomplish two objectives: (1) to demonstrate and verify the use of the LV in the V/STOL tunnel; and (2) to obtain two-dimensional velocity measurements about a wing, to be used later for comparison with theoretical techniques.

SYMBOLS

The axes used for this investigation was presented in figure 1. The units for the physical quantities defined in this paper are in the International System of Units. Most quantities were measured in this system; however, some were measured in the U.S. Customary Units and converted by using factors given in reference 14.

c	wing chord, 0.3048 m
C_i	number of velocity measurements in i^{th} histogram interval as percent of N
D_{sv}	diameter of sample volume, m
DR	average data rate in ensemble, measurements/sec
E	excess (or kurtosis) of histogram
f	signal frequency received from LV, Hz
L_{sv}	length of sample volume, m
L_{fr}	fringe spacing, m
M	free-stream Mach number
N	number of velocity measurements in one ensemble
R_c	airfoil Reynolds number, based on chord
S_R	skewness of histogram
T_R	reset time of the high-speed burst counter, sec
U	local velocity component, direction described by subscript (see fig. 1)
U_R	local total velocity, $\sqrt{U^2 + V^2}$, m/sec
$\pm U$	uncertainty in velocity component (U), m/sec
U_T	free-stream velocity determined from pitot-static probe, m/sec

V	local velocity component, direction described by subscript (see fig. 1)
V_{fr}	velocity of the fringes due to Bragg cell, m/sec
$\pm V$	uncertainty in velocity component (V), m/sec
X_f, Y_f	coordinate axis relative to free stream (fig. 1)
X_c, Y_c	coordinate axis relative to wing chord (fig. 1)
x_c	distance downstream from wing leading edge along chord, m
y_c	distance above (and measured on perpendicular to) wing chord, m
α	wing angle of attack, deg
α_R	local flow angle, $\tan^{-1}\left(\frac{V_f}{U_f}\right)$, deg
Δt	time between two consecutive velocity measurements, sec
Δz	distance between beam focus and sample volume, m
ε	error, percent
θ	angle between crossing laser beam components, deg
λ	laser radiation wave length, m
σ	standard deviation, m/sec
$\pm\sigma$	uncertainty in calculation of standard deviation, m/sec

Subscripts:

B data corrected for Bragg bias and velocity bias

e ensemble-average data

f direction indication of parameters U,V,X,Y parallel and perpendicular to free stream (see fig. 1)

i i^{th} measurement in ensemble

L direction indication of velocity components inclined 44.4° above free stream and 45.6° below free stream (see fig. 1)

t time-average data

u data in direction of U_L component

v data in direction of V_L component

APPARATUS

Laser Velocimeter - Optical System

A fringe-type LV optics system operating in the backscatter mode was used for these tests. The characteristics of the optics system are provided in table 1. The backscatter mode of operation allowed the use of simplified scanning, vertically and horizontally, without compromizing the optical alignment since the output lens is used for both transmitting the output beams and collecting the scattered light. The system was used to consecutively measure the two components of velocity $\pm 45°$ to a parallel to the test section longitudinal geometric centerline (fig. 1). The LV optics are illustrated in figure 2.

A laser beam is a monochromatic and coherent source of light. The LV uses these source characteristics to develop a fringe pattern. The beam is optically split into two parallel beams, which are focused with a lens to the point where

the two beams cross. In the sample volume, at the crossover point, the two light waves interfere constructively and destructively forming a fringe pattern. This is no more than a volume in space which if examined very closely would appear as being a series of alternating light and dark planes, orthogonal to the direction of the velocity measurement and parallel to the optical axis, each with approximately 26 micron size spacing between fringes in the present case.

The spacing between the fringes, as described above, is determined by:

$$L_{fr} = \frac{\lambda}{2 \sin \frac{\theta}{2}} \qquad (1)$$

As a micron-sized particle passes through the fringe pattern, light is scattered with an intensity proportional to the incident intensity in the fringe pattern. If a portion of this scattered light is detected by a photomultiplier tube, an electrical signal proportional to the Doppler frequency is generated.

To obtain two components of velocity, U_L and V_L, two sets of fringes are formed orthogonal to each other. These two fringe patterns are obtained by focusing three parallel laser beams, instead of two at a point, with each beam located at an apex of an isosceles-right triangle. The resulting fringe patterns are illustrated in figure 3. In reference 13, polarization separation was used to make simultaneous measurements in both components; however, in the present test, the 15 dB cross talk separation was due to the modifications in the optics system to accommodate a Bragg cell system. Thus, the measure of both components were made consecutively.

The investigation described in reference 13 experienced problems in four-fold ambiguity in direction measurement and limited low velocity measurement capability; therefore, a Bragg cell was placed in the beam that is common to both velocity components in the present test. The Bragg cell shifts the frequency of the light beam by a small amount. To obtain maximum resolution in the electronic frequency counter, the effective Bragg shift was chosen to be 5 MHz since the expected signal would be on the order of 2 MHz. This shift sets each fringe pattern in motion at a velocity proportional to a Doppler frequency of 5 MHz ($\approx$132 m/sec). For example, a particle with zero velocity would scatter light with a

Doppler frequency of 5 MHz as the fringes move past the particle. A particle traveling in the direction of the fringe motion would provide a signal frequency less than 5 MHz, conversely a particle moving against the direction of the fringe motion would produce a signal oscillation greater than 5 MHz. Thus, directionality of particle motion through the fringe pattern can be determined. The velocity of the particle is determined from measurement of the frequency of oscillation of the scattered light by:

$$U_L \text{ or } V_L = (f - 5 \text{ MHz}) L_{fr} \qquad (2)$$

An Argon-ion continuous wave laser was used in the present LV system. It was operated at about 4 watts output power at a wavelength of 514.5×10^{-9} m. The system was installed in the test chamber of the V/STOL tunnel just outside the test section, and the beams were projected through one of the test-section glass windows into the test area. The beam-crossing optics had a focal length of about 3.86 m (sufficient to reach the centerline of the wing) and a collecting solid angle of 0.00108 steradians. The sample volume was 2.29 cm long with a diameter of 0.314 mm. The optical axis was set approximately 3° off orthogonality to the tunnel free stream to provide for unobstructed measurements very near the leading and trailing edge of the wing. The optical system was mounted on a mechanical two-component traversing mechanism to allow movement of the common volume in the X_f, Y_f directions. The overall assembly, including the traverse system, laser, and the optical system, is presented in figure 4.

Laser Velocimeter - Electronics System

The interface between the optics system and electronics system consisted of two S-20 response photomultiplier tubes, one for each directional component, and signal conditioning electronics. The signal conditioning electronics consisted of line-driving amplifiers attached to the photomultipliers and band-pass filter banks to remove the signal pedestal ("DC bias") and high frequency noise.

The LV electronics system, shown schematically in figure 5, measures the frequency contained in each output signal burst, converts the frequency to velocity, develops velocity histograms, computes the statistical mean velocity and standard deviation of the velocity fluctuations, and stores

the raw velocity data, computed data and tunnel parameters on magnetic tape for later, complete, data reduction.

High-speed burst counter. - The high-speed burst counter is a device designed to measure the period of a high-frequency signal (1 KHz to 100 MHz) contained in a burst of the type received from a LV. An idealized burst received from the LV is illustrated in figure 6(a). The pedestal ("DC bias") is removed by high-pass filters so that the burst is symmetric about 0 volts (fig. 6(b)). A double threshold comparator is used to convert the burst into a digital pulse train (fig. 6(c)). In order for the comparator to work, the signal must cross the positive threshold before crossing 0 volts with a negative slope, and the signal must cross the negative threshold before crossing to 0 volts with a positive slope. Any other combination will not operate the comparator. The first pulse in the digital pulse train is used to clear the counter circuits; the second is used to arm the counters; and the third triggers the counters to begin counting pulses from the 500 MHz reference clock. When the tenth digital pulse occurs, the counters are halted. Thus, each counter now contains the measurement of the period average of 8 signal cycles based on a reference clock of 500 MHz, yielding a period average measurement with a resolution of 2×10^{-9} seconds.

Data gathering system. - The data from the two high-speed burst counters is input to the LV buffer interface which stores the velocity data and measures the time between the arrival of each datum and the immediately preceding datum to a resolution of 0.1×10^{-6} seconds. The interface is described in greater detail in Appendix A. When either 4096 data points are gathered or 1.0 minute of measurement time elapses, the data gathering process halts and the interface flags the minicomputer which begins the data transfer from the interface to the computer. The raw data are converted to velocity values in the computer and stored, along with the interarrival times, on magnetic tape. The statistical quantities, e.g., mean, standard deviation, skew, etc., are computed on-line and output on-line on the CRT. The total time required for measurement, data transfer, storage, computation and output is less than 2 minutes.

Tunnel Model

The model used in this investigation was a simple straight wing with revolved tips. It had a span of 2.438 m, a chord of 0.3048 m, and a NACA 0012 airfoil

section. Velocity measurements were made within a vertical plane at center span to obtain two-dimensional characteristics. The wing was supported by struts from the floor near the tunnel centerline with no balance measurements taken. The location of the strut mount to the wing was chosen as far outboard as structurally feasible. This provided ample space between struts to minimize flow disturbance at the wing centerline. A photograph of the model with crossing laser beams is presented in figure 7.

Local flow velocities were measured about the wing centerline at two geometric angles of attack, 0° and 4.15°. A pitot-static probe was mounted in the tunnel vertical center plane 2.5 m below and 1 m ahead of the wing leading edge to provide accurate reference of the free-stream tunnel dynamic pressure. A hygrometer was used to obtain wet bulb temperatures; the total temperature was measured in the tunnel settling chamber. Thus, the tunnel air density and velocity could accurately be calculated.

Tunnel Seeding

Perhaps the foremost problem in achieving LV measurement accuracy is due to seeding-particle lag. In most applications, the distribution of velocities within a gas medium is the main subject of the measurements; however, the LV measures the velocity of seed particles in the gas. In many cases, these velocities are identical; however, in regions of large velocity gradients, such as along a stagnation streamline, the inertia of comparatively larger seed particles does not allow them to immediately adjust to local flow velocity. Care was taken in the present tests to ensure that the seed particles within the flow were small enough to follow the flow with sufficient accuracy. This problem was addressed in the investigation described in reference 13. It was found in those tests that 3-micron size particles responded to the severe velocity gradient (1540 m/sec/m) along the stagnation line of a hemisphere at a Mach number of 0.55. It was determined from laboratory tests and preliminary calculations that with the LV system and at the focal lengths used in the present investigation, the minimum particle size for reasonable signal intensity was of the order of 2 microns. This then put a restriction on the particulate required for practical use of the LV in the V/STOL tunnel 2 to 3 microns.

The V/STOL tunnel standard smoke generator flow-visualization device was modified to yield the appropriate particle size distribution for this test. The distribution was measured by an optical technique similar to that discussed in reference 13 and is presented in figure 8(a). The smoke generator vaporizes liquid kerosene by adding heat and emits a dense white smoke through a nozzle. The nozzle was positioned in the settling chamber of the tunnel to minimize flow disturbance on the model. The nozzle position was critical in that the particulate was only to be applied in the region of the measurement volume. The smoke plume in the test section was observed to be about 0.4 m in diameter. To keep the sample volume from traversing out of the smoke plume, the nozzle was repositioned as necessary. This was done manually which was very time-consuming (required 20 to 60 minutes). Future LV use for similar purposes in the tunnel will require remote positioning of the smoke nozzle to minimize test times.

DATA ACQUISITION AND REDUCTION

Laser Velocimeter Data Processing

Statistical quantities. - The LV measures velocity events that are Poisson distributed in time at a location in the flow. During the measurement process, two assumptions are made: first, the particles embedded in the flow are not only randomly dispersed in space but are also randomly dispersed in the velocity field; and secondly, that the measurement sample taken over a finite period of time is a good representation of the stationary condition at the measurement location. The statistical quantities of sample mean, standard deviations (and their statistical uncertainties), skew, and excess are computed. Graphical representation of the velocity probability density functions for each velocity component were made by placing each velocity ensemble in histogram form.

The sample mean was calculated by three different methods: (1) arithmetic mean, (2) arithmetic mean with corrections for velocity bias (ref. 15)and Bragg cell bias, and (3) time averaging (ref. 16). The arithmetic mean assumes that all velocities present in the flow at the measurement point have equal probability of being measured. The computations use the classical nonweighted equation:

$$V_e = \frac{V_i}{N} \tag{3}$$

However, from reference 15, it was found that if the seeding particles are uniformally distributed in the flow, the number of measurements will be weighted toward the higher velocities since more gas (and thus more particles) passes through the sample volume per unit time than at lower velocities. Conversely, when a Bragg cell is used for directionality measurements, as in the present study, the number of measurements will be weighted toward the lower velocities since the particle will cross more of the moving fringes than at higher velocities; for example, a particle at 0 velocity will yield an infinite number of measurements. Therefore, the data must be weighted to account for these biases and then the arithmetic mean calculated:

$$V_B = \frac{\dfrac{10\ L_{fr} + T_r\ V_{fr} + T_r\ V_i}{D_{sv}\ (V_{fr} + V_i)}\ V_i}{\dfrac{10\ L_{fr} + T_r\ V_{fr} + T_r\ V_i}{D_{sv}\ (V_{fr} + V_i)}} \tag{3}$$

From reference 16, it has been suggested that all biases are removed if the data are weighted by the amount of time elapsed between each particle arrival. The restriction of this method is that the mean particle arrival rate must be equal to or greater than the highest flow turbulence frequency that contributes to the energy contained in the overall turbulent power spectra. The method for determining the time weighted average is:

$$V_t = \frac{\dfrac{(V_i + V_{i+1})}{2}\ \Delta t_i}{\Delta t_i} \tag{4}$$

From tables 2 to 4, it may be seen that all three averaging techniques yield similar results when the mean data rate is above about 10 particle arrivals per second. Also, in all cases, the simple mean and the corrected mean for velocity bias and Bragg cell bias yield similar results, which infers that when a Bragg cell is used whose frequency is large compared to the signal frequency, the bias errors are self-cancelling. Thus, the statistical quantities calculated from the test data were determined by using simple moment equations:

$$V_e = \frac{\sum V_i}{N} \tag{6}$$

$$\sigma = \sqrt{\frac{\sum (V_i - V_e)^2}{N}} \tag{7}$$

$$S_R = \frac{\sum (V_i - V_e)^3}{N \sigma^3} \tag{8}$$

$$E = \frac{\frac{\sum (V_i - V_e)^4}{4}}{\left(\frac{\sum (V_i - V_e)^2}{N}\right)^2} - 3.0 \tag{9}$$

In order to determine the statistical accuracy of the mean and standard deviation obtained from each measurement ensemble, the measurement uncertainties were calculated. From reference 17, the measurement uncertainty in the mean value is expressed for a 95 percent confidence limit as

$$\text{Uncertainty in } V_e = \pm V_e = \frac{\pm 2\sigma}{\sqrt{N}} \tag{10}$$

where σ is the standard deviation of the histogram and N is the number of discrete velocity measurements in the ensemble. That is, the true stationary mean velocity of the flow lies within a radius of uncertainty about the measured mean calculated from the ensemble. Similarly, the measurement uncertainty in the standard deviation for a 95-percent confidence limit is

$$\text{Uncertainty in } \sigma = \pm\sigma = \pm\sigma\sqrt{\frac{2}{N}}\left(1 + \frac{E}{2}\right)^{1/2} \tag{11}$$

It should be noted that the inclusion of excess in equation 10 allows the measurement uncertainty to be calculated for ensembles with probability densities other than Gaussian.

Since the high-speed burst counters provide data in the form of number of reference clock pulses, the histogram interval width is established. Thus, the histograms are formed by determining the number of occurances of each counter output pattern present in each measurement ensemble. These patterns are converted to velocity and the histograms plotted, either on the CRT for on-line analysis or by plotter off-line.

Instrument precision. The overall measurement precision is obtained by determining the accuracies of all variables in the system which will affect the accuracy of each velocity measurement. From reference 13 these error sources are: cross beam angle measurement, diverging fringes, time jitter, clock synchronization, and quantizing error. The cross beam angle measurement error is a bias error based on the uncertainty in locating the center of each laser beam when the cross beam angle is determined. This error is estimated to be $\pm$1.12 percent in the present study. The diverging fringes, resulting from the focus point of each laser beam being at a different location than the crossover point, yield both a bias error (-0.5 percent in the present test), and a random error ($\pm$0.37 percent in the present test). Time jitter is an error resulting from the threshold detector in the high-speed burst counter triggering at different points on the signal burst when the signal amplitude changes as the particle passes through the Gaussian light intensity distribution in the sample volume. However, in the present system, a double threshold technique with zero crossing detection is used which eliminates the time jitter error. The clock synchronization error, time difference between the high-speed burst counter start pulse and the first reference clock pulse that is counted, yields a bias error (0.29 percent in the present test) and a random error ($\pm$0.29 percent in the present test). The quantizing error is nonexistent in the present test since the 10 bit digital output from the high-speed burst counter is not truncated, that is, the lowest bit is one clock pulse from the 500 MHz reference clock in the present test. It should be noted that the above calculated errors are percentages of the velocity measurement, but they were calculated at signal frequencies which include the Bragg cell frequency; for example, the errors would be much less if the Bragg cell were removed.

The errors mentioned above yield an effective total bias error of -1.33 percent to 0.91 percent calculated by an algebraic sum of the partial bias

errors. The total effect of random error was ±0.47 percent uncertainty, which was obtained by the square root of the sum of the squares of the partial random errors described above.

In large velocity gradients, velocity measurement errors may occur if the measurement point is not at the desired location. The two-component, mechanical traversing system for the LV optics had a placement uncertainty of ±1 mm which yield a worst case (based on the measured velocity flow field) uncertainty of 1.6 percent.

Particle lag. - Since the LV measures particle velocities and not the gas velocity, the final measurement accuracy is dependent on the ability of the particle to faithfully follow the flow. The size distribution of the seed particle was measured using an optical particle size analyzer placed in the test section so as to capture particles from the generator which yielded acceptable LV signals. The resulting distribution is shown in figure 8(a). The particle size necessary from the LV to obtain valid measurements was determined using the computer simulation of the LV developed by Meyers (ref. 18). The probability of a successful measurement is based on the signal level calculated for a given particle size. The effective sample volume size that would yield a successful measurement was calculated and compared to the sample volume size based on the $1/e^2$ power level. For example, if a particle of a certain size whose path is tangent to the $1/e^2$ power circle, and it yielded a successful measurement, that particle size is given a weight of unity. Any particle size that would result in a measure beyond or less than $1/e^2$ is weighted greater than or less than unity, respectively. The probability of a successfull measurement, as a function of particle size is shown in figure 8(b). Thus, the overall measurement probability for this test was found (fig. 8(c)). As mentioned previously, from reference 13 it was determined that a 3-micron particle traveling at Mach 0.55 free stream would faithfully follow a velocity gradient of 1540 m/sec per m. Since this velocity gradient is far greater than any experienced in these tests, it is concluded that the velocity measurements obtained are a true representation of the gas velocity flow field.

TEST AND PROCEDURES

This investigation was conducted in the Langley V/STOL tunnel at a nominal free-stream Mach number of 0.15. The Reynolds number, based on the wing chord

length was approximately 1×10^6. Preliminary free-stream measurements were made with the tunnel clear except for the pitot-static probe used as a reference. These measurements were made in the vicinity where the model would be positioned later. The wing was installed at two geometric angles of attack, 0° and 4.15°.

The scan capability of this particular preliminary LV system was not sufficient to survey above, ahead of, and behind the wing without moving either the wing or LV system platform. There was no survey behind the wing in the $\alpha = 0°$ case. With the wing at 4.15° angle of attack, a complete survey was made. To obtain the measurements behind the trailing edge, the model was moved forward and raised inside the test section with very little change to the LV system platform.

To obtain measurements very near the leading and trailing edges of the model, the optical centerline was inclined off perpendicular to the tunnel vertical center plane such that the laser beam component nearest the leading (or trailing) edge was aligned with the edge. Thus, in these cases, the angle of inclination of the optical centerline was approximately 3°.

At each angle of attack, a series of runs was made by beginning at the uppermost limit of traverse capability at a desired x_c location. The scan was accomplished by making measurements at locations along a line perpendicular to the wing chord line. Runs were taken increasingly closer to the wing surface until blockage by the wing precluded further measurements, or the lower limit of the traverse was reached.

The measurements were obtained as indicated previously and raw data converted to velocity values and stored on magnetic tape for later data reduction. The on-line capability of the computer system was invaluable in the immediate assessment of the acceptability of each data ensemble as it was obtained.

PRESENTATION OF RESULTS

As mentioned previously, all of the velocity measurements at each measurement location were first reduced to histogram form. These histograms are presented in Appendix B with a figure list and a short discussion of interpretation. Statistical analysis of the data was performed as described previously, and the results are presented in tabulated form. The free-stream data are presented

in table 2, data for the wing at two angles of attack are presented in tables 3 and 4.

The statistical characteristics of the data presented in tables 3 and 4 are plotted as a function of vertical height above the wing chord in figures 9 to 39. To summarize some of the statistical characteristics, contour plots were generated using spline-fit routines between data points. They are local total velocity and local flow angle presented as contours of constant values about the wing. These are presented in figures 40 to 47.

DISCUSSSION

Free-Stream Data

The data acquired in the free stream are presented in table 2(a). Analysis of these data indicated that, at the Mach number used for this test, the flow angularity in the tunnel at the model position was, on the average, 0.6° (inclined above the tunnel centerline). The $^{U}f_{e}$ and $^{V}f_{e}$ velocities listed in table 2 are, therefore, referenced to free stream rather than tunnel centerline. The velocity computed from measurements by the pitot-static probe U_T was used to nondimensionalize these velocity components. The ratio provides a means of determining the error in measurement between this device and the LV. The variation of $^{U}R_{e}/^{U}T$ can be accepted as reasonable instrument error as compared to the previously determined LV instrument error.

The standard deviation, , can be considered as a measure of the unsteadiness of the flow. For the first five runs, the Mach number was 0.15. The average ratio σ_u/U_T and σ_v/U_T is 3.4 percent and 2.5 percent, respectively. For runs 6 and 7, the Mach number was 0.37 with average ratio σ_u/U_T and σ_v/U_T of 3.5 percent and 2.9 percent, respectively.

Basic Velocity Data - Wing at α = 4.75° and 0.6°

The wing was installed at 4.15° and 0°, referenced to the tunnel centerline. With the tunnel flow angularity of 0.6, the effective angles of attack were 4.75° and 0.6°; therefore, all analyses were conducted with these values.

The statistical characteristics of the velocity data are presented in figures 9 to 27 for the wing at α = 4.75° and figures 28 to 39 for the wing at

$\alpha = 0.6°$. Each figure represents a scan along a perpendicular to the wing chord. Total velocity and local flow angle plots are consistent and reasonable. The wake defect is evident in the trailing-edge scans in both velocity and local flow angle (figs. 25 to 27). The $^{U}L_{e}$ and $^{V}L_{e}$ component measurements are as expected, except near the surface (at $\alpha = 4.75°$) near the leading edge (figs. 12 to 16). Near the surface, the $^{U}L_{e}$ component decreases rapidly as the measurement approaches the surface, with a corresponding increase in the $^{V}L_{e}$ component. For most of the data, standard deviation, skew, and excess, indicate gradual changes as the surface is approached. Away from the surface, the small values of standard deviation and negative values of excess indicate a flow that is relatively steady and contains fewer larger fluctuations from the mean velocity than the traditional Gaussian model of turbulence (for which the excess is zero). The skew differs little from zero (note the expanded scale). The skewness of the histogram (as discussed in Appendix C) provides a measure of flow angle variation and velocity variation. Large values of excess (fig. 12) can be attributed to the double peaks (see App. B, $\alpha = 4.75°$, runs 51 and 52). However, near the surface, these values change drastically. This behavior of the velocity field in this area suggest drastic change in the field as though the sample volume passed through a shear layer.

The characteristics of the flow field can be seen in the histograms in Appendix B. The cases for the proposed traverse through a shear layer are presented in figures B-5 to B-7. Notice that in runs 50, 63, 67, and 78, the shape of the histogram alters from the data point just above, runs 49, 62, 66, and 77, respectively. Each histogram seems to split into a double-peaked histogram at this point. This indicates that there are two predominant velocity values. The flow experiences an oscillation between the two values, sometimes with greater tendency to be at or near one value than the other, but spends little time between the two general values. Notice figure B-5, runs 51 and 52. The $^{V}L_{e}$ component indicates that, at the position for run 51, the flow experiences the lower velocity value most of the time; however, at the position for run 52, the flow experiences the higher velocity value most of the time. The positions, as listed in table 3(b), are only 0.007 chords apart (2.1 mm). These points, therefore, must be on opposite sides of the proposed shear layer. The most likely explanation of this is that the shear layer is oscillating to provide the double peaks. It is suggested that this is very near the location of the

start of the shear layer. The double peaks are also evident in runs 63, 64, 67, 68, 78 and 79. For the latter run numbers, the double-peaked histograms are broader, and the tendency to favor one velocity over the other is not as evident. The broad histograms are indicative of flow situations with large flow unsteadiness. The double-peaked histograms indicate flow unsteadiness with oscillating velocity fields. If the shear layer was steady, the inner region separated field would be of much lower velocity than the outer. The most probable explanation of these two facts is that the double-peaked histograms were obtained at the region of the shear layer of a laminar separation bubble. This shear layer was oscillatory and possibly a thin vortex sheet was formed between the undisturbed region and separated region. It is postulated that this sheet was the cause of the double peaks.

The broadening of the double-peak histograms for runs 78 and 79 indicate that the separation bubble shear layer has experienced a transition to turbulent flow characteristics, and it is suspected that the flow had reattached further downstream.

A similar situation was reported in reference 19. A NACA 0010 (modified) airfoil was tested to determine its characteristics when laminar separation was developed. Reference 19 report that at a Reynolds number of 1.5×10^6 at 4.75° angle of attack, the NACA 0010 (modified) should have a laminar separation at approximately $x_c/c = 0.02$. The flow should transition from laminar to turbulent at $x_c/c = 0.05$ and should reattach at about $x_c/c = 0.05$.

The laminar separation bubble measured in this investigation began at about $x_c/c = 0.01$, with evidence of its existence reaching to $x_c/c = 0.09$. Realizing that this investigation was conducted with a NACA 0012 airfoil at Reynolds number = 1×10^6, it seems entirely possible that the phenomena observed was a laminar separation bubble.

As described in appendix B, a skewed histogram indicates a fluctuation in flow angle and velocity. The histograms of the measurements leading up to the double-peaked histograms were skewed, thus the flow at this location was experiencing variation in velocity and angle. The position of the laminar separation point, as measured in reference 19, is highly sensitive to slight

wing angle-of-attack changes; therefore, it is possible that the separation point was moving with the tunnel flow angle oscillation. This unsteadiness in separation point would result in unsteadiness in the shear layer of the separation and trigger an undulating shear layer; thus the double histograms with increasing total velocity as the sample volume is traversed downward into the bubble.

The trailing-edge scans show expected results: (1) wake defect behind the trailing edge; (2) flow angle change through the wake; (3) large unsteadiness in the wake. The data for the wing at $\alpha = 0.6°$ indicate that the flow is smooth and can be easily predicted by theories such as that reported in reference 20.

Statistical Characteristics Summarized

In an attempt to summarize the statistical characteristics of the flow field, composites were developed which describe the flow situation over the wing wing as measured.

Total velocity vectors, streamlines, contours of constant local flow angle, and contours of constant U_{R_e}/U_T were computed and plotted. These are presented in figures 40 to 43 for the wing at $\alpha = 4.75°$ and in figures 44 to 47 for the wing at $\alpha = 0.6°$.

At $\alpha = 4.75°$, the velocity vectors near the region of the laminar separation bubble are clearly affected by the calculation of mean velocity from a double-peaked histogram. This fact in turn affects the spline fit of the survey flow angle map in an attempt to compute streamlines (a path a particle would take in the flow). The local flow angle is maximum (25°) at the expected location (near the nose), and approaches the upper surface local angle at the trailing edge. The velocity decreases along the stagnation line is evident at the leading edge in the contours of constant U_{R_e}/U_T plot. The wake region is evident with approximately 70 percent of the free-stream velocity. It is interesting to note in these figures that the presence of the wing was obvious ahead of it as far as the scans were made. This is evident in all of the plots.

At $\alpha = 0.6°$, the velocity vectors are classic, exactly what would be expected for the flow about this airfoil. The streamlines are well-defined and exhibit

no obvious inconsistencies. The plot of constant U_{R_e}/U_T indicates the velocity decrease along the stagnation line. Local flow angles are smoothly varying with maximum value (17°) at the nose upper surface.

CONCLUDING REMARKS

A LV survey about a NACA 0012 wing installed in the Langley V/STOL tunnel has been conducted to accomplish two objectives: (1) demonstrate the applicability of the LV in the V/STOL tunnel; and (2) to obtain two-dimensional velocity measurements to be used later for comparison with theoretical techniques.

The results of this investigation indicated that the LV is a viable tool in fluid flow research with measurement precision calculated to be -1.33 percent to 0.91 percent bias uncertainty and $\pm$0.47 percent random uncertainty in this investigation.

The histogram is one means of analyzing the result of LV measurements and provide invaluable insight into the character of the flow.

Free-stream measurement comparison with calculations from a pitot-static probe measurements agree to within 1 percent.

The data for the wing at α = 4.75° indicated that a laminar separation bubble probably existed with a thin oscillating shear layer. The data for the wing at α = 0.6° indicated that the flow is smooth and can be easily predicted by existing theories.

REFERENCES

1. Wilson, John C.: A General Rotor Model System for Wind-Tunnel Investigations. J. of Aircraft, July 1977

2. Sullivan, John P.: An Experimental Investigation of Vortex Rings and Helicopter Wakes Using a Laser Doppler Velocimeter. TR-183, M.I.T. Aerophysics Lab., June 1973

3. Johnson, B. V.: L.D.V. Measurements in the Periodic Velocity Field Adjacent to a Model Helicopter Rotor. Proc. Sec. Intl. Workshop on Laser Velocimetry, vol. II, March 27-29, 1974, pp. 169-181

4. Landgrebe, A. J.; and Johnson, B. V.: Measurements of Model Helicopter Rotor Flow Velocities with a Laser Doppler Velocimeter. Tech. Note, J. Am. Hel. Soc., vol. 20, no. 1, January 1975, pp. 39-43

5. Biggers, James C.; and Orloff, Kenneth L.: Laser Velocimeter Measurements of the Helicopter Rotor-Induced Flow Field. J. Am. Hel. Soc., vol. 20, no. 1, January 1975, pp. 2-10

6. Goldman, Louis J.; Seasholtz, Richard G.; and McLallin, Kerry L.: Velocity Surveys in a Turbine Stator Annular-Cascade Facility Using Laser Doppler Techniques. NASA TN D-8269, 1976

7. Eggins, P. L.; and Jackson, D. A.: Laser Doppler Velocity Measurements in an an Under-Expanded Free Jet. J. Phys. D: Appl. Phys, vol. 7, 1974, pp. 1894-1906

8. Flack, R. D.; and Thompson, H. D.: Preliminary Results with Purdue's LDV System. Proc. Sec. Intl. Workshop on Laser Velocimeter, March 27-29, 1974, pp. 314-334

9. Meyers, J. F.; Feller, W. V.; and Hepner, T. E.: A Feasibility Test of the Laser Velocimeter in the Mach 5 Nozzle Test Chamber. Proc. Sec. Intl. Workshop on Laser Velocimeter, March 27-29, 1974, pp. 290-313

10. Meyers, J. F.: and Feller, W. V.: Turbulence Measurements in Air. Laser Doppler Anemometer Workshop, June 11-13, 1973

11. Avidor, J. M.: Turbulence Measurements in High Speed Wake Flow Using Laser Velocimetry. Proc. Sec. Intl. Workshop on Laser Velocimeter, March 27-29, 1974, pp. 335-354

12. Whiffen, M. C.; and Meadows, D. M.: Two Axis, Single Particle Laser Velocimeter System for Turbulence Spectral Analysis. Proc. Sec. Intl. Workshop on Laser Velocimetry, March 27-29, 1974, pp. 1-15

13. Young, Warren H., Jr.; Meyers, James F.; and Hepner, Timothy E.: Laser Velocimeter Systems Analysis Applied to a Flow Survey Above a Stalled Wing. NASA TN D-8408, 1977

14. Mechtly, E. A.: The International System of Units - Physical Constants and Conversion Factors (Second Revision). NASA SP-7012, 1973

15. Tiederman, W. G.; McLaughlin, D. K.; and Reischman, M. M.: Individualized Realization Laser-Doppler Technique Applied to Turbulent Channel Flow. 3rd Biennial Sym. on Turbulence in Liquids, Un. of Missouri, 1973

16. Dimotakis, P. E.: Single Scattering Particle Laser Doppler Measurements of Turbulence. AGARD CP-193, May 1976, pp. 10-1 to 10-14

17. Yule, G. V.; and Kendall, M. G.: An Introduction to the Theory of Statistics 12th ed., Charles Griffin Co. (London), 1940

18. Meyers, J. F.: Computer Simulation of a Fringe Type Laser Velocimeter. Proc. Sec. Intl. Workshop on Laser Velocimetry, vol. II, 1974

19. Gault, Donald E.: An Experimental Investigation of Regions of Separated Laminar Flow. NACA TN 3505, 1955

Table 1

Laser Wavelength	514.5 nm
Input Lens Focal Length	3.8649 m
Cross Beam Angle	1.1139 deg
Transmission Coefficient	
Beam A	0.15
Beam B	0.16
Beam C	0.12
Input Laser Power	4.0 W
Diameter of Laser Beam at Input Lens	0.0081 m
Receiving Lens Focal Length	3.8649 m
Rotation Angle of Receiver	
Horizontal	180.0 deg
Vertical	0.0 deg
Effective Receiving Lens Diameter	0.127 m
Transmission Coefficient, Receiver	0.42
Bragg Frequency	5.0 MHz
Photomultiplier Quantum Efficiency	0.14
Photomultiplier Gain	60000
Counter Threshold Voltage	0.015 V
Low Pass Filter Cutoff	8.0 MHz
High Pass Filter Cutoff	0.5 MHz
Counter Count Comparison Accuracy	0.02
System Gain	-4.0 dB

Table 2-A (freestream)

Run	U_{L_e} m/sec	$\pm U_{L_e}$ m/sec	V_{L_e} m/sec	$\pm V_{L_e}$ m/sec	U_{L_B} m/sec	V_{L_B} m/sec	U_{L_t} m/sec	V_{L_t} m/sec	S_{R_u}	S_{R_v}	E_u	E_v	N_u	N_v	DR_u sec^{-1}	DR_v sec^{-1}	Time	Julian day
1	36.7	.0	35.8	.0	36.7	35.9	36.7	35.8	.15	.03	-.2	.1	2347	2397	39	40	9:45	147
2	36.9	.0	36.1	.0	36.9	36.1	36.9	36.0	.06	.01	.3	.0	3064	2302	51	33	9:43	147
3	36.8	.0	36.0	.0	36.8	36.0	36.9	35.9	-.15	-.20	.1	.3	3025	2363	50	39	9:39	147
4	36.7	.0	36.0	.0	36.7	36.0	36.7	36.1	.01	-.07	.3	.4	3054	2439	51	41	9:41	147
5	36.7	.0	36.0	.0	36.8	36.1	36.4	36.0	.22	.22	.6	.2	2252	565	38	10	9:48	147
6	65.6	.1	63.2	.1	65.9	63.8	66.2	60.9	.55	.18	3.6	18.0	3973	3787	169	63	10:24	147
7	66.0	.0	63.9	.0	66.4	64.4	66.8	62.9	.41	-.20	1.6	11.1	4023	3113	166	52	10:26	147

Table 2-B (freestream)

Run	$\frac{x_c}{c}$*	$\frac{y_c}{c}$*	σ_u m/sec	$\pm\sigma_u$ m/sec	σ_v m/sec	$\pm\sigma_v$ m/sec	$\frac{U_{f_e}}{U_T}$	$\frac{V_{f_e}}{U_T}$	$\frac{U_{R_e}}{U_T}$	α_{R_e} deg	$\frac{U_{f_B}}{U_T}$	$\frac{V_{f_B}}{U_T}$	$\frac{U_{R_B}}{U_T}$	α_{R_B} deg	$\frac{U_{f_t}}{U_T}$	$\frac{V_{f_t}}{U_T}$	$\frac{U_{R_f}}{U_T}$	α_{R_t} deg
1	.590	.110	1.2	.0	.9	.0	1.00	.00	1.00	.1	1.00	.00	1.00	.1	1.00	.00	1.00	.1
2	.594	.047	1.3	.0	.9	.0	1.01	.00	1.01	.0	1.01	.00	1.01	.0	1.01	.00	1.01	.1
3	.602	-.066	1.3	.0	.9	.0	1.01	-.00	1.01	-.0	1.01	.00	1.01	.0	1.00	.00	1.00	.2
4	.603	-.075	1.3	.0	.9	.0	1.00	-.00	1.00	-.0	1.00	-.00	1.00	-.0	1.01	-.00	1.01	-.1
5	.607	-.137	1.3	.0	.9	.0	1.01	-.00	1.01	-.1	1.01	-.00	1.01	-.0	1.00	-.00	1.00	-.3
6	.600	-.035	3.4	.1	3.3	.1	1.00	.01	1.00	.4	1.01	.01	1.01	.3	.99	.03	.99	1.8
7	.600	-.035	3.1	.0	2.0	.1	1.01	.01	1.01	.3	1.02	.00	1.02	.3	1.01	.02	1.01	1.1

* referenced to location of wing at $\alpha = 4.75^0$.

Table 3-A ($\alpha = 4.75^0$)

Run	U_{L_e} m/sec	$\pm U_{L_e}$ m/sec	V_{L_e} m/sec	$\pm V_{L_e}$ m/sec	U_{L_B} m/sec	V_{L_B} m/sec	U_{L_t} m/sec	V_{L_t} m/sec	S_{R_u}	S_{R_v}	E_u	E_v	N_u	N_v	DR_u sec^{-1}	DR_v sec^{-1}	Time	Julian day
1	41.2	.1	35.2	.1	41.2	35.1	41.5	35.1	-.26	.03	-.6	.2	165	225	3	4	17:32	133
2	41.7	.0	34.6	.0	41.7	34.5	41.9	34.3	-.54	.20	.2	.8	1008	1072	17	18	17:34	133
3	41.7	.0	34.3	.0	41.7	34.2	41.8	34.2	-.21	.25	.1	.1	1195	1811	20	30	17:35	133
4	41.8	.0	33.5	.0	41.8	33.4	42.0	33.3	-.39	.46	-.0	.6	1332	1329	22	22	17:37	133
5	41.2	.0	32.8	.0	41.2	32.7	41.4	32.6	-.27	.45	.1	.4	1489	1759	25	29	17:38	133
6	40.7	.0	32.1	.0	40.7	32.0	40.8	32.0	-.24	.35	-.1	.2	2087	3398	35	57	17:40	133
7	39.8	.0	31.8	.0	39.9	31.7	40.0	31.5	-.16	.49	.2	.4	2323	2066	39	34	17:42	133
8	39.2	.0	31.5	.0	39.2	31.5	39.3	31.4	.04	.47	.2	.4	1289	1567	21	26	17:43	133
9	38.8	.0	31.5	.0	38.8	31.4	38.7	31.0	.05	.45	.1	.3	2167	1894	36	32	17:45	133
10	38.2	.0	31.5	.0	38.2	31.4	38.2	30.9	.15	.40	.4	.2	2170	1696	36	28	17:46	133
11	37.8	.0	31.8	.0	37.8	31.7	37.8	31.6	.15	.54	.4	.4	1312	1407	22	23	17:48	133
12	43.1	.1	35.6	.1	43.1	35.5	43.2	35.5	-.41	-.10	.1	.3	254	331	4	6	17:52	133
13	43.4	.1	34.9	.1	43.5	34.9	43.6	34.6	-.61	-.01	.0	-.2	262	205	4	3	17:53	133
14	43.9	.1	34.1	.1	44.0	34.1	44.0	34.1	-.74	.19	1.5	.1	474	379	8	6	17:55	133
15	44.1	.0	33.2	.0	44.2	33.1	44.2	33.0	-.41	.24	.0	.7	1651	909	28	15	17:56	133
16	43.8	.0	31.7	.0	43.8	31.7	44.0	31.6	-.27	.16	-.3	-.1	1361	1169	23	19	17:58	133
17	43.1	.0	29.8	.0	43.1	29.8	43.4	29.7	-.30	.84	-.3	.7	1315	1444	22	24	17:59	133
18	42.2	.0	28.7	.1	42.2	28.5	42.3	28.6	-.24	.64	-.1	.6	1242	1060	21	18	18: 1	133
19	41.0	.0	28.1	.1	41.0	28.1	41.1	28.1	-.24	.52	-.0	-.2	1055	989	18	16	18: 2	133
20	39.8	.0	27.8	.1	39.8	27.7	39.9	27.7	-.07	.71	-.2	.4	1239	874	21	15	18: 3	133
21	38.5	.0	30.1	.1	38.6	30.2	38.6	29.9	.10	.21	.2	-.5	2877	1877	48	31	18:58	133
22	38.1	.0	30.4	.1	38.1	30.4	38.1	29.9	.04	.08	.1	-.7	1703	1485	28	25	19: 0	133
23	37.7	.0	31.2	.1	37.7	31.2	37.6	29.9	.13	-.03	-.1	-.9	980	1209	16	20	19: 2	133
24	37.2	.0	30.9	.1	37.1	30.9	37.2	30.1	.25	.09	-.2	-.5	1192	1221	20	20	19: 4	133
25	36.8	.0	31.0	.1	36.8	31.0	36.8	30.3	.35	.21	-.0	-.4	1814	1762	30	29	19: 6	133
26	42.0	.1	35.7	.1	42.2	35.7	42.0	35.7	-.03	.05	-.1	.6	763	954	13	16	19:10	133
27	43.2	.1	35.1	.0	43.3	35.2	43.5	35.1	-.51	.31	.2	1.1	1489	1544	25	26	19:12	133
28	43.4	.1	34.2	.0	43.6	34.2	43.9	34.1	-.49	.15	-.0	1.2	1093	2562	33	43	19:13	133
29	45.5	.0	33.0	.0	45.6	32.9	45.7	33.0	-.59	.19	.2	.4	4073	4078	161	200	19:16	133
30	45.9	.0	32.1	.0	45.9	32.1	46.1	31.9	-.48	.50	.0	1.1	4066	4081	188	208	19:17	133
31	46.4	.0	29.6	.0	46.4	29.5	46.5	29.4	-.40	.32	.1	.3	4076	4044	209	240	19:19	133
32	46.2	.0	27.5	.0	46.2	27.4	46.4	27.3	-.43	.51	-.1	.4	4087	4055	182	254	19:21	133
33	45.2	.0	25.7	.0	45.2	25.6	45.3	25.3	-.35	.66	-.1	.3	4078	4044	162	185	19:23	133
34	43.4	.0	23.1	.0	43.4	22.9	43.5	22.8	-.20	.81	-.2	.5	4091	4033	150	164	19:25	133
35	41.7	.0	21.9	.0	41.7	21.6	41.8	20.6	-.08	.60	-.2	.3	3815	3381	64	56	19:27	133
36	40.0	.0	23.0	.1	40.0	22.7	40.2	22.5	-.17	.90	-.2	.7	781	715	13	12	19:29	133
37	38.1	.1	24.3	.3	38.1	24.2	38.1	24.5	.18	.82	.5	-.4	107	159	2	3	19:32	133
38	37.0	.1	23.8	.3	37.0	23.7	37.1	23.6	.55	1.20	-.7	1.0	58	174	1	3	19:35	133
39	35.7	.1	24.6	.2	35.7	24.3	35.6	23.9	.50	.72	-.3	.6	192	156	3	3	19:39	133
40	34.9	.2	25.9	.4	34.8	25.7	34.8	26.1	.26	.56	-.7	-.2	72	51	1	1	19:43	133
41	34.4	.2	26.0	.2	34.4	25.8	34.3	25.2	.45	1.11	-.5	.0	105	280	2	5	19:46	133
42	28.9	.3	24.4	.3	28.9	24.1	28.9	24.0	.67	.64	.4	.2	24	58	0	1	19:49	133
43	43.9	.0	36.4	.0	43.9	36.4	44.0	36.6	-.36	-.11	.1	.0	4060	4010	153	154	20:25	133
44	44.8	.0	35.7	.0	44.9	35.7	45.0	35.8	-.32	-.03	-.1	.1	3743	2251	62	38	20:27	133
45	45.6	.0	34.8	.0	45.6	34.8	46.3	34.9	-.46	-.08	.2	.4	4053	4085	159	183	20:29	133
46	46.0	.0	33.6	.0	46.0	33.5	46.4	33.5	-.63	-.02	-.1	.5	4074	4078	139	160	20:31	133
47	47.5	.0	31.4	.0	47.5	31.4	48.1	31.4	-.39	.27	-.4	.4	4076	4075	153	150	20:34	133
48	49.8	.1	27.2	.0	49.7	27.1	50.3	27.3	-.34	.53	-.3	.8	4083	3780	127	63	20:36	133
49	51.2	.1	21.7	.0	51.2	21.6	52.0	21.5	-.14	.41	-.6	.4	3456	1967	58	33	20:53	133
50	49.4	.1	17.5	.1	49.4	17.2	49.9	16.1	.11	1.65	.2	2.3	2755	1190	46	20	20:39	133
51	48.4	.1	18.0	.3	48.4	17.3	48.9	17.4	.44	1.80	.5	4.9	934	206	16	3	20:51	133
52	45.7	.3	26.3	.5	45.6	26.1	46.4	24.6	-1.05	-1.93	.1	2.3	163	113	3	2	20:42	133
53	27.2	.1	26.3	.1	27.2	26.1	24.1	25.7	.32	1.17	.1	1.9	542	849	9	14	20:47	133
54	44.5	.0	37.4	.0	44.6	37.4	44.8	37.6	-.37	-.04	.5	.2	2135	1535	36	26	20:56	133
55	45.0	.0	37.2	.0	45.0	37.2	45.1	37.3	-.23	-.21	.3	.1	2129	1250	35	21	20:57	133
56	46.0	.0	37.0	.1	46.1	37.0	46.2	37.2	-.44	-.32	.7	.1	955	624	16	10	20:59	133
57	47.2	.0	35.9	.0	47.3	35.9	47.4	36.1	-.57	-.14	.3	-.1	4037	4082	186	167	21: 1	133
58	48.0	.0	35.2	.0	48.1	35.2	48.5	35.4	-.66	-.23	.1	-.1	4017	4007	143	153	21: 3	133
59	50.0	.0	34.3	.0	50.1	34.3	50.4	34.1	-.59	-.15	-.1	-.3	4053	3614	126	59	21: 4	133
60	52.8	.0	32.3	.0	52.9	32.3	53.4	32.6	-.52	.07	-.2	-.4	4045	3028	127	50	21: 6	133

Table 3-A. - Continued.

Run	U_{L_e} m/sec	$\pm U_{L_e}$ m/sec	V_{L_e} m/sec	$\pm V_{L_e}$ m/sec	U_{L_B} m/sec	V_{L_B} m/sec	U_{L_t} m/sec	V_{L_t} m/sec	S_{R_u}	S_{R_v}	E_u	E_v	N_u	N_v	DR_u sec^{-1}	DR_v sec^{-1}	Time	Julian day
61	56.2	.1	30.4	.0	56.3	30.3	56.7	30.6	-.61	.43	-.2	-.3	3861	2843	64	47	21: 7	133
62	62.0	.1	25.9	.0	62.2	25.8	62.4	26.0	-.67	.84	.3	.6	2605	4041	43	125	21: 9	133
63	63.8	.1	21.9	.1	64.0	21.3	64.4	22.6	-.15	1.68	.3	3.4	2041	2352	34	39	21:14	133
64	63.6	.1	22.0	.1	64.2	21.6	64.2	22.3	-.25	1.80	.8	3.1	1792	2562	30	43	21:15	133
65	52.0	1.1	27.0	.4	51.7	27.0	52.5	25.7	.26	.16	-1.0	-.9	58	159	1	3	21:12	133
66	57.2	.1	29.6	.0	57.3	29.6	58.0	29.9	-.82	.53	-.0	.1	4045	3984	108	135	14:47	136
67	53.2	.1	24.8	.1	53.0	24.7	54.5	24.6	-.47	.99	-.5	.5	4093	4049	111	143	14:39	136
68	54.7	.1	21.1	.1	54.5	21.2	56.3	20.8	-.36	.93	-.4	1.2	3585	3752	60	63	14:41	136
69	56.1	.3	17.4	.3	55.7	16.9	57.7	15.7	-.68	.45	-1.0	-1.4	1073	1249	18	21	14:43	136
70	43.5	.0	37.2	.1	43.6	37.2	43.8	37.3	-.47	-.09	.8	-.0	699	840	12	14	10:17	136
71	43.6	.0	37.0	.0	43.6	37.0	43.6	37.2	-.61	-.22	.4	-.1	2670	3573	44	60	10:18	136
72	45.4	.0	36.9	.0	45.4	36.9	45.5	37.1	-.44	-.29	.3	-.1	4044	4075	152	151	10:20	136
73	47.1	.0	36.7	.0	47.2	36.7	47.3	37.1	-.39	-.23	.3	-.3	4034	4084	181	158	10:22	136
74	49.9	.0	37.0	.0	50.0	37.0	50.1	37.3	-.50	-.27	.6	-.3	4035	4087	202	177	10:24	136
75	51.5	.0	37.0	.0	51.6	37.1	51.7	37.4	-.61	-.25	.9	-.4	4029	4084	224	151	10:26	136
76	53.8	.0	37.4	.0	53.9	37.4	53.9	37.8	-.62	-.39	1.6	-.4	4050	4089	149	136	10:28	136
77	57.0	.0	36.8	.1	57.2	36.8	57.1	37.2	-.07	-.36	.6	-.7	4032	3794	128	63	10:29	136
78	58.2	.1	35.6	.9	58.7	35.4	58.5	36.6	-1.79	.09	7.9	-1.6	470	55	8	1	10:35	136
79	54.0	.6	26.8	3.5	53.8	26.0	55.3	30.1	-.66	-2.36	-1.2	4.2	115	10	2	0	10:34	136
80	61.1	.1	28.2	.1	61.7	28.1	62.0	28.5	-.32	.65	3.1	.3	3996	4078	136	157	14:49	136
81	50.3	.6	29.6	.2	50.0	29.5	50.9	28.6	.67	-.42	-.7	-.1	209	261	3	4	14:52	136
82	44.6	.5	30.1	.8	44.6	30.1	45.4	31.0	.90	-1.27	.1	1.3	52	21	1	0	14:56	136
83	43.0	.1	36.8	.1	43.0	36.8	43.3	36.9	-.33	-.46	.1	.6	357	343	6	6	10:15	136
84	43.4	.0	38.7	.0	43.5	38.7	43.3	38.8	-.20	-.22	.5	-.0	1491	1288	25	21	10:38	136
85	44.5	.0	38.7	.1	44.6	38.7	44.6	39.1	-.04	-.37	.1	.2	1576	1165	26	19	10:40	136
86	45.7	.0	38.9	.1	45.8	7.7	46.1	39.8	.05	-.58	.2	-.3	988	224	16	4	10:41	136
87	46.9	.0	38.0	.0	47.0	38.0	47.1	38.5	-.26	-.10	.3	-.6	4050	4092	231	191	10:43	136
88	49.0	.0	38.3	.0	49.2	38.4	49.2	38.8	-.75	.02	1.4	-.8	4022	4083	184	167	10:45	136
89	50.1	.0	38.9	.1	50.3	39.0	50.5	39.3	-.65	-.10	1.4	-.8	3991	3714	154	62	10:46	136
90	52.0	.0	39.3	.1	52.2	39.5	52.2	39.6	-.58	-.19	1.3	-.7	4000	3258	134	54	10:48	136
91	55.1	.0	38.5	.1	55.4	38.4	55.3	39.1	-.60	.14	1.2	-1.2	3995	3844	140	64	10:50	136
92	44.1	.0	38.3	.0	44.2	38.3	44.2	38.6	-.42	.00	.6	-.2	3671	4085	65	169	10:58	136
93	45.3	.0	38.1	.0	45.4	38.2	45.5	38.3	-.63	.09	1.3	-.5	4080	2988	125	50	10:59	136
94	46.6	.0	39.0	.0	46.6	39.0	46.7	39.5	-.40	-.07	.9	-.6	4069	3828	139	64	11: 1	136
95	48.2	.0	40.4	.0	48.3	40.5	48.4	40.8	-.21	-.27	.8	-.6	4034	4081	136	144	11: 3	136
96	48.7	.0	41.5	.1	48.8	41.5	48.9	41.9	-.84	-.53	1.4	-.6	4045	4085	150	180	12:31	136
97	50.5	.0	43.8	.0	50.5	43.9	50.4	43.9	.42	-.64	-.0	.9	4067	3441	219	57	12:33	136
98	52.7	.0	36.5	.1	52.8	36.6	52.7	36.8	-.29	1.20	.3	1.1	4028	669	129	11	12:41	136
99	42.4	.0	41.0	.0	42.5	41.1	42.5	41.0	.32	-.22	.4	.2	2544	4001	42	171	12:43	136
100	42.8	.0	41.7	.0	42.9	41.7	42.8	41.9	.47	-.43	.1	.2	4082	4087	119	171	12:45	136
101	43.6	.0	42.3	.0	43.6	42.3	43.5	42.7	.24	-.46	-.3	-.1	3056	3560	51	59	12:47	136
102	43.7	.0	43.6	.0	43.7	43.7	43.6	43.9	.47	-.70	-.0	.4	4086	4083	124	168	12:48	136
103	44.2	.0	44.4	.0	44.2	44.4	44.1	44.9	.52	-.54	-.1	-.0	2780	2903	46	48	12:50	136
104	44.8	.0	44.3	.1	44.7	44.4	44.5	44.6	.54	-.36	-.3	-.4	2059	1967	34	33	12:52	136
105	40.4	.0	43.1	.1	40.3	43.2	40.2	43.2	.48	-.03	-.1	2.5	1340	973	22	16	12:56	136
106	40.7	.1	42.6	.0	41.2	42.7	41.0	43.2	1.25	-.36	.7	-.2	166	3160	3	53	12:58	136
107	40.4	.0	42.3	.0	40.5	42.5	40.2	43.1	.81	-.30	.5	-.2	4079	3305	124	55	13: 2	136
108	41.1	.0	43.1	.0	41.1	43.3	40.3	43.5	.53	-.30	-.0	-.1	3990	3560	113	64	13: 5	136
109	42.1	.0	43.5	.1	42.1	43.6	41.9	43.9	.15	-.22	-.3	-.1	3193	2822	53	47	13: 6	136
110	43.0	.0	44.6	.1	43.0	44.7	42.6	45.2	.16	-.22	-.7	.0	2401	2372	47	40	13: 9	136
111	41.0	.0	43.8	.0	41.0	43.9	40.9	44.3	.51	-.70	.0	-.1	1063	3077	133	51	13: 9	143
112	40.5	.0	46.1	.0	40.5	46.3	40.6	46.2	.12	-.01	-.1	.4	1552	963	26	16	13:10	143
113	37.9	.0	43.4	.0	37.9	43.4	37.8	43.1	.59	-.57	.1	1.1	4071	4087	158	186	13:16	136
114	38.7	.0	43.6	.0	38.7	43.6	38.3	43.6	.44	-.49	-.1	1.2	4077	3928	135	148	13:18	136
115	38.5	.0	43.9	.0	38.5	43.9	38.3	43.5	.23	-.42	-.5	1.0	1734	3075	29	173	13:20	136
116	39.5	.0	44.2	.1	39.6	44.2	39.5	44.1	.46	-.41	.0	.5	1567	714	26	13	13:22	136
117	38.5	.0	43.8	.0	38.5	43.9	38.1	44.3	.09	-.74	-.1	1.1	4068	4077	136	153	13:58	136
118	37.7	.0	44.4	.0	37.7	44.5	37.4	44.7	1.16	-1.05	.0	2.1	3695	3750	62	62	14: 0	136
119	37.3	.0	44.7	.0	37.2	44.8	37.0	45.2	1.23	-1.16	1.3	1.3	4059	4082	116	151	14: 2	136
120	38.0	.0	44.4	.0	38.0	44.5	37.4	45.2	.97	-.67	-.1	.5	3754	4064	63	165	14: 4	136

Table 3-A. - Continued.

Run	U_{L_e} m/sec	$\pm U_{L_e}$ m/sec	V_{L_e} m/sec	$\pm V_{L_e}$ m/sec	U_{L_B} m/sec	V_{L_B} m/sec	U_{L_t} m/sec	V_{L_t} m/sec	S_{R_u}	S_{R_v}	E_u	E_v	N_u	N_v	DR_u sec^{-1}	DR_v sec^{-1}	Time	Julian day
121	38.1	.1	45.1	.1	38.1	45.2	37.9	45.4	.66	-1.34	-.5	2.0	1635	2474	27	41	14: 6	136
122	37.6	.0	44.9	.0	37.6	45.0	37.5	45.0	.58	-.06	.2	.9	4079	3703	174	62	13:21	143
123	36.9	.0	45.4	.0	36.9	45.4	36.7	45.5	.38	.10	.1	-.1	2158	795	36	13	13:23	143
124	36.2	.1	45.8	.1	36.2	45.8	36.2	45.9	.05	.10	-.1	-.0	248	102	4	2	13:25	143
125	37.1	.0	42.9	.0	37.3	43.0	36.9	43.1	.53	.04	-.3	1.0	1919	2269	32	38	14:13	136
126	36.3	.0	43.2	.0	36.4	43.3	36.2	43.3	.87	.17	.8	1.6	4073	4080	152	168	14:14	136
127	37.9	.1	42.6	.1	37.9	42.7	37.8	42.4	.31	-.06	-.1	.5	916	752	15	13	14:16	136
128	36.2	.0	42.9	.0	36.4	43.3	35.9	43.4	.75	.30	-.0	2.0	2737	3305	46	55	14:19	136
129	35.8	.0	43.2	.0	35.9	43.5	35.2	43.5	.91	-.36	.3	2.3	4073	3990	120	152	14:21	136
130	35.7	.0	43.9	.0	35.7	44.0	35.2	43.8	.91	-.20	.2	1.6	4076	4076	123	181	14:23	136
131	35.8	.0	43.9	.0	35.8	44.2	35.1	44.0	.73	.12	-.1	2.1	4073	4071	126	172	14:25	136
132	35.9	.0	44.7	.0	35.9	44.8	35.3	44.5	.59	-.14	-.6	2.3	3979	4075	120	160	14:27	136
133	34.8	.1	45.2	.0	34.7	45.2	34.7	45.1	.34	.41	-.2	.7	1018	1937	17	32	14:29	136
134	35.6	.0	43.8	.0	35.8	43.9	35.5	43.8	.33	.09	.0	.3	4065	4069	167	129	13:28	143
135	34.8	.0	44.1	.0	34.8	44.0	34.7	44.0	.19	.15	-.0	.0	3738	3076	62	51	13:30	143
136	33.9	.0	44.4	.0	33.9	44.4	33.8	44.4	.19	.11	.0	-.1	1879	2146	31	36	13:32	143
137	33.3	.0	44.5	.0	33.3	44.5	33.1	44.5	.08	-.12	-.1	-.2	1295	1711	22	29	13:33	143
138	33.7	.0	41.2	.0	33.8	41.2	33.3	41.1	.84	.38	1.0	.1	4063	3609	170	60	13:36	143
139	33.0	.0	41.9	.0	33.0	41.9	33.0	41.8	.50	.08	.3	-.4	3139	1746	52	29	13:38	143
140	31.6	.0	40.8	.0	31.5	40.8	31.6	40.8	.04	.24	.2	-.1	3633	3136	61	52	13:40	143
141	30.8	.0	40.8	.0	30.8	40.8	30.7	40.7	.04	.14	-.0	-.0	2394	3810	40	63	13:42	143
142	30.2	.0	40.7	.0	30.2	40.7	30.3	40.7	-.10	.05	.1	-.2	1075	1423	18	24	13:44	143
143	34.3	.1	31.5	.1	34.4	31.5	34.5	31.4	.04	.12	-.1	-.2	666	369	11	6	8:52	144
144	35.3	.0	32.8	.0	35.3	32.8	35.3	32.8	.06	.11	.0	.2	4079	2670	177	44	8:53	144
145	35.3	.0	33.3	.0	35.3	33.3	35.3	33.3	-.02	.38	.3	.3	4064	2429	168	40	8:55	144
146	35.3	.0	33.6	.0	35.3	33.6	35.2	33.5	.09	.29	.4	.4	4080	3178	150	53	8:56	144
147	35.3	.0	34.0	.0	35.3	33.9	35.5	33.9	.07	.22	.2	.4	3186	2054	53	34	8:59	144
148	35.2	.0	34.2	.0	35.3	34.2	35.2	34.2	.14	.41	.6	.8	2322	1768	39	29	9: 1	144
149	33.1	.0	40.0	.0	33.1	39.9	33.1	39.8	.68	.42	1.2	.2	4065	4059	350	267	14: 7	143
150	33.5	.1	41.1	.1	33.4	41.1	33.7	40.9	.05	.17	-.3	-.5	386	1027	6	17	14: 9	143
151	31.7	.1	39.6	.0	31.7	39.5	31.9	39.7	.21	.42	-.1	.0	380	913	6	15	14:26	143
152	30.9	.0	38.7	.0	30.8	38.7	30.6	38.7	.04	.10	-.1	-.1	2618	2187	44	36	14:28	143
153	30.3	.0	38.1	.0	30.3	38.1	30.2	38.1	-.00	-.06	.0	-.2	2616	961	44	16	14:29	143
154	32.2	.4	28.7	.3	32.3	28.7	32.4	14.3	-.83	.16	1.0	-.6	76	43	1	1	14:37	143
155	34.2	.1	32.3	.1	34.3	32.3	34.1	32.4	.05	-.09	.1	-.3	450	202	7	3	14:38	143
156	35.0	.1	32.7	.0	35.0	32.7	34.9	32.8	.26	-.07	.4	.1	538	986	9	16	14:40	143
157	35.4	.0	33.3	.0	35.4	33.3	35.4	33.2	.03	.08	.1	.3	3757	3064	63	51	14:41	143
158	35.6	.0	33.9	.0	35.7	33.9	35.5	33.8	.30	.54	.8	.6	4084	4058	159	137	14:42	143
159	35.6	.0	34.4	.0	35.8	34.3	35.5	34.2	.43	.54	.8	.5	3662	3621	61	60	14:44	143
160	35.5	.0	34.6	.0	35.7	34.6	35.0	34.5	.44	.50	1.0	.7	4079	3496	140	58	14:46	143
161	35.6	.0	34.8	.0	35.7	34.8	35.6	34.8	.42	.60	1.1	1.5	4081	4084	152	125	14:47	143
162	35.8	.0	35.1	.0	35.8	35.1	35.7	35.1	.11	.32	.4	.5	3710	1966	62	33	14:49	143
163	35.1	.0	34.6	.0	35.1	34.6	34.9	34.6	.08	.12	.7	.3	4080	4069	258	152	8:44	144
164	33.4	.1	39.7	.0	33.7	39.8	32.6	39.6	1.23	.39	1.4	-.4	1977	2178	33	36	9:23	144
165	32.7	.1	39.6	.1	32.6	39.6	32.6	39.6	.27	.14	.4	-.5	373	862	6	14	9:24	144
166	31.5	.0	37.7	.0	31.5	37.7	31.6	37.8	-.07	.17	.1	.1	4075	4055	207	274	9:26	144
167	31.1	.0	36.7	.0	31.1	36.7	31.1	36.8	-.01	.07	-.1	-.0	4079	2452	143	41	9:28	144
168	31.4	.0	36.2	.0	31.4	36.1	31.3	36.2	.07	-.06	-.1	-.2	853	995	14	17	9:29	144
169	30.8	.1	34.9	.2	30.8	35.0	31.0	35.2	-.04	-1.17	.2	2.1	94	63	2	1	9:30	144
170	28.2	.2	34.0	.4	28.2	34.0	28.1	34.1	-.35	-1.16	.1	.9	70	35	1	1	9:37	144
171	25.4	.3	33.2	.6	25.3	33.2	25.3	33.0	-.46	-.35	.9	-.4	36	13	1	0	9:39	144
172	23.9	.7	22.2	.6	23.8	22.2	24.8	22.4	.55	.30	-.7	-.0	45	29	1	0	9:40	144
173	25.6	.6	22.1	.3	25.9	22.0	26.6	22.1	.25	-.36	-1.0	-.3	92	73	2	1	9:42	144
174	29.7	.4	26.3	.3	29.6	26.3	29.9	26.5	-.86	-.41	.1	-.4	136	115	2	2	9:44	144
175	32.4	.1	31.5	.1	32.5	31.5	33.0	31.6	-.20	-.30	.0	.5	413	248	7	4	9:46	144
176	32.7	.1	33.7	.0	32.9	33.7	33.3	33.3	-.21	.15	.7	-.0	1235	939	21	16	9:48	144
177	33.3	.0	34.0	.0	33.2	34.0	33.5	33.9	-.19	.48	.4	.9	2162	1651	36	28	9:50	144
178	33.9	.0	33.9	.0	33.9	34.0	33.9	33.8	.32	.58	1.0	2.0	4069	2928	139	49	9:53	144
179	34.6	.0	34.5	.0	34.6	34.5	34.4	34.4	.23	.45	.9	1.2	4077	4061	179	151	9:55	144
180	34.7	.0	34.9	.0	35.0	34.8	34.8	34.7	.53	.39	1.0	.7	4061	4074	203	183	9:56	144

Table 3-A. - Concluded.

Run	U_{L_e} m/sec	$\pm U_{L_e}$ m/sec	V_{L_e} m/sec	$\pm V_{L_e}$ m/sec	U_{L_B} m/sec	V_{L_B} m/sec	U_{L_t} m/sec	V_{L_t} m/sec	S_{R_u}	S_{R_v}	E_u	E_v	N_u	N_v	DR_u sec^{-1}	DR_v sec^{-1}	Time	Julian day
181	34.7	.0	34.9	.0	35.0	35.0	34.5	34.8	.60	.55	1.2	1.0	4065	4075	175	157	9:58	144
182	34.9	.0	35.0	.0	35.1	35.1	34.9	34.9	.50	.24	1.4	.8	4070	4068	161	137	10: 0	144
183	34.9	.0	35.2	.0	35.2	35.2	35.0	35.1	.55	.44	1.2	1.2	4064	4076	149	119	10: 2	144
184	33.0	.0	38.9	.0	33.1	38.9	32.9	38.7	.86	.57	1.8	-.1	4064	4086	264	201	10: 6	144
185	32.4	.0	38.9	.0	32.4	38.9	32.3	38.6	.06	.34	1.2	-.5	4078	4086	196	160	10: 7	144
186	32.0	.0	37.4	.0	32.0	37.4	31.7	37.4	-.08	.18	.3	.0	4089	3727	250	62	10:10	144
187	32.0	.0	36.3	.0	32.0	36.3	32.0	36.4	-.10	.06	.2	-.1	2606	2387	47	40	10:11	144
188	32.1	.1	36.0	.1	32.1	36.0	32.4	36.0	.09	-.07	-.3	-.2	419	250	7	4	10:13	144
189	30.6	.1	35.2	.1	30.6	35.3	30.8	35.4	.12	.18	.1	-.3	137	122	2	2	10:14	144
190	28.1	.5	33.3	.9	28.0	33.3	28.8	33.5	-1.00	-.09	1.5	-.6	21	7	0	0	10:16	144
191	25.6	.9	29.7	1.9	25.5	29.6	26.0	.0	.39	1.12	-.8	-.7	22	4	0	0	10:17	144
192	26.1	1.1	23.9	.5	26.0	23.2	23.6	22.1	.80	.93	.5	2.1	13	10	0	0	10:26	144
193	26.0	1.0	25.4	.6	26.0	25.3	25.8	25.7	.52	.72	-.9	-.2	15	49	0	1	10:30	144
194	28.3	.6	24.7	.4	28.2	24.7	28.1	24.3	-.44	.14	-.4	-.7	51	33	1	1	10:32	144
195	26.6	.8	25.2	.4	26.5	25.2	26.0	25.3	-.17	.34	-.8	-.9	25	25	0	0	10:33	144
196	32.4	.2	30.9	.1	32.5	30.9	32.0	30.9	-.50	-.20	.4	.2	290	390	5	6	10:35	144
197	33.0	.1	32.6	.1	33.1	32.6	33.0	33.0	-.10	.09	.5	.4	704	645	12	11	10:36	144
198	33.3	.0	34.5	.0	33.3	34.4	33.1	34.5	-.13	.29	.8	.1	3353	2251	56	38	10:38	144
199	33.8	.0	34.4	.0	33.8	34.4	33.7	34.4	.07	.04	.4	.3	4083	1912	170	32	10:39	144
200	34.2	.0	34.6	.0	34.3	34.6	34.0	34.4	.33	.17	1.0	.9	4084	4071	192	134	10:41	144
201	34.3	.0	34.7	.0	34.3	34.7	34.2	34.7	.54	.07	1.3	.8	4078	2838	157	47	10:42	144
202	34.5	.0	34.9	.0	34.5	34.9	34.4	34.9	.42	.10	1.0	1.3	4084	2411	142	40	10:44	144
203	34.6	.0	35.0	.0	34.6	35.0	34.5	35.1	.33	.23	1.1	.7	2648	1749	44	29	10:46	144

Table 3-B ($\alpha = 4.75^0$)

Run	$\frac{x_c}{c}$	$\frac{y_c}{c}$	σ_u m/sec	$\pm\sigma_u$ m/sec	σ_v m/sec	$\pm\sigma_v$ m/sec	$\frac{U_{f_e}}{U_T}$	$\frac{V_{f_e}}{U_T}$	$\frac{U_{R_e}}{U_T}$	α_{R_e} deg	$\frac{U_{f_B}}{U_T}$	$\frac{V_{f_B}}{U_T}$	$\frac{U_{R_B}}{U_T}$	α_{R_B} deg	$\frac{U_{f_t}}{U_t}$	$\frac{V_{f_t}}{U_t}$	$\frac{U_{R_t}}{U_t}$	α_{R_t} deg
1	-.173	.277	1.6	.1	1.4	.1	1.03	.07	1.04	3.9	1.03	.07	1.04	4.0	1.04	.08	1.04	4.2
2	-.171	.239	1.5	.0	1.4	.0	1.03	.08	1.04	4.7	1.03	.09	1.04	4.8	1.03	.09	1.04	5.2
3	-.166	.201	1.4	.0	1.4	.0	1.03	.09	1.03	5.0	1.03	.09	1.03	5.0	1.03	.09	1.03	5.1
4	-.164	.161	1.4	.0	1.5	.0	1.02	.10	1.02	5.6	1.02	.10	1.02	5.7	1.02	.11	1.02	6.0
5	-.163	.120	1.3	.0	1.4	.0	1.00	.10	1.01	5.9	1.00	.10	1.01	6.0	1.00	.11	1.01	6.2
6	-.161	.082	1.3	.0	1.4	.0	.99	.11	.99	6.1	.99	.11	.99	6.2	.99	.11	.99	6.3
7	-.163	.041	1.2	.0	1.5	.0	.97	.10	.97	5.8	.97	.10	.97	5.9	.97	.11	.97	6.2
8	-.161	.021	1.2	.0	1.5	.0	.96	.09	.96	5.6	.96	.10	.96	5.7	.96	.10	.96	5.7
9	-.162	.001	1.1	.0	1.5	.0	.95	.09	.96	5.3	.95	.09	.96	5.4	.95	.09	.95	5.7
10	-.160	-.020	1.1	.0	1.4	.0	.94	.08	.95	5.0	.94	.08	.95	5.0	.94	.09	.94	5.4
11	-.162	-.040	1.0	.0	1.5	.0	.94	.07	.95	4.4	.94	.07	.94	4.4	.94	.07	.94	4.5
12	-.090	.276	1.5	.1	1.3	.1	1.07	.09	1.07	4.8	1.06	.09	1.07	4.9	1.07	.09	1.07	5.0
13	-.086	.240	1.5	.1	1.2	.1	1.06	.10	1.07	5.6	1.06	.11	1.07	5.7	1.06	.11	1.07	6.0
14	-.084	.199	1.5	.1	1.2	.0	1.06	.12	1.07	6.5	1.06	.12	1.07	6.6	1.06	.12	1.07	6.6
15	-.083	.160	1.5	.0	1.3	.0	1.04	.14	1.05	7.5	1.04	.14	1.05	7.6	1.04	.14	1.05	7.6
16	-.080	.121	1.6	.0	1.4	.0	1.02	.15	1.03	8.5	1.02	.15	1.03	8.6	1.03	.16	1.04	8.7
17	-.078	.080	1.5	.0	1.7	.0	.99	.17	1.00	9.7	.99	.17	1.00	9.7	.99	.17	1.01	10.0
18	-.077	.061	1.3	.0	1.6	.0	.96	.17	.98	10.2	.96	.18	.97	10.4	.96	.18	.98	10.3
19	-.080	.040	1.2	.0	1.8	.0	.94	.16	.95	9.9	.94	.16	.95	10.0	.94	.17	.95	10.0
20	-.077	.021	1.1	.0	1.9	.1	.92	.15	.93	9.5	.91	.15	.93	9.6	.92	.16	.93	9.7
21	-.079	.010	1.2	.0	2.9	.0	.94	.10	.94	6.4	.94	.10	.94	6.4	.93	.11	.94	6.6
22	-.077	.002	1.2	.0	3.3	.0	.93	.10	.94	5.8	.93	.10	.94	5.8	.93	.10	.93	6.2
23	-.078	-.010	1.2	.0	3.3	.0	.94	.08	.94	4.8	.94	.08	.94	4.8	.92	.09	.92	5.8
24	-.078	-.019	1.2	.0	3.0	.1	.93	.07	.93	4.6	.93	.08	.93	4.7	.92	.09	.92	5.4
25	-.078	-.030	1.4	.0	2.7	.0	.92	.07	.93	4.3	.92	.07	.92	4.3	.91	.08	.92	4.9
26	-.048	.280	2.1	.1	1.7	.0	1.06	.08	1.06	4.1	1.06	.08	1.06	4.2	1.06	.07	1.06	4.0
27	-.045	.240	2.1	.0	1.7	.0	1.06	.10	1.07	5.3	1.07	.10	1.07	5.3	1.07	.10	1.07	5.5
28	-.044	.200	2.5	.0	1.7	.0	1.06	.11	1.06	6.2	1.06	.12	1.07	6.3	1.06	.12	1.07	6.6
29	-.041	.159	2.0	.0	1.5	.0	1.07	.16	1.08	8.5	1.07	.16	1.08	8.5	1.07	.16	1.09	8.5
30	-.038	.140	2.0	.0	1.6	.0	1.06	.18	1.08	9.4	1.06	.18	1.08	9.4	1.06	.18	1.08	9.7
31	-.036	.100	2.2	.0	1.5	.0	1.04	.22	1.06	11.9	1.03	.22	1.06	12.0	1.04	.22	1.06	12.1
32	-.034	.080	2.3	.0	1.8	.0	1.01	.24	1.03	13.6	1.00	.25	1.03	13.7	1.01	.25	1.04	13.9
33	-.037	.060	2.0	.0	2.2	.0	.97	.26	1.00	14.8	.97	.26	1.00	14.9	.97	.26	1.00	15.2
34	-.036	.041	1.8	.0	2.5	.0	.91	.27	.95	16.4	.91	.27	.94	16.6	.90	.27	.94	16.7
35	-.034	.030	1.4	.0	2.4	.0	.87	.26	.91	16.7	.86	.26	.90	17.0	.85	.28	.90	18.2
36	-.036	.021	1.0	.0	3.2	.1	.86	.22	.89	14.5	.86	.23	.89	14.8	.86	.23	.89	15.2
37	-.036	.010	.9	.1	4.4	.2	.85	.18	.87	11.8	.85	.18	.87	11.9	.85	.18	.87	11.7
38	-.036	.001	1.0	.1	3.6	.2	.83	.17	.85	11.6	.83	.17	.85	11.8	.83	.18	.85	12.0
39	-.037	-.009	1.3	.1	2.7	.2	.82	.14	.83	9.8	.82	.15	.83	10.1	.81	.15	.83	10.6
40	-.036	-.019	1.4	.1	2.8	.3	.83	.11	.84	7.8	.83	.12	.83	7.9	.83	.11	.84	7.6
41	-.036	-.029	1.8	.1	2.7	.1	.82	.11	.83	7.4	.82	.11	.83	7.5	.81	.12	.82	8.1
42	-.006	-.030	1.6	.3	2.0	.2	.73	.05	.73	4.2	.72	.06	.72	4.5	.72	.06	.72	4.8
43	-.006	.279	1.3	.0	1.4	.0	1.10	.09	1.10	4.7	1.10	.09	1.10	4.7	1.10	.09	1.11	4.7
44	-.003	.240	1.4	.0	1.3	.0	1.10	.11	1.11	5.9	1.10	.11	1.11	5.9	1.11	.11	1.11	5.9
45	-.000	.199	1.6	.0	1.5	.0	1.10	.14	1.11	7.1	1.10	.14	1.11	7.1	1.11	.14	1.12	7.4
46	.002	.160	2.5	.0	1.5	.0	1.09	.16	1.10	8.2	1.09	.16	1.10	8.3	1.09	.16	1.11	8.5
47	.002	.119	2.8	.0	1.5	.0	1.08	.21	1.10	10.9	1.08	.21	1.10	11.0	1.09	.22	1.11	11.3
48	.005	.080	3.5	.0	1.6	.0	1.06	.30	1.10	15.7	1.05	.30	1.09	15.8	1.06	.30	1.11	16.0
49	.005	.058	3.9	.0	1.7	.0	1.00	.39	1.08	21.4	1.00	.39	1.07	21.6	1.01	.41	1.09	21.9
50	.005	.040	3.9	.1	4.8	.1	.92	.43	1.02	25.0	.92	.43	1.01	25.2	.91	.45	1.01	26.5
51	.005	.038	2.9	.1	3.6	.3	.91	.41	1.00	24.0	.90	.42	1.00	24.7	.91	.42	1.00	24.8
52	.006	.031	3.6	.2	6.1	.5	.99	.25	1.02	14.5	.98	.26	1.02	14.6	.97	.29	1.02	16.5
53	.011	.035	3.2	.1	2.0	.1	.73	.01	.73	.4	.73	.01	.73	.6	.68	-.03	.68	-2.4
54	.035	.290	1.3	.0	1.4	.0	1.12	.09	1.12	4.4	1.12	.09	1.12	4.4	1.12	.09	1.13	4.4
55	.037	.273	1.2	.0	1.4	.0	1.12	.09	1.13	4.8	1.12	.09	1.13	4.8	1.13	.09	1.13	4.8
56	.039	.231	1.3	.0	1.5	.0	1.14	.11	1.14	5.6	1.14	.11	1.14	5.6	1.14	.11	1.15	5.6
57	.042	.193	1.7	.0	1.6	.0	1.14	.14	1.15	7.1	1.14	.14	1.15	7.2	1.14	.14	1.15	7.1
58	.045	.163	2.2	.0	1.7	.0	1.14	.16	1.15	8.2	1.14	.16	1.15	8.2	1.15	.17	1.16	8.3
59	.047	.133	2.5	.0	1.8	.0	1.15	.20	1.17	10.0	1.15	.20	1.17	10.0	1.16	.21	1.18	10.3
60	.046	.102	3.0	.0	2.1	.0	1.16	.27	1.19	12.9	1.17	.27	1.20	13.0	1.19	.27	1.21	13.0

Table 3-B. - Continued.

Run	x_c/c	y_c/c	σ_u m/sec	$\pm\sigma_u$ m/sec	σ_v m/sec	$\pm\sigma_v$ m/sec	U_{f_e}/U_T	V_{f_e}/U_T	U_{R_e}/U_T	α_{R_e} deg	U_{f_B}/U_T	V_{f_B}/U_T	U_{R_B}/U_T	α_{R_B} deg	U_{f_t}/U_T	V_{f_t}/U_T	U_{R_t}/U_T	α_{R_t} deg
61	.048	.083	3.4	.0	2.4	.0	1.18	.34	1.23	16.0	1.19	.34	1.23	16.1	1.20	.34	1.24	16.0
62	.046	.063	3.5	.1	2.7	.0	1.21	.48	1.30	21.7	1.21	.48	1.30	21.9	1.21	.49	1.31	21.8
63	.046	.057	3.5	.1	3.8	.1	1.18	.56	1.30	25.5	1.17	.57	1.30	26.0	1.19	.56	1.32	25.1
64	.046	.056	4.0	.1	4.1	.1	1.18	.56	1.30	25.3	1.18	.57	1.31	25.8	1.19	.56	1.32	25.2
65	.047	.052	8.4	.6	4.7	.2	1.08	.33	1.13	17.0	1.08	.33	1.13	16.8	1.07	.35	1.13	18.3
66	.026	.064	6.5	.1	3.4	.0	1.08	.38	1.15	19.4	1.08	.38	1.14	19.4	1.10	.40	1.17	20.1
67	.027	.055	7.1	.1	4.7	.1	1.05	.45	1.15	23.3	1.05	.45	1.14	23.2	1.07	.48	1.17	24.1
68	.026	.045	8.7	.1	8.9	.1	1.02	.52	1.15	27.2	1.01	.53	1.14	27.5	1.02	.57	1.17	29.2
69	.076	.328	1.4	.1	1.6	.1	1.11	.07	1.11	3.8	1.11	.07	1.11	3.8	1.12	.08	1.12	3.9
70	.078	.303	1.2	.0	1.5	.0	1.13	.08	1.13	3.9	1.13	.08	1.13	3.9	1.13	.08	1.13	4.0
71	.082	.264	1.7	.0	1.8	.0	1.12	.08	1.13	4.0	1.12	.08	1.13	4.1	1.12	.08	1.13	3.9
72	.085	.224	1.4	.0	1.8	.0	1.15	.11	1.15	5.3	1.15	.11	1.15	5.3	1.15	.10	1.16	5.2
73	.088	.186	1.5	.0	2.0	.0	1.17	.13	1.17	6.4	1.17	.13	1.18	6.5	1.17	.13	1.18	6.3
74	.088	.146	1.5	.0	2.4	.0	1.21	.17	1.22	7.8	1.21	.17	1.22	7.9	1.22	.16	1.23	7.7
75	.089	.126	1.7	.0	2.7	.0	1.23	.19	1.25	8.7	1.23	.19	1.25	8.7	1.24	.19	1.25	8.5
76	.089	.105	1.5	.0	2.9	.0	1.27	.21	1.28	9.6	1.27	.21	1.29	9.6	1.27	.21	1.29	9.4
77	.089	.085	1.6	.0	4.0	.0	1.30	.27	1.33	11.5	1.31	.27	1.33	11.6	1.31	.26	1.34	11.3
78	.087	.066	1.9	.1	6.7	.3	1.30	.30	1.33	12.9	1.30	.31	1.34	13.3	1.32	.29	1.35	12.4
79	.088	.066	6.9	.3	11.1	4.4	1.12	.37	1.18	18.0	1.11	.37	1.17	18.6	1.18	.34	1.23	16.9
80	.059	.077	4.4	.0	3.1	.0	1.20	.37	1.26	17.0	1.21	.37	1.26	17.1	1.22	.38	1.28	17.1
81	.058	.069	5.8	.1	3.8	.0	1.24	.44	1.31	19.7	1.24	.45	1.32	19.9	1.25	.45	1.33	19.7
82	.059	.059	8.1	.3	3.6	.2	1.11	.27	1.14	13.9	1.10	.27	1.13	13.8	1.10	.30	1.14	15.1
83	.060	.053	3.4	.3	3.4	.7	1.03	.19	1.05	10.4	1.03	.19	1.05	10.4	1.06	.19	1.07	10.1
84	.119	.308	1.2	.0	1.6	.0	1.14	.05	1.14	2.7	1.14	.05	1.14	2.7	1.14	.05	1.14	2.5
85	.121	.271	1.2	.0	1.9	.0	1.15	.07	1.16	3.4	1.15	.07	1.16	3.4	1.16	.06	1.16	3.1
86	.123	.231	1.2	.0	1.9	.1	1.17	.08	1.18	4.0	.75	.52	.91	34.9	1.19	.08	1.19	3.6
87	.128	.191	1.5	.0	2.5	.0	1.18	.11	1.18	5.4	1.18	.11	1.18	5.4	1.19	.11	1.19	5.2
88	.128	.151	1.9	.0	3.0	.0	1.21	.14	1.22	6.4	1.22	.14	1.22	6.4	1.22	.13	1.23	6.1
89	.132	.131	2.0	.0	3.4	.0	1.23	.14	1.24	6.5	1.24	.14	1.24	6.6	1.24	.14	1.25	6.5
90	.130	.112	2.1	.0	3.8	.0	1.26	.16	1.27	7.3	1.27	.16	1.28	7.3	1.27	.16	1.28	7.2
91	.130	.091	2.2	.0	4.7	.0	1.29	.22	1.31	9.5	1.30	.22	1.32	9.6	1.31	.21	1.32	9.2
92	.162	.274	1.8	.0	2.2	.0	1.14	.07	1.14	3.5	1.14	.07	1.14	3.4	1.14	.07	1.14	3.3
93	.165	.236	1.7	.0	2.4	.0	1.15	.09	1.16	4.4	1.16	.09	1.16	4.3	1.16	.09	1.16	4.3
94	.169	.196	1.8	.0	2.7	.0	1.18	.09	1.18	4.5	1.18	.09	1.18	4.5	1.19	.09	1.19	4.1
95	.171	.156	1.7	.0	3.1	.0	1.22	.10	1.23	4.5	1.23	.10	1.23	4.5	1.23	.09	1.23	4.3
96	.171	.136	2.3	.0	3.5	.0	1.25	.09	1.25	4.0	1.25	.09	1.25	4.0	1.26	.08	1.26	3.8
97	.172	.116	1.6	.0	2.6	.0	1.30	.08	1.31	3.5	1.31	.08	1.31	3.4	1.31	.08	1.31	3.4
98	.170	.101	2.1	.0	3.4	.1	1.24	.21	1.26	9.7	1.24	.21	1.26	9.7	1.24	.21	1.26	9.5
99	.287	.317	1.6	.0	2.0	.0	1.15	.01	1.15	.3	1.15	.01	1.15	.4	1.16	.00	1.16	.1
100	.288	.280	1.6	.0	2.1	.0	1.17	.00	1.17	.2	1.17	.00	1.17	.2	1.17	.00	1.17	.0
101	.293	.240	1.6	.0	2.4	.0	1.19	.01	1.19	.3	1.19	.01	1.19	.3	1.19	-.00	1.19	-.1
102	.295	.201	1.6	.0	2.4	.0	1.21	-.01	1.21	-.6	1.21	-.01	1.21	-.6	1.21	-.02	1.21	-.8
103	.297	.161	1.8	.0	2.7	.0	1.23	-.02	1.23	-.7	1.23	-.02	1.23	-.8	1.23	-.02	1.23	-1.2
104	.296	.141	2.0	.0	2.9	.0	1.23	-.01	1.23	-.3	1.23	-.01	1.23	-.4	1.23	-.01	1.23	-.7
105	.411	.314	1.5	.0	1.8	.1	1.15	-.05	1.15	-2.5	1.15	-.05	1.15	-2.6	1.15	-.05	1.15	-2.6
106	.414	.277	1.8	.1	2.7	.0	1.15	-.04	1.15	-1.9	1.16	-.03	1.16	-1.7	1.16	-.04	1.16	-2.1
107	.413	.277	1.7	.0	2.8	.0	1.14	-.04	1.14	-1.9	1.14	-.04	1.14	-2.0	1.15	-.05	1.15	-2.6
108	.418	.238	1.9	.0	2.8	.0	1.16	-.04	1.16	-2.0	1.16	-.04	1.16	-2.1	1.16	-.05	1.17	-2.4
109	.419	.199	2.1	.0	2.8	.0	1.18	-.03	1.18	-1.5	1.18	-.03	1.18	-1.6	1.18	-.04	1.18	-1.9
110	.422	.158	2.5	.0	2.7	.0	1.21	-.04	1.21	-1.7	1.21	-.04	1.21	-1.7	1.21	-.05	1.21	-2.3
111	.421	.148	2.2	.0	2.2	.0	1.18	-.05	1.18	-2.5	1.18	-.05	1.18	-2.5	1.18	-.06	1.18	-2.9
112	.422	.118	1.8	.0	1.1	.0	1.20	-.09	1.20	-4.3	1.20	-.09	1.20	-4.4	1.20	-.09	1.20	-4.3
113	.579	.304	1.6	.0	2.0	.0	1.12	-.09	1.12	-4.4	1.12	-.09	1.12	-4.5	1.12	-.09	1.12	-4.6
114	.578	.287	1.9	.0	1.9	.0	1.13	-.08	1.13	-4.0	1.13	-.08	1.14	-4.0	1.13	-.09	1.13	-4.3
115	.581	.268	2.0	.0	2.1	.0	1.13	-.09	1.14	-4.3	1.14	-.09	1.14	-4.4	1.13	-.08	1.13	-4.3
116	.582	.249	1.9	.0	2.0	.1	1.15	-.08	1.16	-3.8	1.15	-.08	1.16	-3.8	1.15	-.08	1.15	-3.7
117	.584	.228	2.4	.0	2.5	.0	1.14	-.09	1.14	-4.3	1.14	-.09	1.14	-4.4	1.14	-.10	1.14	-4.9
118	.586	.207	2.3	.0	2.0	.0	1.13	-.10	1.14	-5.3	1.14	-.11	1.14	-5.3	1.13	-.11	1.14	-5.6
119	.586	.187	2.2	.0	2.4	.0	1.13	-.11	1.13	-5.7	1.13	-.12	1.13	-5.8	1.13	-.12	1.14	-6.3
120	.587	.167	3.0	.0	2.6	.0	1.14	-.10	1.14	-5.0	1.14	-.10	1.14	-5.1	1.14	-.12	1.15	-6.0

Table 3-B. - Continued.

Run	$\frac{x_c}{c}$	$\frac{y_c}{c}$	σ_u m/sec	$\pm\sigma_u$ m/sec	σ_v m/sec	$\pm\sigma_v$ m/sec	$\frac{U_{f_e}}{U_T}$	$\frac{V_{f_e}}{U_T}$	$\frac{U_{R_e}}{U_T}$	α_{R_e} deg	$\frac{U_{f_B}}{U_T}$	$\frac{V_{f_B}}{U_T}$	$\frac{U_{R_B}}{U_T}$	α_{R_B} deg	$\frac{U_{f_t}}{U_T}$	$\frac{V_{f_t}}{U_T}$	$\frac{U_{R_t}}{U_T}$	α_{R_t} deg
121	.589	.158	2.7	.0	2.8	.1	1.15	-.11	1.15	-5.4	1.15	-.11	1.16	-5.5	1.15	-.12	1.16	-5.7
122	.578	.145	2.2	.0	1.1	.0	1.14	-.11	1.15	-5.6	1.14	-.11	1.15	-5.7	1.14	-.12	1.14	-5.8
123	.578	.126	1.8	.0	.9	.0	1.14	-.13	1.14	-6.5	1.14	-.13	1.14	-6.5	1.14	-.13	1.14	-6.7
124	.579	.106	1.3	.1	.8	.1	1.13	-.14	1.14	-7.3	1.13	-.14	1.14	-7.3	1.13	-.15	1.14	-7.3
125	.744	.309	2.1	.0	1.9	.0	1.10	-.09	1.11	-4.8	1.11	-.09	1.11	-4.7	1.10	-.10	1.11	-5.0
126	.746	.291	2.0	.0	1.7	.0	1.10	-.11	1.10	-5.6	1.10	-.11	1.10	-5.6	1.09	-.11	1.10	-5.7
127	.746	.271	1.8	.0	1.9	.1	1.11	-.08	1.11	-4.0	1.11	-.08	1.12	-4.0	1.11	-.08	1.11	-3.9
128	.747	.251	2.4	.0	2.1	.0	1.09	-.10	1.10	-5.4	1.10	-.11	1.10	-5.6	1.09	-.11	1.10	-5.8
129	.750	.232	2.4	.0	2.1	.0	1.09	-.11	1.09	-5.9	1.09	-.12	1.10	-6.1	1.08	-.13	1.09	-6.6
130	.751	.212	2.5	.0	2.0	.0	1.10	-.12	1.10	-6.5	1.10	-.13	1.11	-6.5	1.09	-.13	1.10	-6.8
131	.751	.192	2.8	.0	2.0	.0	1.10	-.12	1.11	-6.4	1.10	-.13	1.11	-6.6	1.09	-.15	1.10	-7.1
132	.754	.171	2.8	.0	1.9	.0	1.11	-.13	1.12	-6.8	1.11	-.13	1.12	-6.9	1.10	-.14	1.11	-7.2
133	.755	.151	1.8	.0	1.5	.0	1.10	-.16	1.11	-8.0	1.10	-.16	1.11	-8.1	1.10	-.16	1.11	-8.1
134	.743	.149	2.3	.0	1.2	.0	1.10	-.12	1.10	-6.4	1.10	-.12	1.10	-6.4	1.09	-.13	1.10	-6.6
135	.745	.130	1.9	.0	1.0	.0	1.09	-.14	1.10	-7.3	1.09	-.14	1.10	-7.3	1.08	-.14	1.09	-7.4
136	.746	.111	1.5	.0	1.0	.0	1.08	-.16	1.09	-8.2	1.08	-.16	1.09	-8.2	1.08	-.16	1.09	-8.3
137	.749	.091	1.3	.0	.9	.0	1.07	-.17	1.09	-8.8	1.07	-.17	1.09	-8.8	1.07	-.17	1.08	-8.9
138	.952	.185	2.3	.0	1.4	.0	1.03	-.11	1.04	-6.3	1.03	-.11	1.04	-6.2	1.03	-.12	1.03	-6.5
139	.954	.145	1.9	.0	1.4	.0	1.03	-.13	1.04	-7.4	1.03	-.13	1.04	-7.4	1.03	-.13	1.04	-7.3
140	.957	.107	1.4	.0	1.0	.0	1.00	-.14	1.01	-7.9	1.00	-.14	1.01	-7.9	1.00	-.14	1.01	-7.9
141	.961	.087	1.3	.0	.9	.0	.99	-.15	1.00	-8.6	.99	-.15	1.00	-8.6	.98	-.15	1.00	-8.6
142	.960	.068	1.2	.0	.9	.0	.98	-.16	.99	-9.0	.98	-.16	.99	-9.0	.98	-.15	.99	-8.9
143	1.007	-.009	1.6	.0	1.1	.0	.92	.03	.92	1.9	.92	.03	.92	1.9	.92	.03	.92	2.2
144	1.005	-.029	1.3	.0	.9	.0	.95	.03	.95	1.5	.95	.03	.95	1.5	.95	.02	.95	1.5
145	1.005	-.039	1.3	.0	1.0	.0	.96	.02	.96	1.1	.96	.02	.96	1.1	.96	.02	.96	1.0
146	1.007	-.059	1.3	.0	.9	.0	.96	.01	.96	.8	.96	.01	.96	.8	.96	.01	.96	.8
147	1.006	-.078	1.3	.0	.9	.0	.97	.01	.97	.5	.97	.01	.97	.5	.97	.01	.97	.7
148	1.006	-.099	1.3	.0	1.0	.0	.97	.00	.97	.2	.97	.00	.97	.2	.97	.00	.97	.2
149	1.014	.188	1.8	.0	1.3	.0	1.01	-.11	1.01	-6.0	1.01	-.11	1.01	-6.0	1.01	-.10	1.01	-5.9
150	1.017	.149	1.5	.1	1.6	.0	1.03	-.12	1.04	-6.5	1.03	-.12	1.03	-6.5	1.03	-.11	1.03	-6.1
151	1.021	.110	1.4	.0	1.2	.0	.98	-.12	.99	-6.9	.98	-.12	.99	-6.9	.99	-.12	.99	-6.8
152	1.021	.080	1.2	.0	.8	.0	.96	-.12	.97	-7.1	.96	-.12	.97	-7.1	.96	-.12	.96	-7.3
153	1.024	.060	1.1	.0	.7	.0	.94	-.12	.95	-7.1	.94	-.12	.95	-7.1	.94	-.12	.95	-7.1
154	1.025	.000	3.8	.4	1.6	.1	.84	.04	.84	2.7	.84	.04	.85	2.8	.65	.24	.69	20.6
155	1.028	-.010	1.5	.1	1.0	.0	.92	.02	.92	1.1	.92	.02	.92	1.2	.92	.01	.92	.9
156	1.026	-.019	1.3	.0	.9	.0	.94	.02	.94	1.4	.94	.02	.94	1.4	.94	.02	.94	1.1
157	1.027	-.030	1.4	.0	1.0	.0	.95	.02	.95	1.2	.95	.02	.95	1.2	.95	.02	.95	1.2
158	1.027	-.039	1.5	.0	1.3	.0	.96	.01	.96	.8	.96	.01	.96	.9	.96	.01	.96	.8
159	1.026	-.060	1.6	.0	1.2	.0	.97	.01	.97	.4	.97	.01	.97	.6	.96	.01	.96	.5
160	1.026	-.079	1.5	.0	1.2	.0	.97	.00	.97	.1	.97	.00	.97	.3	.96	-.00	.96	-.2
161	1.027	-.099	1.5	.0	1.2	.0	.97	.00	.97	.1	.98	.00	.98	.2	.97	.00	.97	.0
162	1.026	-.140	1.4	.0	1.2	.0	.98	-.00	.98	-.0	.98	.00	.98	.0	.98	-.00	.98	-.1
163	1.027	-.141	1.4	.0	1.0	.0	.97	-.00	.97	-.2	.97	-.00	.97	-.2	.97	-.01	.97	-.3
164	1.076	.177	2.4	.0	1.8	.0	1.02	-.10	1.02	-5.5	1.02	-.09	1.03	-5.3	1.00	-.11	1.01	-6.1
165	1.078	.139	1.7	.1	1.7	.0	1.00	-.11	1.01	-6.1	1.00	-.11	1.01	-6.1	1.00	-.11	1.01	-6.1
166	1.083	.100	1.3	.0	1.0	.0	.96	-.10	.97	-5.8	.96	-.10	.97	-5.8	.97	-.10	.97	-5.7
167	1.085	.061	1.2	.0	.8	.0	.94	-.09	.95	-5.4	.94	-.09	.95	-5.4	.94	-.09	.95	-5.4
168	1.086	.041	1.2	.0	.8	.0	.94	-.08	.94	-4.7	.94	-.08	.94	-4.6	.94	-.08	.94	-4.7
169	1.088	.032	1.4	.1	1.8	.2	.91	-.07	.92	-4.2	.91	-.07	.92	-4.3	.92	-.07	.92	-4.2
170	1.087	.026	1.5	.1	2.4	.3	.86	-.09	.87	-5.9	.86	-.09	.87	-5.9	.86	-.09	.87	-6.1
171	1.088	.021	2.0	.3	2.2	.4	.81	-.12	.82	-8.2	.81	-.12	.82	-8.2	.81	-.12	.82	-8.2
172	1.088	.015	4.6	.4	3.0	.3	.64	.03	.64	1.4	.64	.03	.64	1.4	.66	.03	.66	2.3
173	1.089	.012	5.8	.3	2.6	.2	.66	.04	.66	3.6	.67	.05	.67	4.0	.68	.06	.68	4.7
174	1.088	.007	4.7	.3	3.0	.2	.78	.04	.78	2.9	.78	.04	.78	2.8	.79	.04	.79	2.5
175	1.088	.001	2.5	.1	1.7	.1	.89	.00	.89	.2	.89	.00	.89	.3	.90	.01	.90	.7
176	1.089	-.004	2.0	.0	1.4	.0	.93	-.02	.92	-1.4	.93	-.02	.93	-1.3	.92	-.03	.93	-1.9
177	1.089	-.008	1.5	.0	1.2	.0	.93	-.02	.93	-1.2	.93	-.02	.93	-1.2	.94	-.01	.94	-.9
178	1.088	-.019	1.5	.0	1.1	.0	.94	-.01	.94	-.6	.94	-.01	.94	-.7	.94	-.01	.94	-.6
179	1.088	-.029	1.6	.0	1.3	.0	.96	-.01	.96	-.6	.96	-.01	.96	-.5	.95	-.01	.95	-.6
180	1.089	-.038	1.8	.0	1.4	.0	.97	-.01	.97	-.7	.97	-.01	.97	-.5	.97	-.01	.97	-.5

Table 3-B. - Concluded.

Run	$\frac{x_c}{c}$	$\frac{y_c}{c}$	σ_u m/sec	$\pm\sigma_u$ m/sec	σ_v m/sec	$\pm\sigma_v$ m/sec	$\frac{U_{f_e}}{U_T}$	$\frac{V_{f_e}}{U_T}$	$\frac{U_{R_e}}{U_T}$	α_{R_e} deg	$\frac{U_{f_B}}{U_T}$	$\frac{V_{f_B}}{U_T}$	$\frac{U_{R_B}}{U_T}$	α_{R_B} deg	$\frac{U_{f_t}}{U_T}$	$\frac{V_{f_t}}{U_T}$	$\frac{U_{R_t}}{U_T}$	α_{R_t} deg
181	1.091	-.058	1.7	.0	1.4	.0	.97	-.01	.97	-.8	.97	-.01	.97	-.6	.96	-.01	.96	-.8
182	1.089	-.078	1.7	.0	1.3	.0	.97	-.01	.97	-.7	.98	-.01	.98	-.6	.97	-.01	.97	-.6
183	1.089	-.099	1.7	.0	1.3	.0	.97	-.01	.97	-.8	.98	-.01	.98	-.6	.97	-.01	.97	-.7
184	1.116	.178	1.9	.0	1.6	.0	1.00	-.09	1.00	-5.3	1.00	-.09	1.00	-5.2	.99	-.09	1.00	-5.2
185	1.120	.139	1.5	.0	1.6	.0	.99	-.10	1.00	-5.8	.99	-.10	1.00	-5.8	.99	-.10	.99	-5.7
186	1.122	.100	1.4	.0	1.0	.0	.97	-.09	.97	-5.1	.97	-.09	.97	-5.1	.96	-.09	.97	-5.3
187	1.126	.060	1.1	.0	.8	.0	.95	-.07	.95	-4.2	.95	-.07	.95	-4.2	.95	-.07	.95	-4.2
188	1.127	.041	1.1	.0	.9	.0	.95	-.06	.95	-3.8	.95	-.06	.95	-3.9	.95	-.06	.95	-3.6
189	1.128	.031	1.4	.1	1.4	.1	.91	-.07	.92	-4.6	.92	-.07	.92	-4.7	.92	-.07	.92	-4.6
190	1.128	.026	2.2	.4	2.4	.5	.85	-.08	.86	-5.5	.85	-.08	.86	-5.5	.87	-.07	.87	-4.9
191	1.128	.021	4.1	.5	3.8	1.1	.77	-.07	.77	-4.9	.77	-.07	.77	-4.9	.37	.36	.51	44.4
192	1.128	.019	3.9	.9	2.3	.5	.70	.02	.70	1.9	.69	.03	.69	2.7	.64	.01	.64	1.3
193	1.128	.018	3.9	.5	4.3	.4	.72	.00	.72	.1	.71	.00	.71	.2	.72	-.01	.72	-.5
194	1.129	.013	4.3	.4	2.5	.2	.74	.04	.74	3.3	.74	.04	.74	3.2	.73	.04	.73	3.5
195	1.129	.013	4.2	.4	1.9	.2	.72	.01	.72	.9	.72	.01	.72	.9	.71	.00	.71	.2
196	1.129	.005	2.8	.1	1.7	.1	.88	.01	.88	.8	.88	.01	.88	.9	.88	.01	.88	.4
197	1.130	.001	2.2	.1	1.6	.0	.91	-.00	.91	-.2	.92	-.00	.92	-.2	.92	-.01	.92	-.6
198	1.132	-.010	1.6	.0	1.1	.0	.94	-.03	.94	-1.6	.94	-.03	.94	-1.6	.94	-.03	.94	-1.8
199	1.132	-.018	1.4	.0	1.0	.0	.95	-.02	.95	-1.1	.95	-.02	.95	-1.1	.95	-.02	.95	-1.3
200	1.130	-.039	1.5	.0	1.1	.0	.96	-.02	.96	-.9	.96	-.02	.96	-.9	.95	-.02	.95	-.9
201	1.132	-.060	1.5	.0	1.1	.0	.96	-.02	.96	-1.0	.96	-.02	.96	-.9	.96	-.02	.96	-1.0
202	1.131	-.079	1.5	.0	1.1	.0	.97	-.02	.97	-.9	.97	-.02	.97	-.9	.97	-.02	.97	-1.0
203	1.131	-.100	1.4	.0	1.0	.0	.97	-.02	.97	-.9	.97	-.02	.97	-.9	.97	-.02	.97	-1.1

Table -4 ($\alpha = 0.6^0$)

Run	U_{L_e} m/sec	$\pm U_{L_e}$ m/sec	V_{L_e} m/sec	$\pm V_{L_e}$ m/sec	S_{R_u}	S_{R_v}	E_u	E_v	N_u	N_v	DR_u sec^{-1}	DR_v sec^{-1}	Time	Julian day
1	36.9	.0	33.6	.0	-.28	.36	.1	1.3	482	248	8	4	13:52	130
2	36.7	.1	33.0	.0	-.19	.05	.0	.1	258	374	4	6	13:55	130
3	36.5	.1	33.1	.0	-.07	-.15	.2	.9	161	353	3	6	13:57	130
4	36.5	.0	32.8	.0	-.33	-.27	-.1	.6	307	356	5	6	13:58	130
5	36.4	.0	32.5	.0	-.06	-.12	-.1	.5	362	245	6	4	14: 0	130
6	36.3	.0	32.2	.0	-.34	-.09	-.3	.2	287	257	5	4	14: 1	130
7	36.2	.1	32.3	.0	-.39	.20	-.3	.4	221	236	4	4	14: 3	130
8	35.8	.1	31.9	.0	.09	.47	-.6	1.0	145	266	2	4	14: 4	130
9	35.4	.0	31.8	.0	-.02	.54	-.1	.4	593	679	10	11	14: 6	130
10	35.3	.0	31.8	.0	-.29	.42	-.1	.7	416	859	7	14	14:10	130
11	34.8	.0	32.0	.1	-.09	.67	-.1	.3	660	252	11	4	14:38	130
12	34.6	.0	32.0	.1	.18	.51	-.4	-.2	221	149	4	2	14:41	130
13	34.2	.1	32.1	.1	.02	.39	-.3	-.3	157	136	3	2	14:43	130
14	33.9	.0	32.3	.1	.19	.28	-.2	-.7	198	87	3	1	14:44	130
15	33.6	.0	32.6	.1	.34	-.44	.1	.6	198	105	3	2	14:46	130
16	33.4	.1	33.0	.1	.26	.34	-.4	.2	123	64	2	1	14:48	130
17	37.2	.0	33.4	.0	-.67	1.03	.8	1.0	3769	1352	63	23	9:19	131
18	37.3	.0	32.9	.0	-.28	.53	.2	1.2	3990	2376	144	40	9:21	131
19	37.4	.0	32.5	.0	-.32	-.01	.4	.4	4014	2356	125	39	9:23	131
20	37.2	.0	31.8	.0	-.29	.23	.3	.3	4005	2575	133	43	9:25	131
21	37.1	.0	31.4	.0	-.22	.46	.1	1.0	4011	2638	129	44	9:27	131
22	36.9	.0	31.0	.0	-.21	.18	.0	.8	3995	2780	141	46	9:28	131
23	36.7	.0	30.5	.0	-.22	.31	.1	2.3	3915	2771	137	46	9:30	131
24	36.4	.0	29.9	.0	-.04	.54	.1	1.4	3777	2730	63	45	9:32	131
25	36.0	.0	29.6	.0	.00	.24	.3	1.1	3714	2634	62	44	9:33	131
26	35.3	.0	29.1	.0	-.06	.47	.2	.7	3597	2573	60	43	9:35	131
27	34.5	.0	28.8	.0	.02	.10	-.1	.4	3427	2648	57	44	9:37	131
28	33.8	.0	28.8	.0	.11	.13	.1	.8	3555	2392	59	40	9:38	131
29	33.2	.0	28.9	.0	.03	.61	.0	1.3	3675	2538	61	42	9:40	131
30	32.7	.0	29.1	.0	.19	.41	.2	.0	3822	2417	64	40	9:42	131
31	32.3	.0	29.7	.0	.29	.47	-.1	-.6	3892	2774	65	46	9:44	131
32	31.9	.0	29.9	.0	.31	.28	-.2	-.6	3948	2942	144	49	9:45	131
33	31.8	.0	30.8	.0	.37	.59	-.1	-.3	3951	3683	129	61	9:50	131
34	31.5	.0	30.7	.0	.33	.57	-.1	-.2	4044	3847	132	64	9:47	131
35	31.4	.0	31.0	.0	.31	.53	-.1	.0	3967	3877	96	65	9:48	131
36	38.2	.0	33.5	.0	-.12	.63	.4	.8	2930	1081	49	13	9:59	131
37	38.1	.0	33.0	.0	-.20	.50	.2	1.6	3842	973	64	16	10: 1	131
38	38.3	.0	32.6	.0	-.17	-.09	.0	1.4	4052	2129	117	35	10: 3	131
39	38.5	.0	31.7	.0	-.12	.41	-.0	.5	4056	1140	120	19	10: 5	131
40	38.5	.0	31.2	.0	-.17	.63	-.2	1.2	3894	1886	65	31	10: 7	131
41	38.4	.0	30.6	.0	-.27	-.09	.0	1.4	3824	2153	64	36	10: 9	131
42	38.2	.0	30.0	.0	-.24	-.17	-.0	1.6	3976	2332	170	39	10:12	131
43	37.8	.0	29.4	.0	-.15	-.26	-.1	1.7	4000	2401	159	40	10:15	131
44	37.4	.0	28.6	.0	-.02	-.17	-.2	1.7	3995	2483	158	41	10:18	131
45	36.6	.0	27.7	.0	-.01	.27	-.0	.2	3951	2287	151	38	10:20	131
46	35.7	.0	26.8	.0	-.36	.33	.2	.8	3725	1997	62	33	10:22	131
47	34.2	.0	26.2	.1	-.23	.53	1.1	-.1	2407	367	40	6	10:25	131
48	32.9	.0	26.5	.2	-.03	-.05	.7	-.8	485	41	8	1	10:58	131
49	32.0	.0	26.6	.2	.20	.18	.5	-.1	372	23	6	0	11: 1	131
50	31.8	.1	26.8	.3	.44	-.00	.2	-1.5	453	15	8	0	11: 5	131
51	30.9	.3	27.1	.2	-.24	-.27	-.2	-.9	21	17	0	0	11:10	131
52	30.7	.1	30.5	.1	.23	.09	.3	-.1	365	255	6	4	11:13	131
53	30.0	.1	30.2	.1	-.27	.50	-.1	-.1	160	285	3	5	11:15	131
54	38.3	.0	34.0	.0	-.75	.27	.7	.3	1193	1036	20	17	13:34	131
55	38.4	.0	33.3	.0	-.72	.23	1.0	.5	2086	1495	35	25	13:35	131
56	38.6	.0	32.7	.0	-.49	.73	1.5	.5	2143	996	36	17	13:37	131
57	38.9	.0	31.7	.0	-.45	.03	.6	3.0	2442	2119	41	35	13:39	131
58	39.4	.0	31.2	.0	-.26	.25	-.1	2.2	3933	2476	115	41	13:40	131
59	39.5	.0	30.6	.0	-.33	-.18	-.1	1.5	3947	2358	126	39	13:42	131
60	39.7	.0	29.9	.0	-.39	-.19	-.1	.7	3989	2458	138	41	13:44	131

Table 4-A. - Continued.

Run	U_{L_e} m/sec	$\pm U_{L_e}$ m/sec	V_{L_e} m/sec	$\pm V_{L_e}$ m/sec	S_{R_u}	S_{R_v}	E_u	E_v	N_u	N_v	DR_u sec^{-1}	DR_v sec^{-1}	Time	Julian day
61	39.8	.0	28.9	.0	-.26	-.07	-.1	.9	4017	2232	139	37	13:45	131
62	39.7	.0	27.6	.0	-.31	.07	-.2	.3	4055	1482	125	25	13:47	131
63	39.5	.0	25.6	.0	-.31	.74	-.3	.9	4068	549	110	9	13:48	131
64	39.1	.0	23.5	.1	-.18	.40	-.5	.9	4073	338	103	6	13:50	131
65	38.6	.0	22.3	.1	-.11	.09	-.5	.3	4079	182	98	3	13:52	131
66	37.3	.0	22.8	.5	.12	.71	-.5	-.1	1816	33	30	1	13:54	131
67	34.4	.1	24.0	1.1	.41	.49	.2	-1.3	219	7	4	0	13:57	131
68	39.4	.0	34.4	.0	.03	.04	-.1	1.6	2391	283	40	5	14: 4	131
69	39.3	.0	33.6	.0	-.01	.12	-.1	.3	2768	422	46	7	14: 7	131
70	40.5	.0	33.2	.0	.00	.26	-.1	-.5	2031	305	34	5	15:12	131
71	40.7	.0	32.4	.0	-.21	-.07	-.0	1.8	4005	2108	283	35	15:24	131
72	40.7	.0	32.1	.0	-.55	.53	.1	2.1	3805	1480	63	25	15:26	131
73	41.0	.0	31.4	.0	-.19	-.28	-.0	2.3	3826	1767	64	29	15:28	131
74	41.7	.0	30.8	.0	-.36	-.27	-.0	1.6	3867	1734	64	29	15:29	131
75	42.5	.0	30.1	.0	-.57	-.04	.0	.5	3923	1690	184	28	15:31	131
76	43.2	.0	28.8	.0	-.50	.36	-.1	.7	3945	1042	181	17	15:33	131
77	44.7	.0	27.2	.1	-.55	.87	-.2	.5	3977	453	200	8	15:35	131
78	47.3	.0	24.1	.2	-.57	1.66	-.2	2.3	3873	91	65	2	15:37	131
79	39.8	.0	34.8	.0	-.09	1.02	.1	1.1	2770	735	46	12	15:47	131
80	40.3	.0	34.4	.1	-.16	.12	.1	.2	2176	226	36	4	15:48	131
81	40.3	.0	33.9	.0	-.23	.68	.2	.4	2628	411	44	7	15:50	131
82	41.7	.0	33.4	.0	-.30	-.14	.2	-.1	2351	938	39	16	15:52	131
83	42.1	.0	33.1	.0	-.21	-.15	.0	-.2	1996	763	33	13	15:54	131
84	42.6	.0	32.7	.0	-.52	-.01	.2	-.5	1166	372	19	6	15:56	131
85	43.6	.0	32.6	.1	-.05	-.14	.1	-.1	1149	179	19	3	15:58	131
86	43.2	.0	32.7	.0	-.79	-.46	.8	.4	2852	644	48	11	16: 1	131
87	45.2	.0	32.7	.0	-1.11	-.45	3.0	.6	3427	582	57	10	16: 2	131
88	45.7	.0	32.1	.0	-.70	-.53	.7	.0	3970	1046	275	17	16:24	131
89	46.3	.0	31.3	.1	-.88	-.06	.9	-.8	3872	632	65	11	16:26	131
90	46.9	.0	30.8	.1	-.93	-.03	.7	-.5	3790	528	63	9	16:28	131
91	48.3	.0	30.6	.1	-.84	-.34	.7	-.1	3815	343	64	6	16:30	131
92	50.5	.0	30.5	.2	-.76	-.92	2.2	.2	3500	64	58	1	16:37	131
93	40.0	.0	35.6	.0	-.01	.80	-.0	1.1	3887	2145	65	36	16:45	131
94	40.3	.0	35.0	.0	-.07	-.19	-.1	.7	2848	733	47	12	16:47	131
95	41.1	.0	34.4	.0	-.25	-.76	.5	.7	3653	1349	61	22	16:51	131
96	41.9	.0	33.9	.0	-.37	-.61	1.0	1.2	3486	1770	58	29	16:53	131
97	42.5	.0	34.1	.0	-.59	-.58	1.7	1.2	3616	2027	60	34	16:55	131
98	43.2	.0	34.0	.0	-.73	-.54	2.1	.7	3677	1701	61	29	16:57	131
99	43.8	.0	33.8	.0	-.78	-.60	1.2	.6	3714	1883	62	31	16:58	131
100	44.7	.0	34.0	.0	-.81	-.67	1.3	.8	3650	1939	61	32	17: 0	131
101	46.3	.0	34.4	.0	-.72	-.62	1.5	1.0	3672	2020	61	34	17: 2	131
102	47.7	.0	34.7	.0	-.62	-.33	1.3	.3	3532	1930	59	32	17: 4	131
103	48.8	.0	34.0	.1	-.64	-.61	1.5	.3	3651	1181	61	20	17: 6	131
104	40.1	.0	35.9	.0	-.16	.12	.3	.5	3827	2164	64	36	17:14	131
105	40.6	.0	35.8	.0	-.11	.30	.2	.5	3868	2261	64	33	17:15	131
106	41.4	.0	35.9	.0	-.21	-.22	.6	.8	3635	2562	61	43	17:17	131
107	42.5	.0	35.5	.0	.00	.02	.2	1.2	3879	1702	65	28	17:19	131
108	42.9	.0	35.6	.0	.00	.21	.7	.6	3832	2013	64	34	17:20	131
109	43.6	.0	36.0	.0	-.01	-.02	.3	.5	3929	3046	152	51	17:22	131
110	44.2	.0	36.4	.0	-.09	-.26	.5	.5	4015	2955	149	49	17:24	131
111	45.0	.0	36.7	.0	.09	-.22	.1	1.5	4029	3250	164	54	17:26	131
112	46.1	.0	37.1	.0	.22	-.37	.1	.8	3789	2634	63	44	17:28	131
113	38.8	.0	37.4	.0	-.04	.19	.5	.7	3937	3866	112	64	9: 6	132
114	39.3	.0	37.6	.0	.08	.25	.5	.7	3960	3864	125	64	9: 8	132
115	39.8	.0	38.0	.0	.07	.14	.0	.3	4012	3883	130	65	9:10	132
116	40.2	.0	38.7	.0	.24	.34	.3	2.4	3999	3928	135	176	9:12	132
117	40.5	.0	39.1	.0	.21	-.02	.4	2.1	3994	3955	117	158	9:14	132
118	40.7	.0	39.4	.0	.34	.10	.3	2.7	2810	3864	47	64	9:16	132
119	41.1	.0	39.8	.0	.37	.30	2.2	3.0	1726	2753	29	46	9:18	132
120	41.0	.0	40.1	.0	.52	.92	.7	2.1	2596	2268	43	38	9:23	132

Table 4-A. - Concluded.

Run	U_{L_e} m/sec	$\pm U_{L_e}$ m/sec	V_{L_e} m/sec	$\pm V_{L_e}$ m/sec	S_{R_u}	S_{R_v}	E_u	E_v	N_u	N_v	DR_u sec^{-1}	DR_v sec^{-1}	Time	Julian day
121	41.6	.0	42.8	.0	.61	-.06	.7	.5	2906	857	48	14	9:27	132
122	42.7	.1	43.3	.1	.03	-.49	.3	1.1	117	248	2	4	9:26	132
123	36.1	.0	37.9	.0	.04	-.02	-.2	-.1	4050	3923	170	306	9:30	132
124	38.3	.0	38.6	.0	.02	-.26	-.2	.2	4067	4026	178	294	9:32	132
125	38.5	.0	39.2	.0	-.04	-.29	-.3	.2	4050	4026	170	356	9:34	132
126	38.5	.0	39.3	.0	.03	-.24	-.3	.2	4047	4019	180	349	9:36	132
127	38.5	.0	39.7	.0	.15	-.16	-.2	.5	4029	4027	119	299	9:37	132
128	38.7	.0	40.2	.0	.30	.13	.3	1.0	3678	3992	61	211	9:39	132
129	39.0	.0	40.5	.0	.21	.38	1.4	.7	1446	3849	24	64	9:41	132
130	39.9	.1	40.8	.1	.45	.26	-.3	.0	693	663	12	11	9:45	132
131	40.7	.2	41.1	.1	-.43	-.07	.2	.1	51	110	1	2	9:43	132
132	37.0	.0	38.8	.0	.61	-.32	1.2	.2	2355	3966	39	141	9:48	132
133	36.9	.0	39.0	.0	.35	-.29	.5	-.1	2711	3977	45	143	9:49	132
134	36.9	.0	39.5	.0	.37	-.80	.6	1.4	3365	3957	56	212	9:51	132
135	37.0	.0	39.6	.0	.56	-.70	.2	.6	2229	3902	37	94	9:53	132
136	36.9	.0	39.7	.0	.87	-.57	.7	.2	2278	3731	38	62	9:55	132
137	37.2	.0	40.1	.0	1.04	-1.13	.6	1.4	1341	3238	22	54	9:57	132
138	38.2	.1	40.3	.0	.10	-1.12	-.8	1.5	533	2064	9	34	9:59	132
139	39.7	.2	39.6	.2	.52	-.73	.6	2.2	33	87	1	1	10: 1	132
140	36.3	.1	38.4	.0	.76	-.75	.1	.5	225	1958	4	33	10:25	132
141	36.0	.0	38.9	.0	.58	-.60	.7	1.0	1703	2971	28	50	10:32	132
142	35.6	.0	39.2	.0	.17	-1.01	.4	2.4	1399	2255	23	38	10:34	132
143	35.5	.0	39.7	.0	.42	-.57	1.6	2.0	766	1747	13	29	10:35	132
144	36.0	.0	39.8	.0	1.28	-1.31	1.5	3.3	921	2558	15	43	10:39	132
145	35.7	.0	40.0	.0	1.63	-1.03	2.5	3.5	1026	1948	17	32	10:41	132
146	35.7	.1	40.1	.0	1.57	-1.23	1.8	2.4	790	855	13	14	10:43	132
147	39.6	.1	40.1	.0	-.27	-.29	-.5	2.3	237	2160	4	36	10:46	132
148	39.4	.1	39.6	.1	-.22	-.18	-.7	1.4	96	292	2	5	10:44	132

Table 4-B ($\alpha = 0.6^0$)

Run	$\frac{x_c}{c}$	$\frac{y_c}{c}$	σ_u m/sec	$\pm\sigma_u$ m/sec	σ_v m/sec	$\pm\sigma_v$ m/sec	$\frac{U_{f_e}}{U_T}$	$\frac{V_{f_e}}{U_T}$	$\frac{U_{R_e}}{U_T}$	α_{R_e} deg
1	-.173	.315	.8	.0	.6	.0	.97	.04	.97	2.1
2	-.171	.250	1.0	.0	.6	.0	.96	.04	.96	2.4
3	-.173	.230	.9	.1	.6	.0	.96	.04	.96	2.3
4	-.173	.211	.8	.0	.7	.0	.96	.04	.95	2.5
5	-.172	.190	.7	.0	.6	.0	.95	.04	.95	2.6
6	-.173	.170	.7	.0	.6	.0	.94	.05	.94	2.8
7	-.171	.151	.8	.0	.7	.0	.95	.04	.95	2.6
8	-.172	.130	.8	.0	.7	.0	.94	.04	.94	2.7
9	-.172	.110	.8	.0	.8	.0	.93	.04	.93	2.4
10	-.173	.100	.7	.0	.7	.0	.93	.04	.93	2.3
11	-.173	.079	.8	.0	.9	.0	.92	.03	.92	1.8
12	-.171	.059	.7	.0	.9	.0	.92	.03	.92	1.6
13	-.172	.039	.6	.0	1.0	.1	.91	.02	.91	1.2
14	-.172	.021	.7	.0	.8	.1	.91	.01	.91	.8
15	-.172	.001	.7	.0	.8	.1	.91	.00	.91	.3
16	-.172	-.019	.7	.0	.6	.1	.92	-.00	.92	-.3
17	-.093	.319	1.2	.0	1.3	.0	.98	.04	.98	2.5
18	-.090	.279	1.0	.0	.9	.0	.97	.05	.97	3.0
19	-.088	.240	1.0	.0	.6	.0	.97	.06	.97	3.4
20	-.089	.201	1.0	.0	.6	.0	.96	.07	.96	3.9
21	-.089	.181	1.0	.0	.6	.0	.95	.07	.95	4.1
22	-.089	.161	1.0	.0	.6	.0	.94	.07	.94	4.4
23	-.089	.141	1.0	.0	.8	.0	.93	.08	.93	4.6
24	-.089	.121	.9	.0	.7	.0	.91	.08	.92	5.0
25	-.088	.101	1.0	.0	.7	.0	.90	.08	.91	5.0
26	-.088	.082	.9	.0	.6	.0	.89	.08	.89	4.9
27	-.088	.060	.9	.0	.7	.0	.88	.07	.88	4.6
28	-.088	.041	.9	.0	.8	.0	.87	.06	.87	4.0
29	-.087	.031	.8	.0	.9	.0	.86	.05	.86	3.4
30	-.088	.021	.8	.0	.8	.0	.86	.04	.86	2.8
31	-.088	.011	.9	.0	1.0	.0	.86	.03	.86	1.8
32	-.088	.002	.9	.0	.9	.0	.86	.02	.86	1.3
33	-.088	-.002	.9	.0	1.5	.0	.86	.00	.86	.3
34	-.088	-.010	.9	.0	1.3	.0	.86	.00	.86	.2
35	-.088	-.018	1.0	.0	1.1	.0	.86	-.00	.86	-.3
36	-.047	.317	1.0	.0	.8	.0	.99	.05	.99	3.2
37	-.047	.280	.9	.0	.8	.0	.98	.06	.98	3.5
38	-.046	.240	.9	.0	.7	.0	.98	.07	.98	4.0
39	-.045	.201	.9	.0	.6	.0	.97	.08	.97	4.9
40	-.047	.181	1.0	.0	.7	.0	.97	.09	.97	5.4
41	-.046	.160	1.0	.0	.8	.0	.96	.10	.96	5.8
42	-.048	.141	1.1	.0	.8	.0	.94	.10	.95	6.2
43	-.047	.121	1.2	.0	.7	.0	.93	.11	.94	6.6
44	-.047	.101	1.2	.0	.7	.0	.91	.11	.92	6.9
45	-.047	.081	1.1	.0	.7	.0	.89	.11	.90	7.3
46	-.047	.060	1.0	.0	.9	.0	.86	.11	.87	7.5
47	-.047	.041	1.0	.0	1.0	.0	.83	.10	.84	7.0
48	-.047	.031	1.0	.0	1.1	.1	.82	.08	.82	5.5
49	-.045	.021	.9	.0	.9	.1	.81	.07	.81	4.6
50	-.047	.011	1.1	.0	1.0	.1	.81	.06	.81	4.3
51	-.046	.002	1.2	.2	.7	.1	.80	.04	.80	3.1
52	-.047	-.009	1.5	.1	1.3	.1	.84	-.01	.84	-.4
53	-.047	-.018	1.5	.1	1.3	.1	.83	-.01	.83	-.9
54	-.004	.317	1.3	.0	1.2	.0	1.00	.05	1.00	2.8
55	-.006	.279	1.3	.0	1.0	.0	.99	.06	.99	3.5
56	-.006	.241	1.3	.0	1.2	.0	.99	.07	.99	4.1
57	-.005	.201	1.2	.0	1.1	.0	.97	.09	.98	5.2
58	-.006	.181	1.1	.0	.7	.0	.97	.10	.98	6.0
59	-.006	.160	1.2	.0	.8	.0	.97	.11	.97	6.7
60	-.006	.140	1.3	.0	.8	.0	.96	.12	.97	7.4

Table 4-B. - Continued.

Run	$\frac{x_c}{c}$	$\frac{y_c}{c}$	σ_u m/sec	$\pm\sigma_u$ m/sec	σ_v m/sec	$\pm\sigma_v$ m/sec	$\frac{U_{f_e}}{U_T}$	$\frac{V_{f_e}}{U_T}$	$\frac{U_{R_e}}{U_T}$	α_{R_e} deg
61	-.004	.121	1.3	.0	.6	.0	.95	.14	.96	8.5
62	-.005	.101	1.4	.0	.6	.0	.93	.16	.94	9.6
63	-.005	.081	1.6	.0	.7	.0	.90	.18	.91	11.4
64	-.005	.060	1.8	.0	.9	.0	.86	.21	.89	13.4
65	-.006	.050	1.9	.0	1.1	.1	.84	.21	.86	14.4
66	-.004	.041	1.9	.0	2.7	.3	.83	.19	.85	12.9
67	-.006	.031	1.4	.1	3.0	.5	.80	.13	.81	9.5
68	.037	.317	.8	.0	.7	.0	1.02	.06	1.02	3.3
69	.037	.280	.8	.0	.6	.0	1.02	.07	1.02	4.2
70	.036	.241	.9	.0	.6	.0	1.02	.09	1.02	5.0
71	.037	.201	1.1	.0	1.0	.0	1.01	.10	1.01	5.9
72	.038	.181	1.3	.0	1.1	.0	1.00	.11	1.01	6.2
73	.037	.160	1.5	.0	.9	.0	1.00	.12	1.00	7.0
74	.036	.141	1.6	.0	.8	.0	1.00	.14	1.01	7.9
75	.037	.122	1.7	.0	.8	.0	1.00	.16	1.01	9.1
76	.037	.101	1.9	.0	.8	.0	.99	.19	1.01	10.8
77	.037	.081	2.1	.0	1.3	.0	.99	.23	1.02	13.1
78	.037	.059	2.7	.0	1.8	.2	.98	.31	1.03	17.4
79	.078	.318	.9	.0	1.0	.0	1.02	.06	1.02	3.2
80	.078	.278	.9	.0	1.0	.1	1.02	.07	1.03	3.9
81	.078	.240	.9	.0	.7	.0	1.02	.08	1.03	4.7
82	.078	.201	1.1	.0	.6	.0	1.03	.10	1.04	5.7
83	.077	.181	1.0	.0	.7	.0	1.04	.11	1.04	6.2
84	.076	.160	1.1	.0	.8	.0	1.04	.13	1.05	6.9
85	.077	.140	1.2	.0	.8	.0	1.05	.14	1.06	7.7
86	.077	.121	2.1	.0	.9	.0	1.05	.14	1.06	7.8
87	.078	.111	1.5	.0	.7	.0	1.07	.16	1.09	8.6
88	.078	.102	1.6	.0	1.3	.0	1.07	.18	1.08	9.4
89	.073	.091	1.9	.0	1.5	.0	1.07	.19	1.08	10.3
90	.079	.081	2.3	.0	1.4	.0	1.07	.21	1.09	11.1
91	.078	.071	2.3	.0	1.4	.1	1.08	.23	1.11	12.0
92	.078	.060	1.6	.0	1.8	.2	1.11	.26	1.14	13.3
93	.117	.318	.9	.0	1.1	.0	1.04	.05	1.04	2.7
94	.117	.279	.8	.0	.7	.0	1.03	.06	1.04	3.4
95	.119	.240	1.0	.0	1.2	.0	1.04	.08	1.05	4.5
96	.119	.201	1.1	.0	1.2	.0	1.05	.10	1.05	5.4
97	.119	.181	1.2	.0	1.3	.0	1.06	.11	1.06	5.7
98	.119	.160	1.4	.0	1.5	.0	1.06	.11	1.07	6.1
99	.119	.141	1.4	.0	1.6	.0	1.07	.13	1.08	6.7
100	.117	.121	1.5	.0	1.5	.0	1.08	.14	1.09	7.2
101	.118	.101	1.4	.0	1.6	.0	1.11	.15	1.12	7.8
102	.118	.081	1.5	.0	1.5	.0	1.13	.17	1.14	8.4
103	.118	.072	1.4	.0	1.9	.0	1.14	.19	1.16	9.5
104	.160	.318	.8	.0	.7	.0	1.05	.05	1.05	2.5
105	.160	.278	.9	.0	.7	.0	1.05	.05	1.05	3.0
106	.161	.240	.8	.0	.7	.0	1.06	.06	1.07	3.5
107	.160	.201	1.0	.0	.9	.0	1.07	.09	1.08	4.5
108	.161	.180	1.0	.0	.8	.0	1.08	.09	1.08	4.7
109	.160	.160	1.0	.0	.9	.0	1.09	.09	1.10	4.8
110	.160	.141	1.0	.0	.8	.0	1.11	.10	1.11	4.9
111	.160	.121	1.0	.0	.9	.0	1.13	.10	1.13	5.2
112	.160	.101	1.0	.0	1.1	.0	1.14	.11	1.15	5.6
113	.293	.318	.7	.0	.8	.0	1.05	.01	1.05	.5
114	.294	.280	.8	.0	.8	.0	1.07	.01	1.07	.7
115	.294	.241	.7	.0	.7	.0	1.08	.01	1.08	.7
116	.293	.202	.7	.0	.9	.0	1.09	.01	1.09	.5
117	.294	.181	.8	.0	.9	.0	1.10	.01	1.10	.4
118	.294	.161	.8	.0	1.0	.0	1.11	.01	1.11	.3
119	.294	.142	1.0	.0	1.1	.0	1.13	.01	1.13	.3
120	.294	.121	.8	.0	1.2	.0	1.13	.00	1.13	.1

Table 4-B. - Concluded.

Run	$\frac{x_c}{c}$	$\frac{y_c}{c}$	σ_u m/sec	$\pm\sigma_u$ m/sec	σ_v m/sec	$\pm\sigma_v$ m/sec	$\frac{U_{f_e}}{U_T}$	$\frac{V_{f_e}}{U_T}$	$\frac{U_{R_e}}{U_T}$	α_{R_e} deg
121	.293	.107	1.0	.0	1.5	.0	1.17	-.03	1.17	-1.4
122	.295	.102	1.4	.1	1.4	.1	1.19	-.02	1.19	-1.0
123	.409	.319	.6	.0	.6	.0	1.05	-.01	1.05	-.5
124	.410	.280	.6	.0	.7	.0	1.06	-.02	1.06	-.9
125	.410	.240	.6	.0	.7	.0	1.07	-.02	1.07	-1.1
126	.410	.201	.6	.0	.7	.0	1.07	-.02	1.07	-1.2
127	.411	.180	.7	.0	.7	.0	1.08	-.03	1.08	-1.5
128	.411	.161	.7	.0	.8	.0	1.08	-.03	1.09	-1.7
129	.413	.141	.8	.0	.8	.0	1.09	-.03	1.09	-1.6
130	.411	.128	1.4	.0	1.4	.0	1.11	-.02	1.11	-1.2
131	.412	.121	1.3	.1	1.2	.1	1.13	-.02	1.13	-.9
132	.578	.318	.8	.0	.8	.0	1.04	-.03	1.04	-1.9
133	.578	.280	.7	.0	.9	.0	1.05	-.04	1.05	-2.1
134	.578	.241	.8	.0	.8	.0	1.06	-.05	1.06	-2.6
135	.578	.201	1.0	.0	1.0	.0	1.06	-.05	1.06	-2.6
136	.578	.180	1.0	.0	1.1	.0	1.06	-.05	1.06	-2.7
137	.578	.161	1.3	.0	1.1	.0	1.07	-.05	1.07	-2.7
138	.577	.140	1.7	.0	1.1	.0	1.08	-.04	1.08	-2.2
139	.578	.127	1.2	.2	1.6	.2	1.09	-.01	1.09	-.5
140	.701	.317	1.0	.0	1.0	.0	1.03	-.04	1.03	-2.2
141	.702	.279	.8	.0	.9	.0	1.03	-.05	1.03	-2.9
142	.702	.240	.7	.0	.8	.0	1.03	-.06	1.04	-3.4
143	.703	.202	.7	.0	.6	.0	1.04	-.07	1.04	-3.8
144	.702	.181	1.4	.0	.9	.0	1.04	-.06	1.04	-3.4
145	.703	.161	1.5	.0	1.0	.0	1.04	-.07	1.04	-3.8
146	.703	.140	1.7	.1	1.3	.0	1.04	-.07	1.04	-3.9
147	.701	.127	1.5	.1	.7	.0	1.09	-.02	1.09	-1.0
148	.703	.121	1.4	.1	1.1	.1	1.09	-.01	1.09	-.8

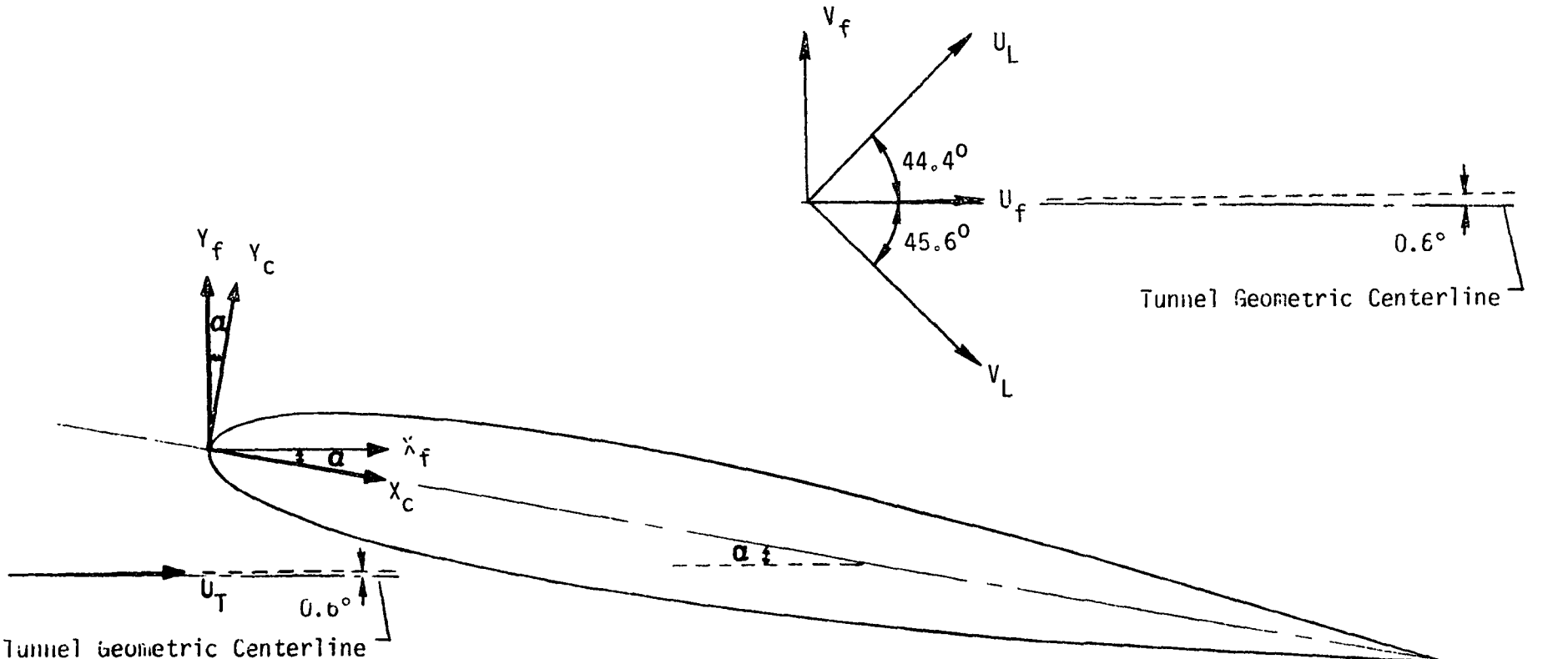

Figure 1. - Sketch of axis system used including directions of velocity components computed.

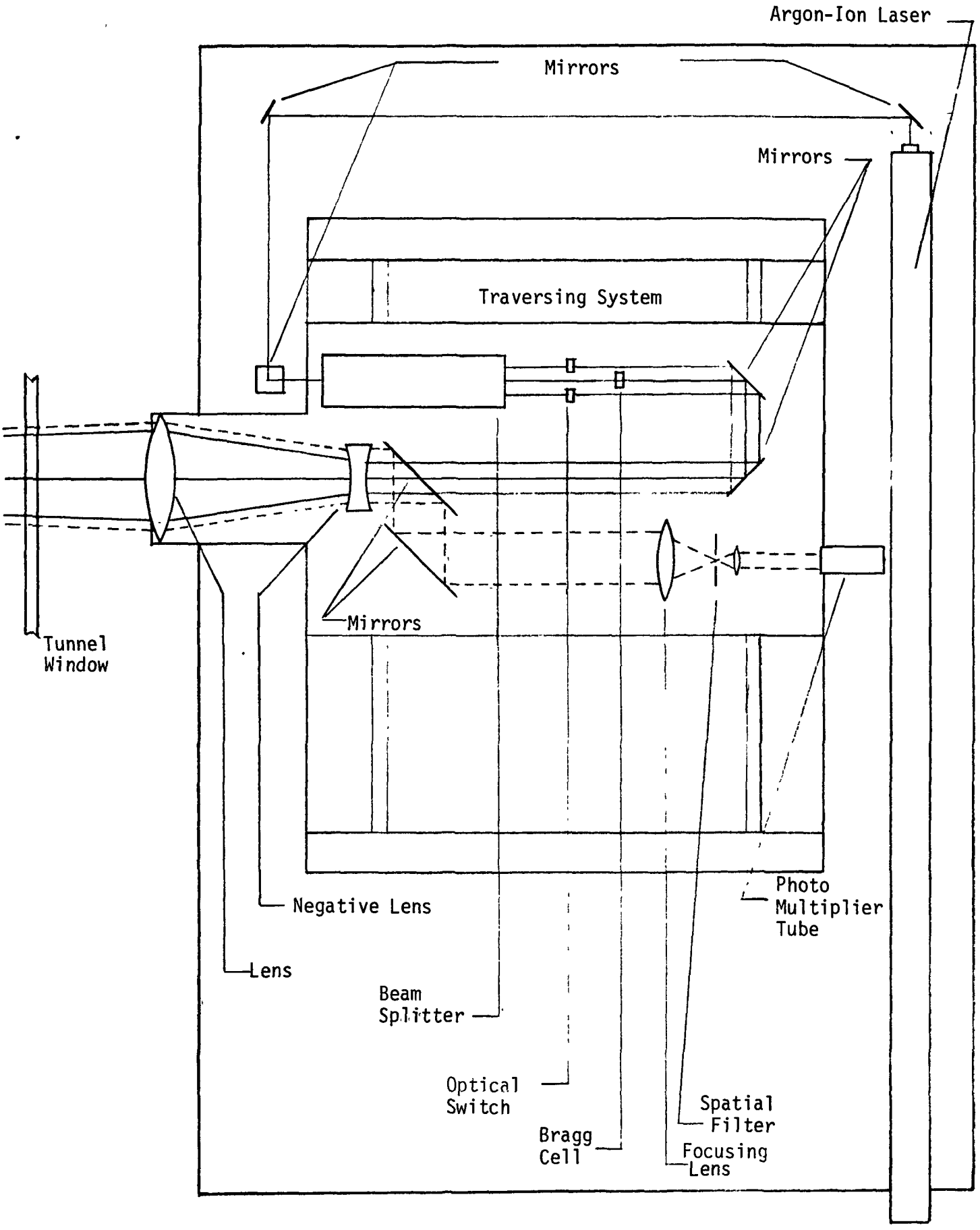

Figure 2.- Schematic of the laser velocimeter optics..

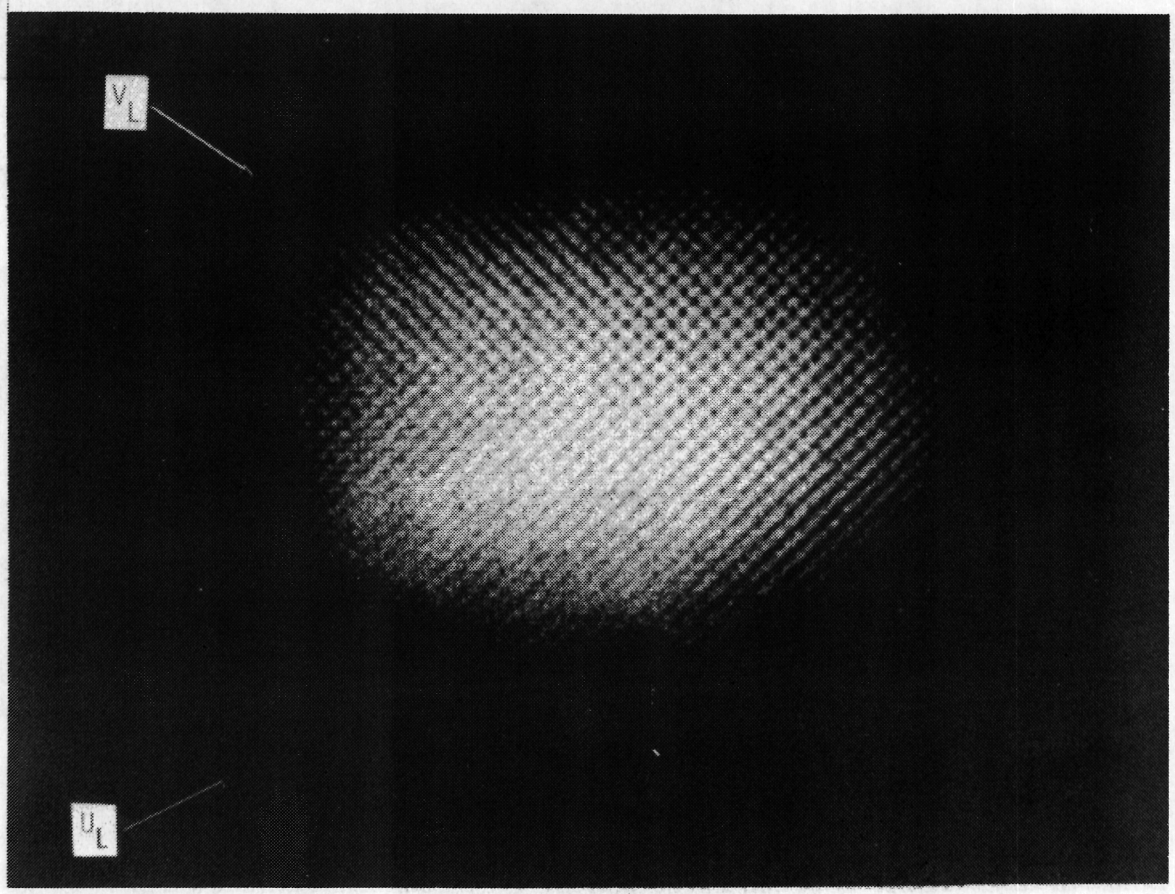

Figure 3. - Two-velocity-component fringes in the sample volume.

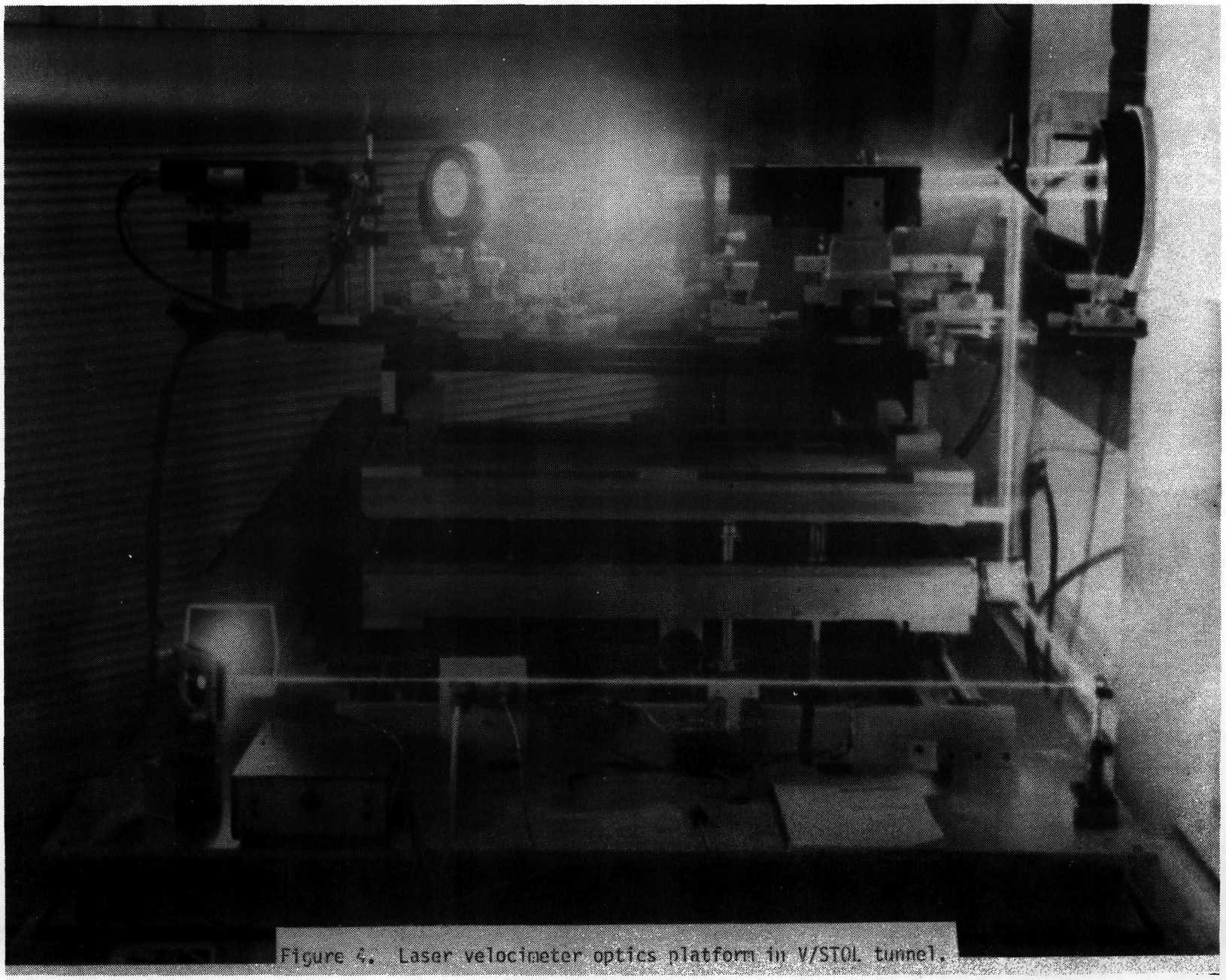

Figure 4. Laser velocimeter optics platform in V/STOL tunnel.

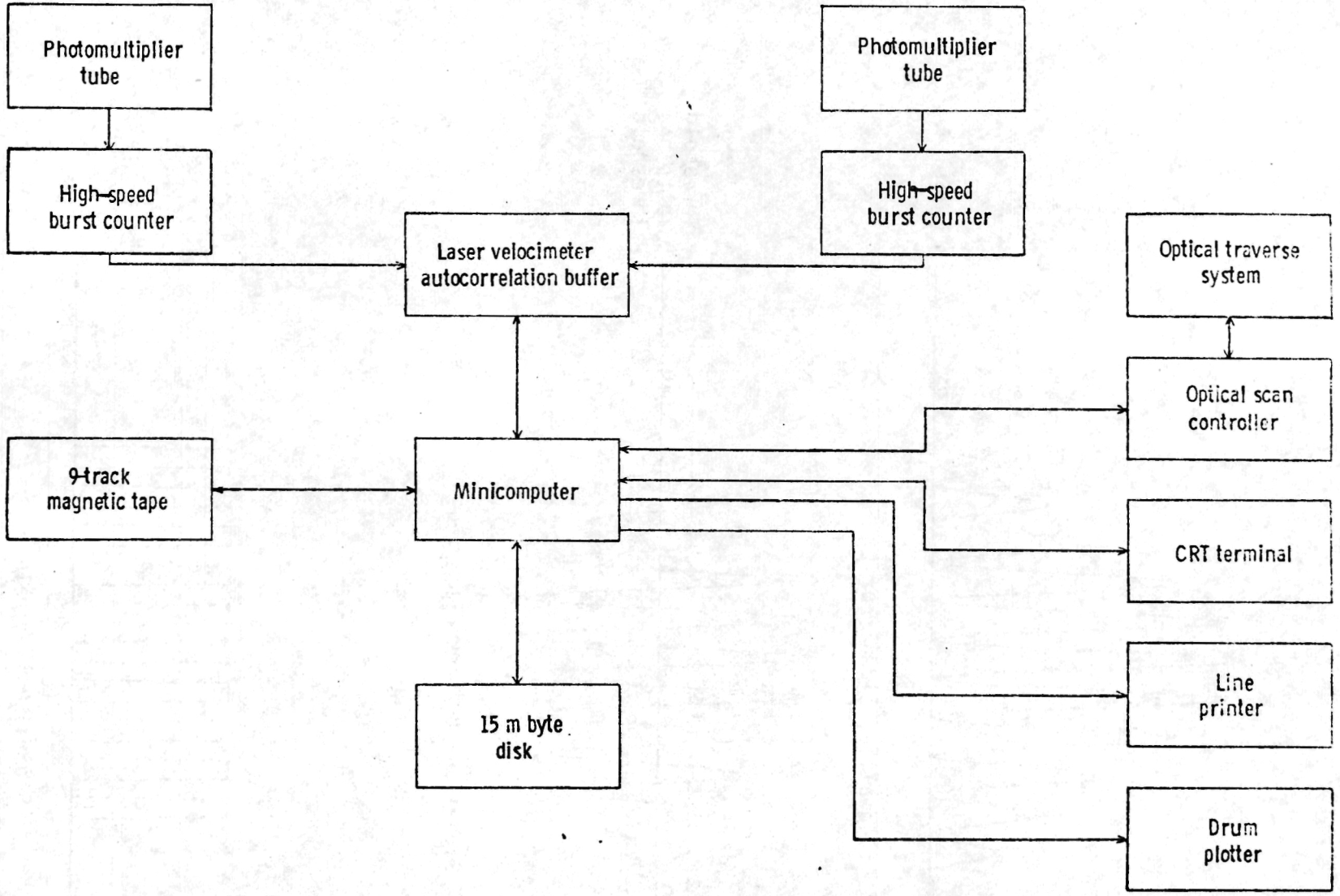

Figure 5.- Block diagram of the laser velocimeter data acquisition system.

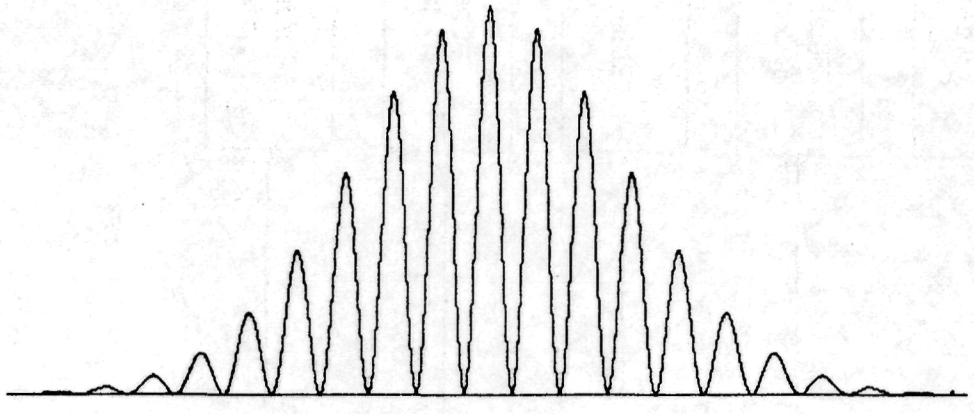

(a)
Idealized Signal Burst

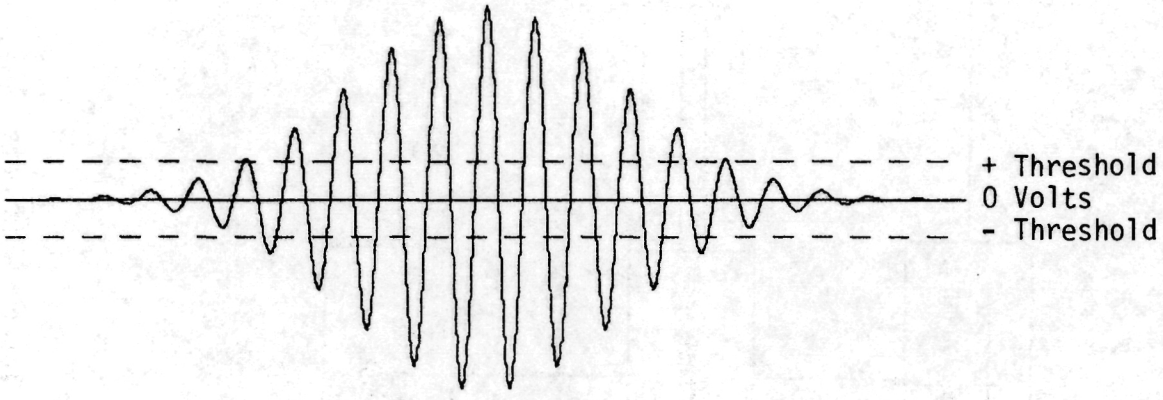

(b)
Signal Burst After Filtering

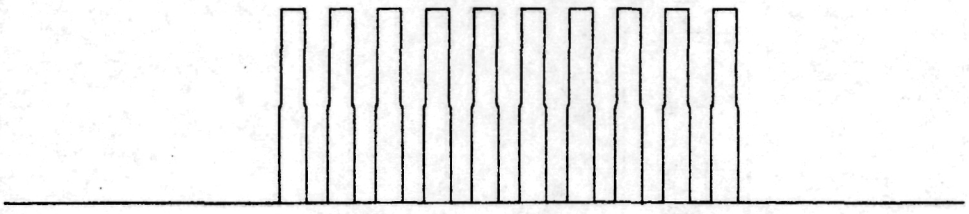

(c)
Digital Pulse Train

Figure 6. - Processing of burst received from laser velocimeter.

Figure 7. - Straight wing with NACA 0012 airfoil sections installed in the 4- by 7-meter low-speed (V/STOL) tunnel.

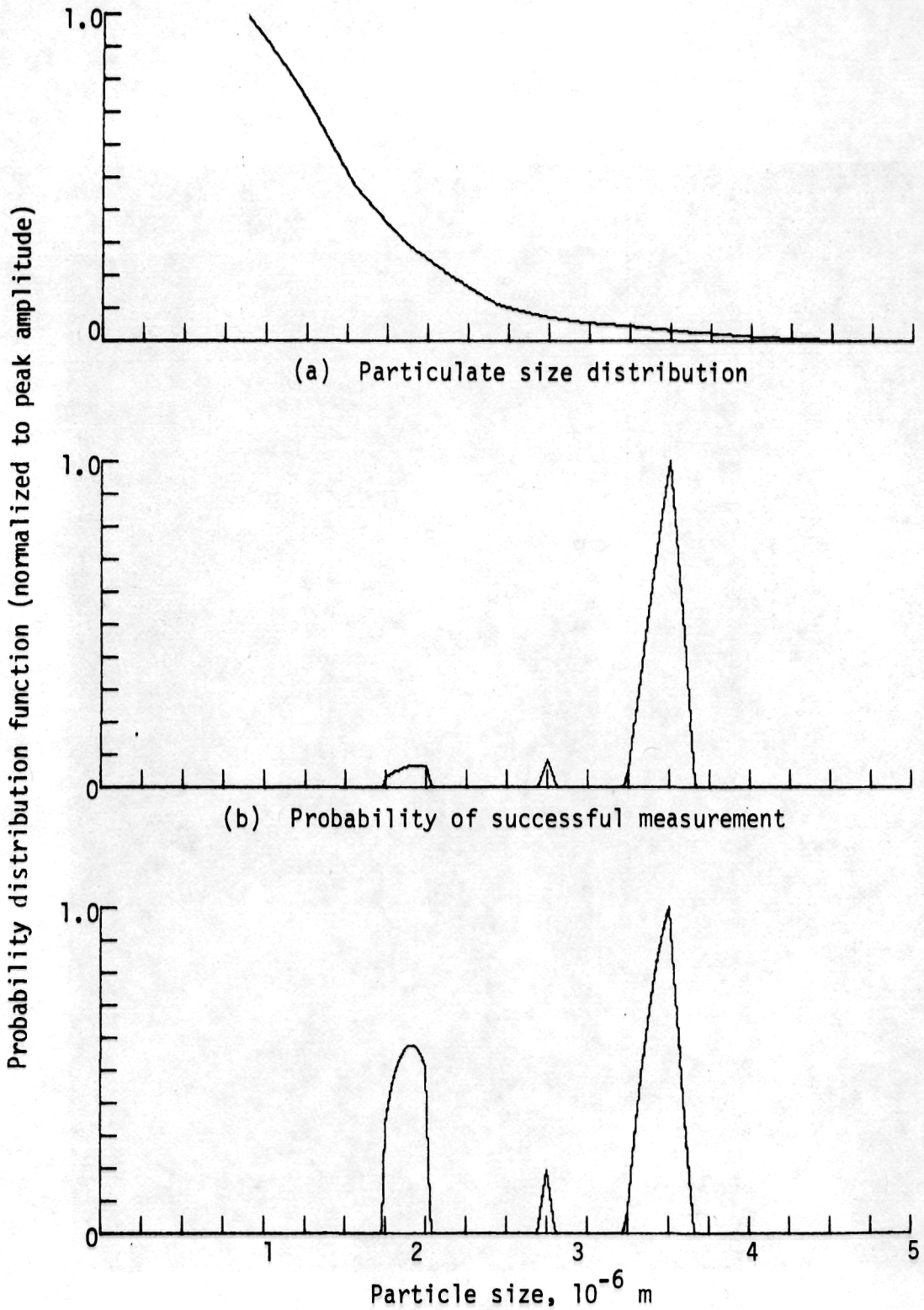

Figure 8. - Particle size distribution measured by the laser velocimeter.

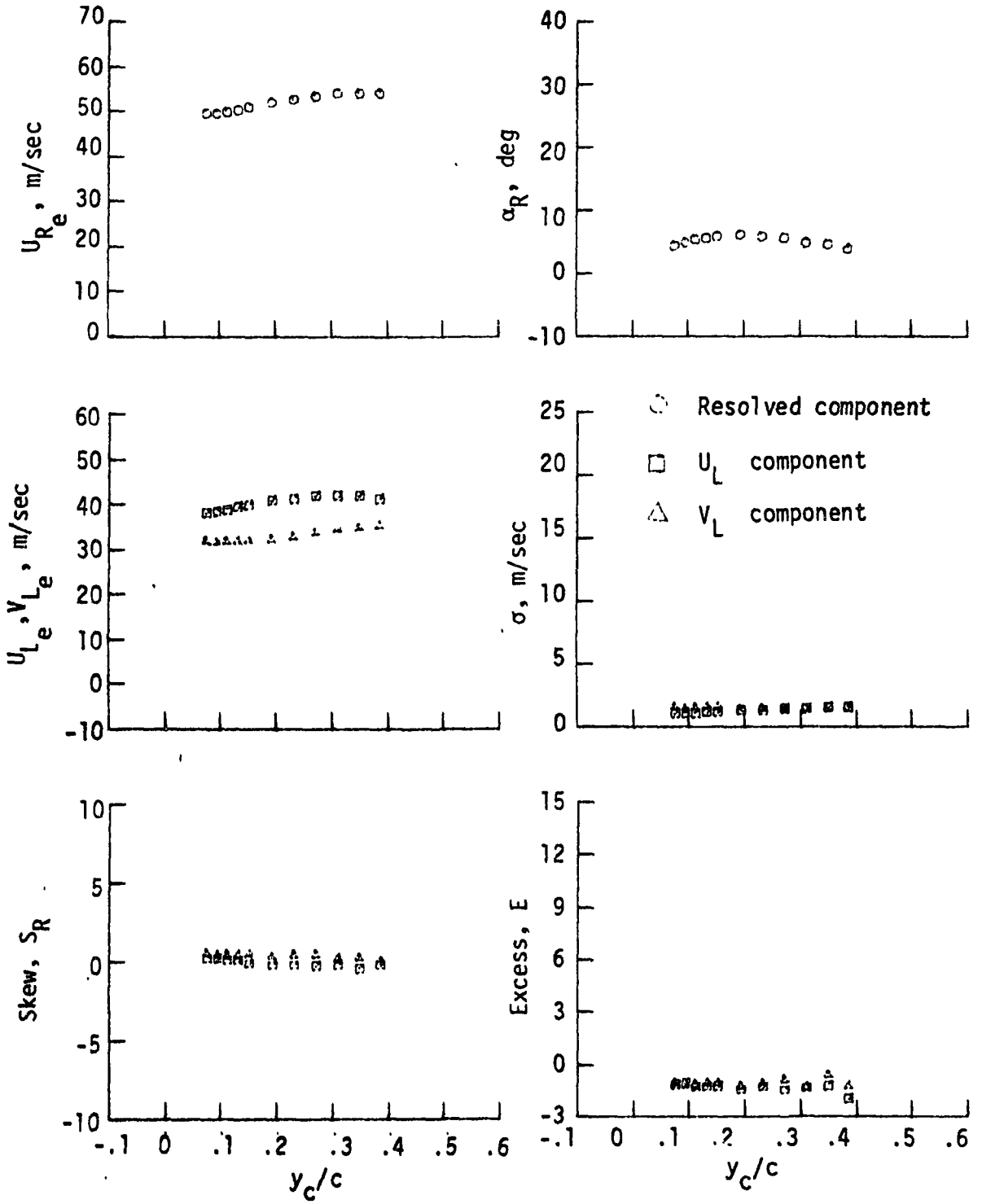

Figure 9. Statistical characteristics of the LV measured velocities at constant $x_c/c = -.16$. $\alpha = 4.75°$.

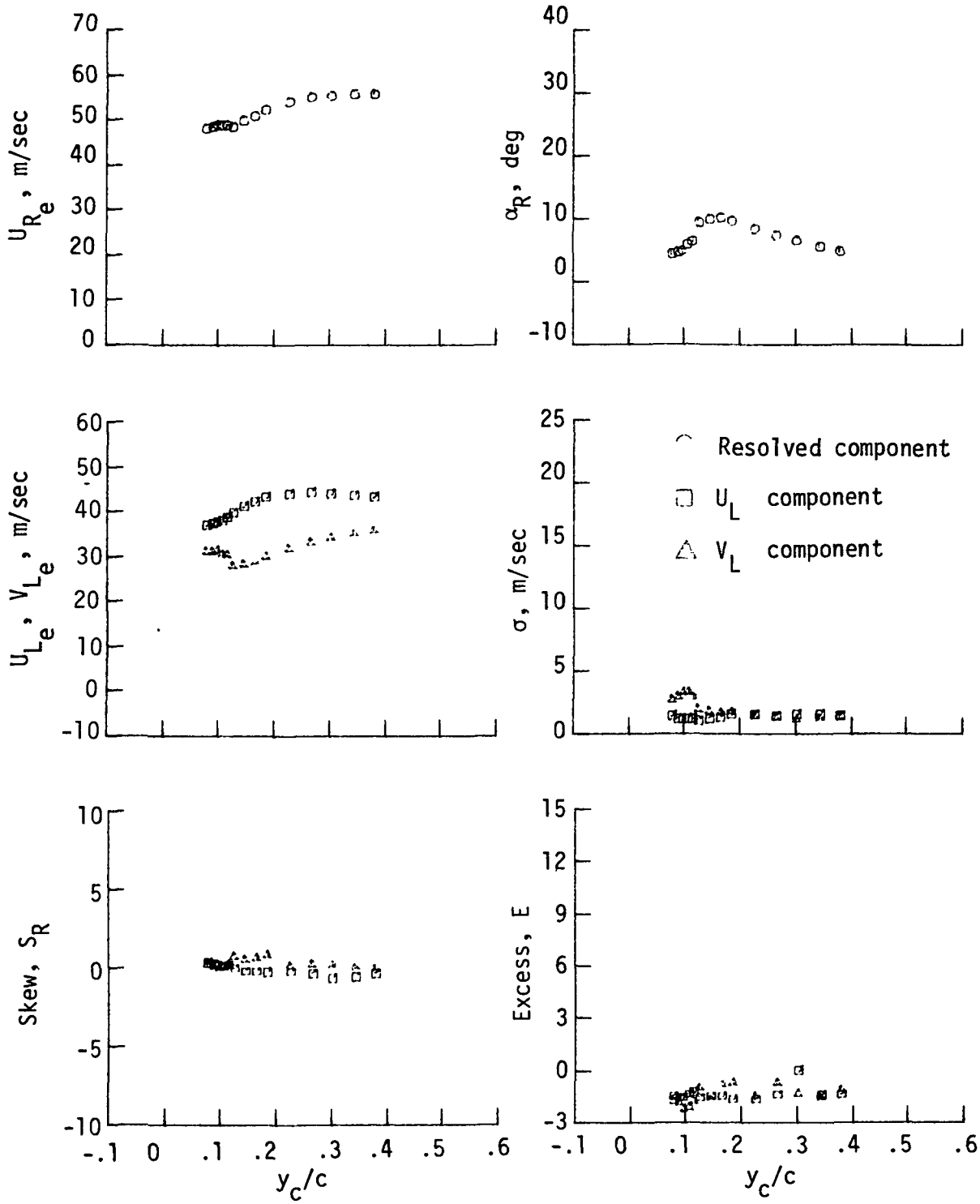

Figure 10. Statistical characteristics of the LV measured velocities at constant x_c/c = -.08. α = 4.75°.

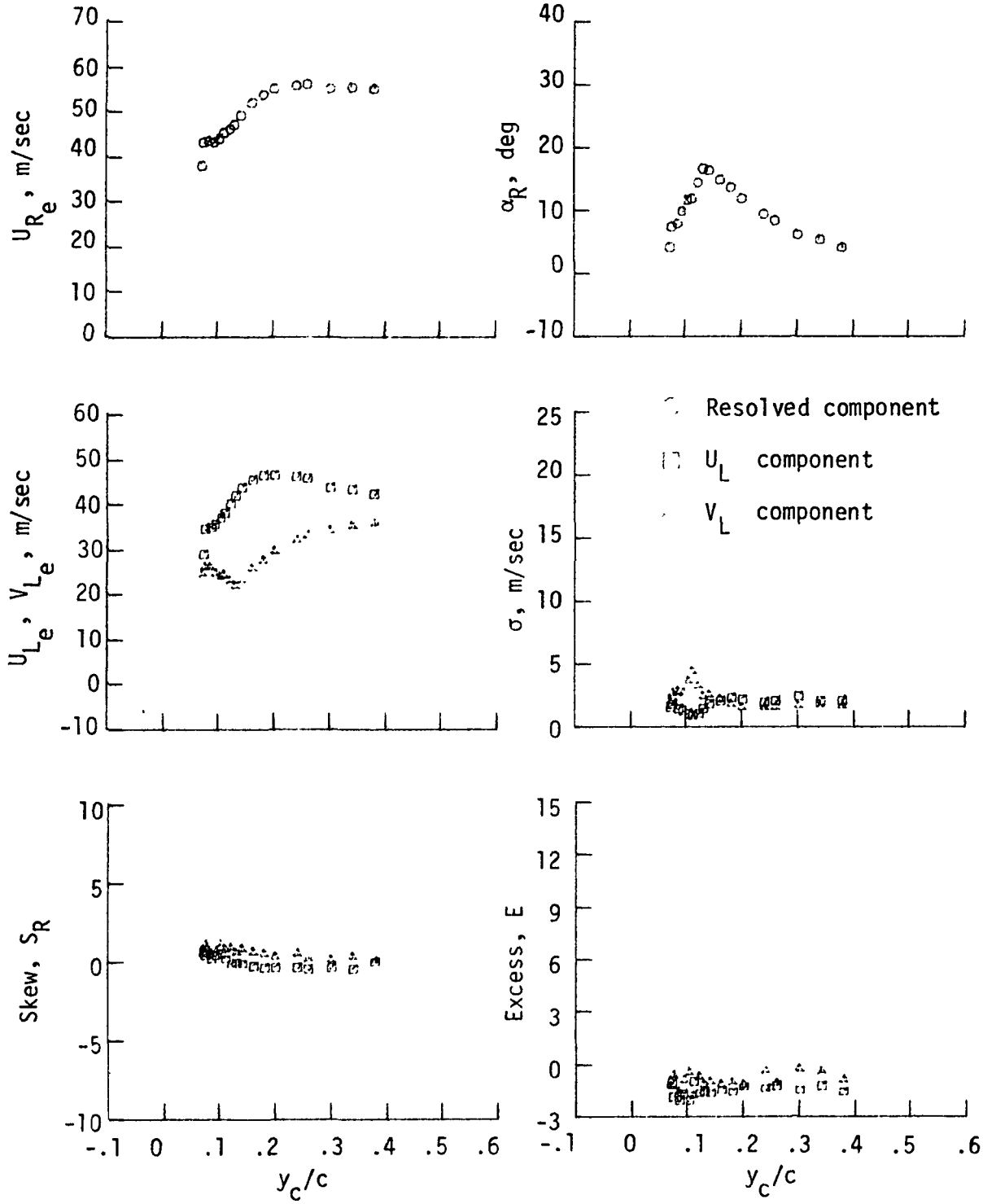

Figure 11. Statistical characteristics of the LV measured velocities at constant x_c/c = -.04. α = 4.75°.

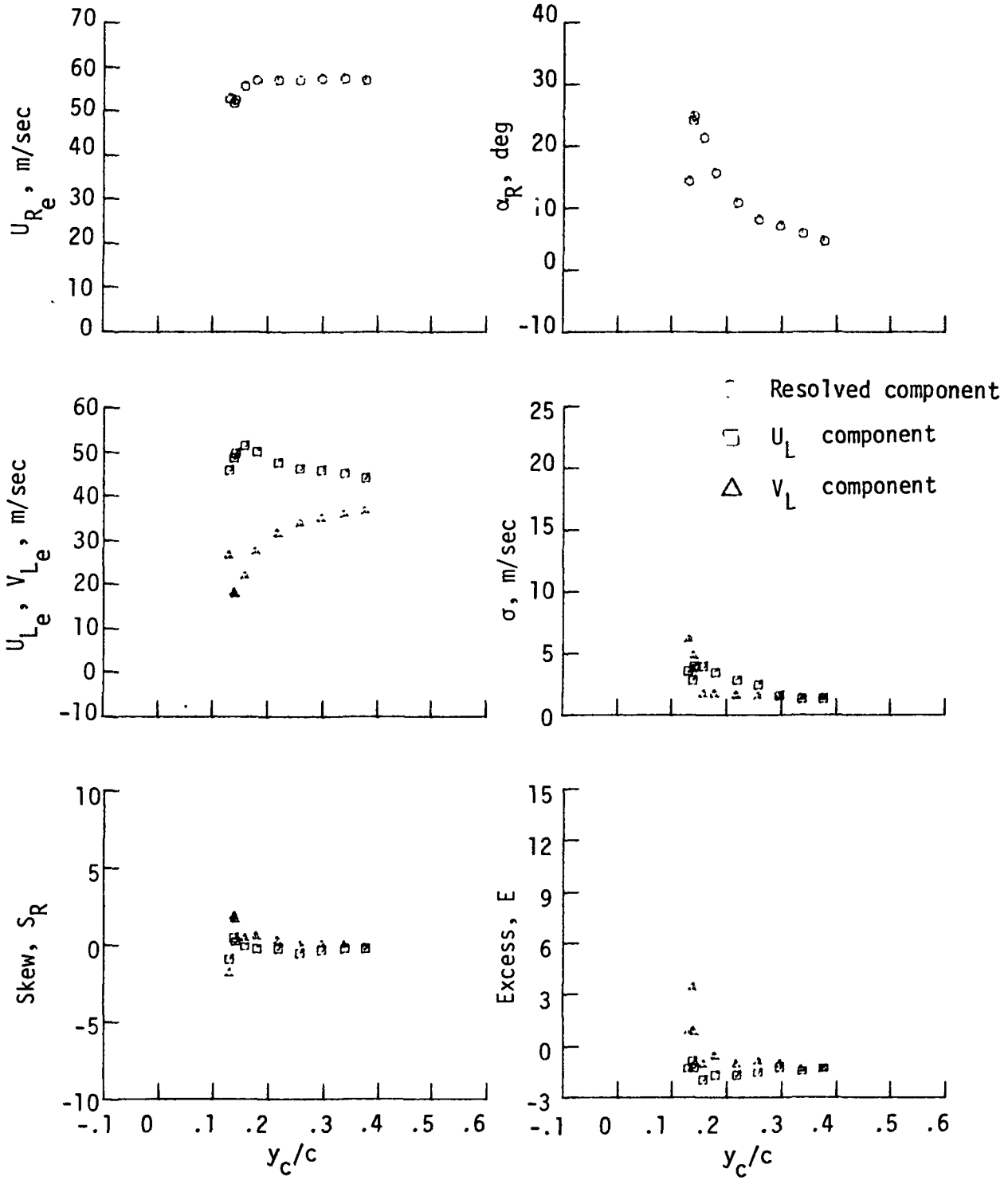

Figure 12. Statistical characteristics of the LV measured velocities at constant $x_c/c = .02$. $\alpha = 4.75°$.

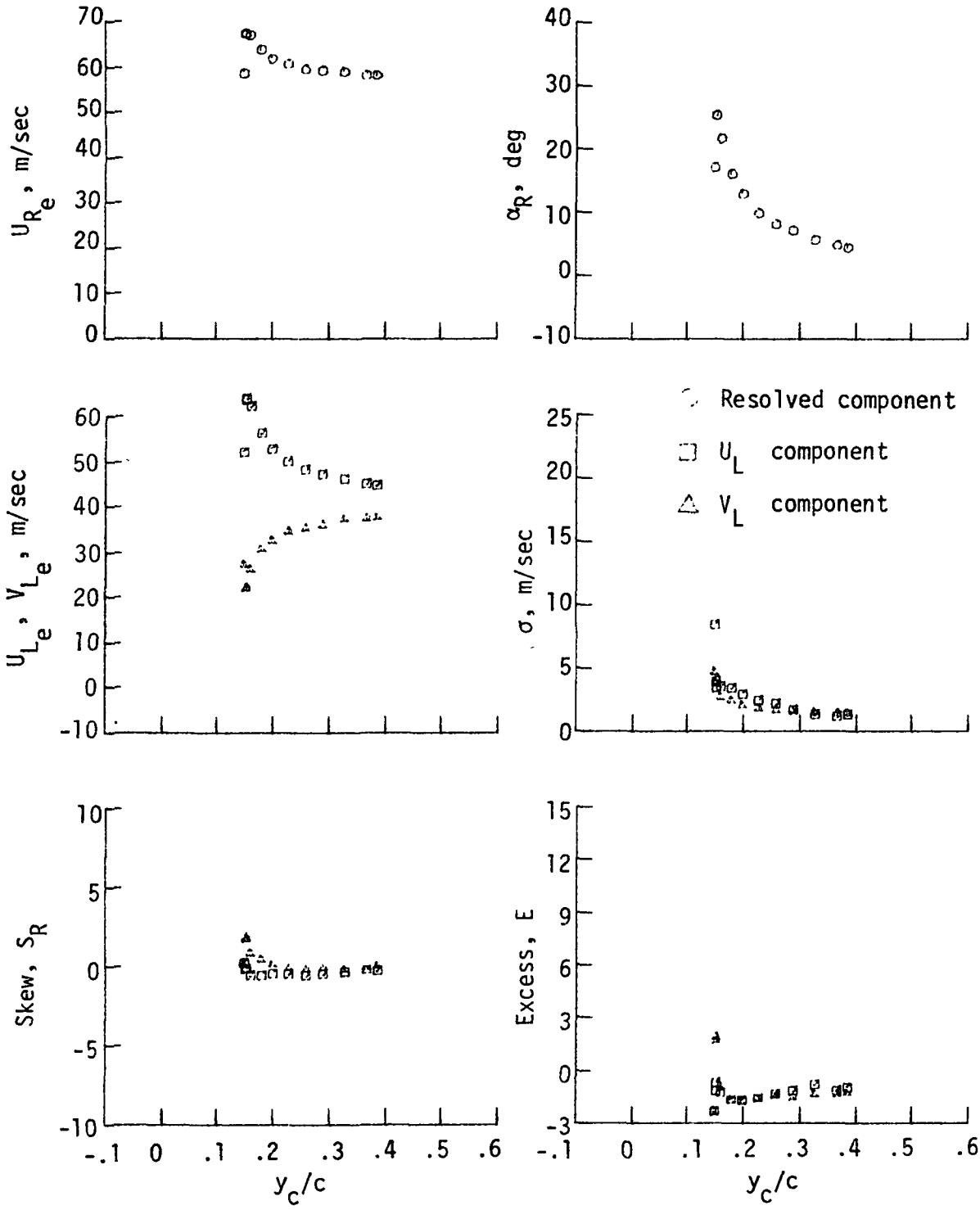

Figure 13. Statistical characteristics of the LV measured velocities at constant $x_c/c = .03$. $\alpha = 4.75°$.

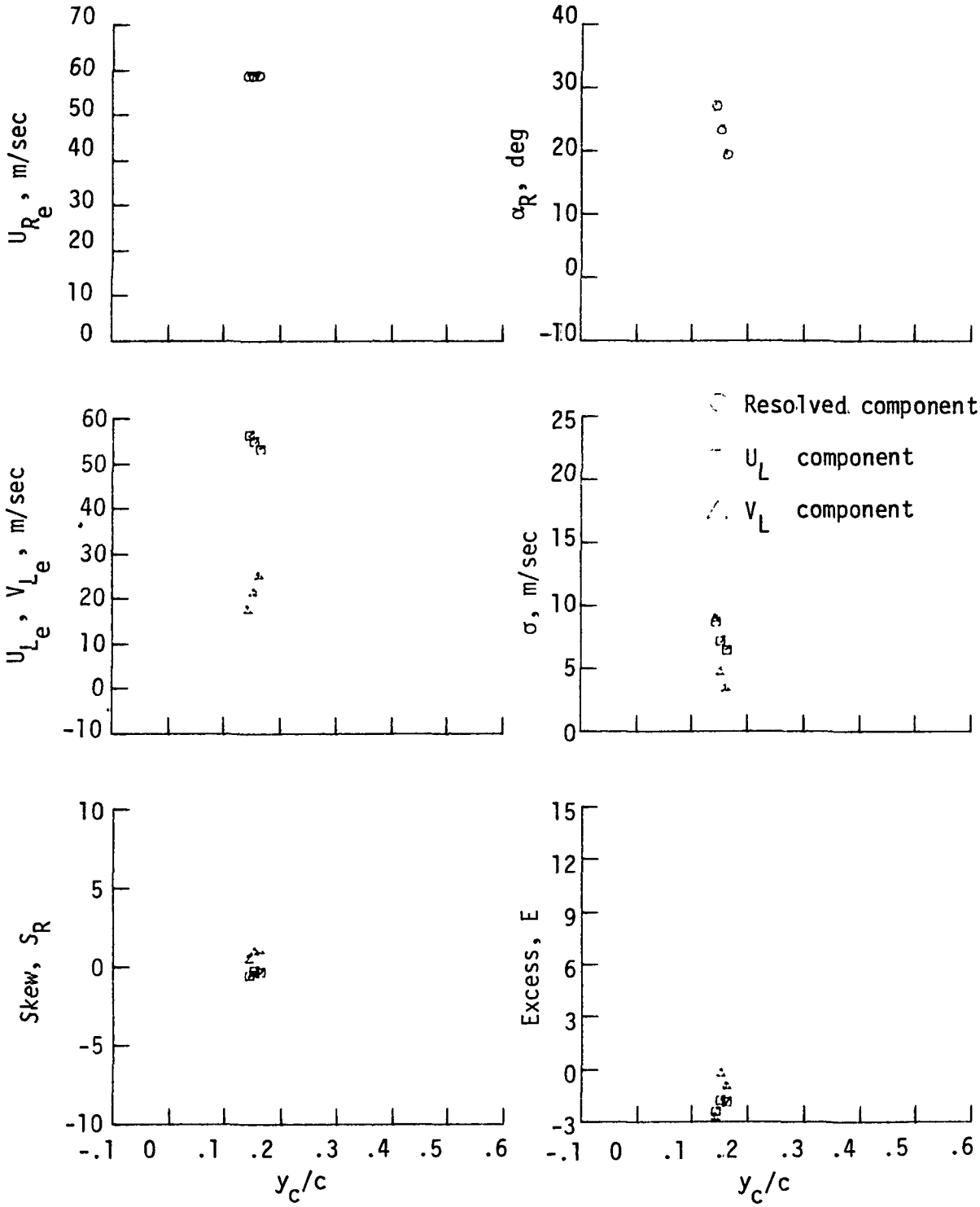

Figure 14. Statistical characteristics of the LV measured velocities at constant $x_c/c = .04$. $\alpha = 4.75°$.

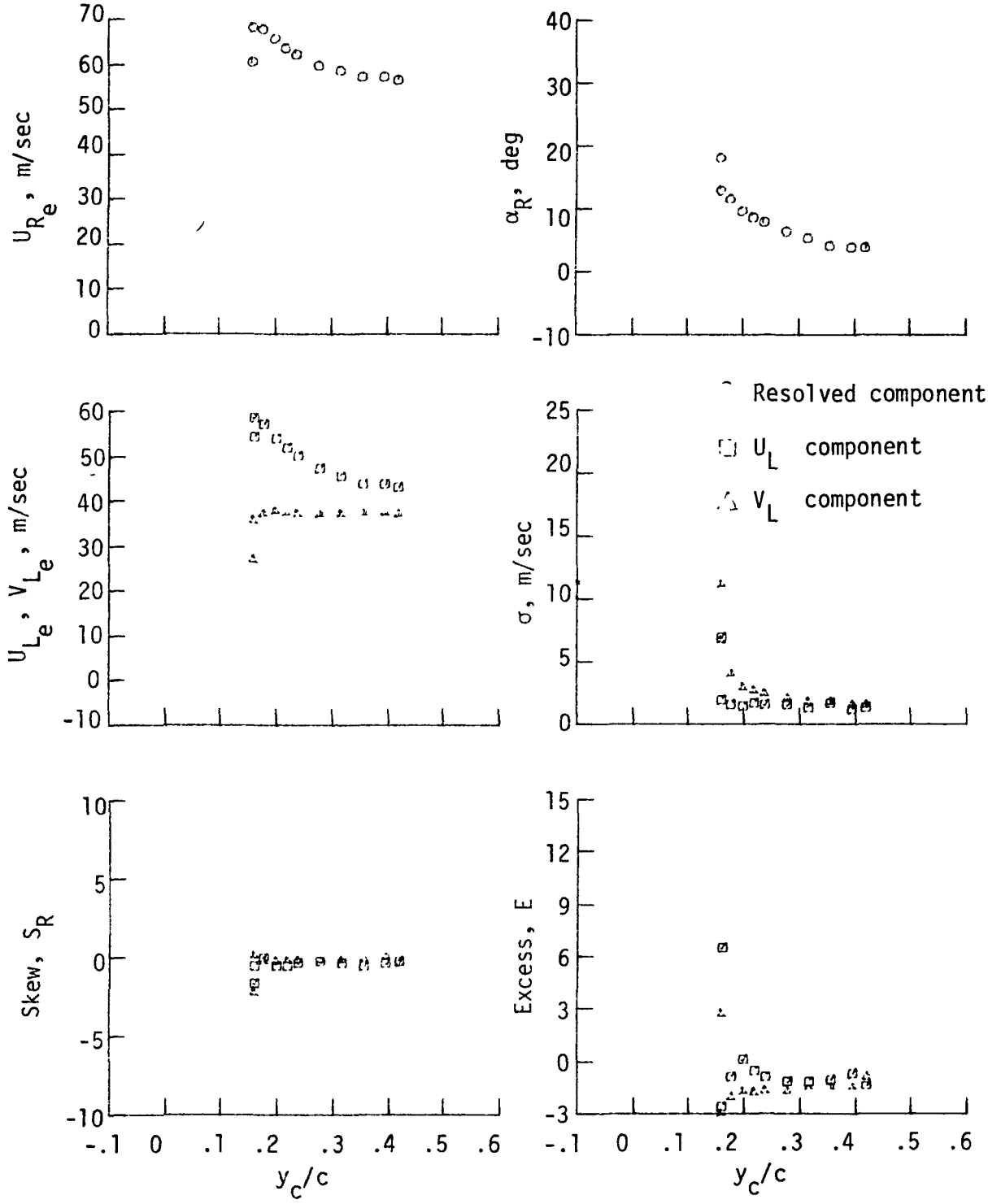

Figure 15. Statistical characteristics of the LV measured velocities at constant $x_c/c = .06$. $\alpha = 4.75$

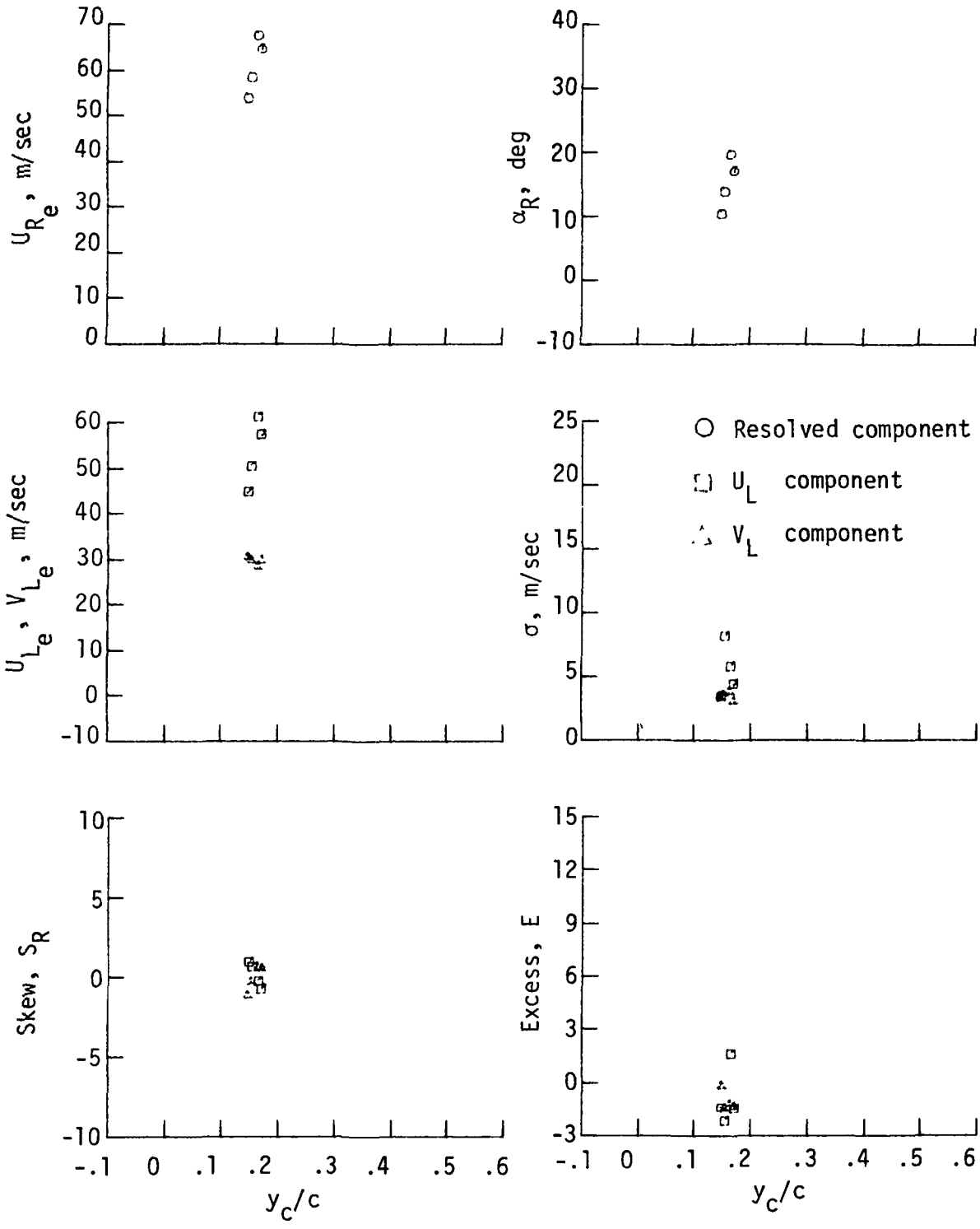

Figure 16. Statistical characteristics of the LV measured velocities at constant x_c/c = .09. α = 4.75°.

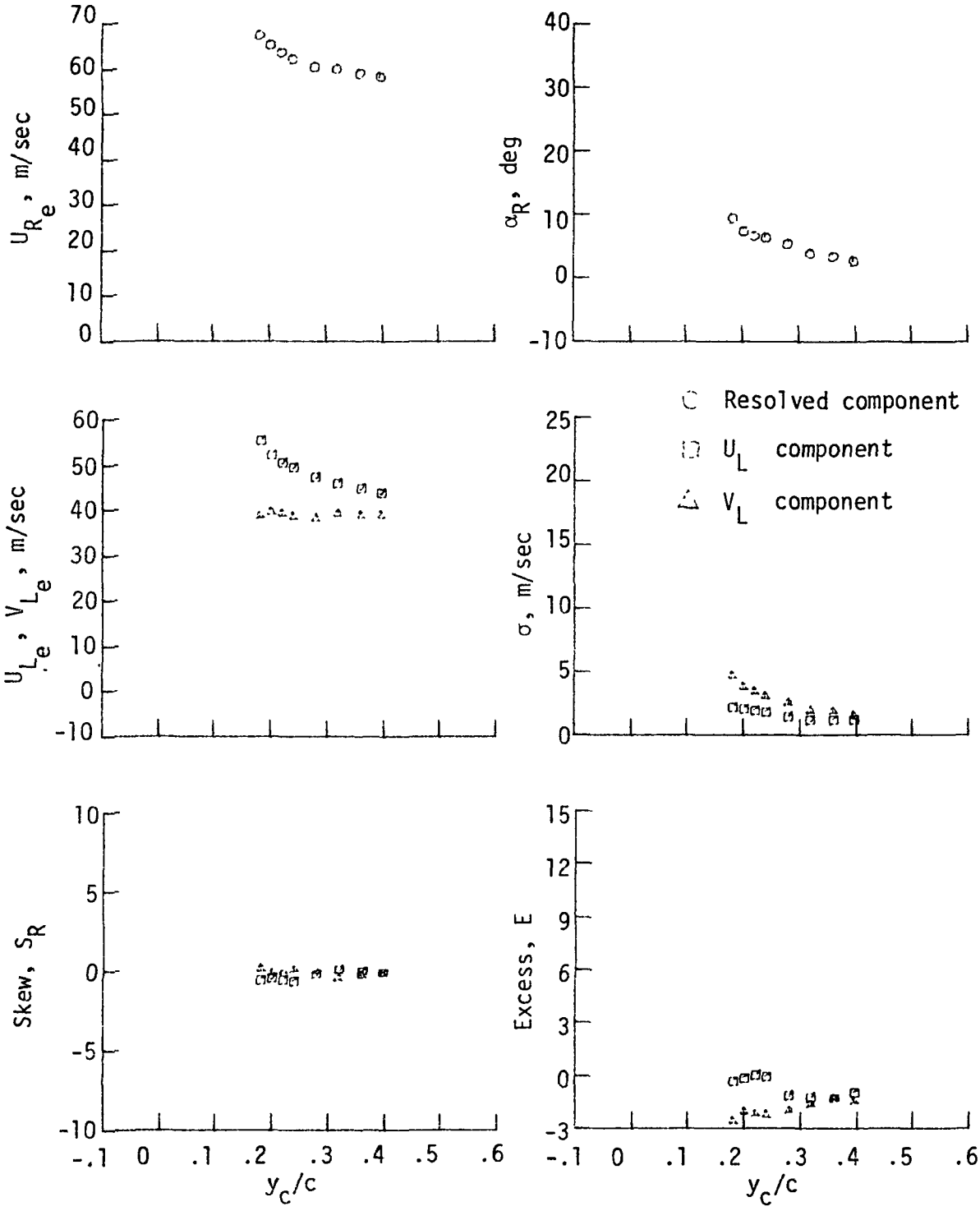

Figure 17. Statistical characteristics of the LV measured velocities at constant $x_c/c = .13$. $\alpha = 4.75°$.

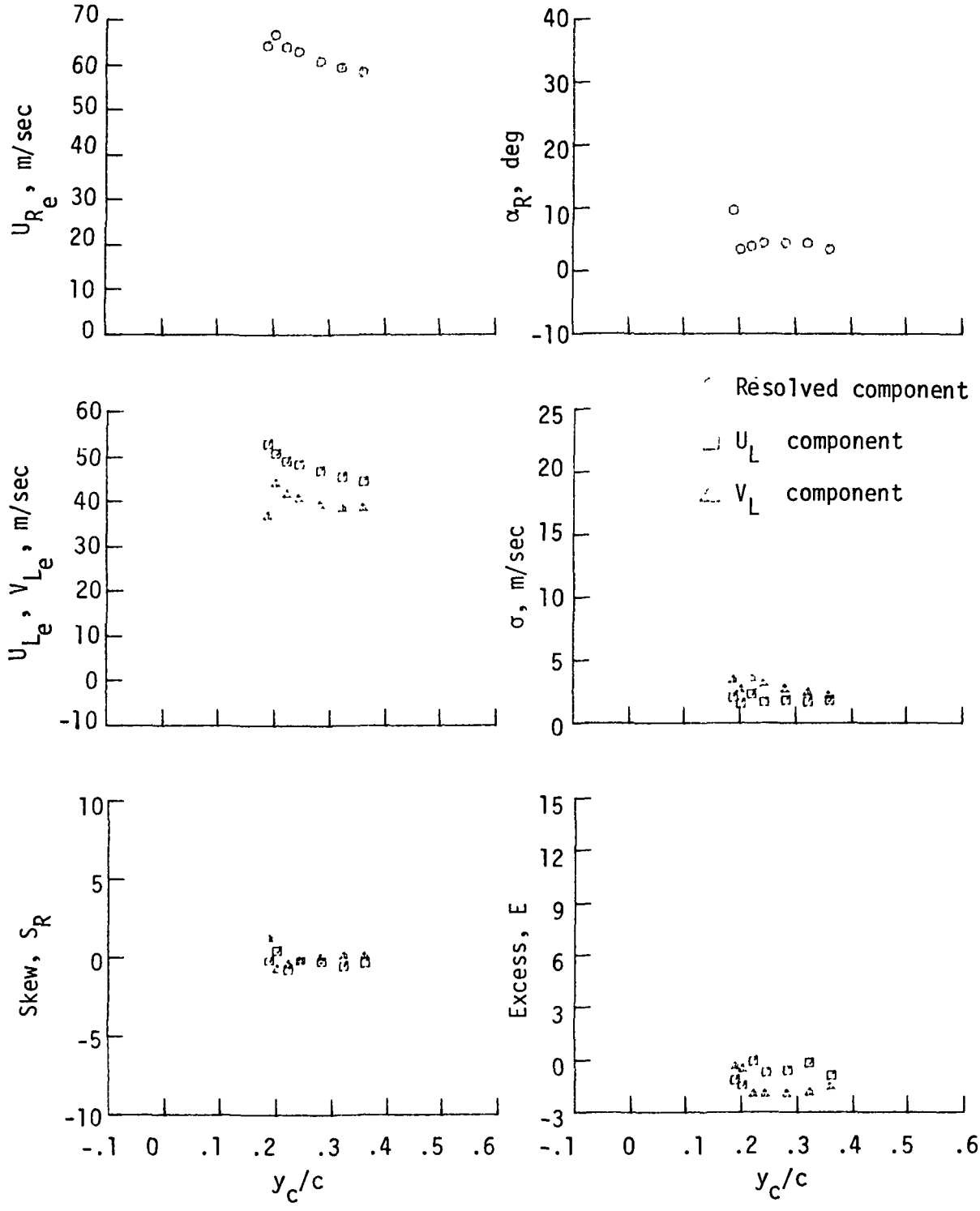

Figure 18. Statistical characteristics of the LV measured velocities at constant $x_c/c = .17$. $\alpha = 4.75°$.

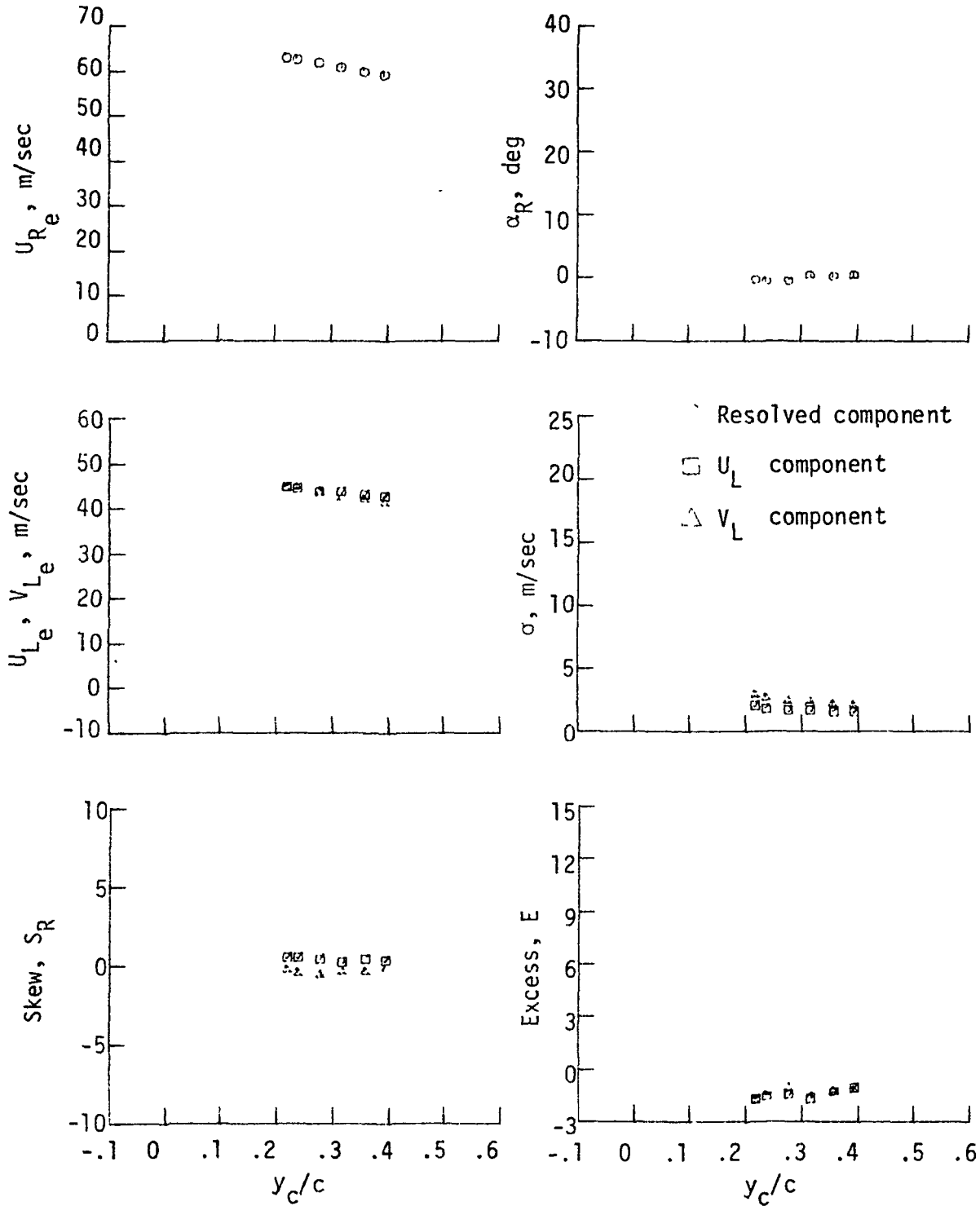

Figure 19. Statistical characteristics of the LV measured velocities at constant $x_c/c = .29$. $\alpha = 4.75°$.

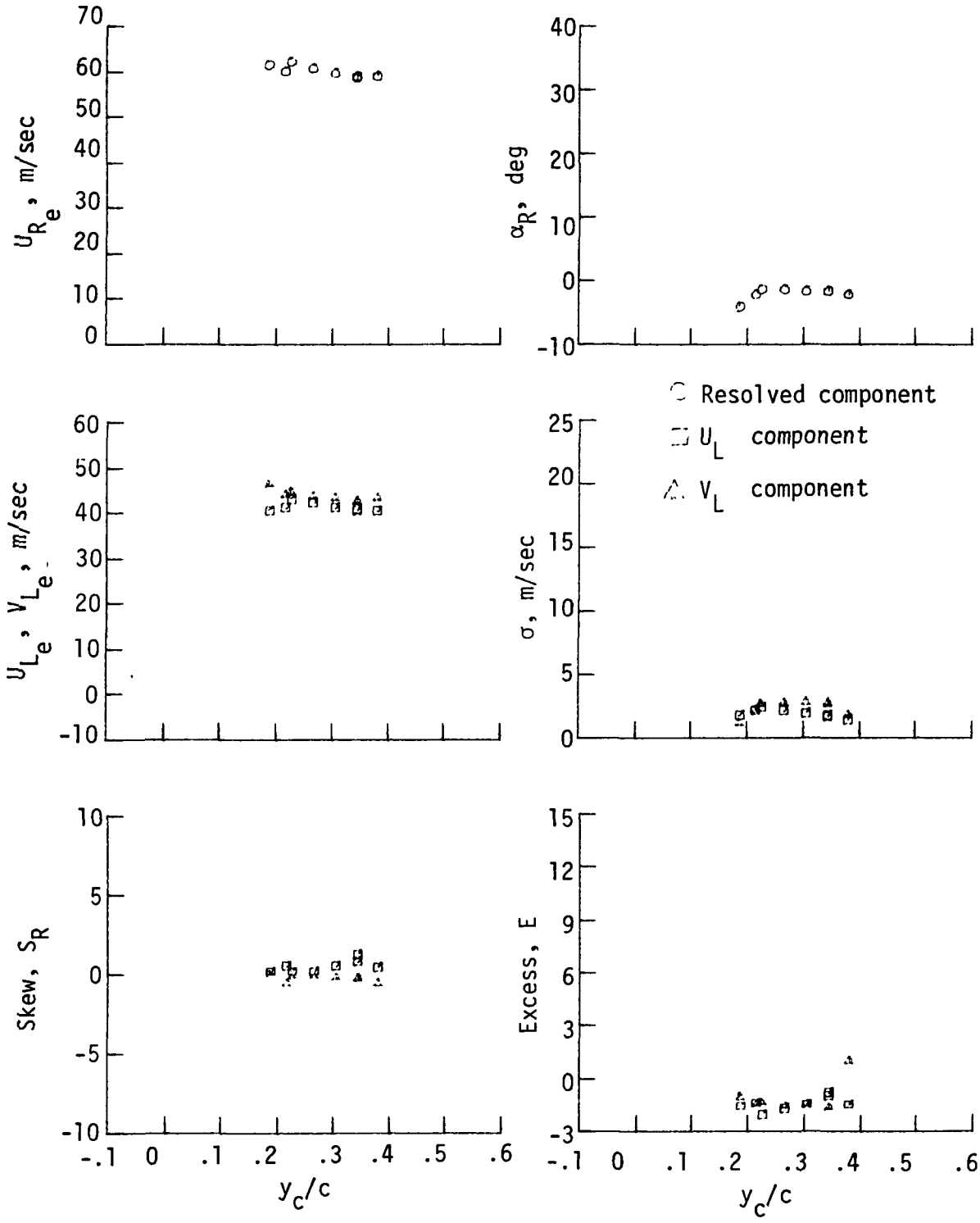

Figure 20. Statistical characteristics of the LV measured velocities at constant $x_c/c = .42$. $\alpha = 4.75°$.

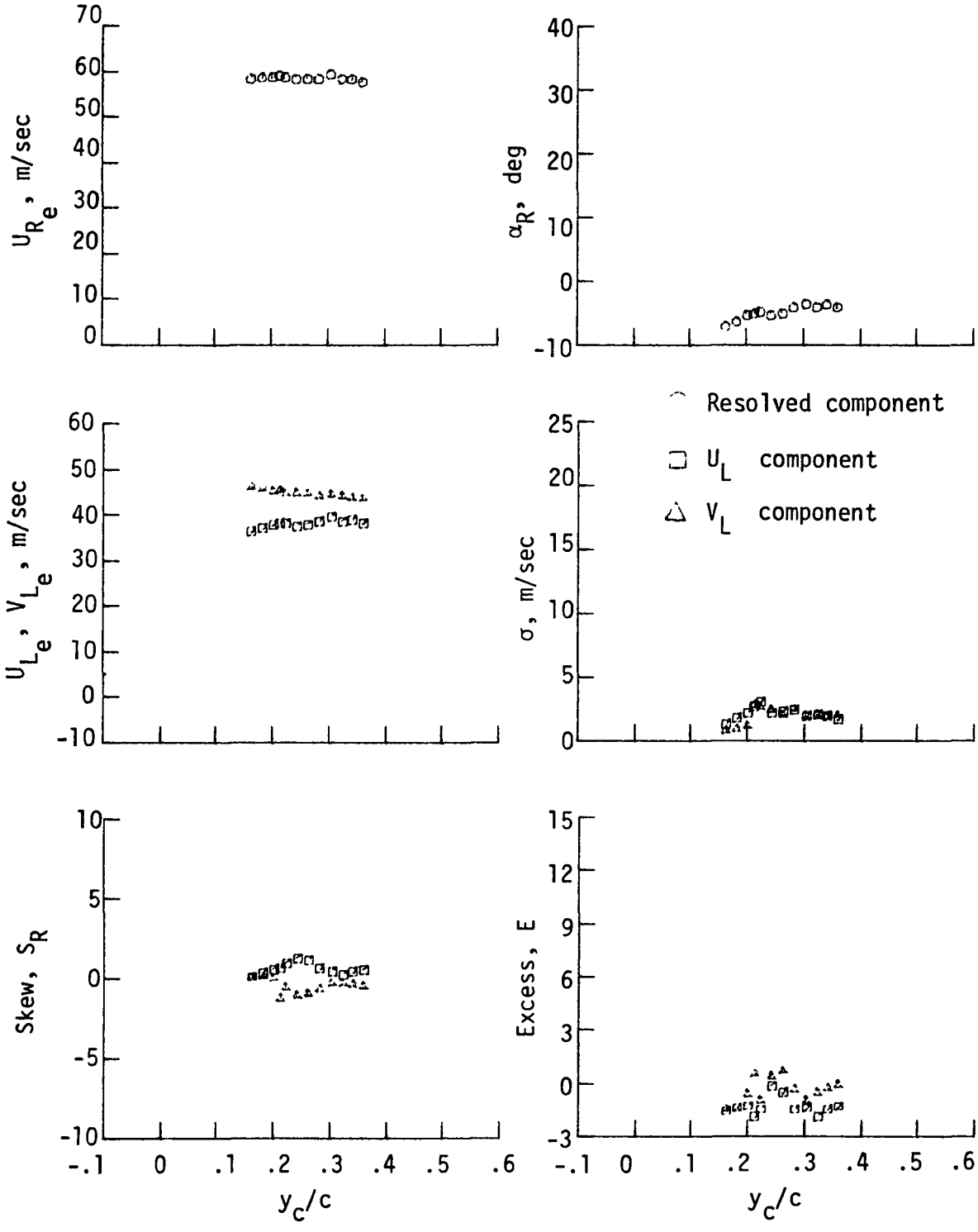

Figure 21. Statistical characteristics of the LV measured velocities at constant $x_c/c = .58$. $\alpha = 4.75°$.

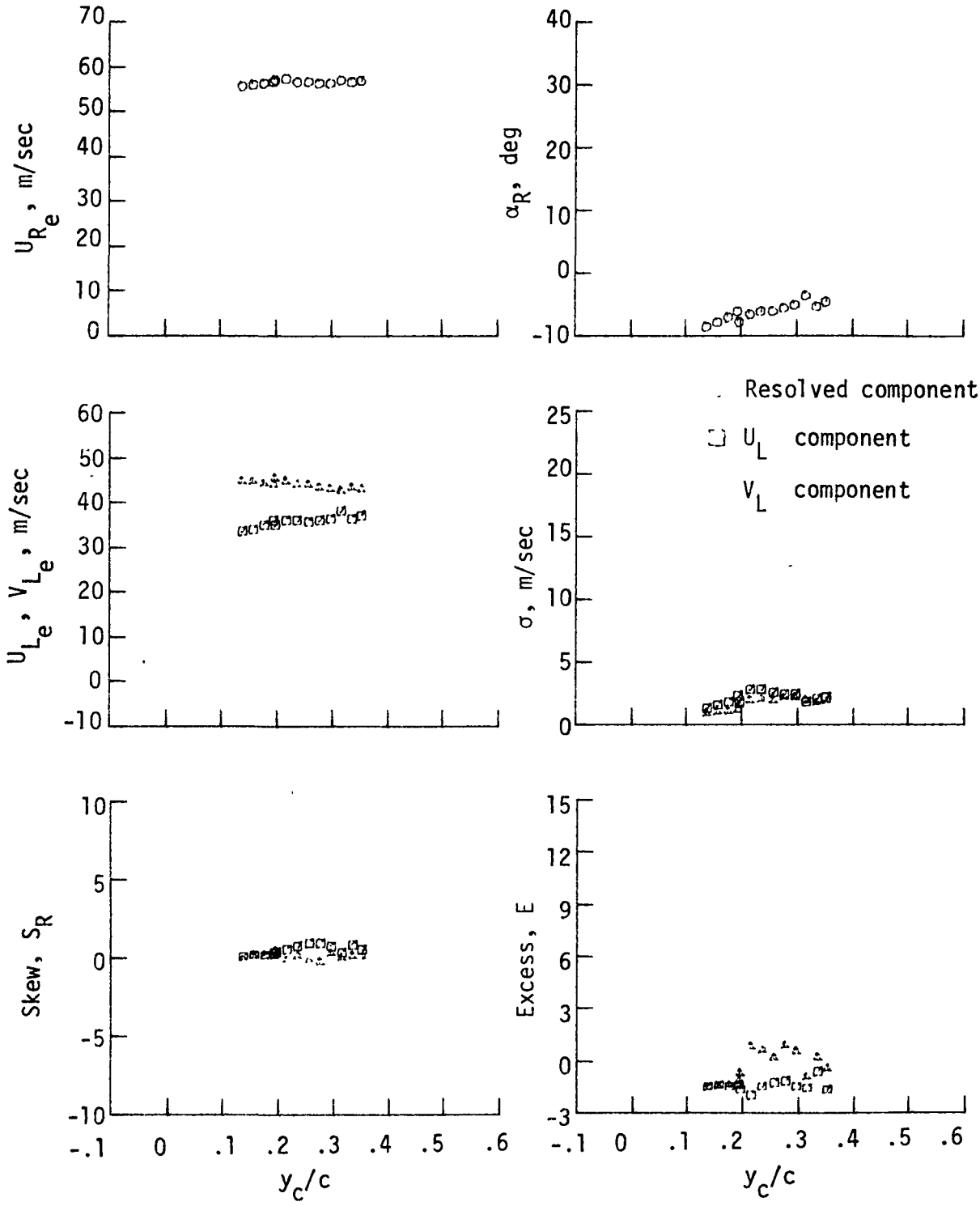

Figure 22. Statistical characteristics of the LV measured velocities at constant $x_c/c = .75$, $\alpha = 4.75°$.

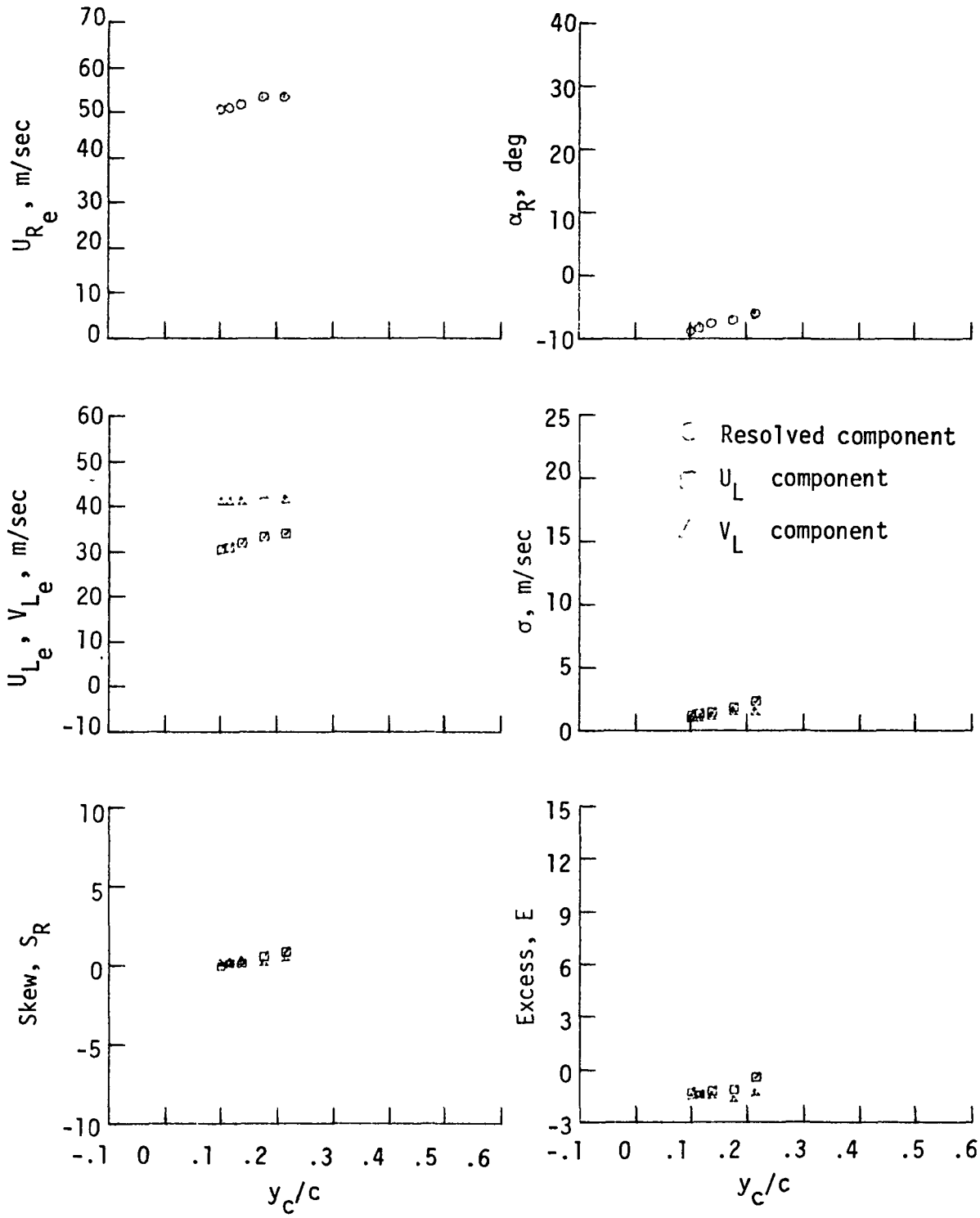

Figure 23. Statistical characteristics of the LV measured velocities at constant x_c/c = .96. α = 4.75°.

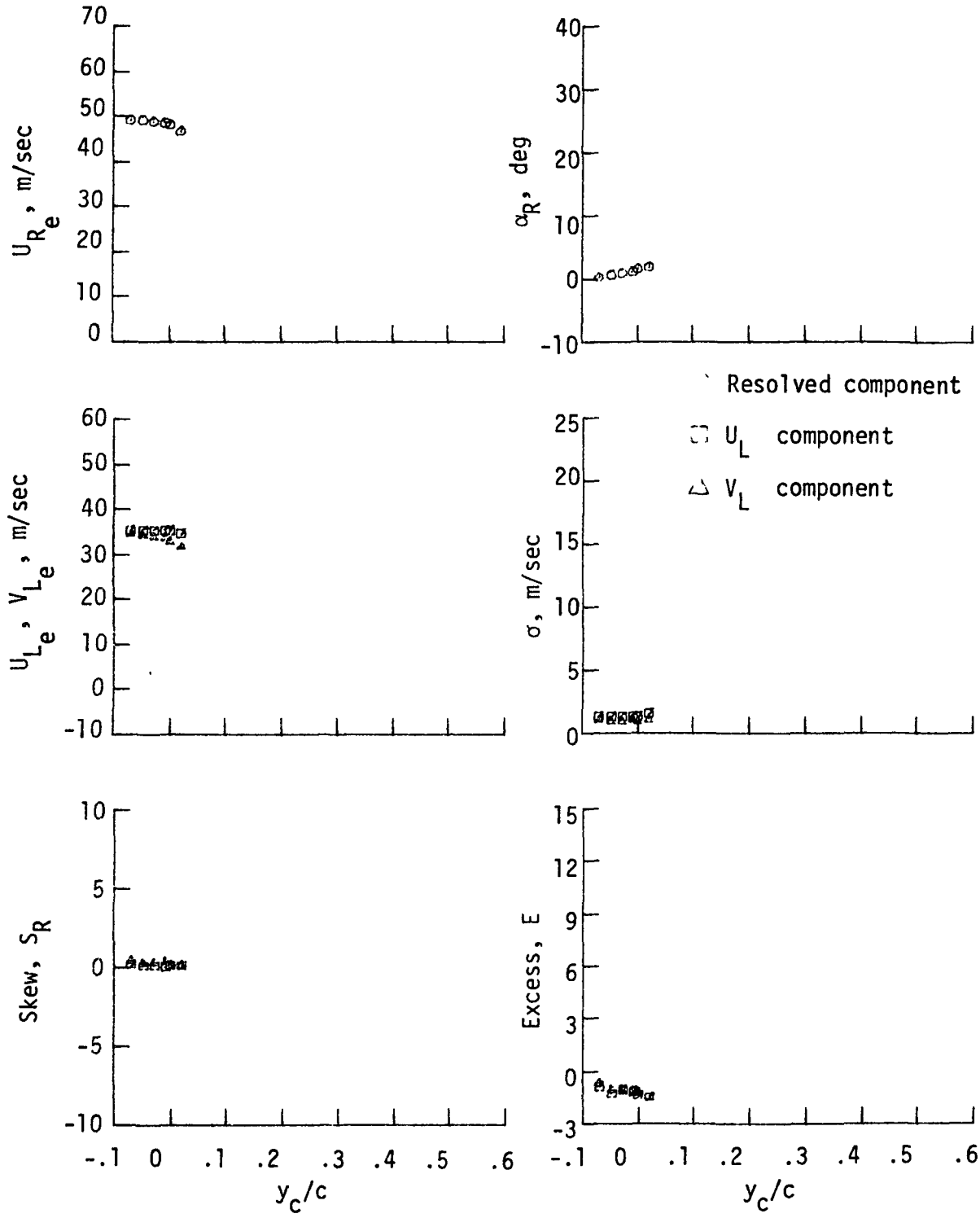

Figure 24. Statistical characteristics of the LV measured velocities at constant x_c/c = 1.01. α = 4.75°.

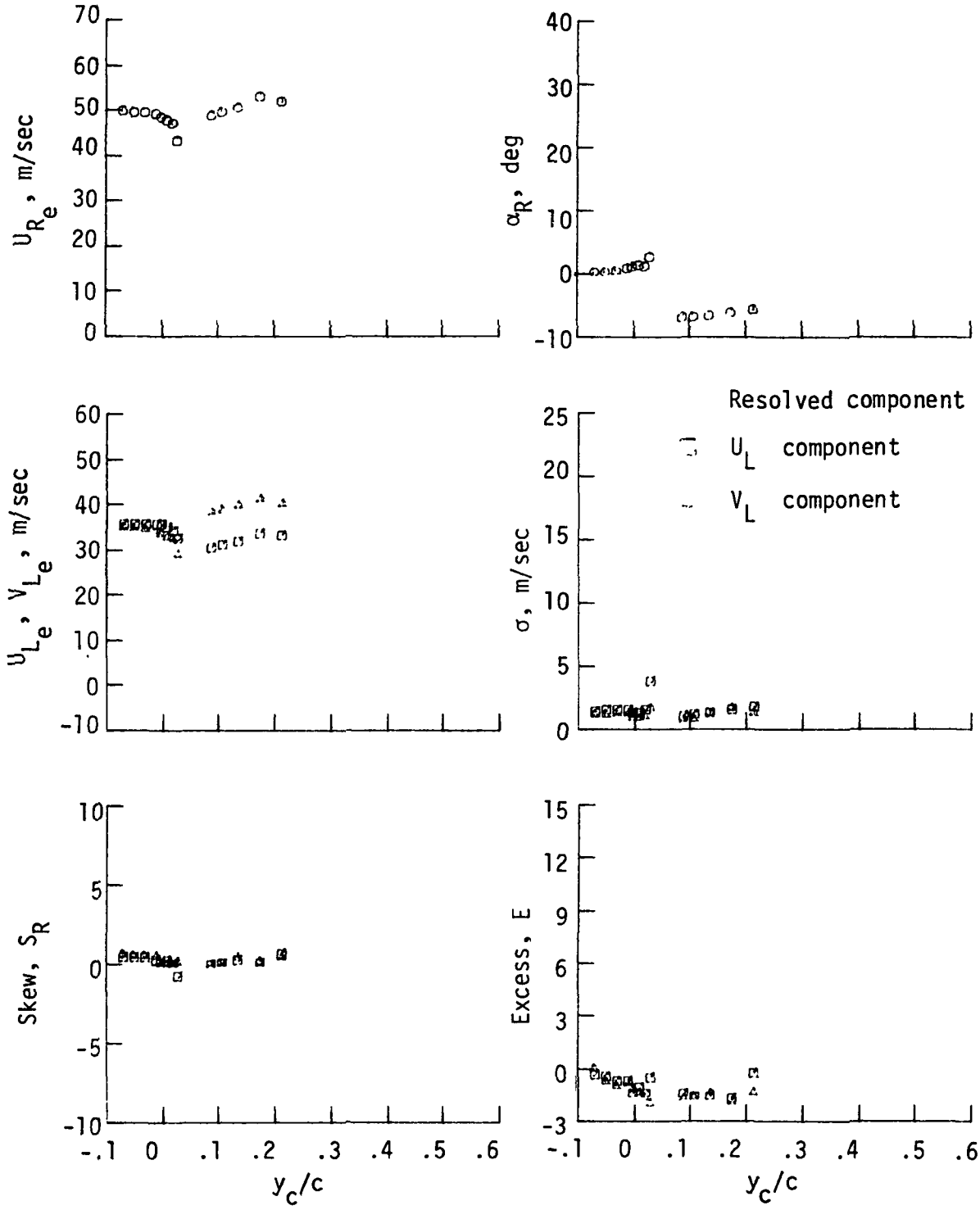

Figure 25. Statistical characteristics of the LV measured velocities at constant $x_c/c = 1.03$. $\alpha = 4.75°$.

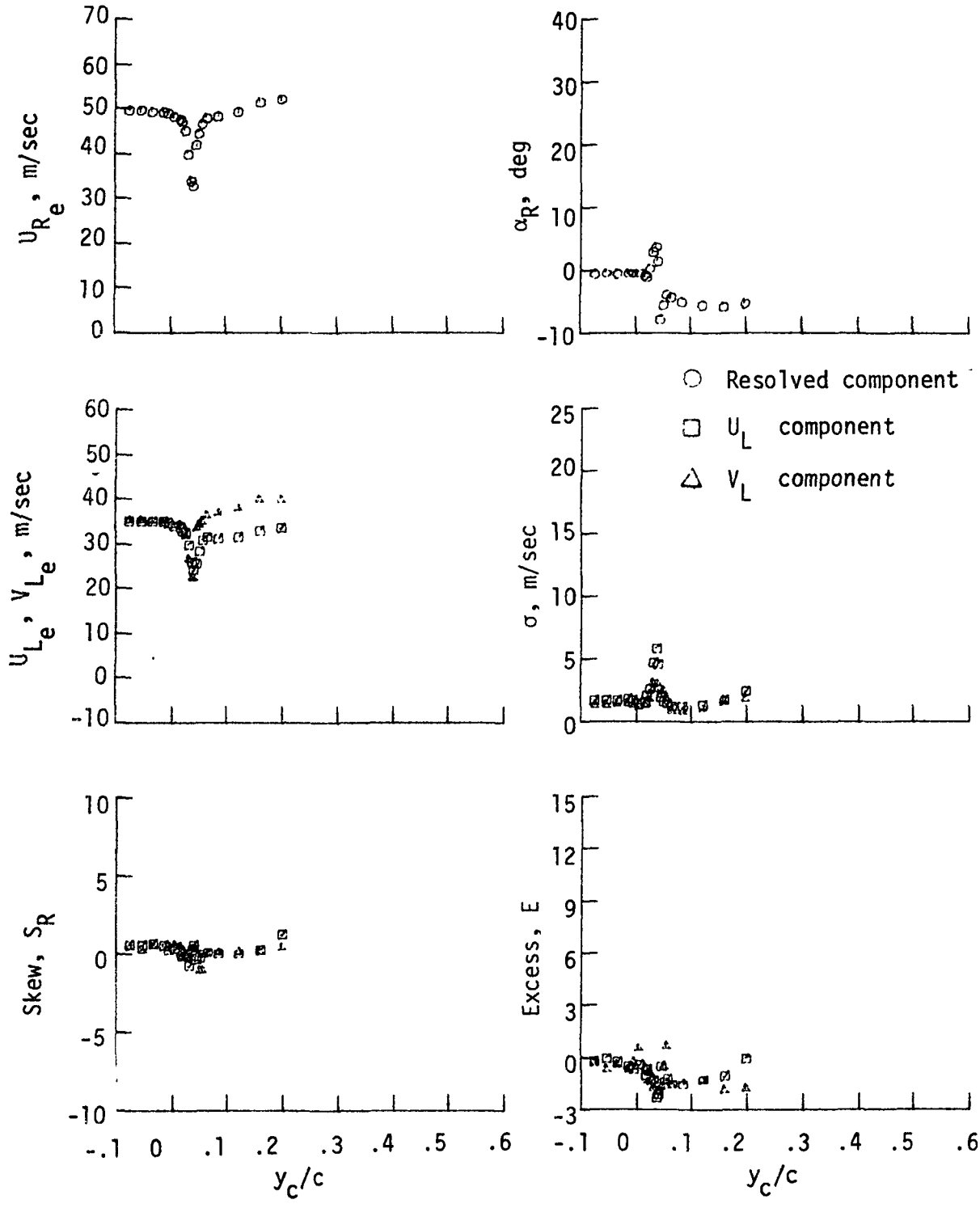

Figure 26. Statistical characteristics of the LV measured velocities at constant $x_c/c = 1.09$. $\alpha = 4.75°$.

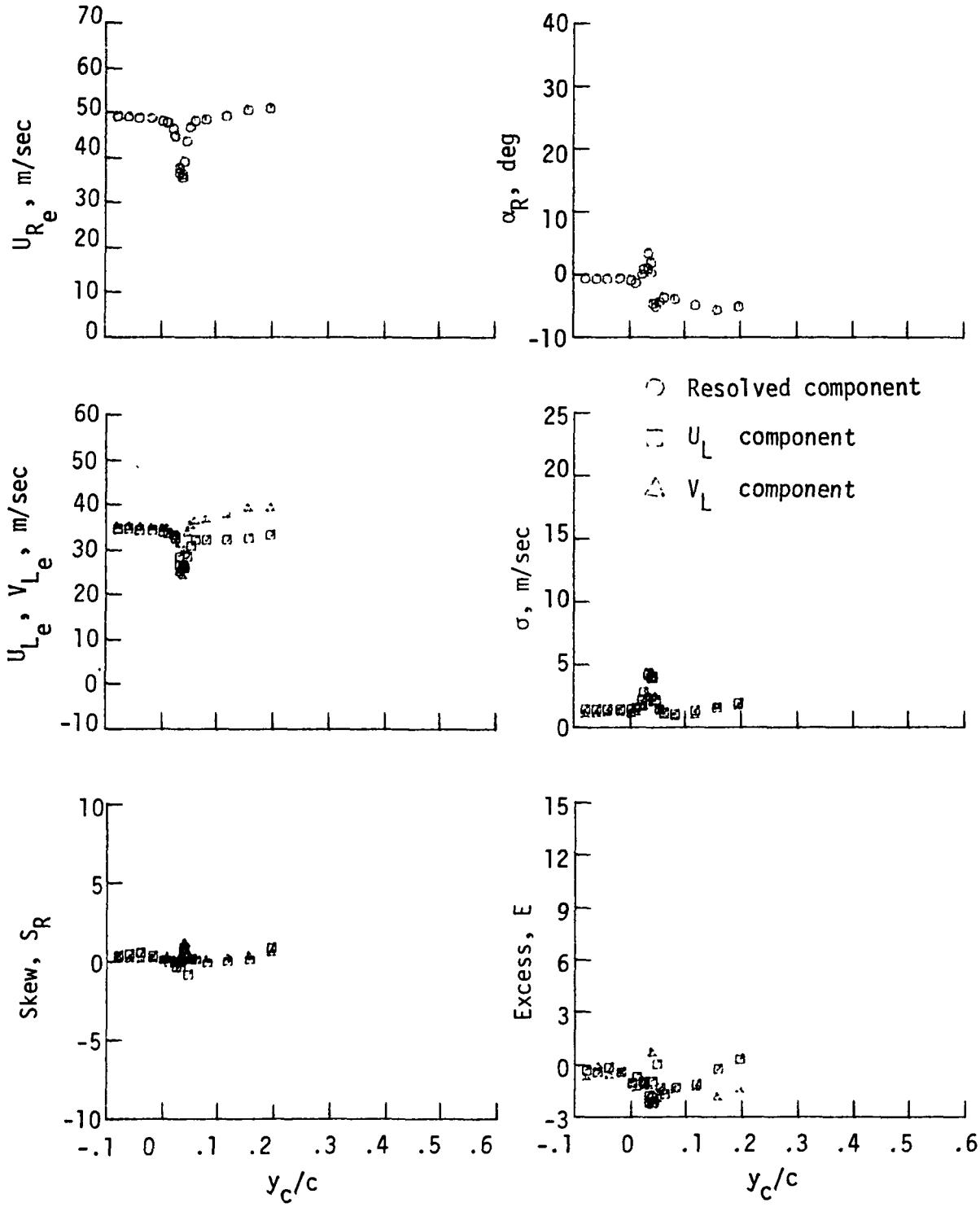

Figure 27. Statistical characteristics of the LV measured velocities at constant $x_c/c = 1.13$. $\alpha = 4.75°$.

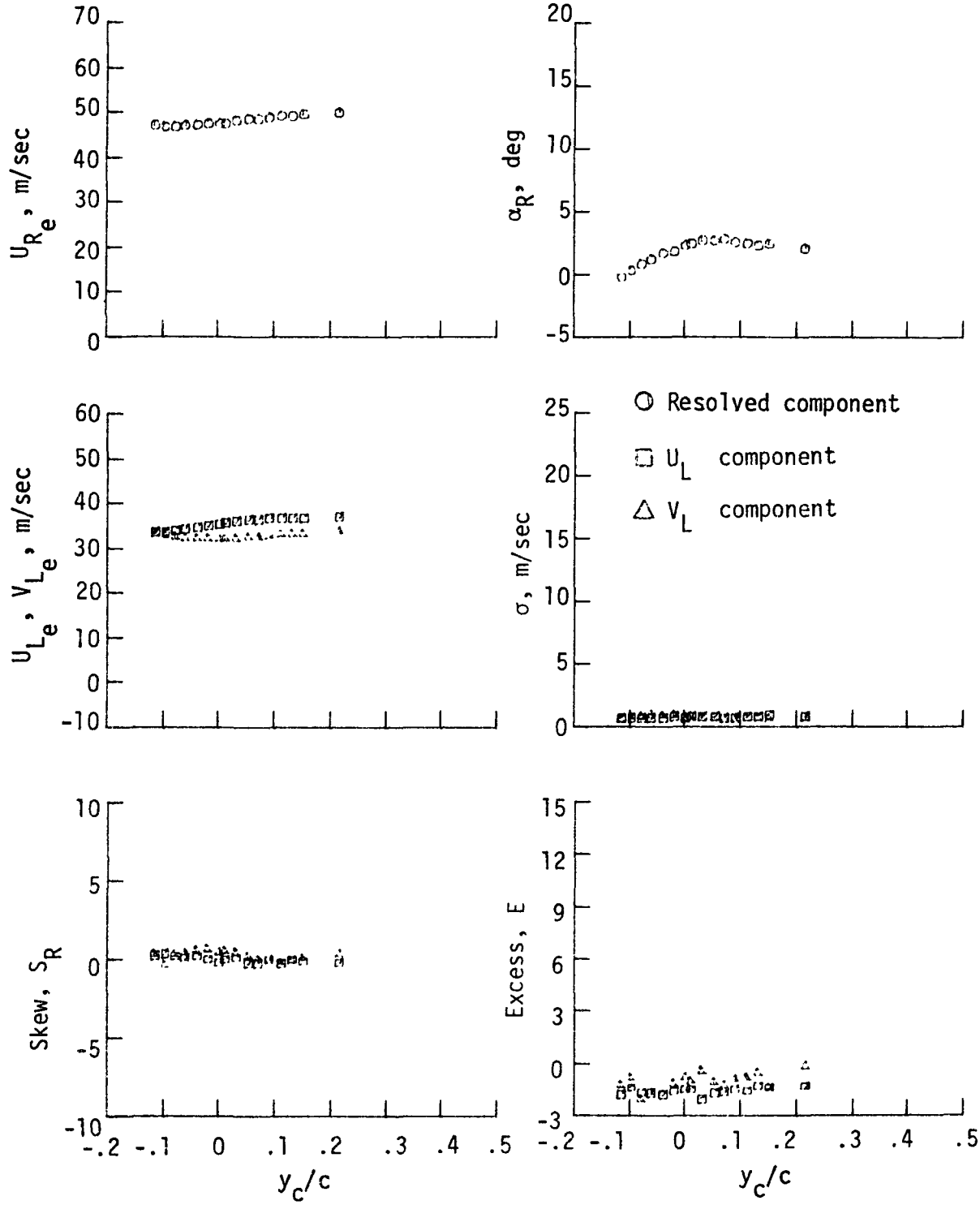

Figure 28. Statistical characteristics of the LV measured velocities at constant x_c/c =-0.17. α = 0.6°.

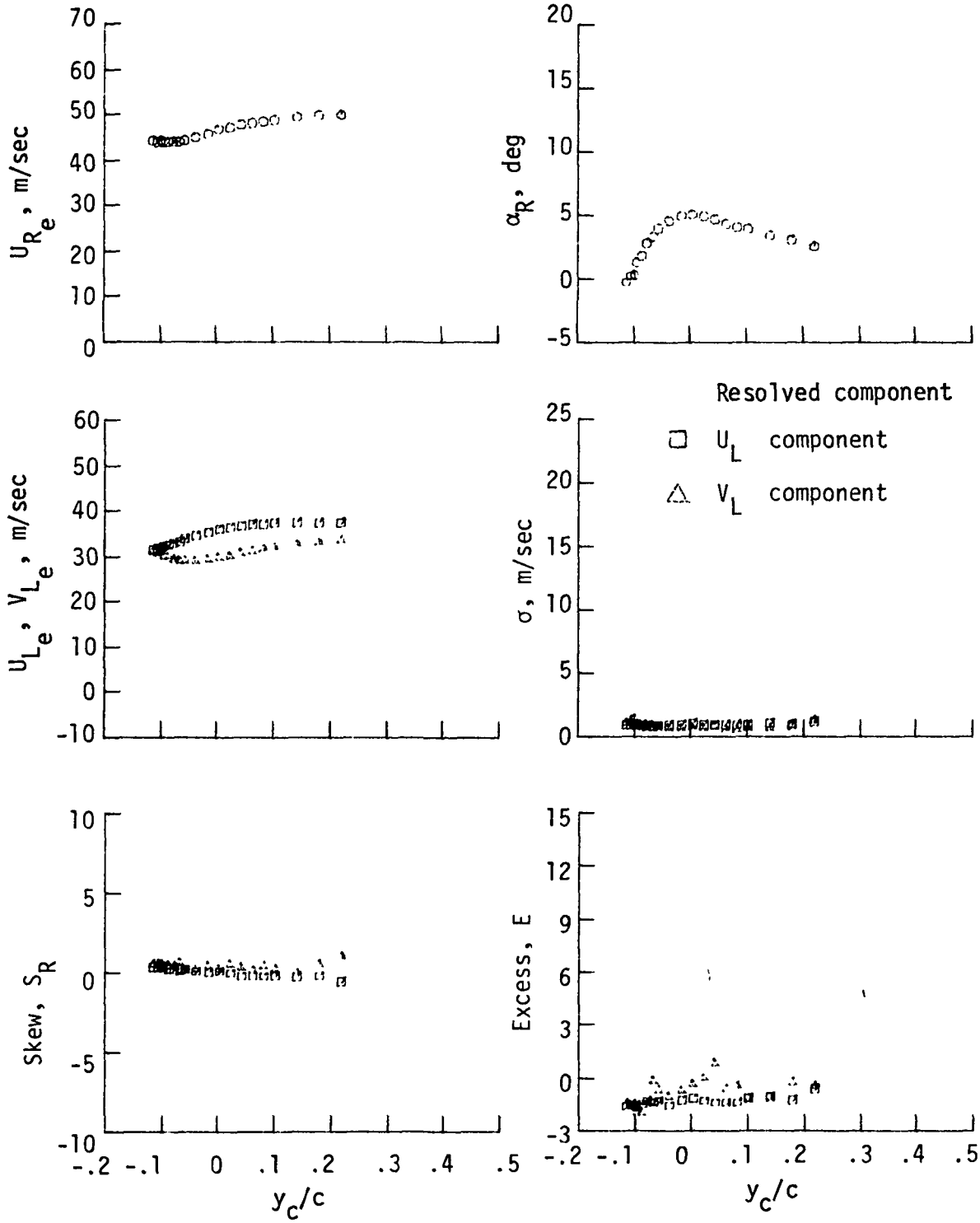

Figure 29. Statistical characteristics of the LV measured velocities at constant x_c/c =-0.09. α = 0.6°.

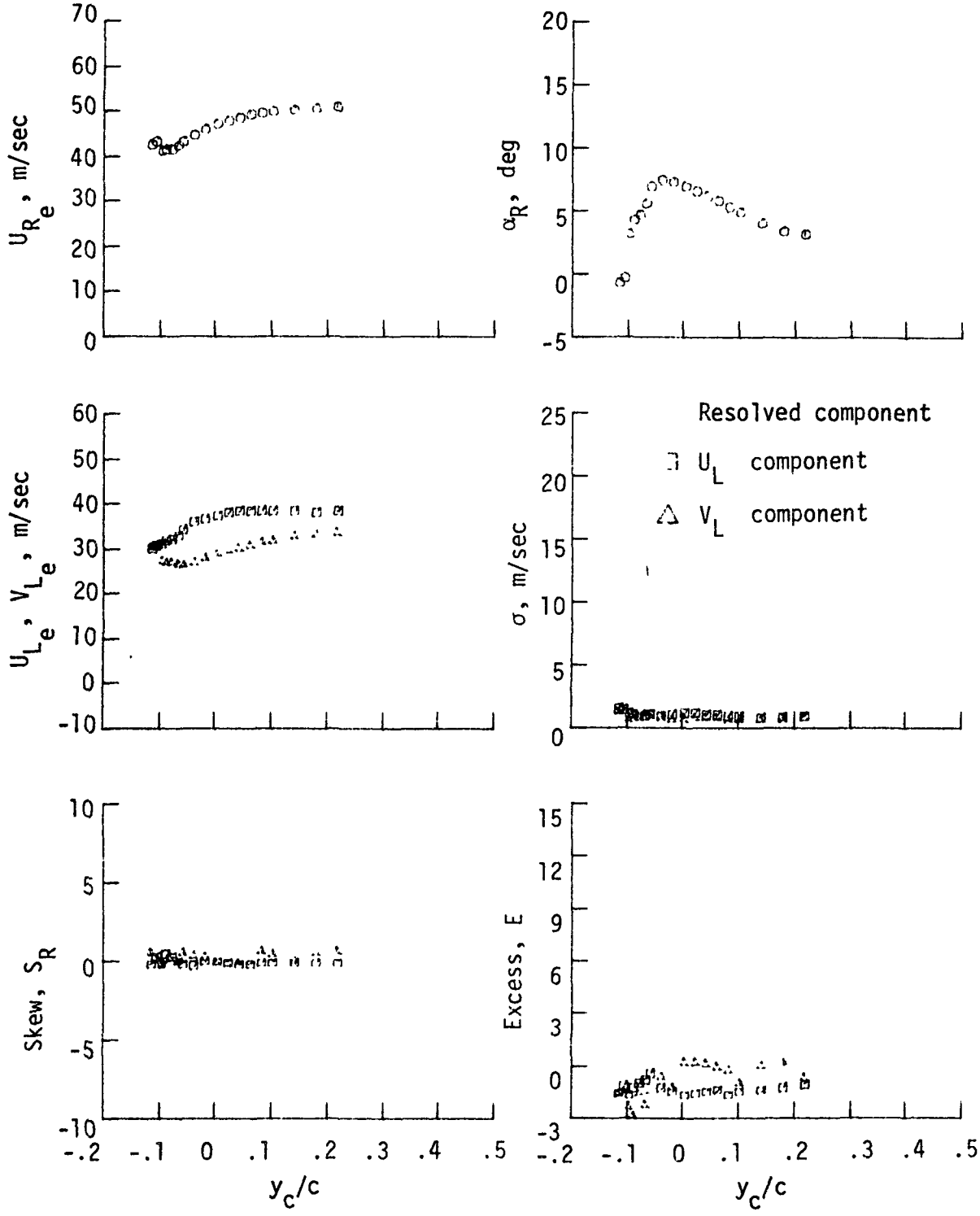

Figure 30. Statistical characteristics of the LV measured velocities at constant x_c/c =-0.05. α = 0.6°.

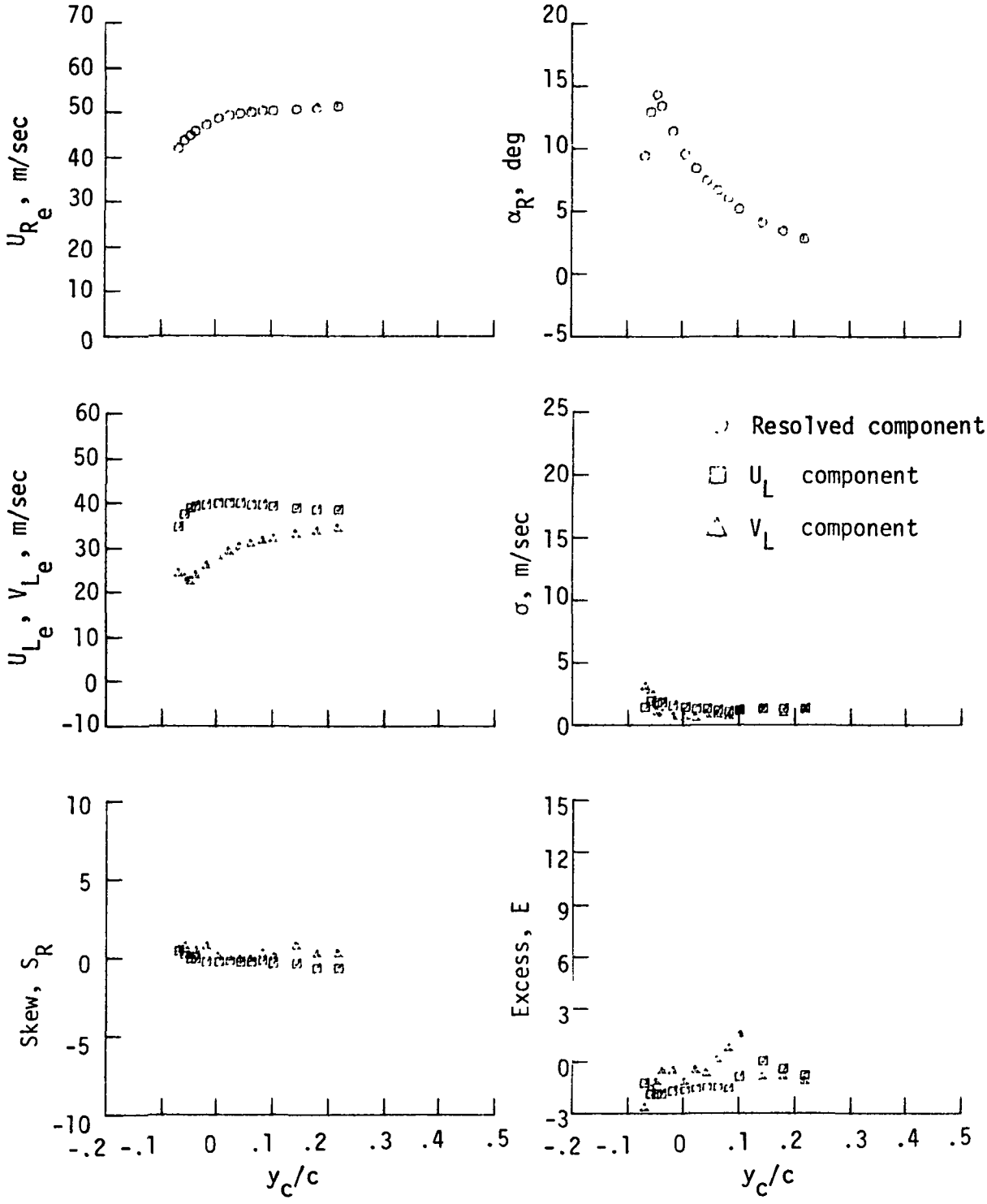

Figure 31. Statistical characteristics of the LV measured velocities at constant $x_c/c = 0$. $\alpha = 0.6°$.

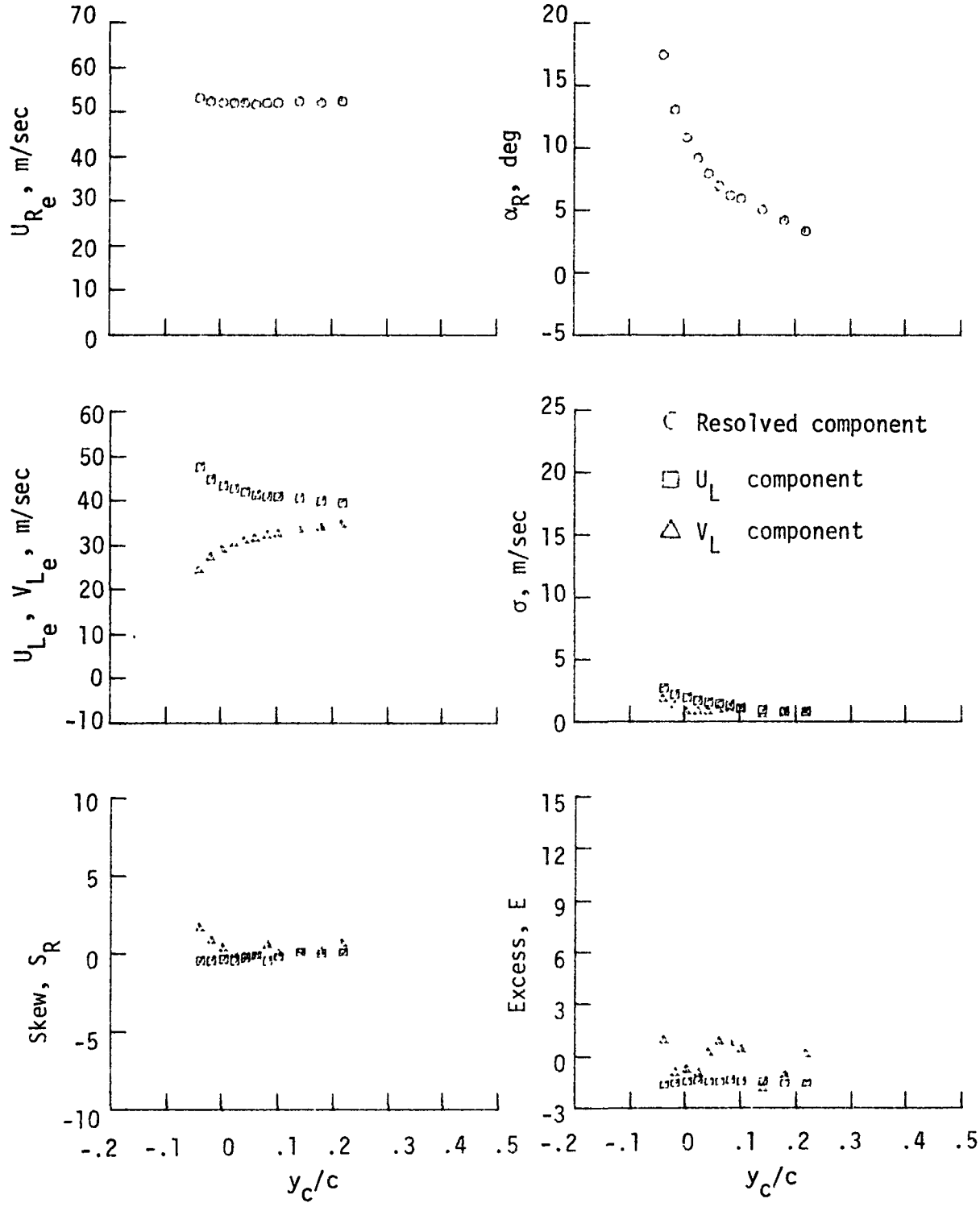

Figure 32. Statistical characteristics of the LV measured velocities at constant $x_c/c = 0.04$. $\alpha = 0.6°$.

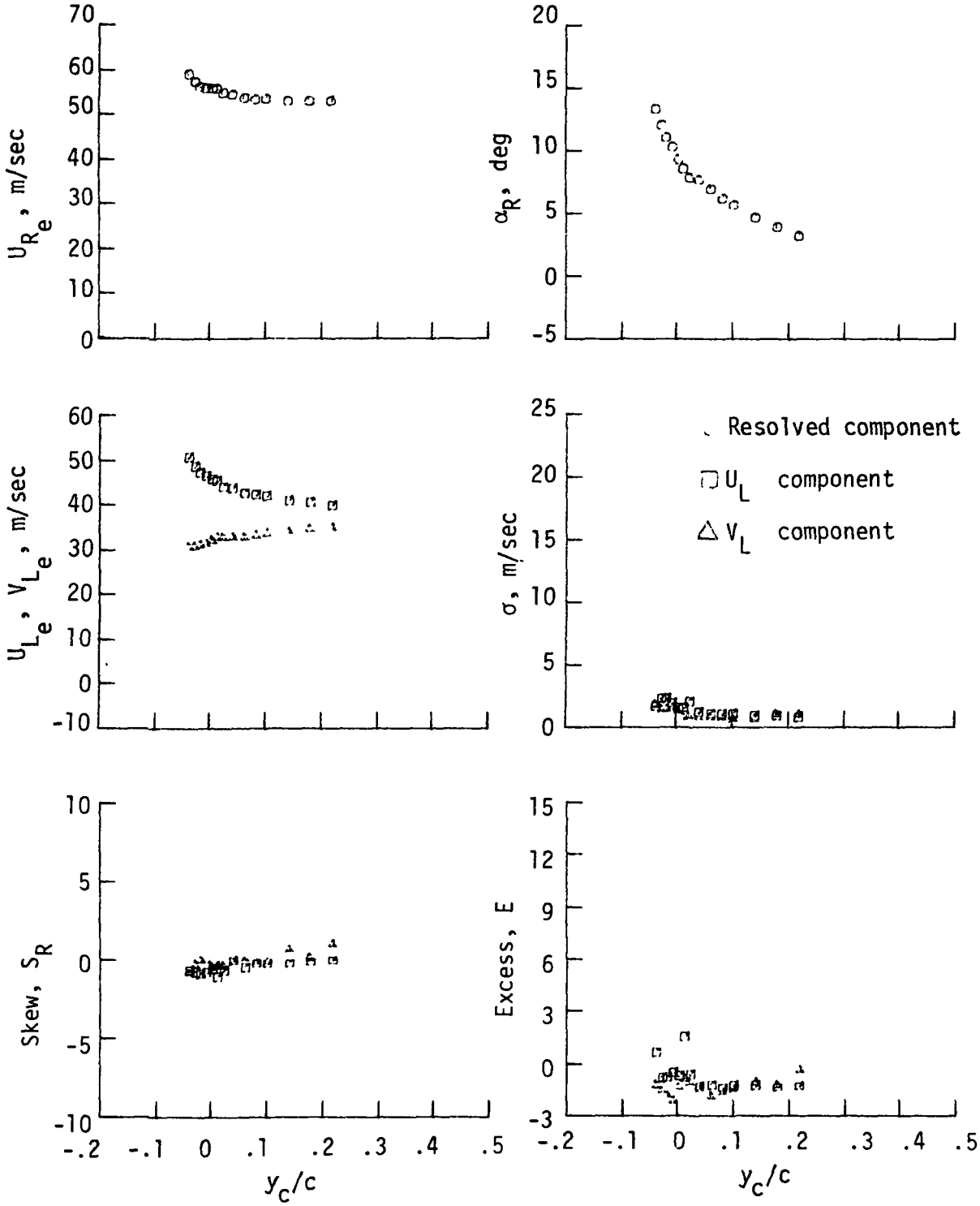

Figure 33. Statistical characteristics of the LV measured velocities at constant $x_c/c = 0.08$. $\alpha = 0.6°$.

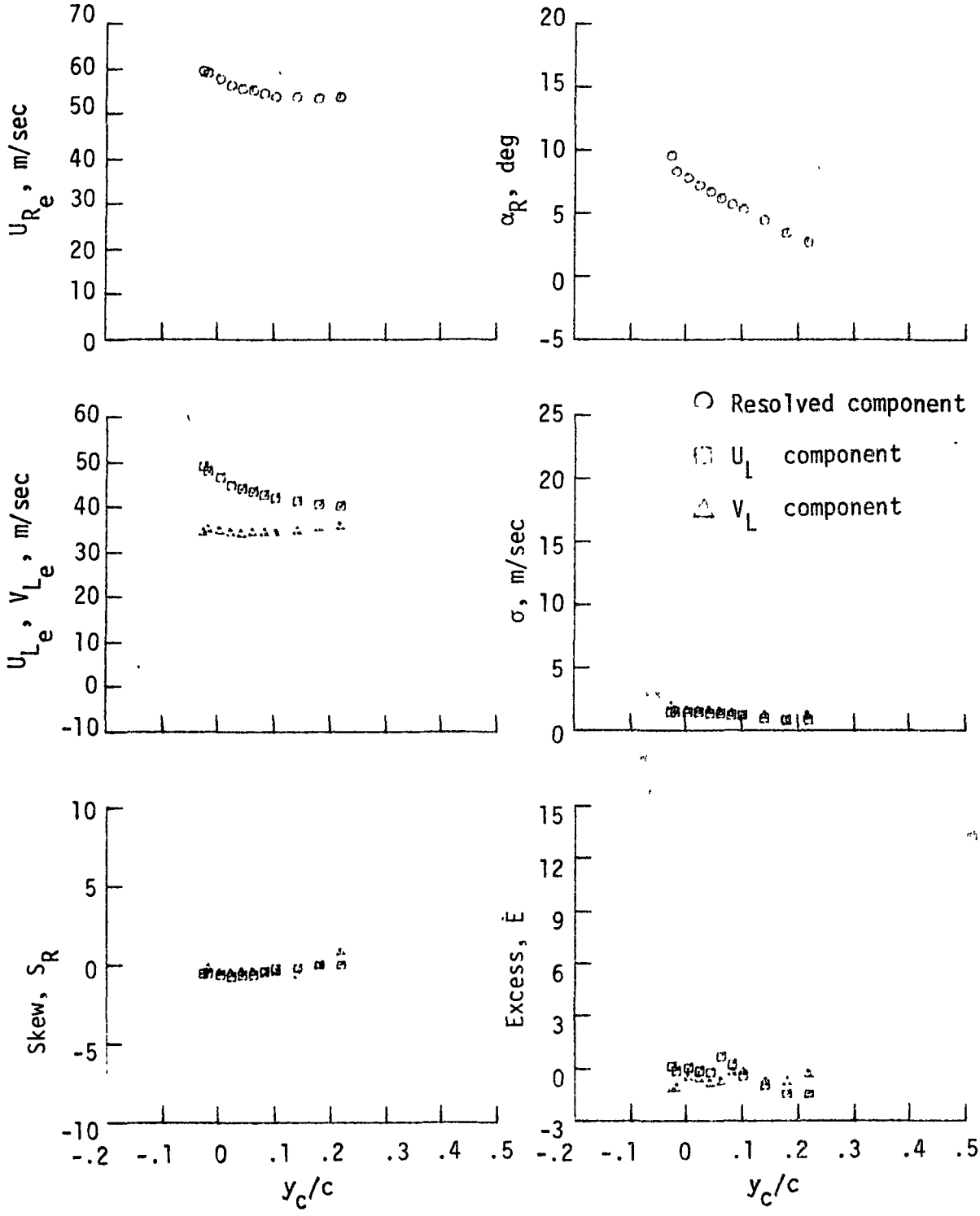

Figure 34. Statistical characteristics of the LV measured velocities at constant $x_c/c = 0.12$, $\alpha = 0.6°$.

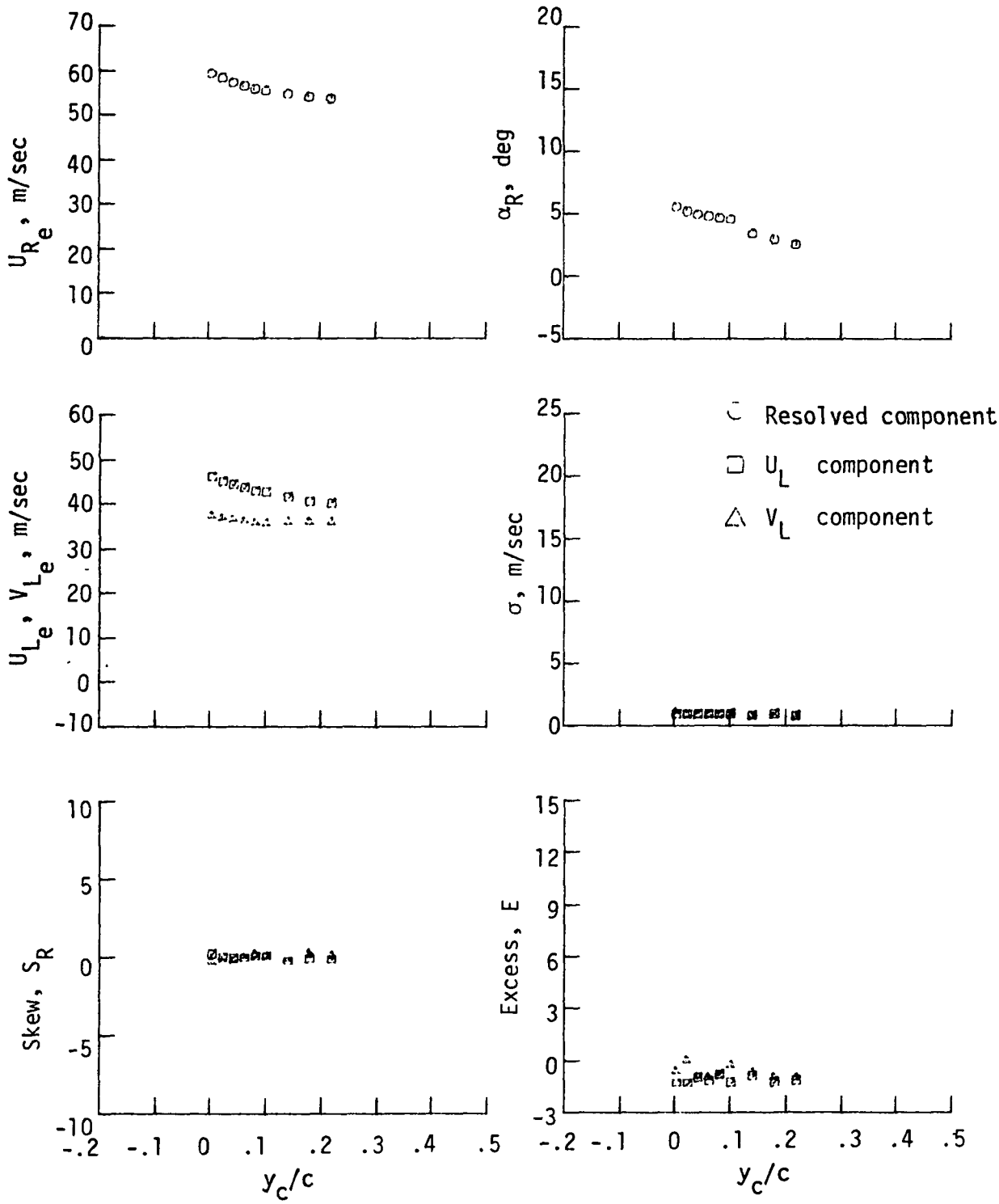

Figure 35. Statistical characteristics of the LV measured velocities at constant $x_c/c = 0.16$. $\alpha = 0.6°$.

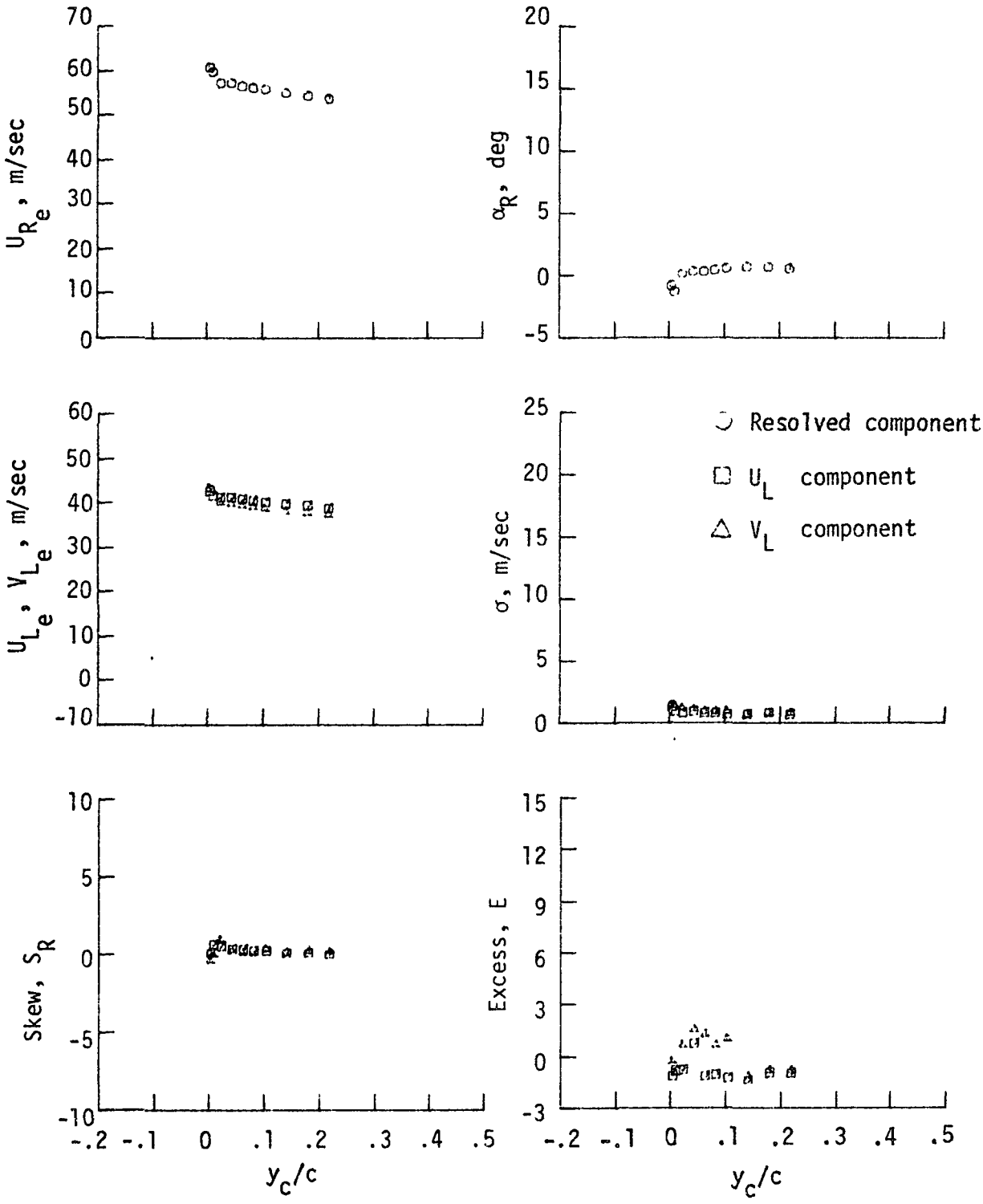

Figure 36. Statistical characteristics of the LV measured velocities at constant $x_c/c = 0.29$. $\alpha = 0.6°$.

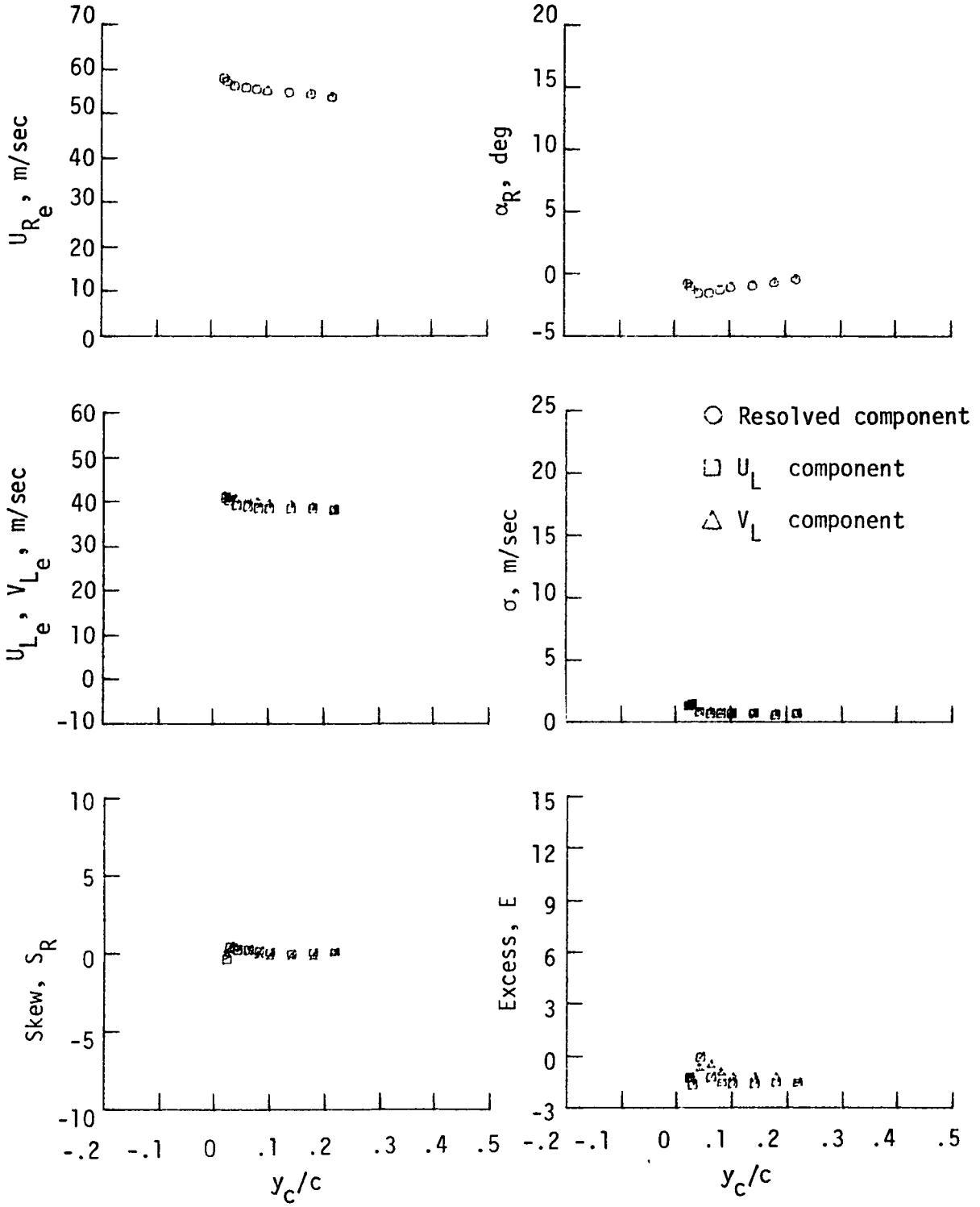

Figure 37. Statistical characteristics of the LV measured velocities at constant $x_c/c = 0.41$. $\alpha = 0.6°$.

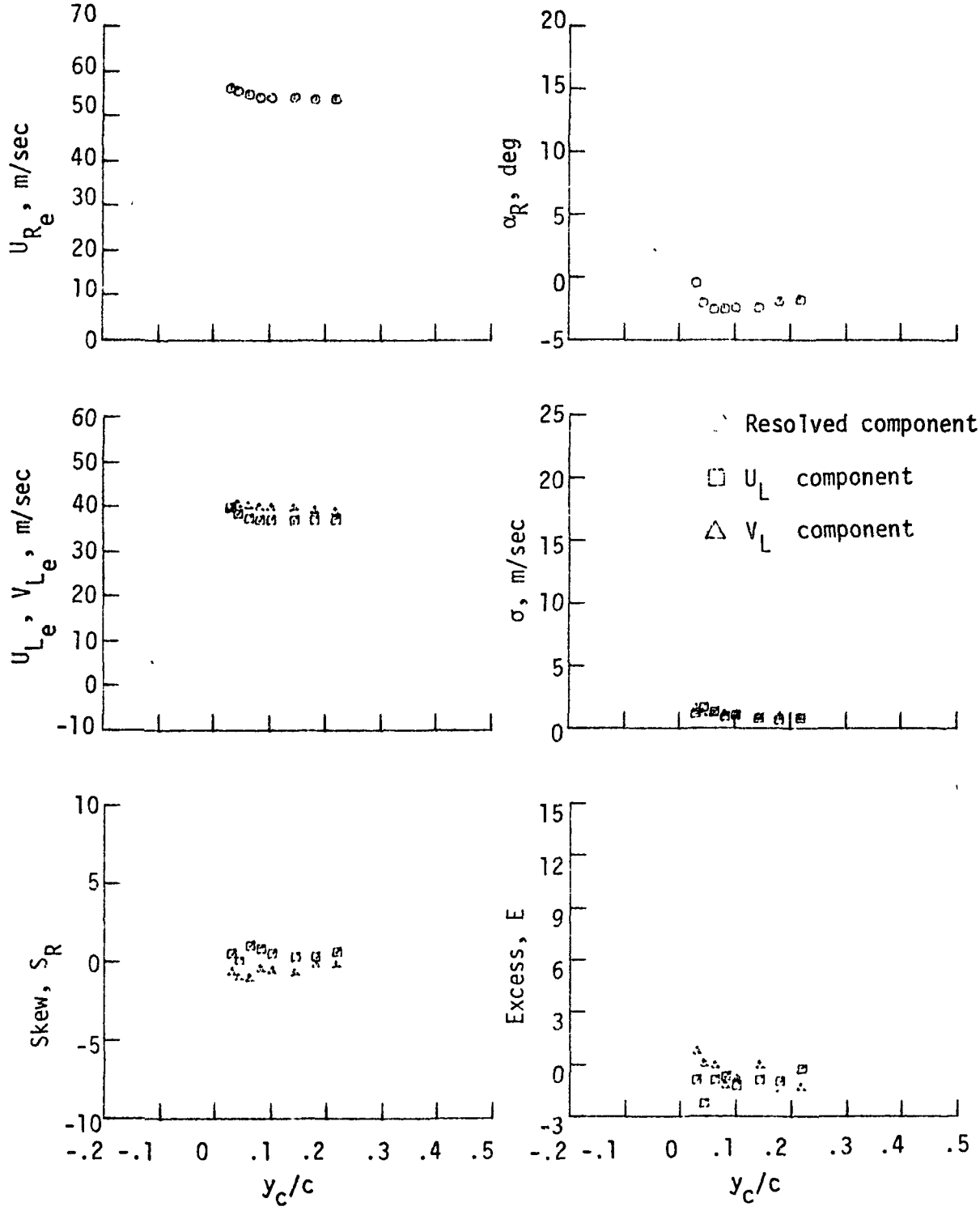

Figure 38. Statistical characteristics of the LV measured velocities at constant $x_c/c = 0.58$. $\alpha = 0.6°$.

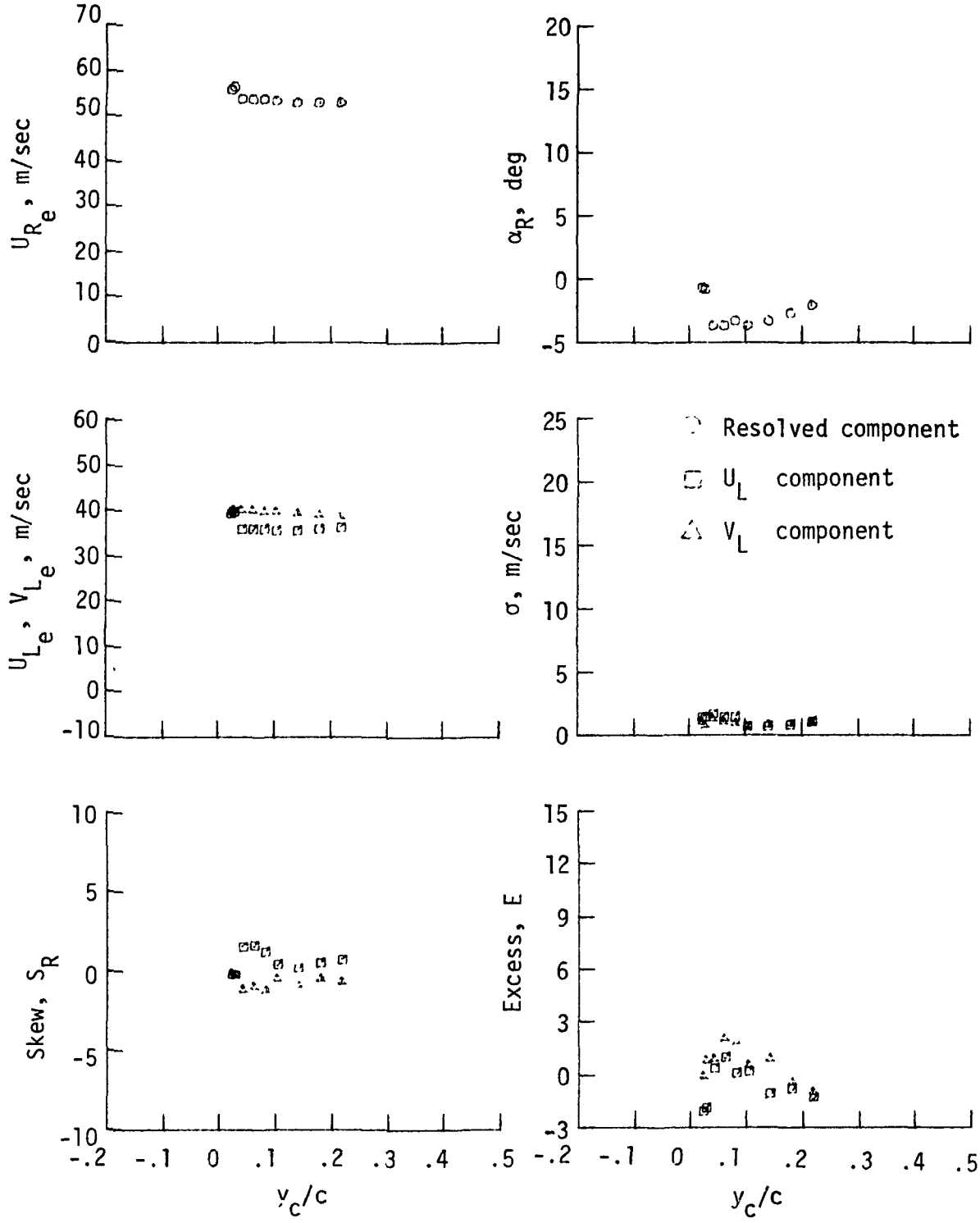

Figure 39. Statistical characteristics of the LV measured velocities at constant $x_c/c = 0.70$. $\alpha = 0.60°$.

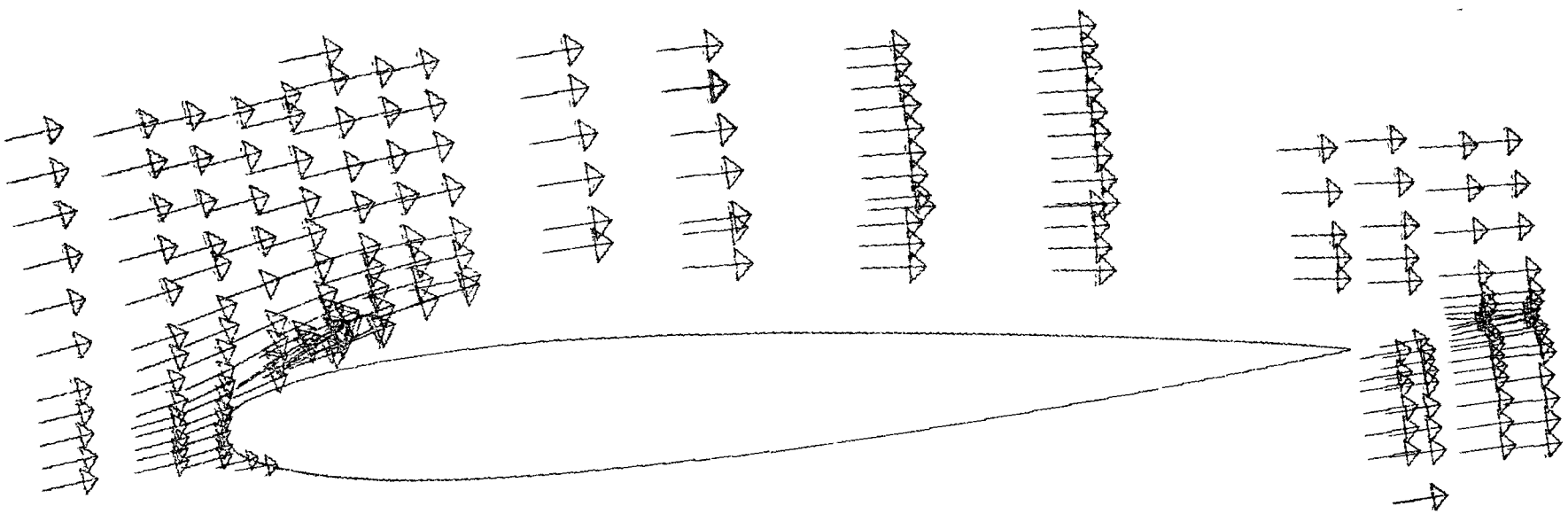

Figure 40.- Velocity vectors computed from measurements over the wing at $\alpha = 4.75^{0}$.

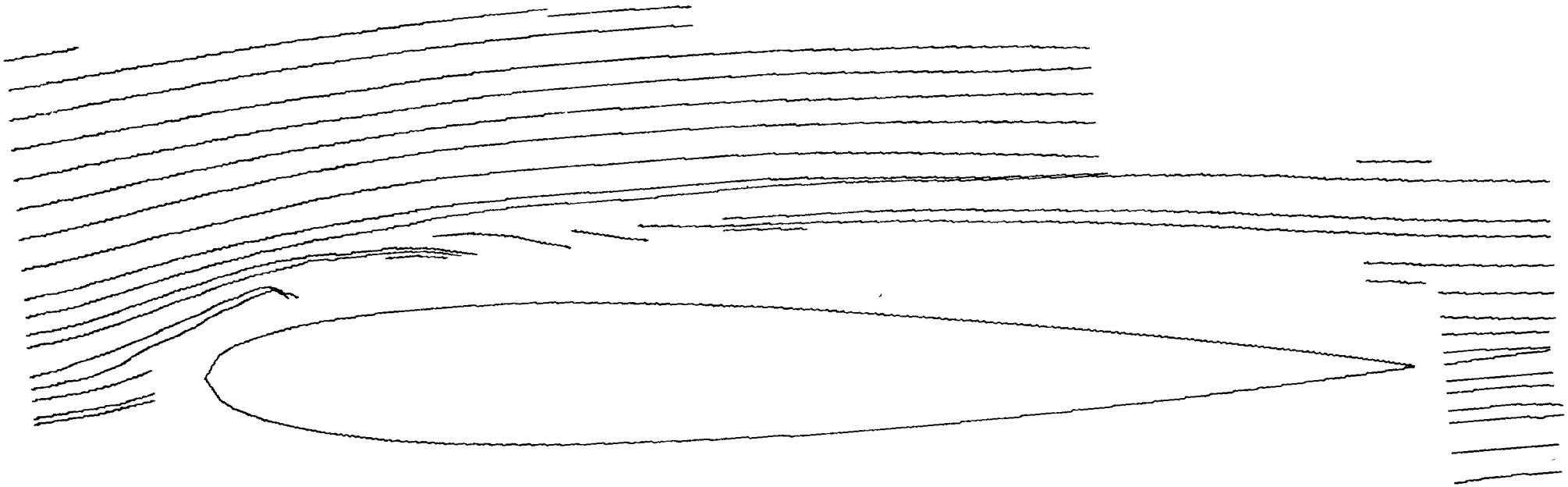

Figure 41.- Streamlines computed from interpolated flow angle distribution over the wing at $\alpha = 4.75^{o}$.

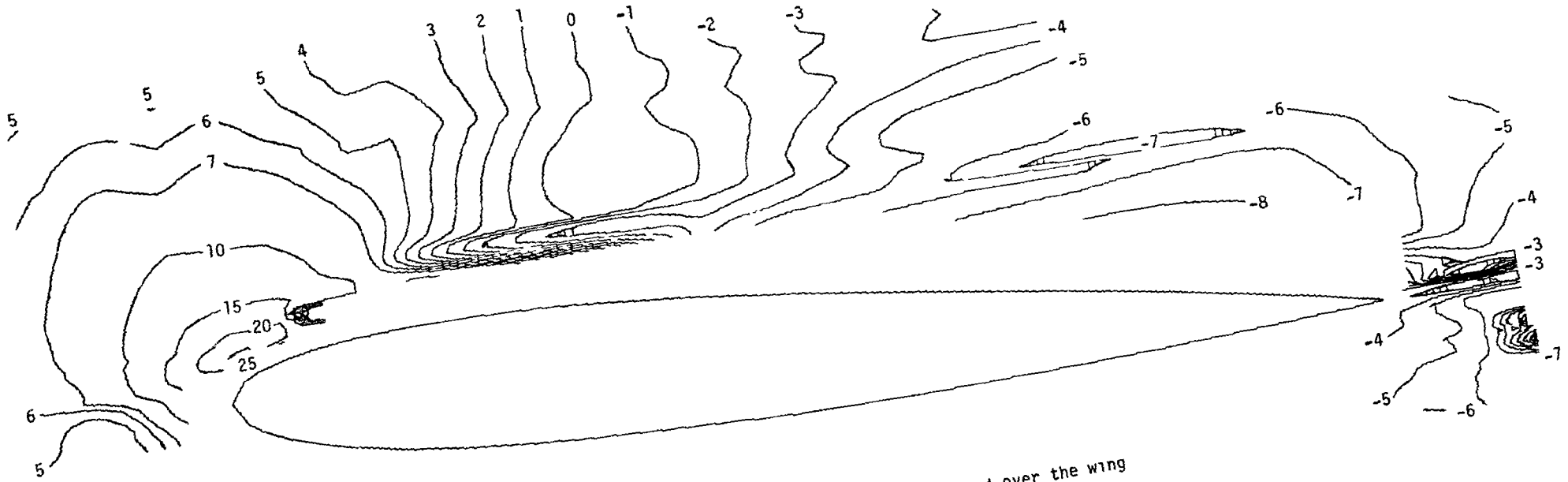

Figure 42.- Contours of constant local flow angle measured over the wing at $\alpha = 4.75^{0}$.

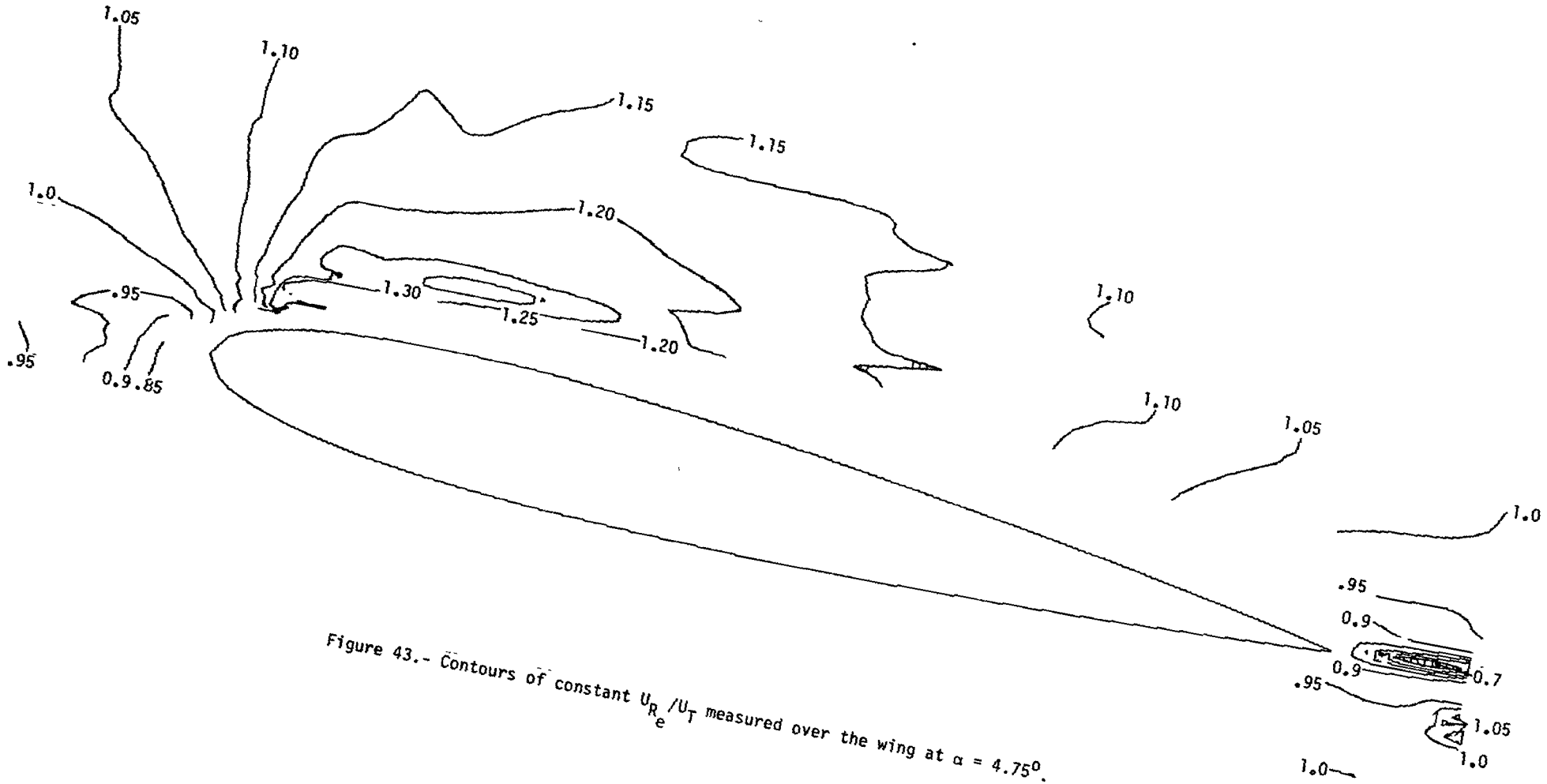

Figure 43.- Contours of constant U_{R_e}/U_T measured over the wing at $\alpha = 4.75^{o}$.

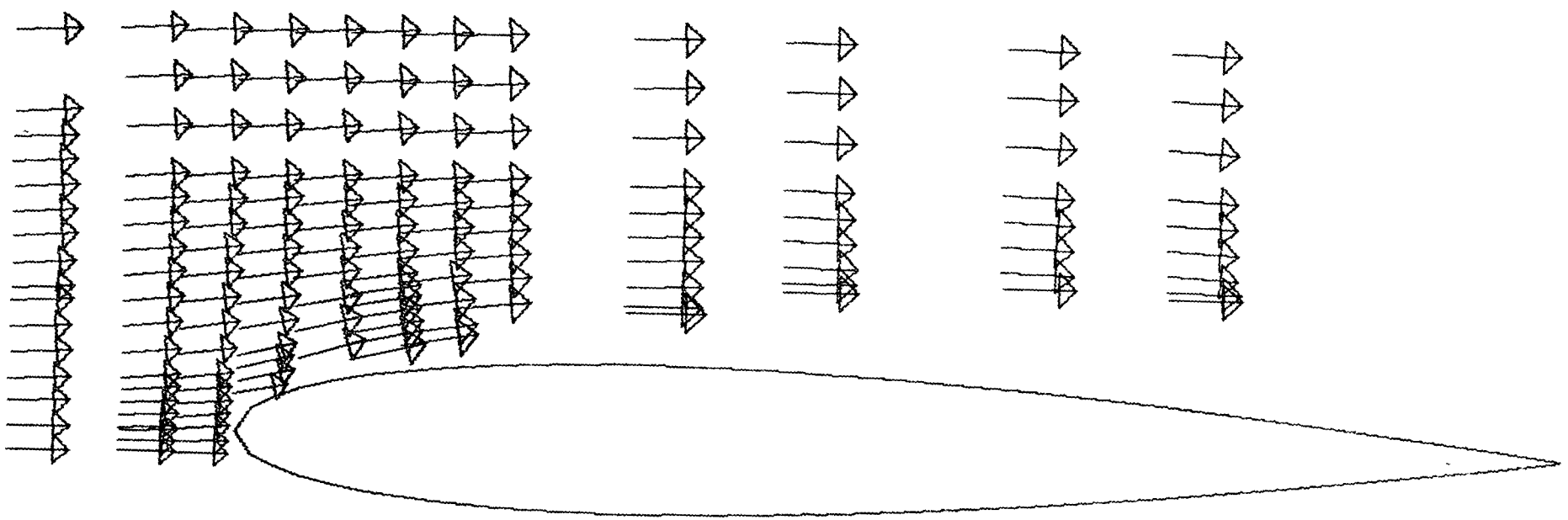

Figure 44.- Velocity vectors computed from measurements over the wing at $\alpha = 0.6^{o}$.

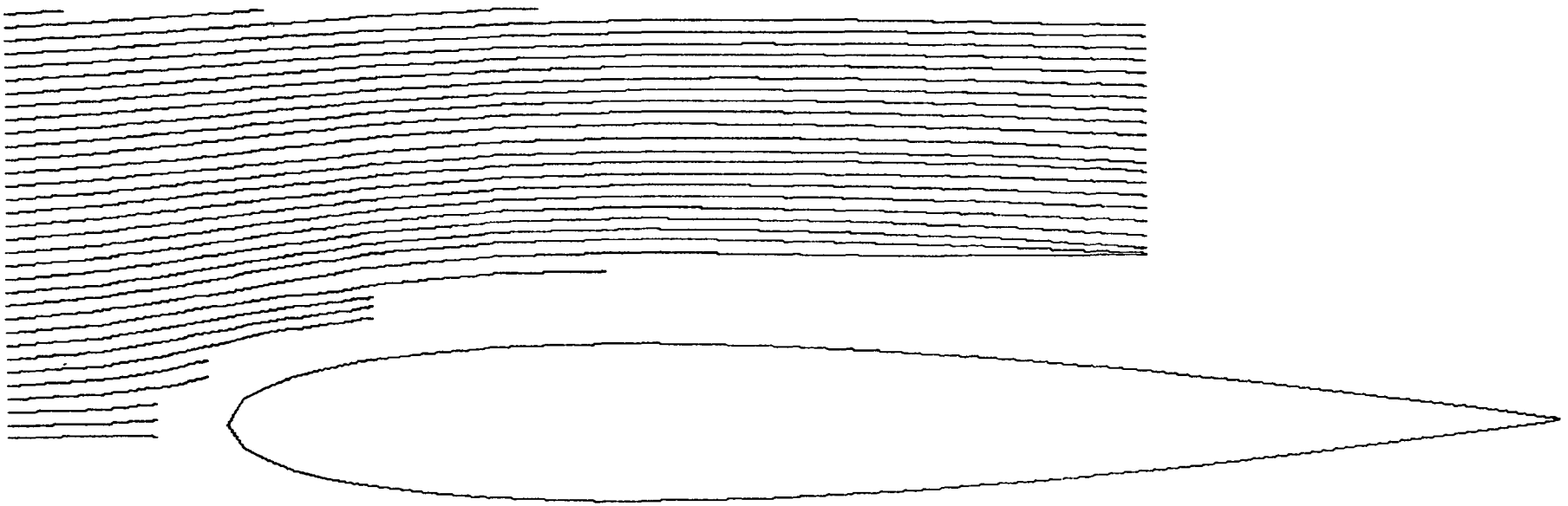

Figure 45.- Streamlines computed from interpolated flow angle distribution over the wing at $\alpha = 0.6^{o}$.

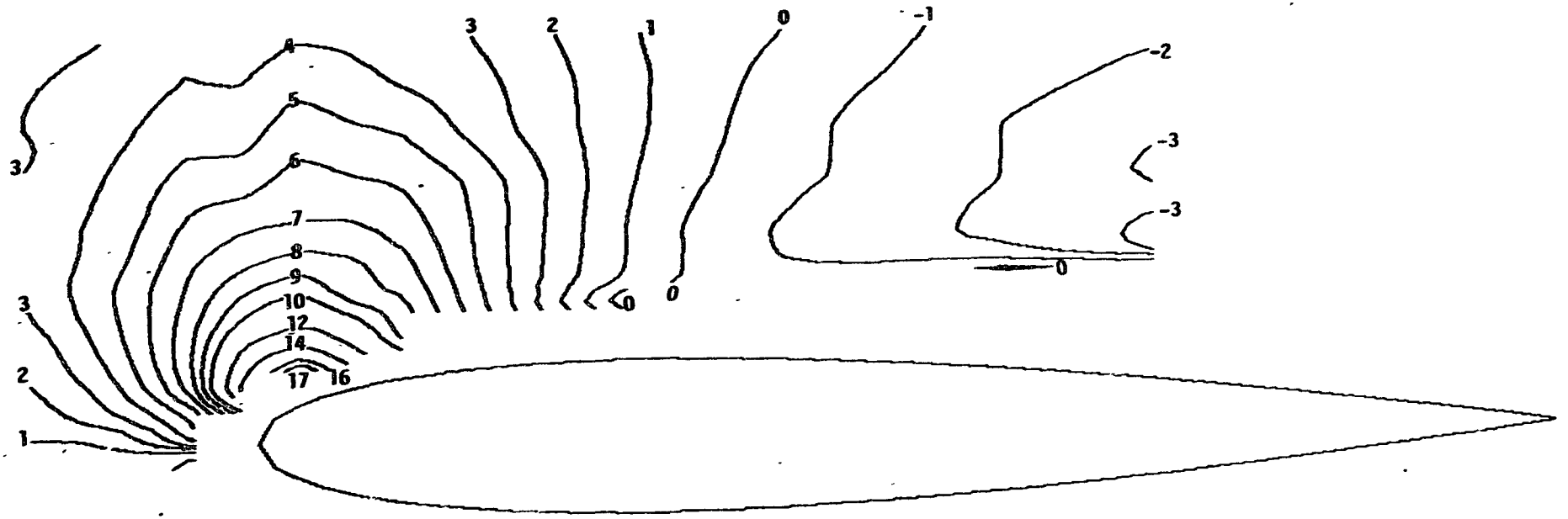

Figure 46.- Contours of constant local flow angle measured over the wing at $\alpha = 0.6^{0}$.

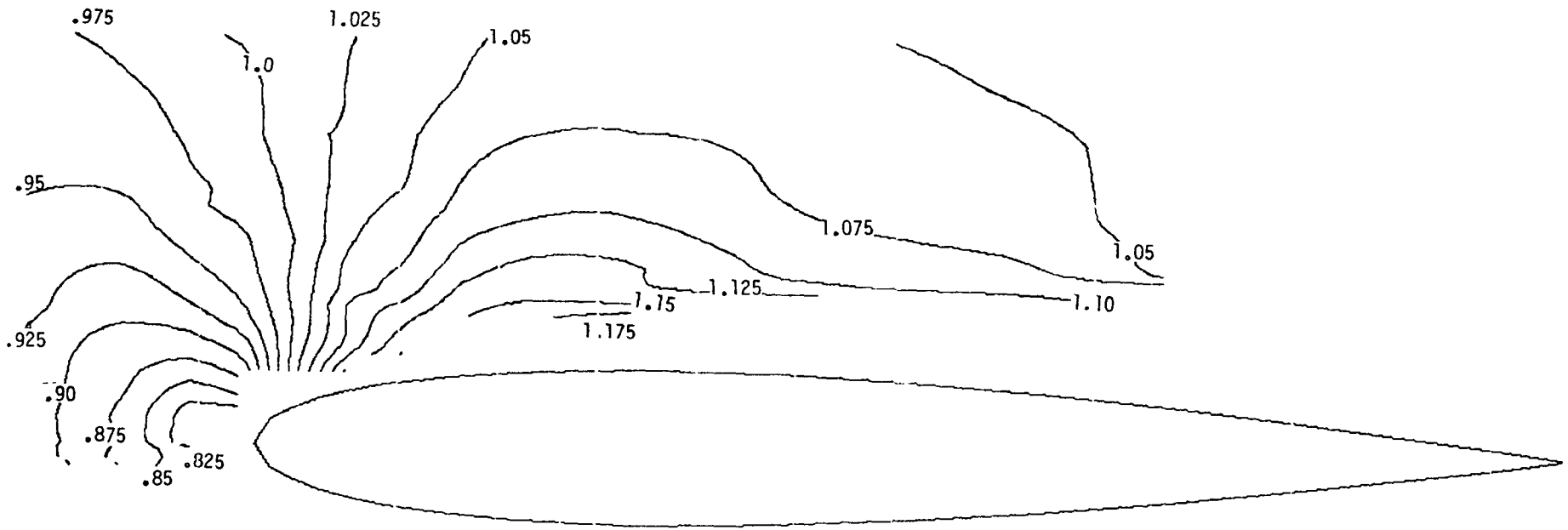

Figure 47.- Contours of constant U_{R_e}/U_T measured over the wing at $\alpha = 0.6^{\circ}$.

APPENDIX A

A LASER VELOCIMETER BUFFER INTERFACE

By James I. Clemmons, Jr.

The laser velocity buffer interface (LVBI) is an electronic instrument for determining the interarrival times of laser velocimeter (LV) data and for the temporary storage of the LV velocity data and the interarrival time data. Interarrival time is an important parameter which can be used for autocorrelation, or as in this case, used to evaluate an approximate time average for comparison with ensemble average. One or two LV high-speed burst counters provide inputs to the LVBI. The velocity data and interarrival time data are sent to a computer for processing. The computer also provides various controls for the proper operation of the interface.

General purpose computers do not have the hardware or software capability for determining the interarrival times of LV data at a rate of 1 million measurements per second. Also, few if any, general purpose computers can input data at a high enough rate and not impair the functioning of the two-component LV. The LVBI has two data acquisition channels each independently capable of receiving data at a rate of up to 1 million velocity measurements per second and determining the interarrival time between successive measurements. Each data acquisition channel has its own data storage memory.

A computer program uses the velocity data and the interarrival time data to produce a history of the velocity of the tunnel flow and to produce a power spectra analysis of the flow at the points of observation (ref. 12). A program is also used to control the LVBI enabling computer definition of the number of data sets (velocity/interarrival time pair) to be acquired, control of data transfer from the LVBI to the computer, and the testing of the LVBI. Figure A-1 is a block diagram of the LVBI, Table A-1 gives the specifications for the LVBI and figure A-2 shows how a typical data set is stored in memory.

CIRCUIT DESCRIPTION

The LVBI has two major divisions: the data acquisition circuits and the computer interface circuits. There may be two data acquisition circuits

(two-channel operation) each having its own interarrival time circuit, memory, and necessary control circuits. The computer interface circuitry serves both data acquisition circuits (fig. A-1).

Interarrival Time Circuits

The interarrival time circuit does not directly produce a value of the real time between two successive LV velocity measurements. It instead counts the number of cycles of a very precise square wave reference signal that occur during successive LV velocity measurements. The period of the square wave specifies the resolution to which the interarrival time may be measured. In order to achieve a reasonable resolution at a 1-MHz data rate, a 10-MHz square wave reference is used. The period for 10 MHz is 100 nsec, therefore resolving the 1 MHz data rate interval to one part in ten.

If a 16-bit wide word is used for the transferring of data to the computer and if a single 16-bit word is used for the interarrival time measurement, then the maximum interarrival time that could be measured is $(2^{16} - 1)$ x (100 nsec) or 65,535 x 100 nsec or 6.5535 msec. If two 16-bit words were used for the interarrival time measurement then the maximum interarrival time that could be measured is $(2^{32} - 1)$x(100 nsec) or 4,294,967,304 x 100 nsec or 429.4967304 sec. The use of a 32-bit interarrival time data word would require an excessively large memory (4096 46-bit memory), and it would require the transferring of three 16-bit words per data set per data acquisition channel to the computer. In order to solve these problems, the LVBI uses a variable resolution interarrival time circuit allowing the use of a single 16-bit data word for the storage and transfer of the interarrival time. As previously discussed, a 16-bit interarrival time data word will alow time measurement to 6.5535 msec when using a 10-MHz reference signal. If a 1-MHz signal were used, then a time measurement to 65.535 msec could be made with a resolution of 1 μsec, and if a 100-KHz reference signal were used, then the maximum time measurement would be 655.35 msec with a resolution of 10 μsec. The change in the reference signal is noted by generating a 2-bit reference signal status (Δt status). These two bits may be stored with the 14-bit LV velocity data making up a 16-bit-wide data word (fig. A-2).

The interarrival time circuit thus consists of a 16-bit $(2^{16} - 1)$ binary cycle counter, a 2-bit binary reference signal status counter, and controls

(fig. A-3). The counters are started by a data ready signal from the LV high-speed burst counter. If the interarrival time being measured is less than 6.5535 msec, the resultant cycle and the 2-bit status (00_2) is stored into the memory along with the LV velocity data. During data reduction, the computer will multiply the cycle count by the resolution indicated by the status bits (00_2), 100 nsec in this case, to obtain the real-time value.

If the interarrival time exceeds 6.5535 msec, the 16-bit cycle counter overflows, incrementing the 2-bit status counter (01_2). The overflow also switches the reference signal to 1 MHz and a correction value of 6553 is loaded into the interarrival time 16-bit cycle counter. The correction value adjusts the counter to the count which would have occurred had the 1-MHz reference signal been used from the beginning of the interval. The worse-case error when using the 1-MHz reference signal is one part in 6553.

Should the cycle counter overflow again, the status counter is incremented (10_2), the 100-KHz reference signal is switched in, the correction value of 6553 is loaded into the cycle counter, and counting resumes. If an additional overflow occurs, the status counter is incremented (11_2), and the cycle counter is filled with zeroes. Either the cycle count, now zero, or the status information (11_2) may be used to indicate that the interarrival time was greater than 655.35 msec and that the interarrival time cannot be computed. A subsequent data ready will reset the status counter to zero (00_2) and switch the reference to 10-MHz allowing normal operation. All calculations involving power spectra will be resumed with this new count.

Data Storage Circuits

The data storage circuits consists of a 4096 x 32-bit memory. The semiconductor memory circuits used allow data to be stored or retrieved in 250 nsec assuring the high-speed operation of the LVBI.

Memory address, the location in memory where data will be stored or retrieved, is generated by a 12-bit (2^{12}) binary counter (fig. A-4). During the data acquisition phase, the entire data set (velocity and interarrival time data) is stored simultaneously, and the address counter is incremented awaiting the next data set. The address counter is usually set to zero at the beginning of the data acquisition phase, but it may be set to any desired value by the computer.

The last memory location into which data is stored or retrieved is set by the computer. This information is stored in the last address latch. Continuous comparison is made between the memory address and the last address and when a true comparison is made the data acquisition is terminated and the computer is flagged.

Computer Interface Circuit

The LVBI communicates with the computer vis two-computer input/output (I/O) channels. Each channel has a 16-bit wide input bus and a 16-bit wide output bus. The first channel is the control/status channel over which the computer sends all major control commands to the LVBI and the LVBI returns information on its status. The data portion of the control commands and the LV velocity/interarrival time data stored in the LVBI memory are transferred over the second channel, the data channel. Stored LVBI data are always transferred to the computer in an LV velocity-interarrival time status/interarrival time data word sequence beginning and ending at the memory address as defined by the computer software. Data from a single data acquisition channel may be transferred or data from both data acquisition channels, in a channel 1/channel 2 sequence, may be transferred. Table A-II gives a listing of the various functions of the two computer I/O channels and figure A-5 is a detailed block diagram of the LVBI.

TABLE A-I -LVBI SPECIFICATIONS

LV data acquisition rates:	1 million data words/second/LV component 14 bits (10-bit mantissa, 4-bit exponent; 2-bit LV counter mode information (not stored))
Interarrival time measured:	1 microsecond to 655.35 milliseconds
Interarrival time resolution:	1 μsec to 6.5535 msec; 100 nsec resolution 6.5535 msec to 65.535 msec; 1 μsec resolution 65.535 msec to 655.35 msec; 10 μsec resolution
Interarrival time data word:	18 bits (16 bits time data, 2-bit status)
Data storage:	4096 32-bit data sets (LV velocity, Δt, Δt status) per data acquisition channel
Computer interface	16-bit data I/O (input/output) 16-bit control I/O
Data transfer rate:	1 million 16-bit data or control words/second

Operational specifications:

Software - computer definition of:
- first data storage location in memory
- last data storage location in memory
- time alloted for LV data acquisition (0 to 9 minutes, 59 seconds; 1 second resolution)
- data for memory diagnostic tests

Electronics: Transistor-transistor logic (TTL), Schottky and low-power Schottky TTL integrated circuits except memory.

Memory - 1K static N-channel metal-oxide-semiconductor (NMOS) circuits.

TABLE A-II

LVBI/COMPUTER I/O SPECIFICATIONS

Control/Status Channel (type of control/status)	Data Channel (Type of data)
Computer to LVBI (Control)	**Computer to LVBI**
Set memory address	Memory address
Set last data address	Last data address
Set real-time clock	Time
Send diagnostic data	Diagnostic data
Start data acquisition	No action
Stop data acquisition	No action
Computer to LVBI (Control)	**LVBI to Computer**
Send LVBI data to computer	Data
Read memory address, channel 1	Memory address, channel 1
Read memory address, channel 2	Memory address, channel 2
LVBI to Computer (Status)	**LVBI to Computer**
Memory full/time limit	No action
Channel 1 active	"
Channel 2 active	"
Channel 1 transferring data	"
Channel 2 transferring data	"
LV or Δt data being transferred	"
LV counters in 5/8 or 10/16 mode	"
LV counters in time or velocity mode	"

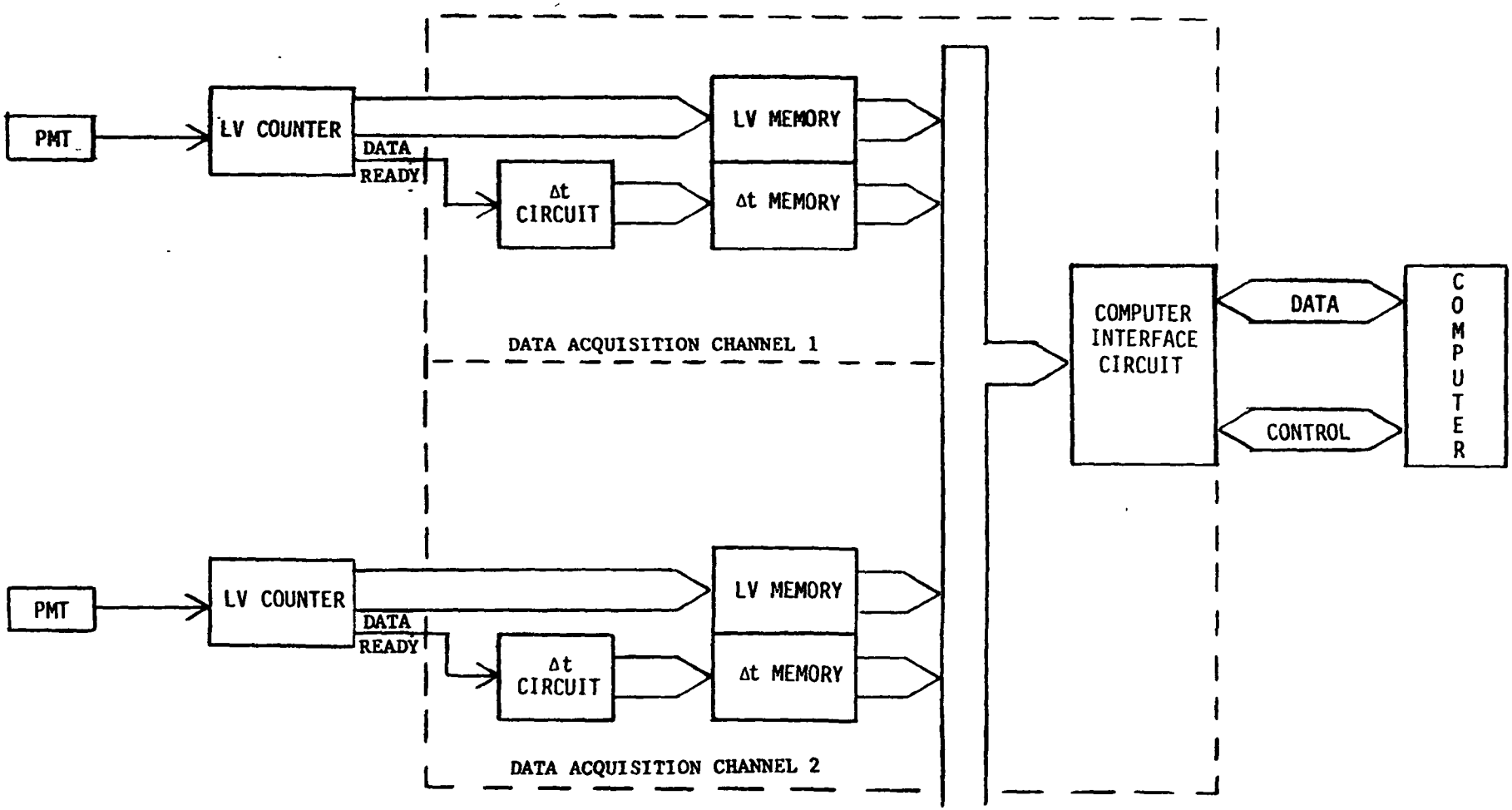

Figure A1. - Laser velocimeter buffer interface (2-component configuration).

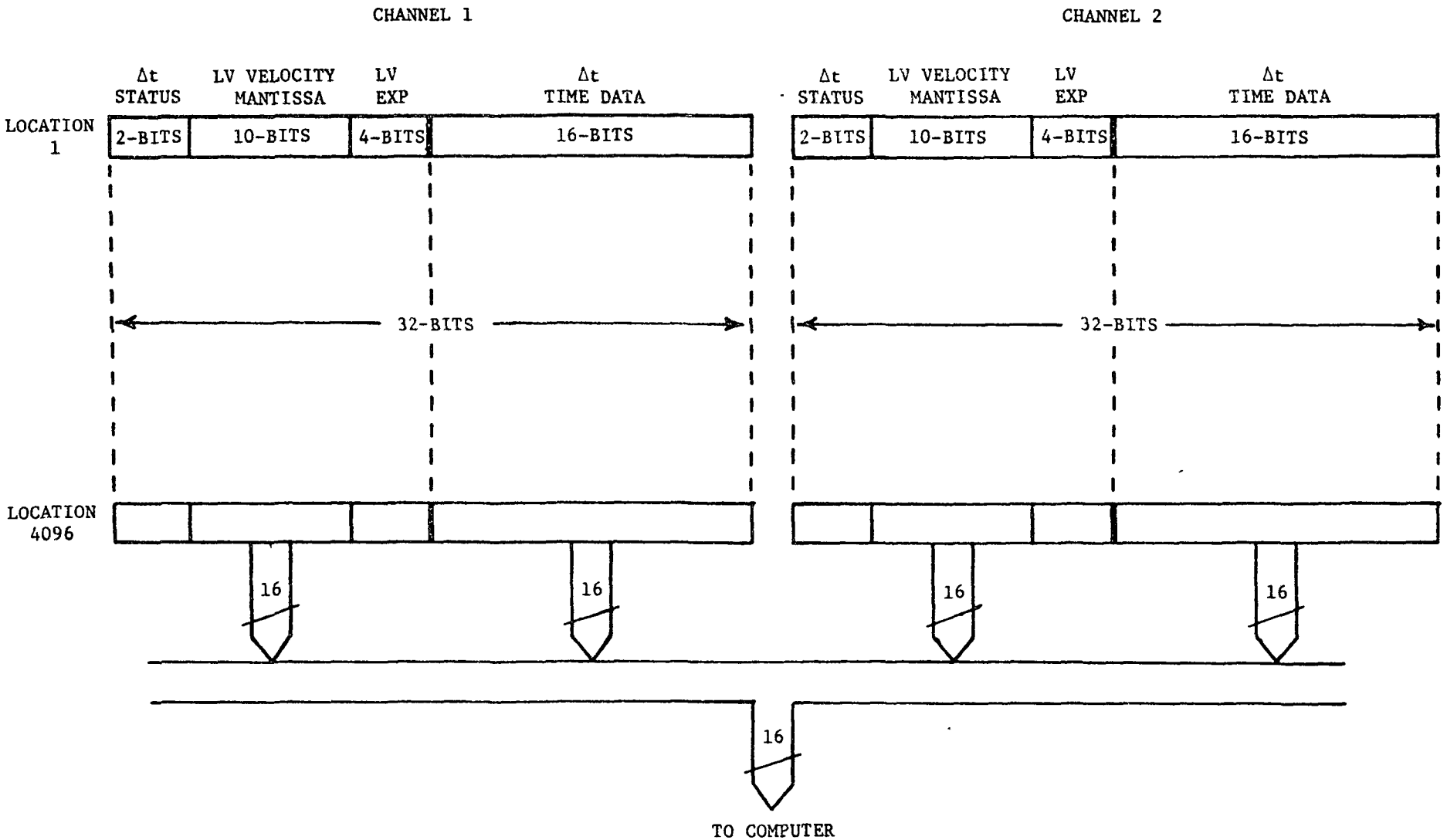

Figure A2.- Data store diagram.

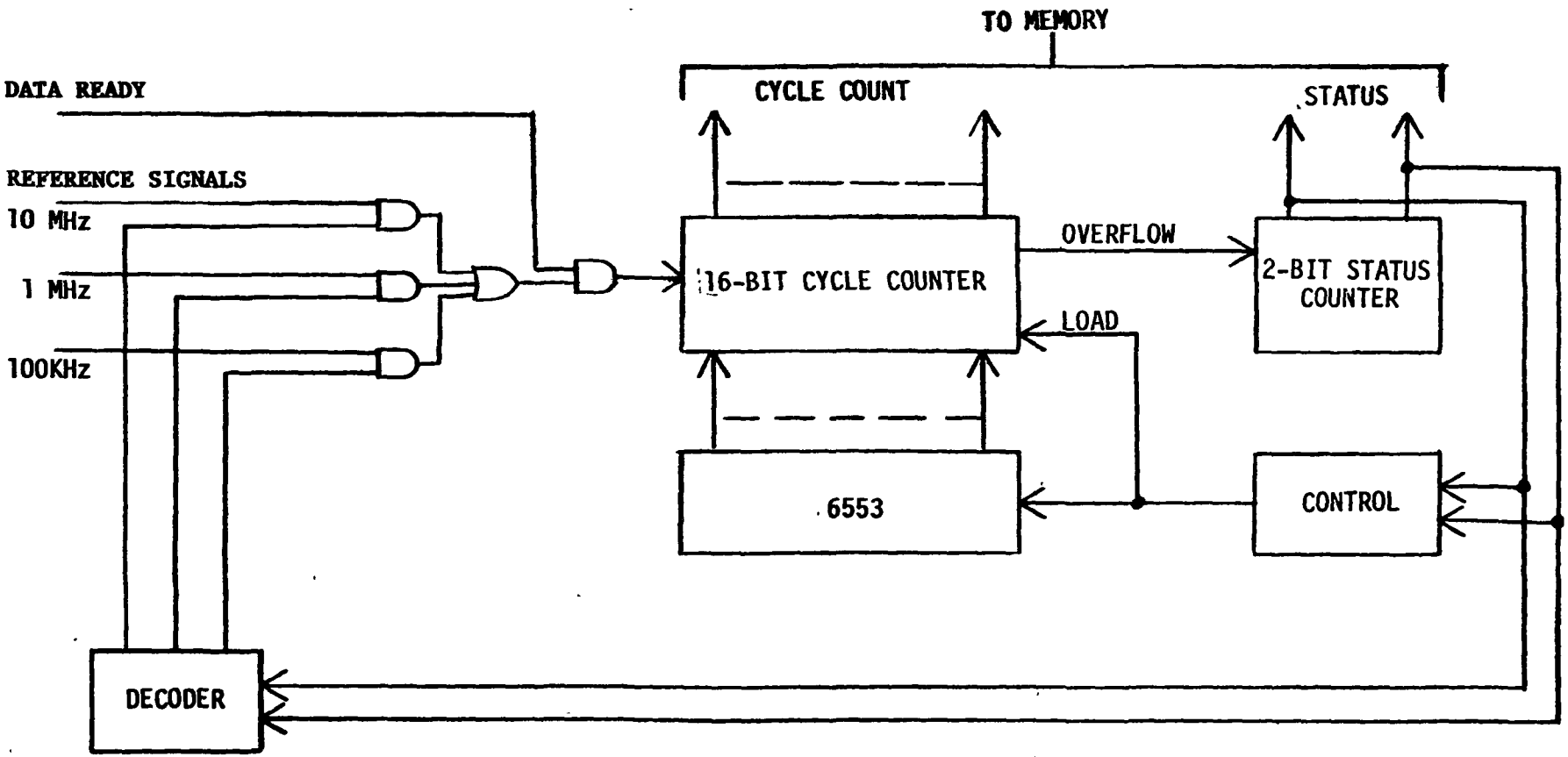

Figure A3.- Interarrival time circuit.

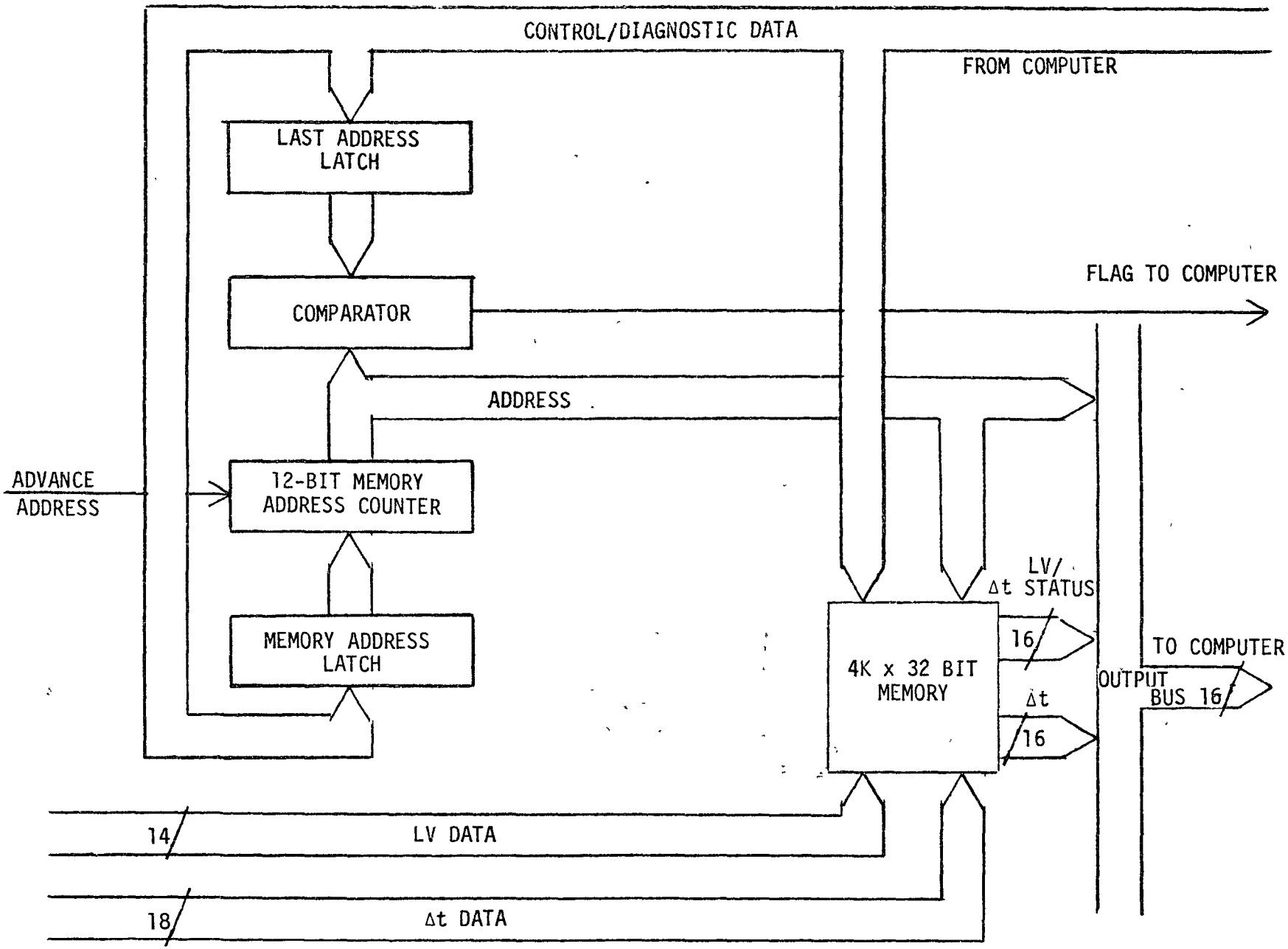

Figure A4. - Data Storage Circuits

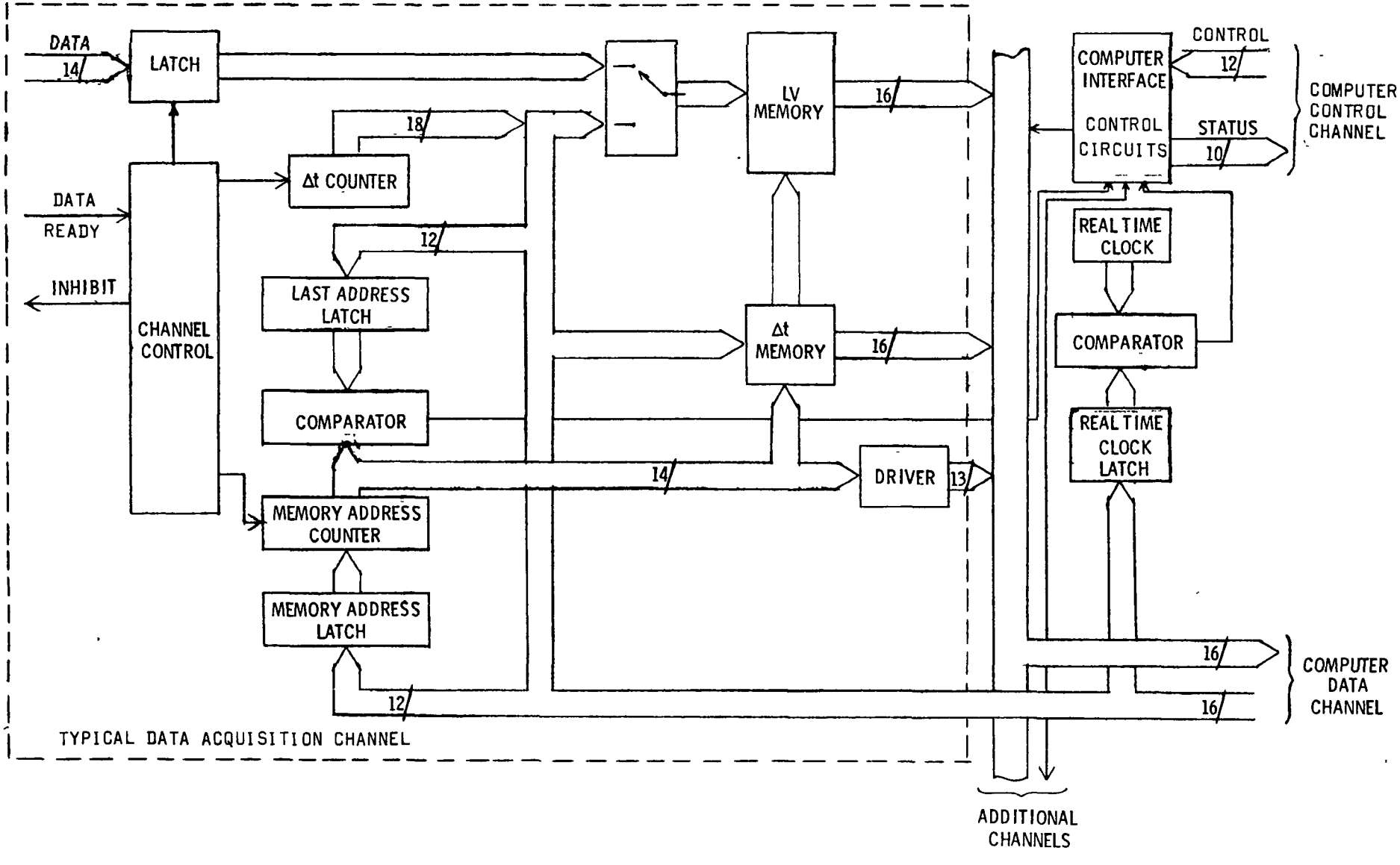

Figure A5. - Laser velocimeter and buffer memory.

APPENDIX B

LASER VELOCIMETER HISTOGRAMS WITH INTERPRETATION

The histograms for every data run recorded during this investigation are presented in this appendix. The order of presentation is as follows:

	Figure
Free Stream	B-1
Wing at $\alpha = 4.75°$	B-2 to B-15
Wing at $\alpha = 0.6°$	B-16 to B-22

Each figure is presented (except free-stream data) with a sketch of the wing cross section with arrows indicating the position, direction, and relative magnitude of the mean velocity vector. A run consisted of an ensemble of data acquired at the position desired. The scan, therefore, is a series of runs at various y_c/c positions at constant chordwise position. The histogram is a graphical representation of the variation of velocity measured over a time period as mentioned in the text. Statistical analysis of each run can be found in corresponding tables.

To interpret the histograms, one must be prepared to consider a velocity measurement not as a single measurement, but as a large number of measurements (ensemble) which is assumed to describe the time-average nature of the flow at the measurement location. Thus, more than just the average velocity can be obtained from the velocity measurements. It is necessary to mention that the LV is not a continuous measurement device such as a hot-wire anemometer but acquires data randomly (Poisson distributed in time) depending upon the rate at which particles of proper size pass through the sample volume. Only when this data rate is continuously large can the system be considered to be quasi-continuous.

The histograms are presented with C_i, percentage of that number of measurements within incremental velocity band, as a function of velocity. In all cases, the U_L component is presented on the left and the V_L component on the right.

The method of determining the expected value of the velocity from a histogram is described in the text. The breadth of the histogram provides a means of

relative determination on the unsteadiness of the flow. For example, the last two runs in figure B-1 are data for higher tunnel speeds than the first five. These histograms would indicate that the unsteadiness of the flow is greater at higher speeds.

Most of the histograms have a form of being Gaussian in nature indicating that the flow has just as great a probability to fluctuate towards lower velocities as to higher velocities. In some cases, particularly near the leading edge of the wing (see fig. B-4, runs 31-37), the histogram is skewed. A histogram resulting from a random velocity unsteadiness in magnitude would be symmetrical about the peak. However, if a steady velocity were oscillating in angle, skewness in the histogram would result. Consider the measurement direction $\pm 45°$ to free stream. A steady free-stream flow oscillating in angle would have mean velocity components of magnitude cos 45° in the two measurement directions. A positive oscillation in angle would result in positive deviation from the mean in the -45° histogram. Similarly, the negative oscillation in angle affects the component histograms. Thus, an unsteadiness in flow angle could, if the mean unsteady angle is nonzero, generate the skewed histograms in the measurement directions $\pm 45°$ to flow direction.

In many situations, a velocity measurement at a point experiences a peculiar phenomenon. If the velocity at a point does not fluctuate randomly, but oscillates between two pronounced velocity values, a so-called double-peaked histogram will occur. (See figs. B-4, B-5, B-6, and B-7, runs 37, 50-53, 63-68, and 78-79, respectively.) These double-peaked histograms indicate that for a large percentage of the time the velocities are centered about one velocity, and at other times they are centered at another velocity. This unexpected phenomenon, at least for the wing at $\alpha = 4.75°$, is discussed fully in the text.

An intuitive confidence in the velocity measurement can be obtained by analysis of the histograms. If the histogram generated is a well-defined shape (whatever it may be), then one may consider that there is a sufficient number of samples in the ensemble to obtain a reasonable measure of the velocity characteristics. However, if the histogram is very ragged (see fig. B-15, runs 190, 191, and 192), it can be very difficult to associate a great detail of confidence in the

statistical parameters calculated from such an ensemble. In these cases, however, realizing that the measurements were obtained very close together in space, the mean velocity calculations are reasonable.

The statistical parameters calculated from these histograms are presented in: Table 2 for the free-stream condition; Table 3 for the wing at $\alpha = 4.75°$; and Table 4 for the wing at $\alpha = 0.6°$.

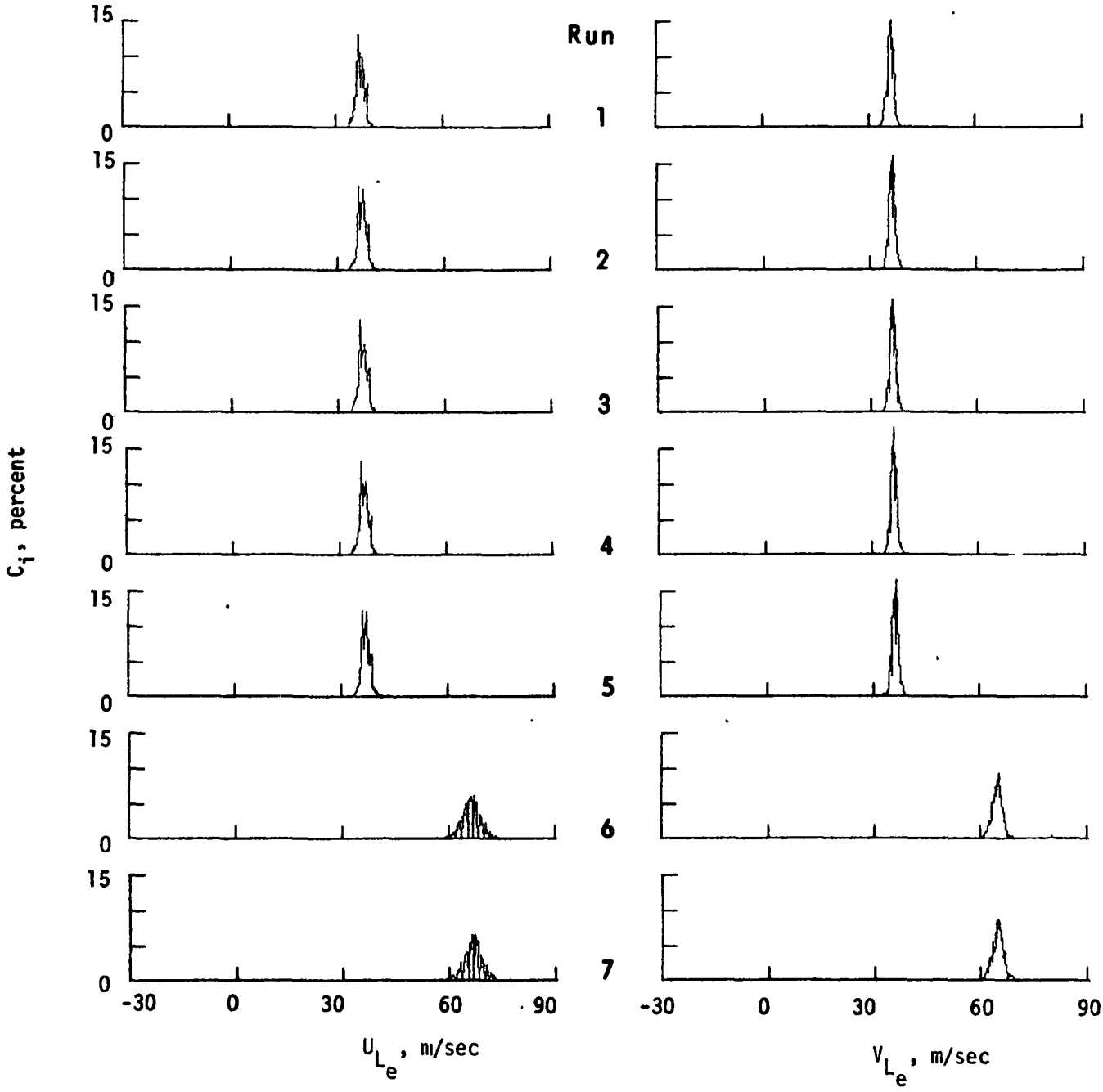

Figure B-1.- Histograms for free-stream measurements.

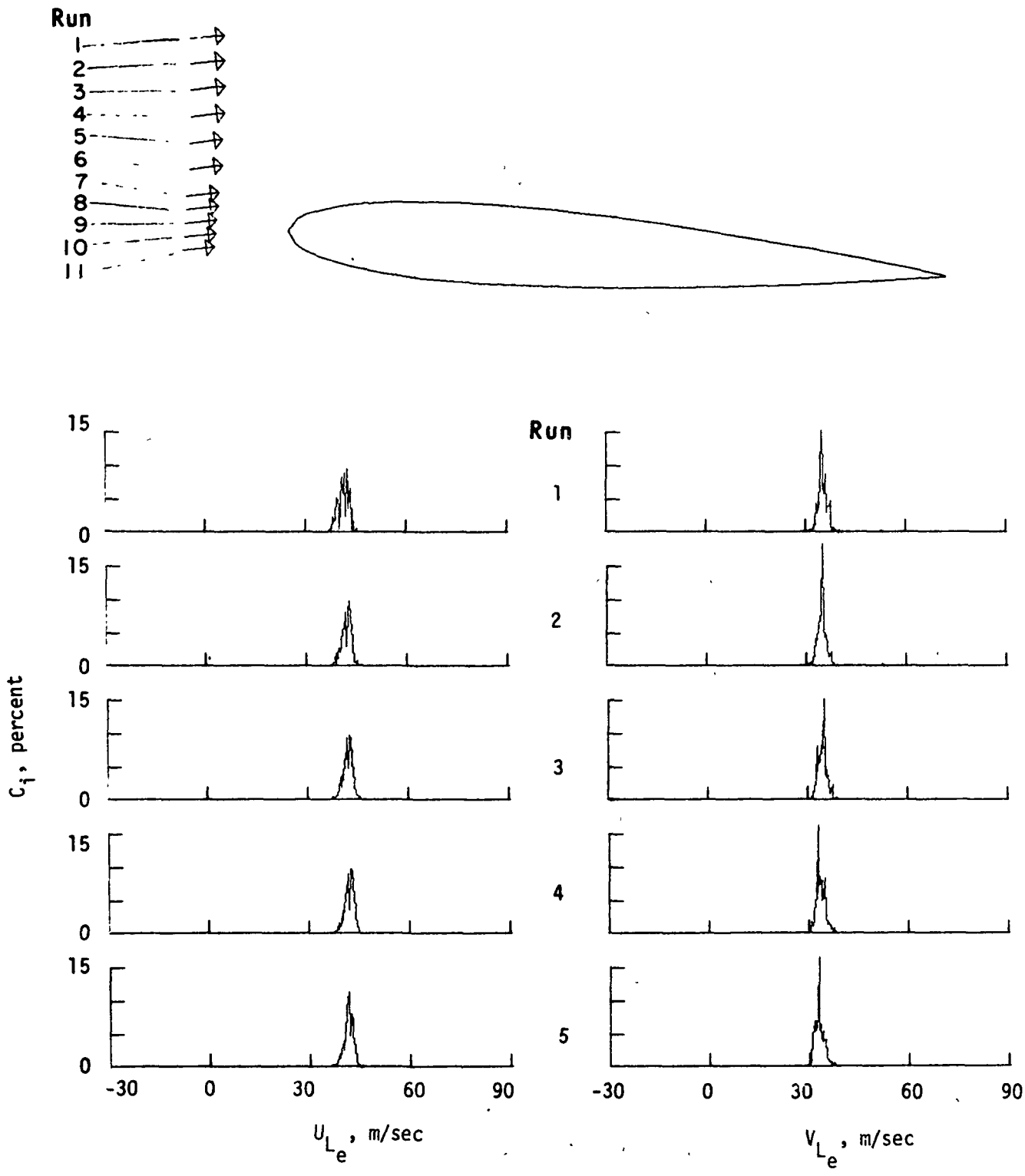

Figure B-2.- Histograms in scan at constant $x_c/c = -0.16$, $\alpha = 4.75^0$.

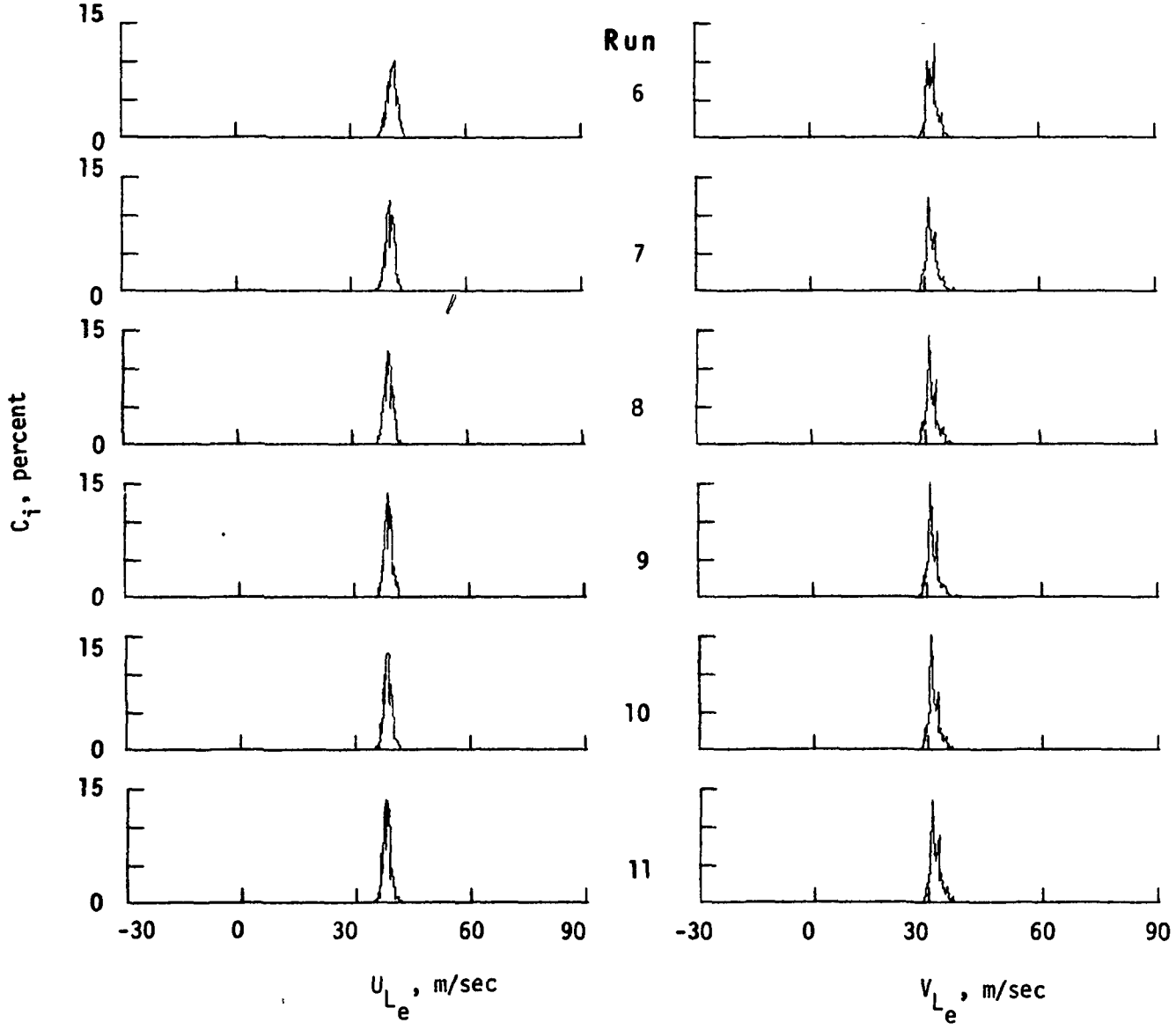

Figure B-2.- Concluded.

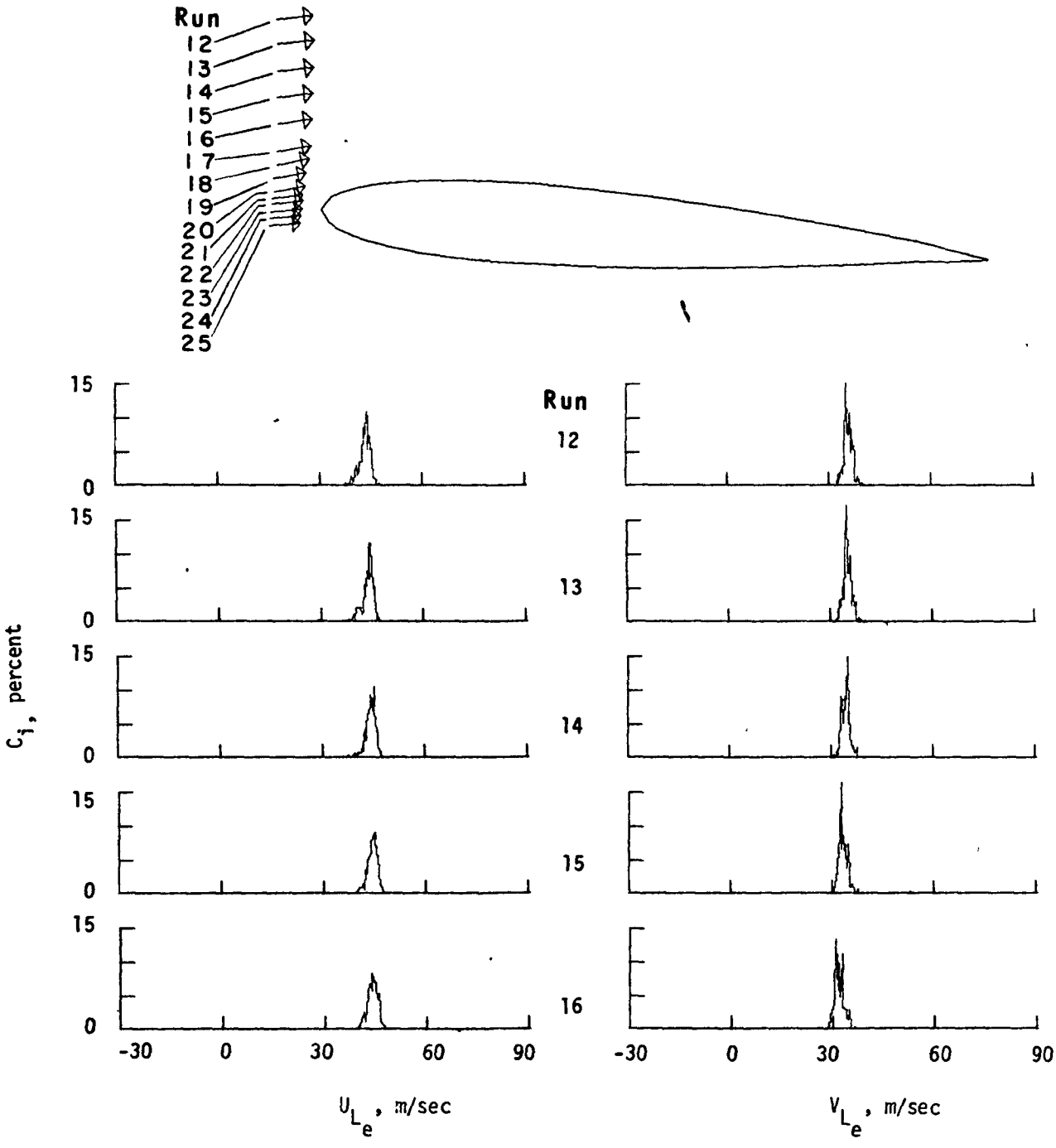

Figure B-3.- Histograms in scan at constant $x_c/c = -0.08$, $\alpha = 4.75^{o}$.

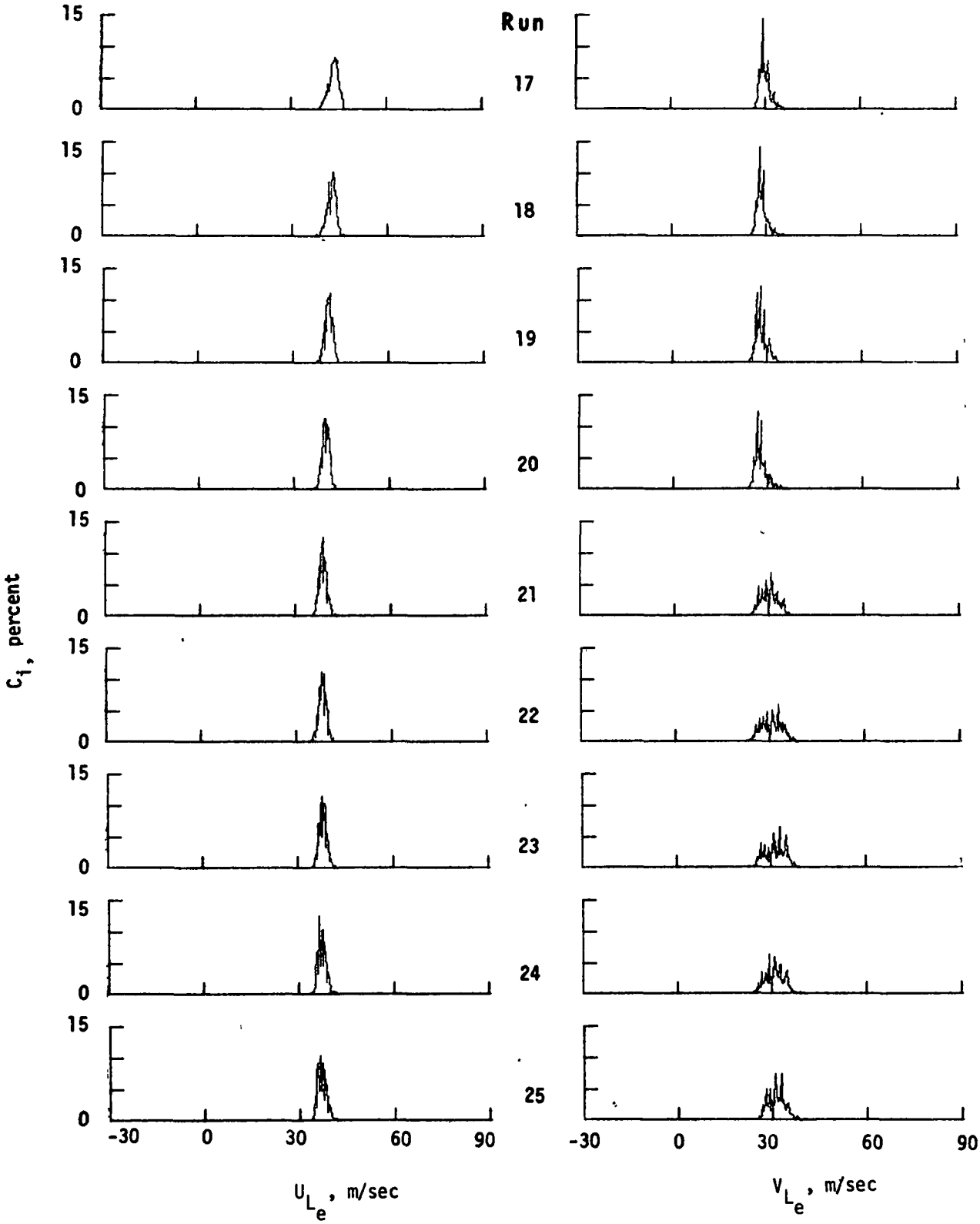

Figure B-3.- Concluded.

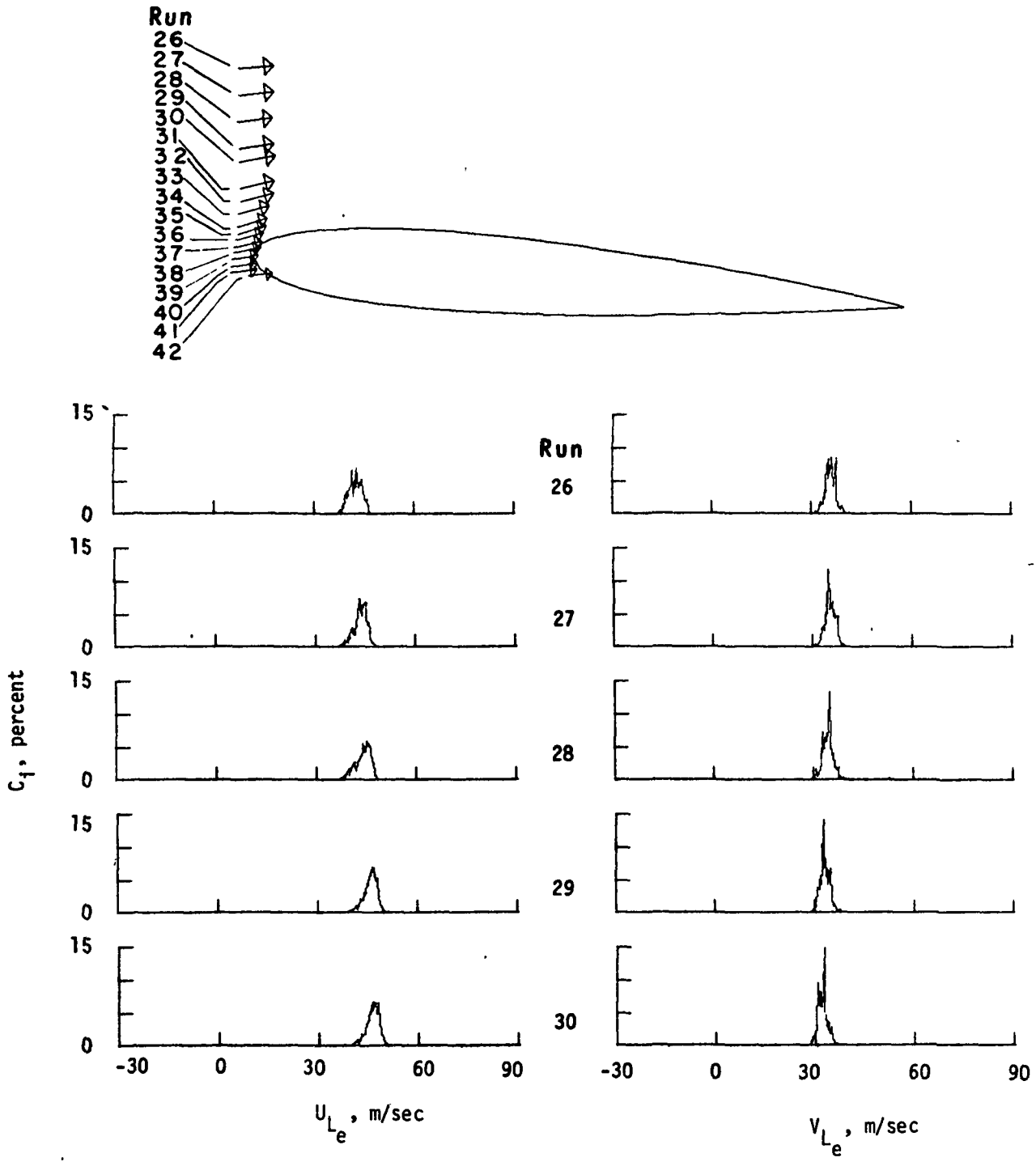

Figure B-4.- Histograms in scan at constant $x_c/c = -0.04$, $\alpha = 4.75^{o}$.

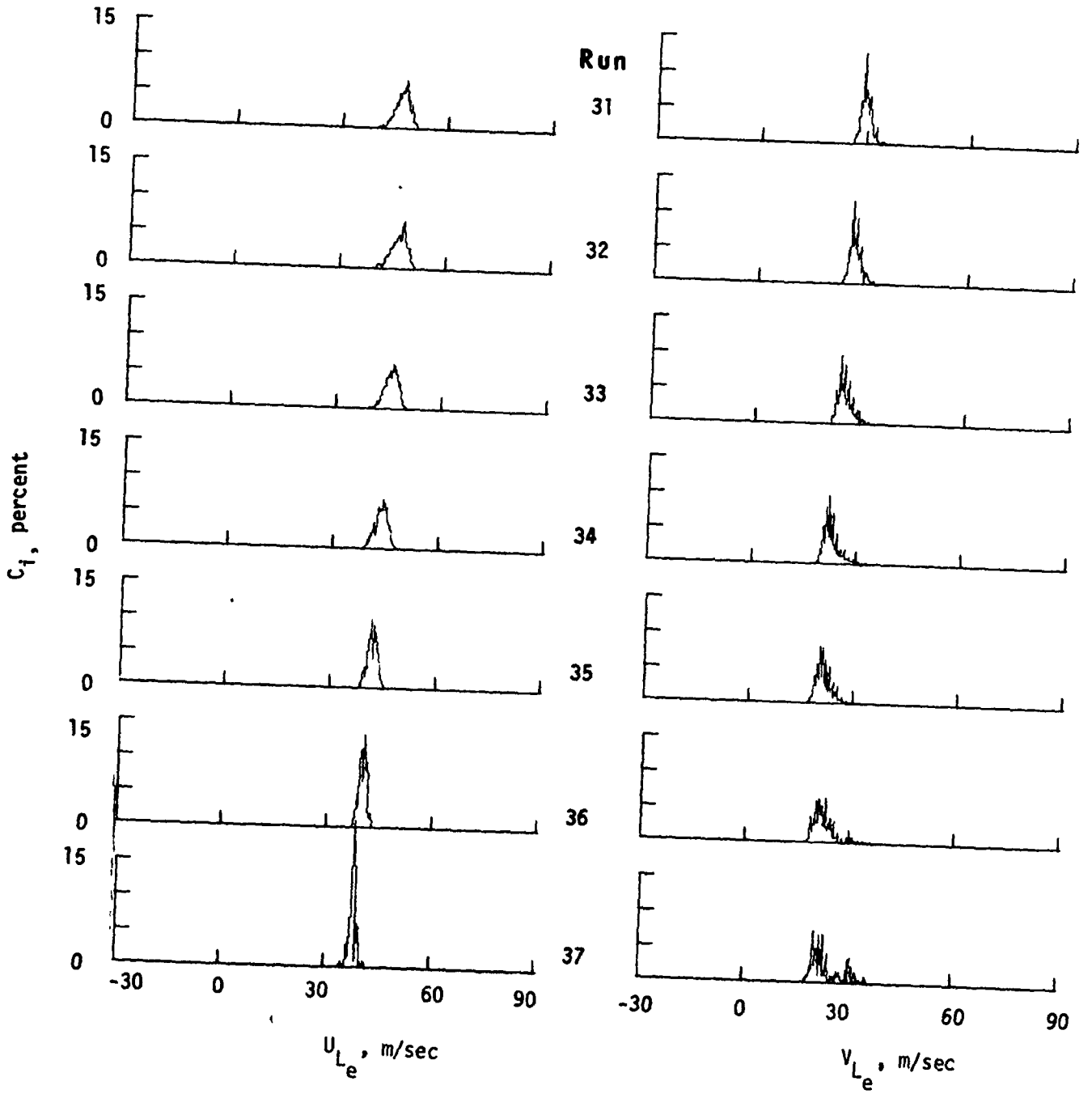

Figure B-4.- Continued.

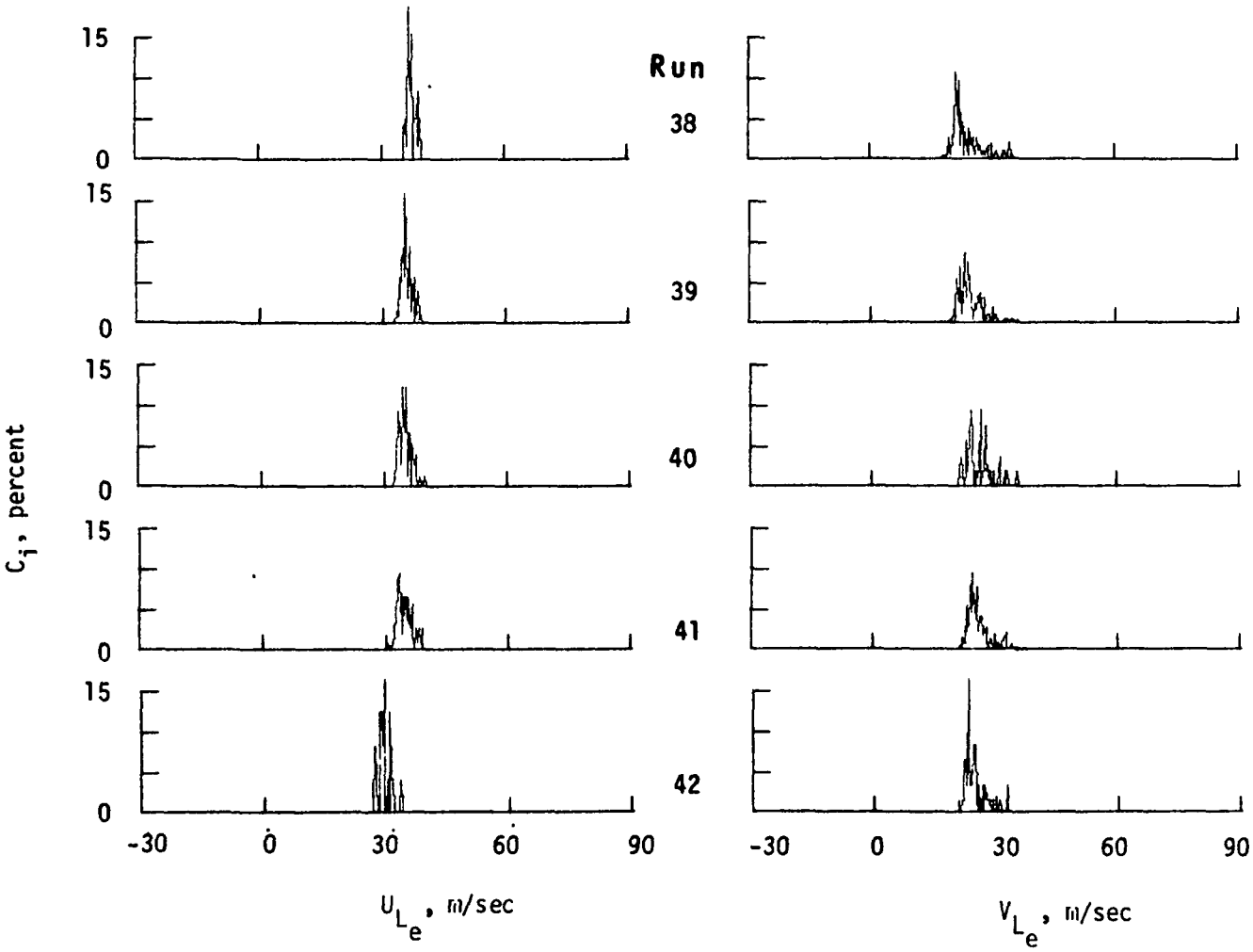

Figure B-4.- Concluded.

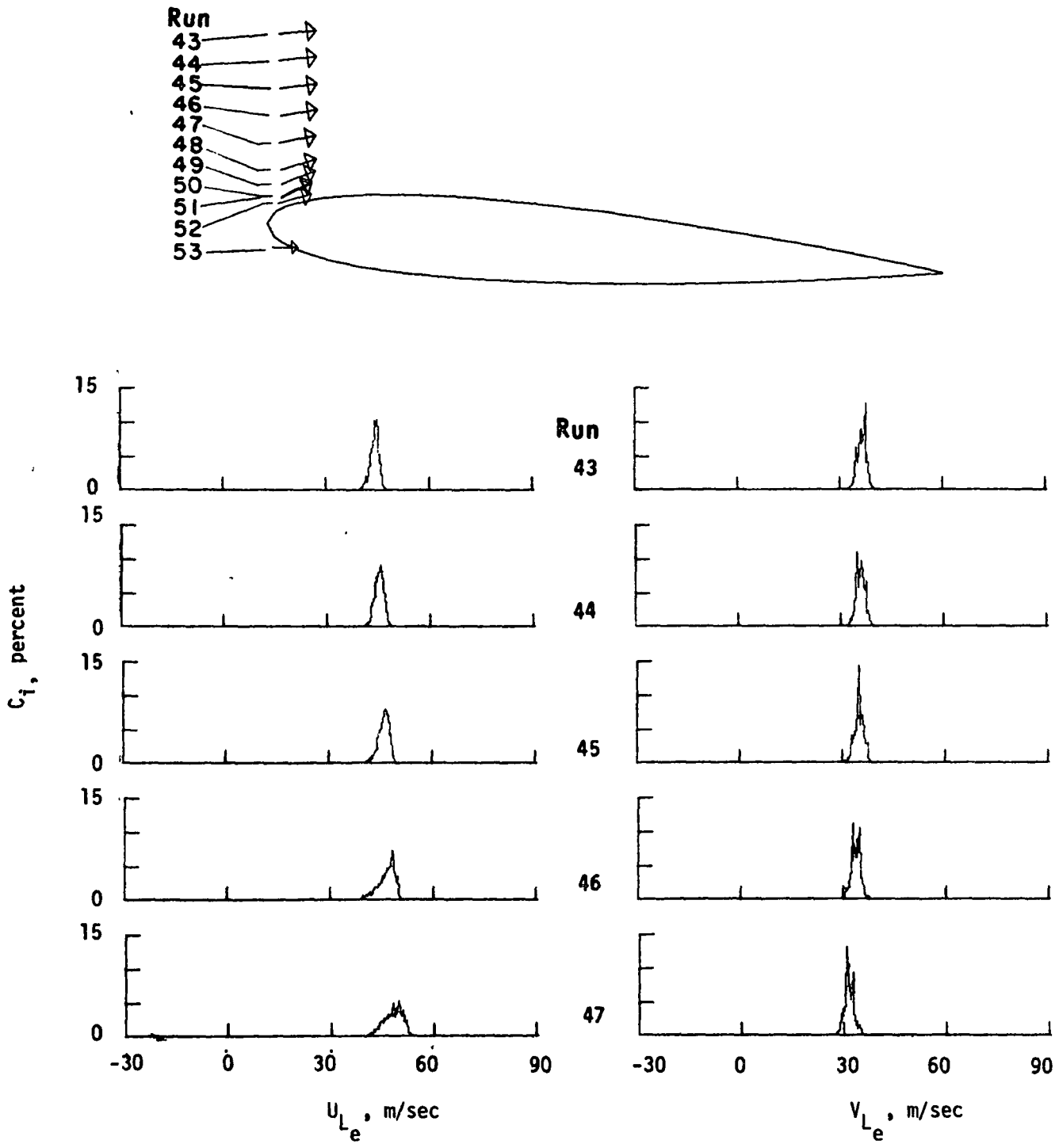

Figure B-5.- Histograms in scan at constant $x_c/c = 0$, $\alpha = 4.75^o$.

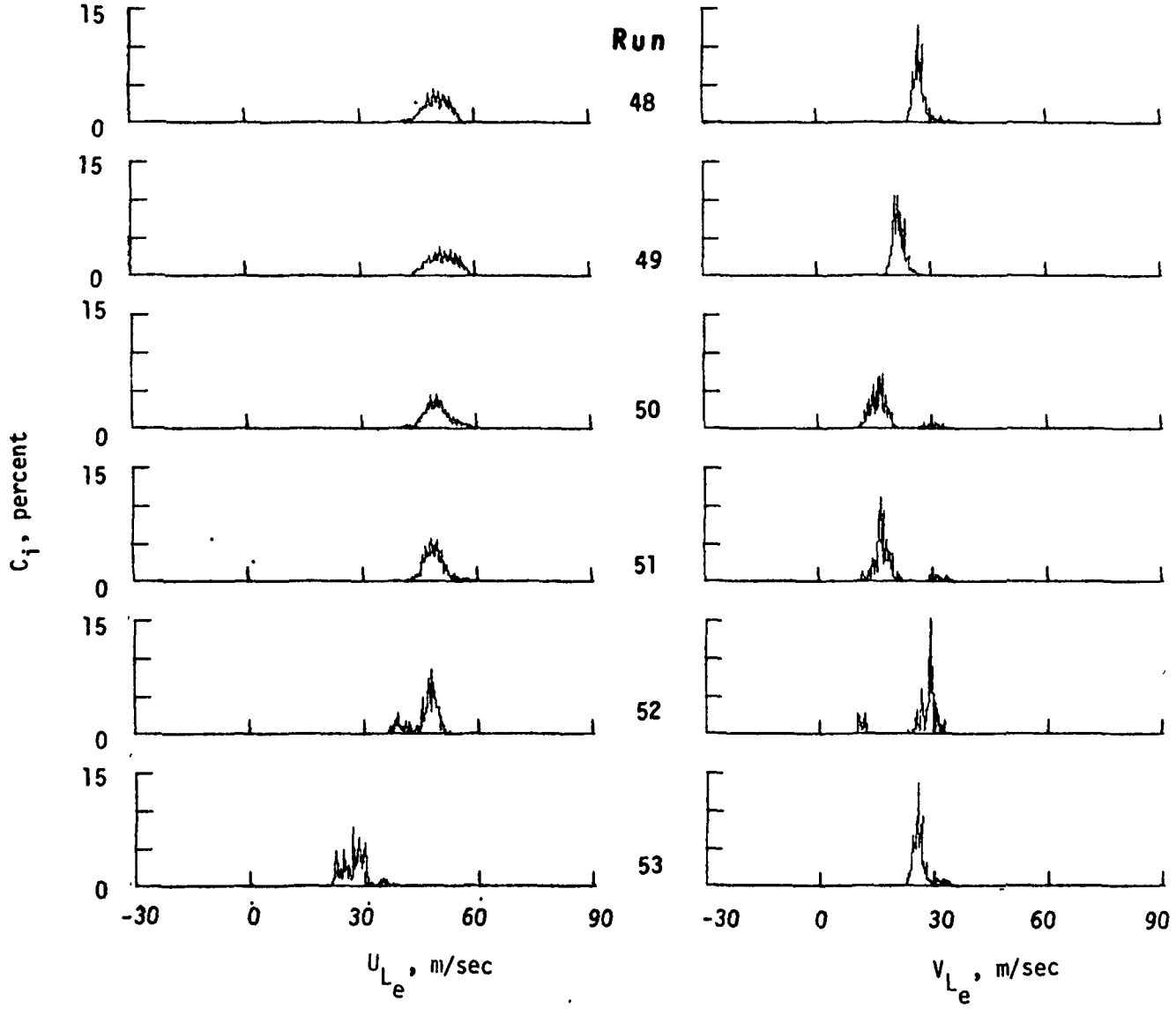

Figure B-5.- Concluded.

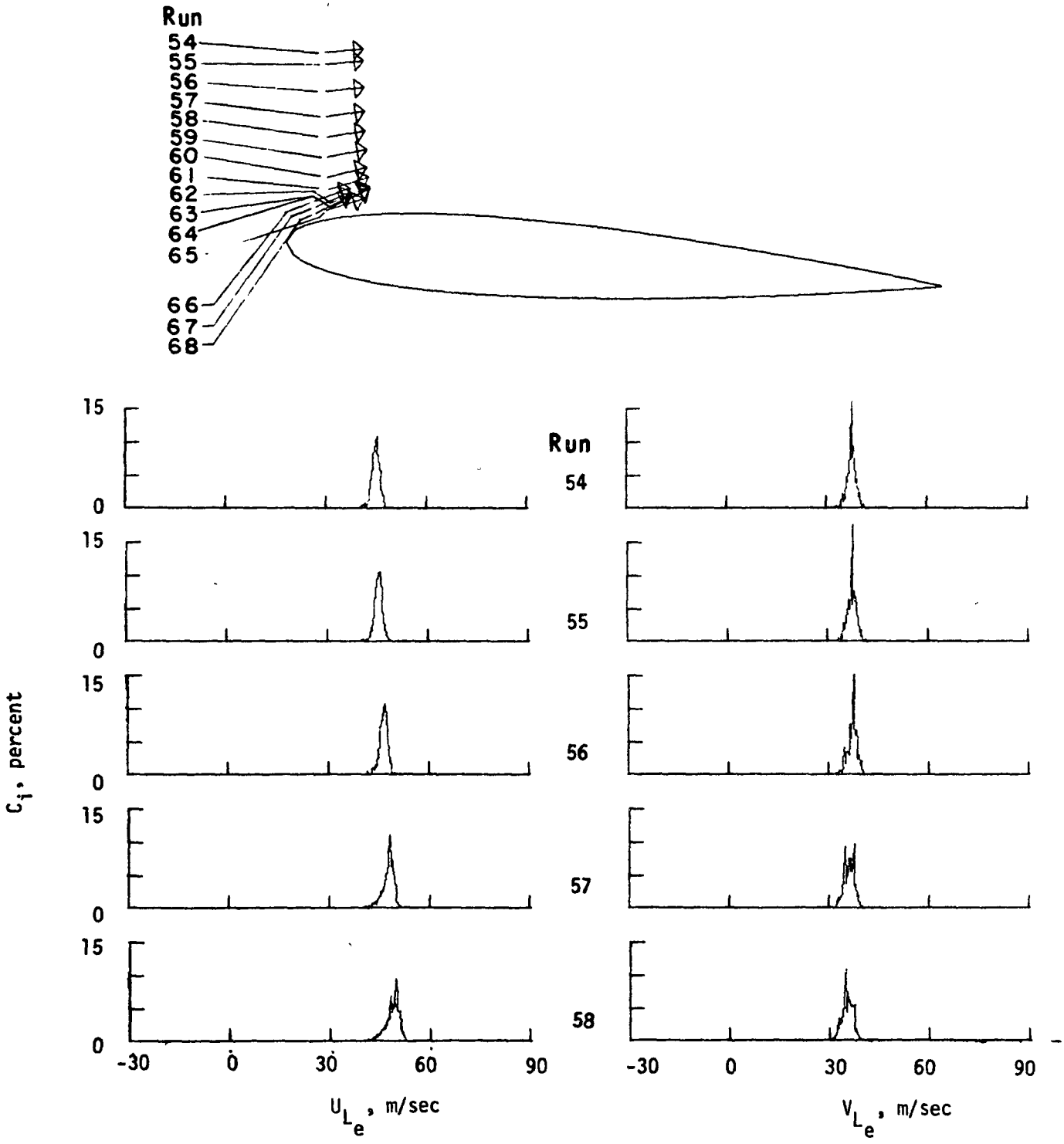

Figure B-6.- Histograms in scan at constant x_c/c = 0.03 and 0.04, α = 4.75°.

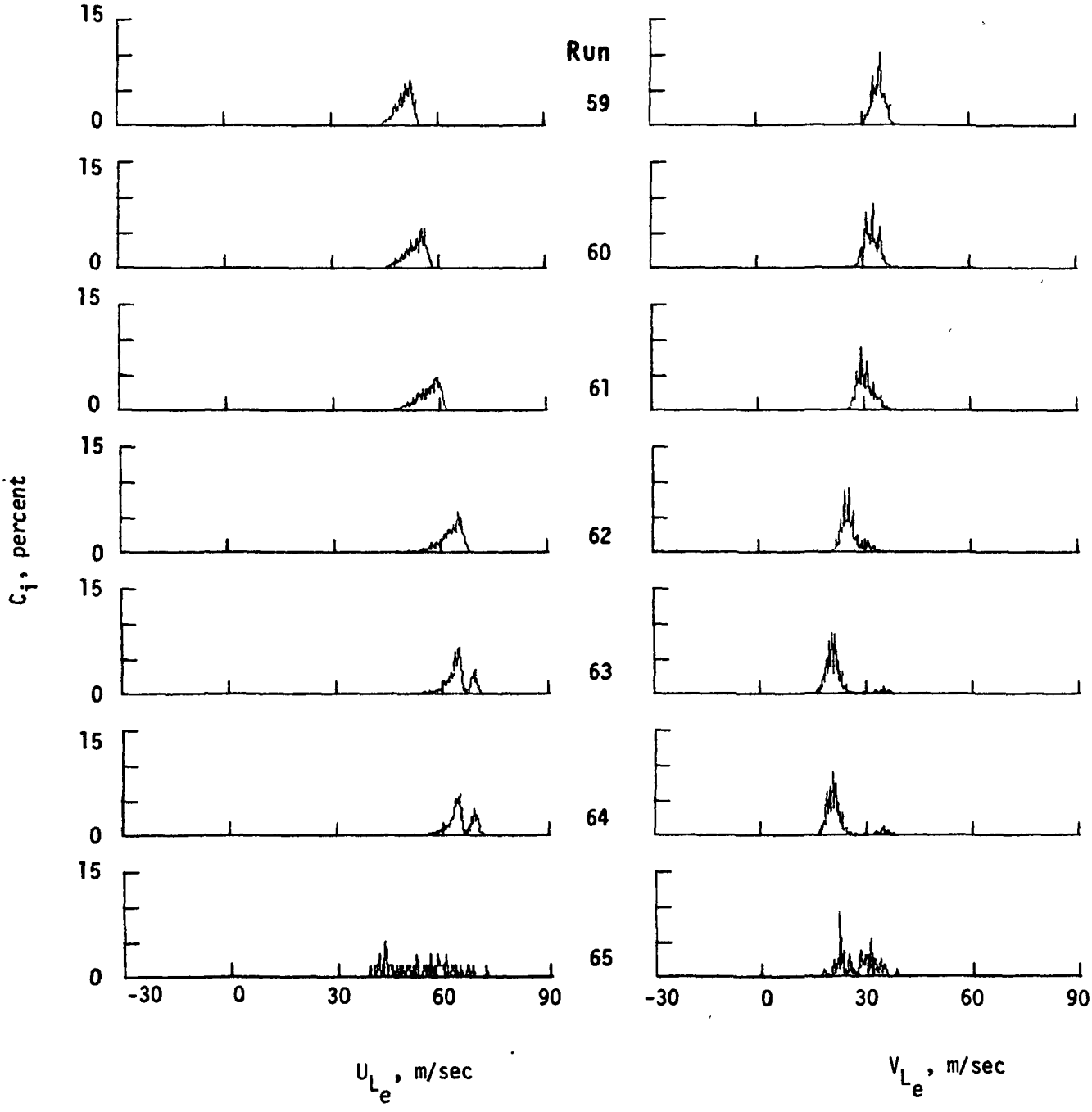

Figure B-6.- Continued.

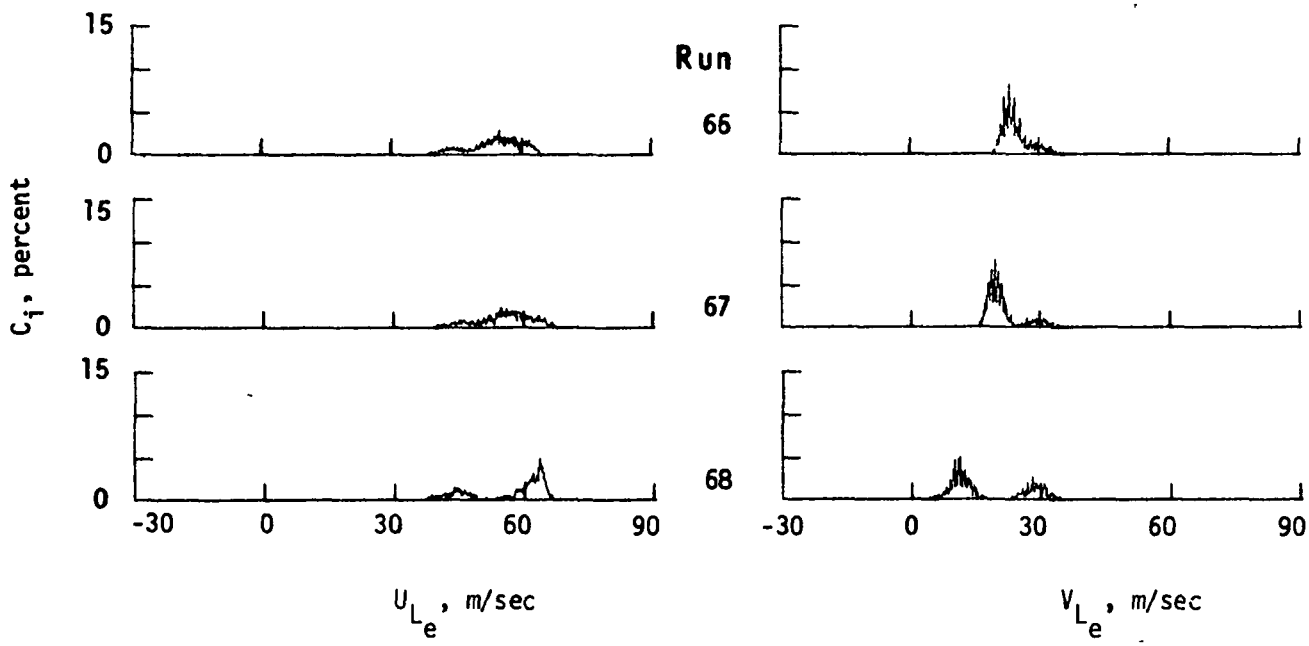

Figure B-6.- Concluded.

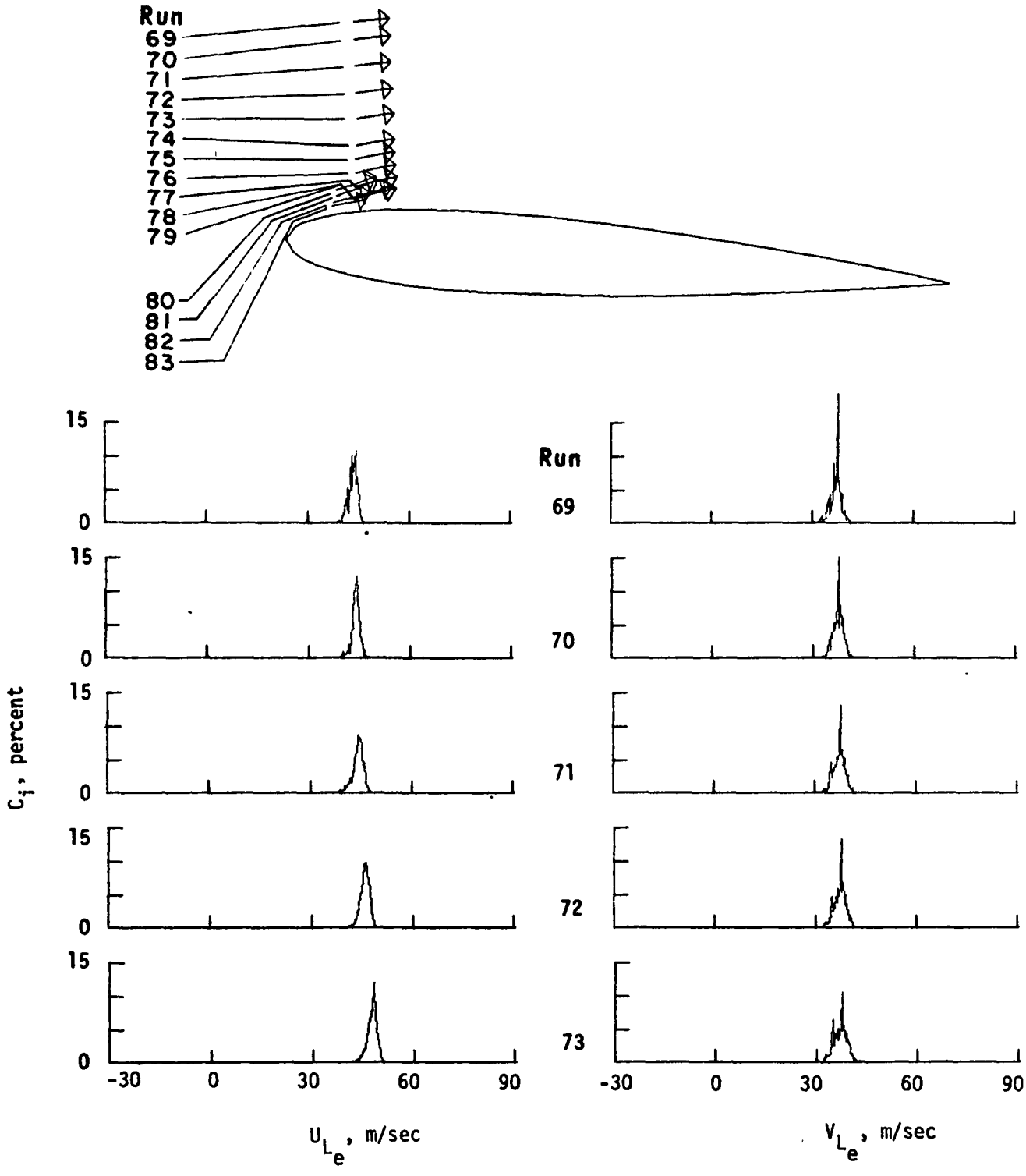

Figure B-7.- Histograms in scan at constant x_c/c = 0.06 and 0.09, $\alpha = 4.75^{o}$.

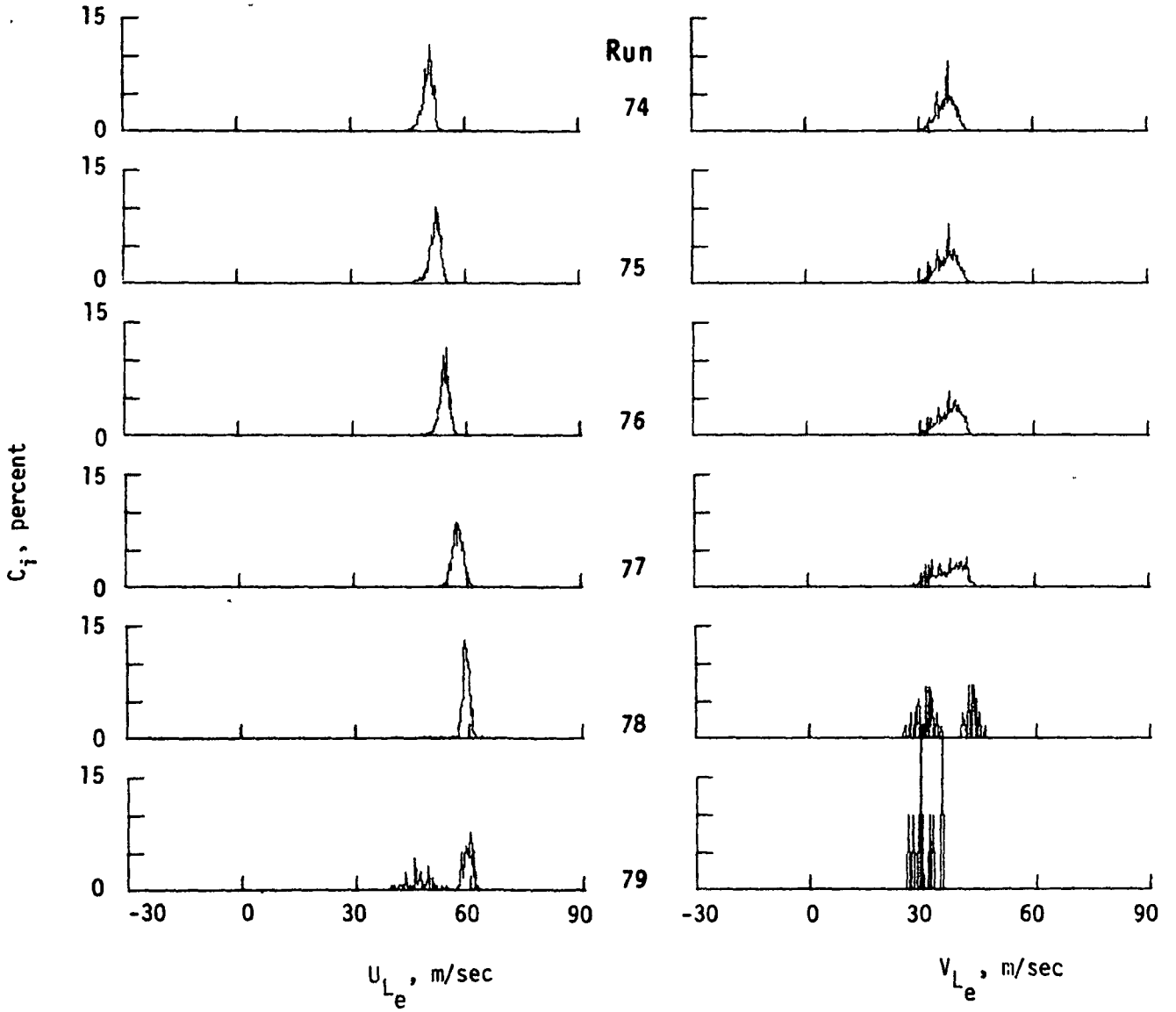

Figure B-7.- Continued.

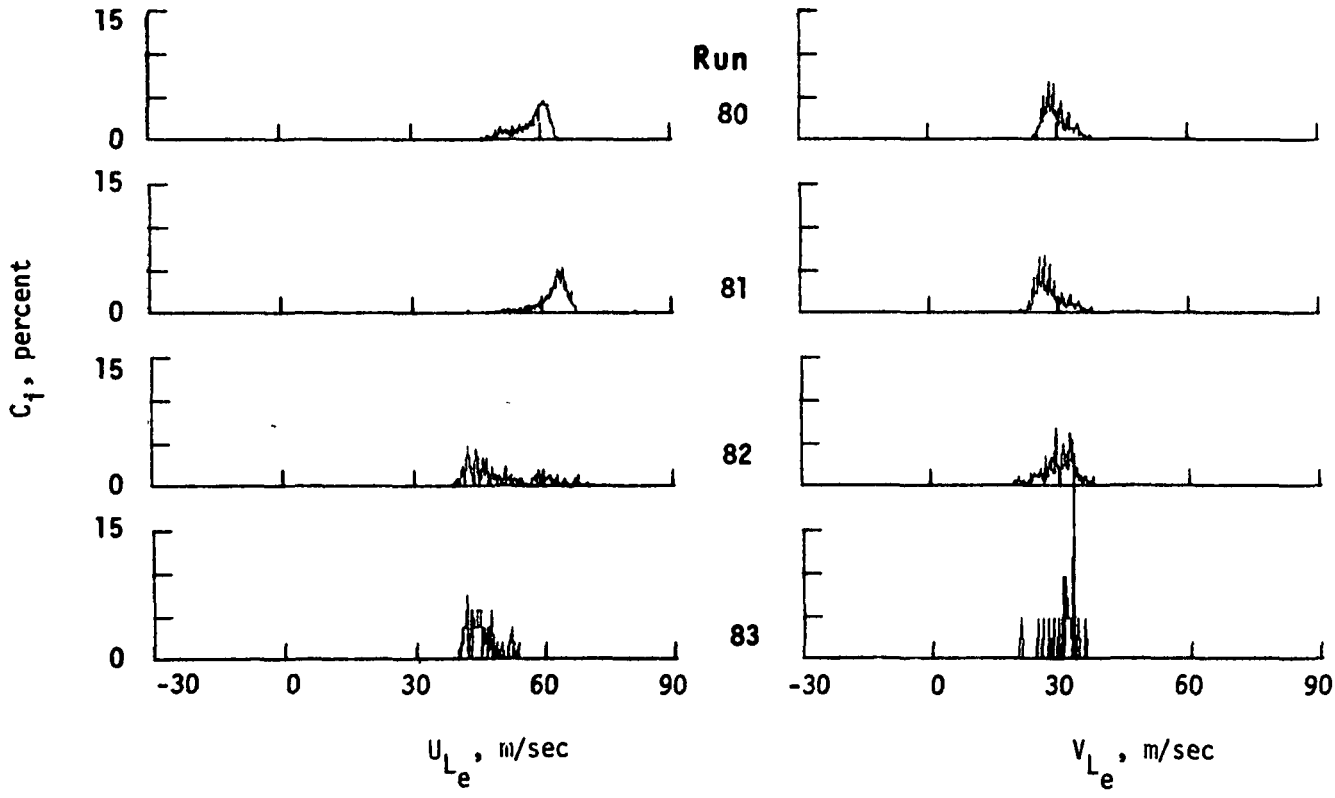

Figure B-7.- Concluded.

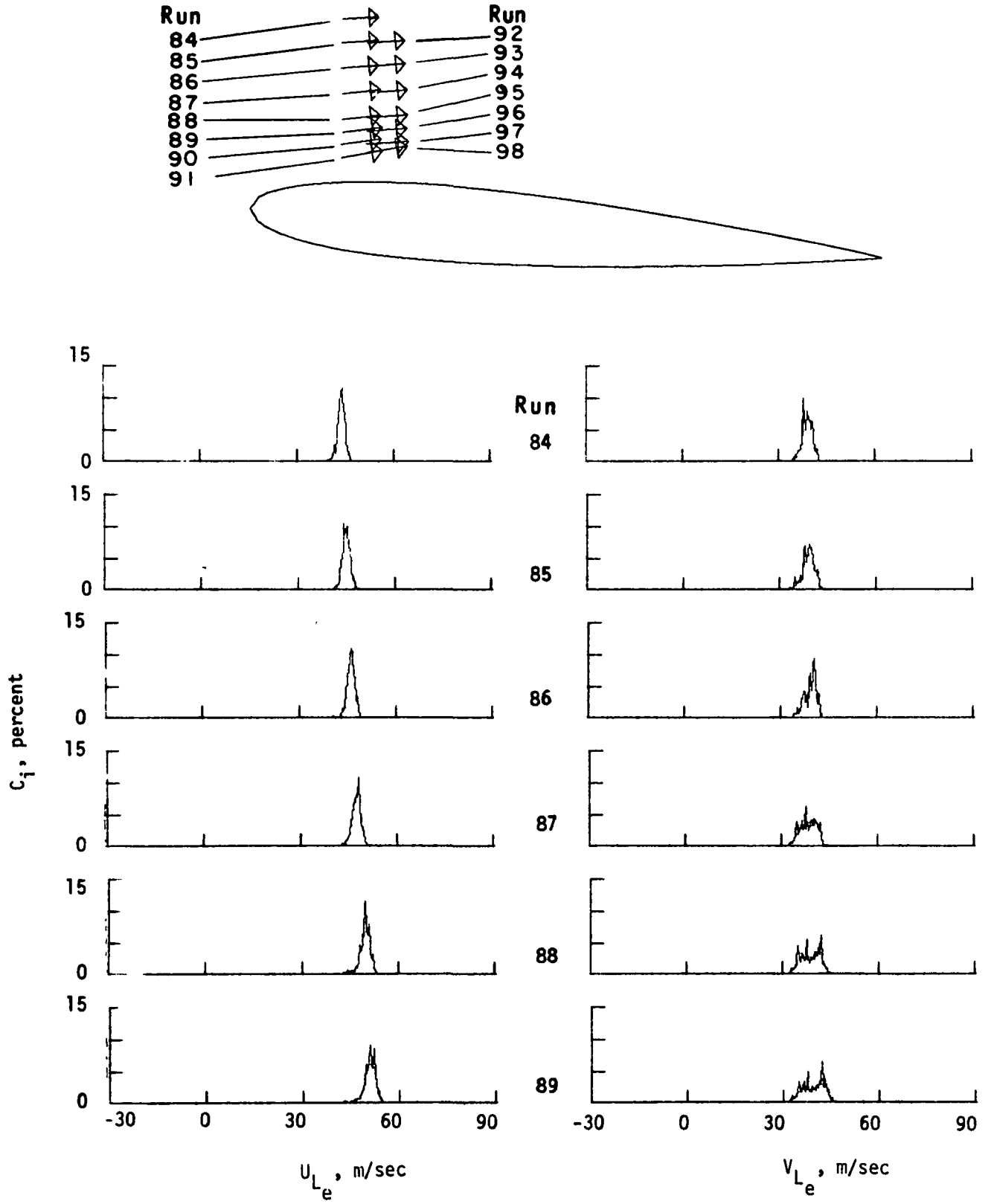

Figure B-8.- Histograms in scan at constant x_c/c = 0 13 and 0.17, $\alpha = 4.75^{o}$.

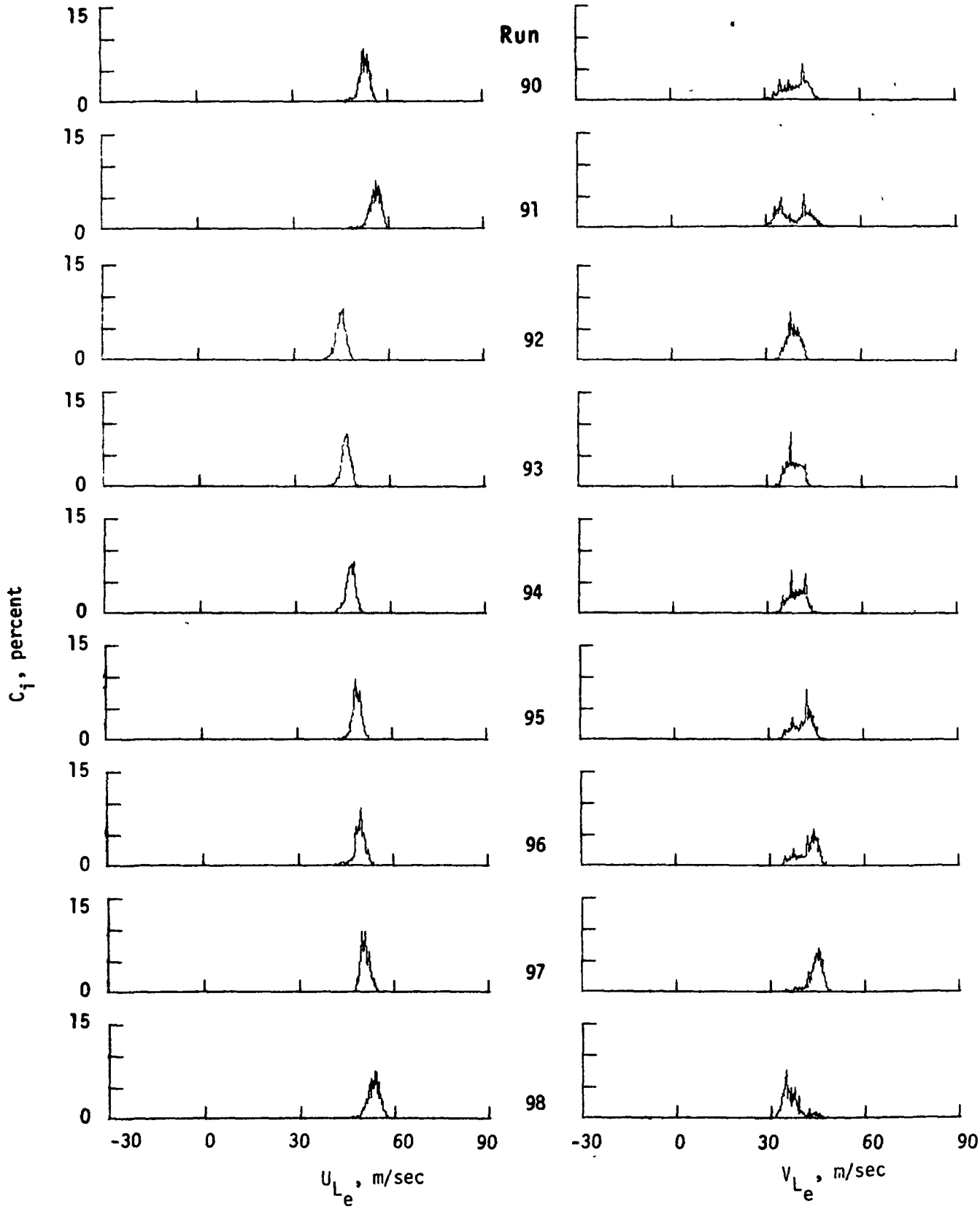

Figure B-8.- Concluded.

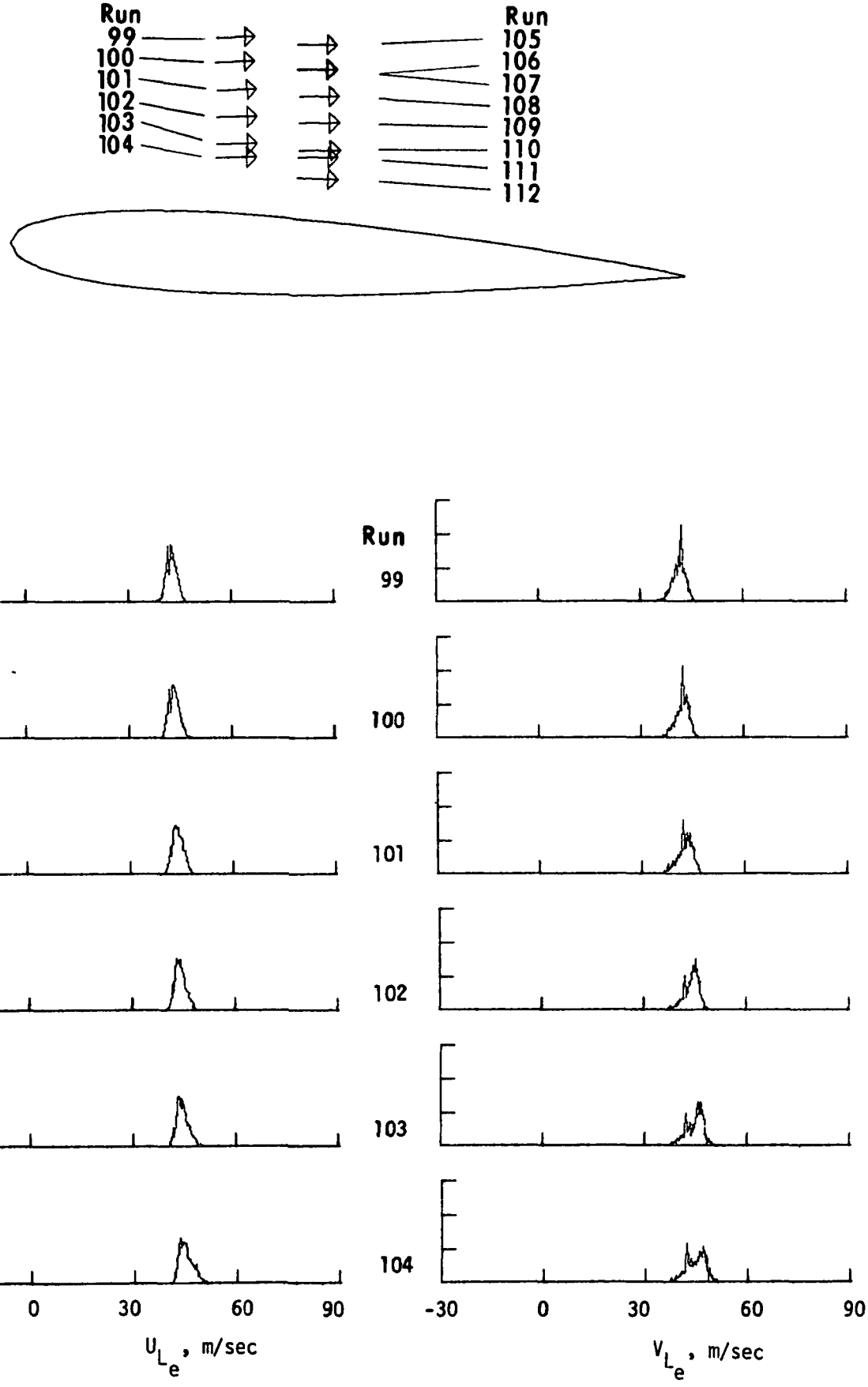

Figure B-9.- Histograms in scan at constant x_c/c = 0.29 and 0.42, α = 4.75°.

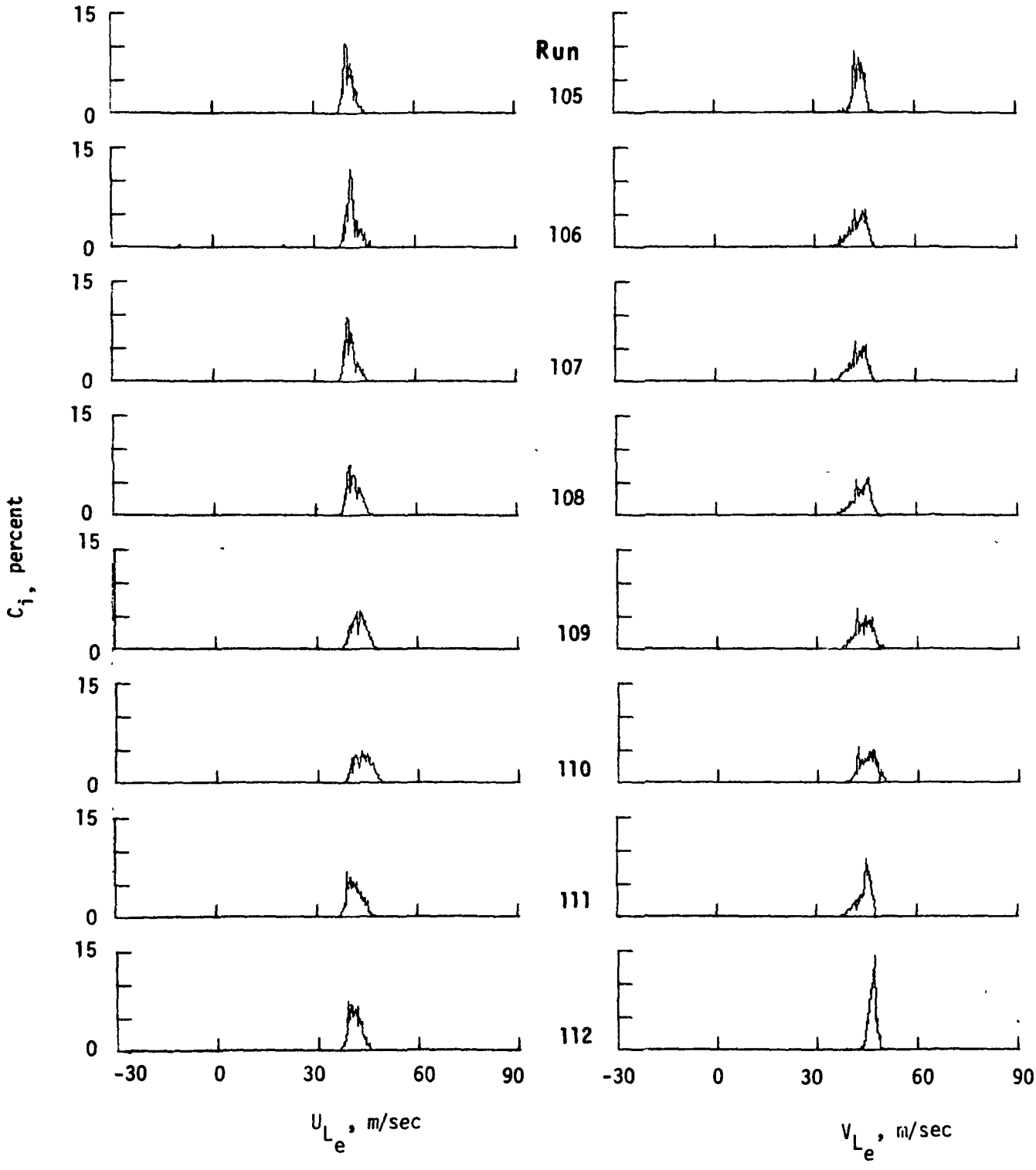

Figure B-9.- Concluded.

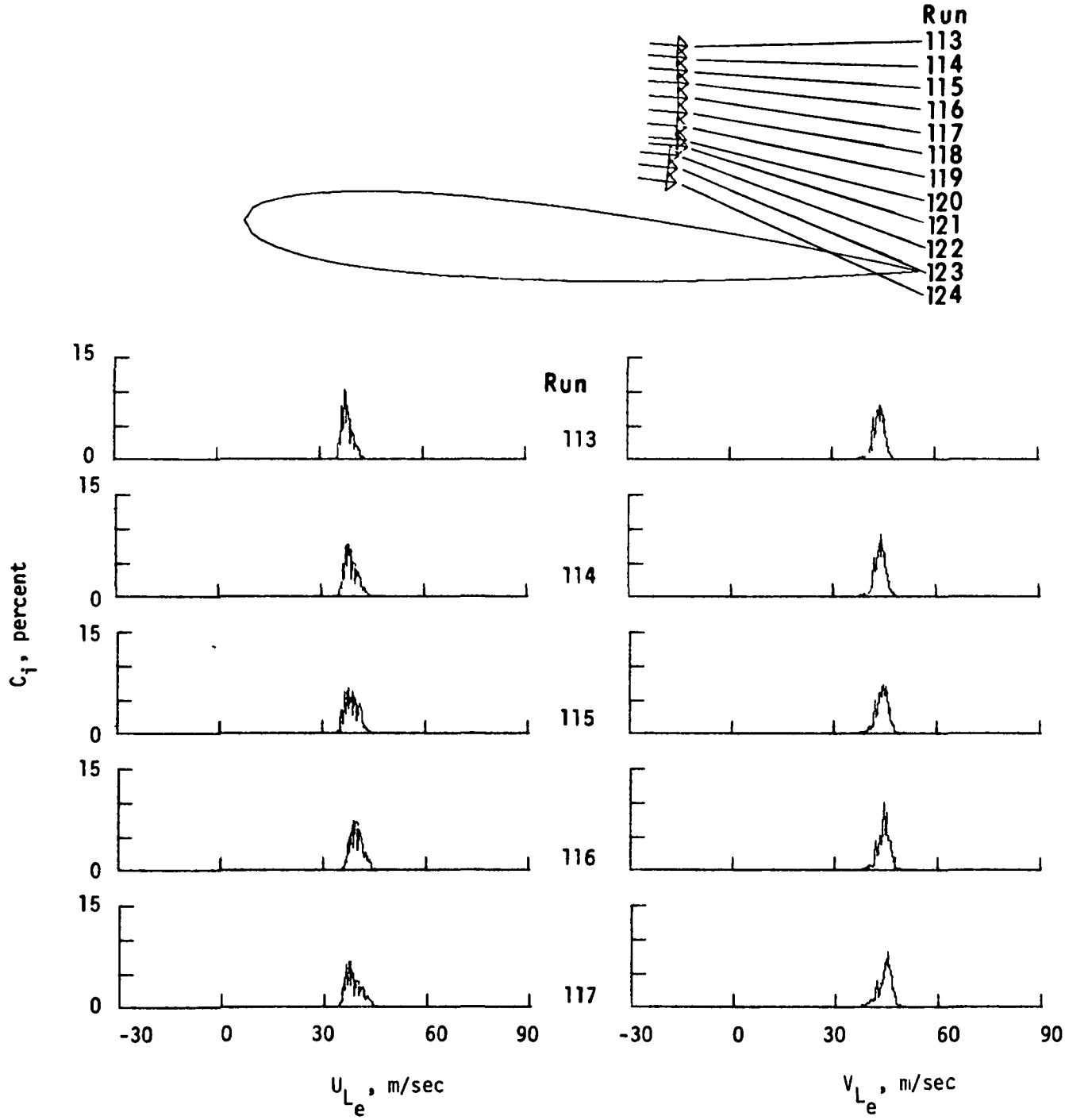

Figure B-10.- Histograms in scan at constant $x_c/c = 0.58$, $\alpha = 4.75^{o}$.

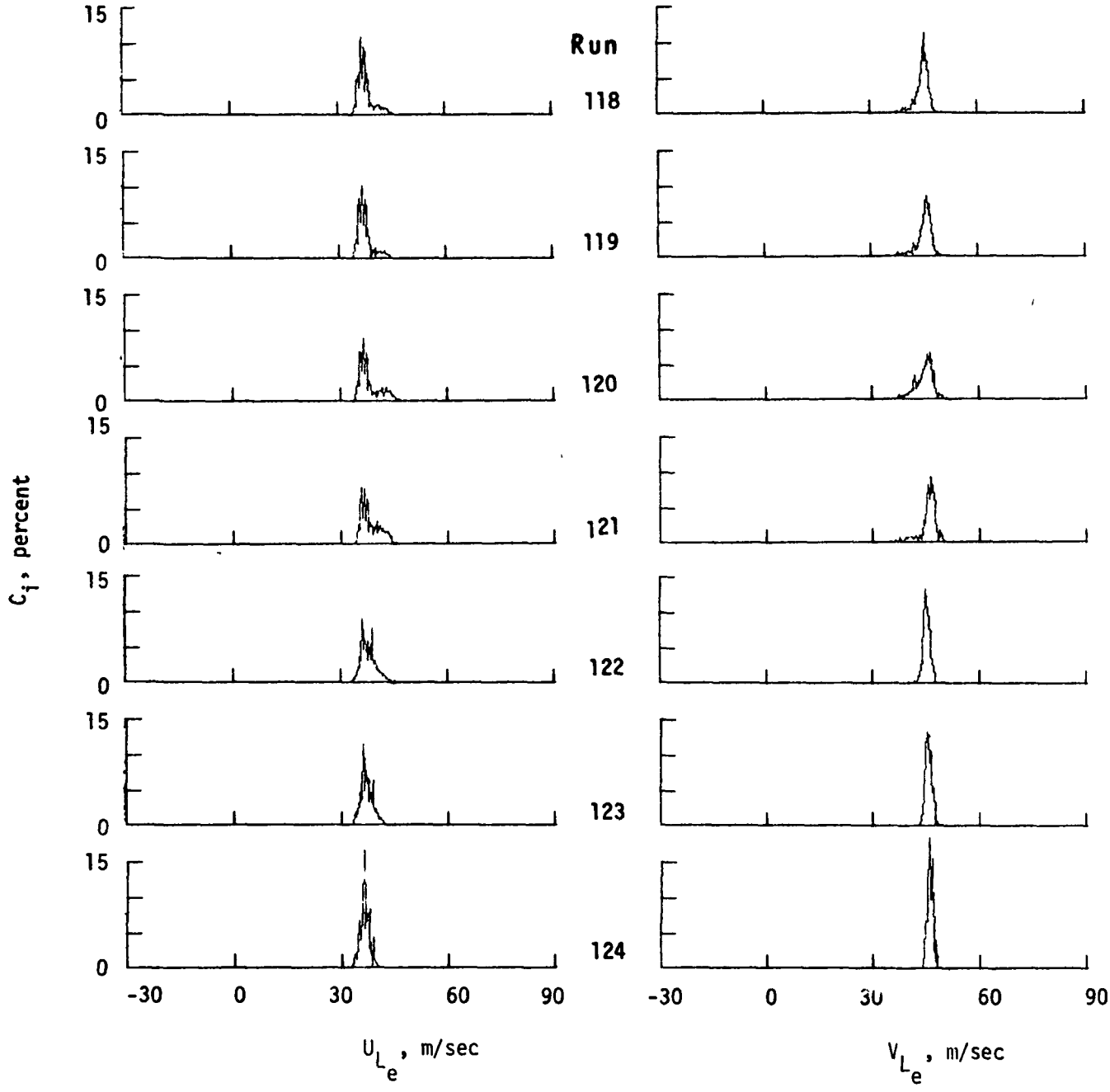

Figure B-10.-Concluded.

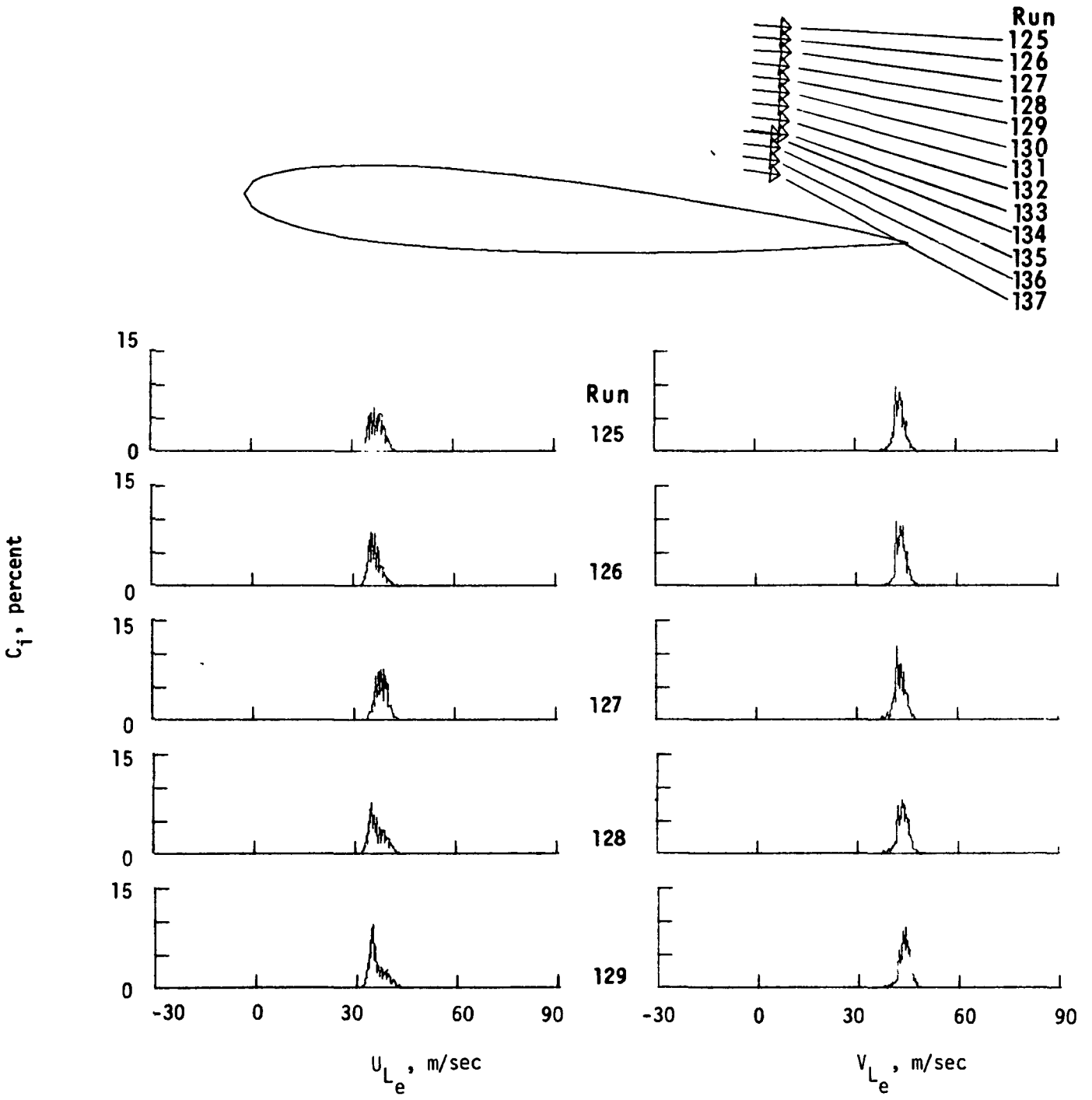

Figure B-11.- Histograms in scan at constant $x_c/c = 0.75$, $\alpha = 4.75^{o}$.

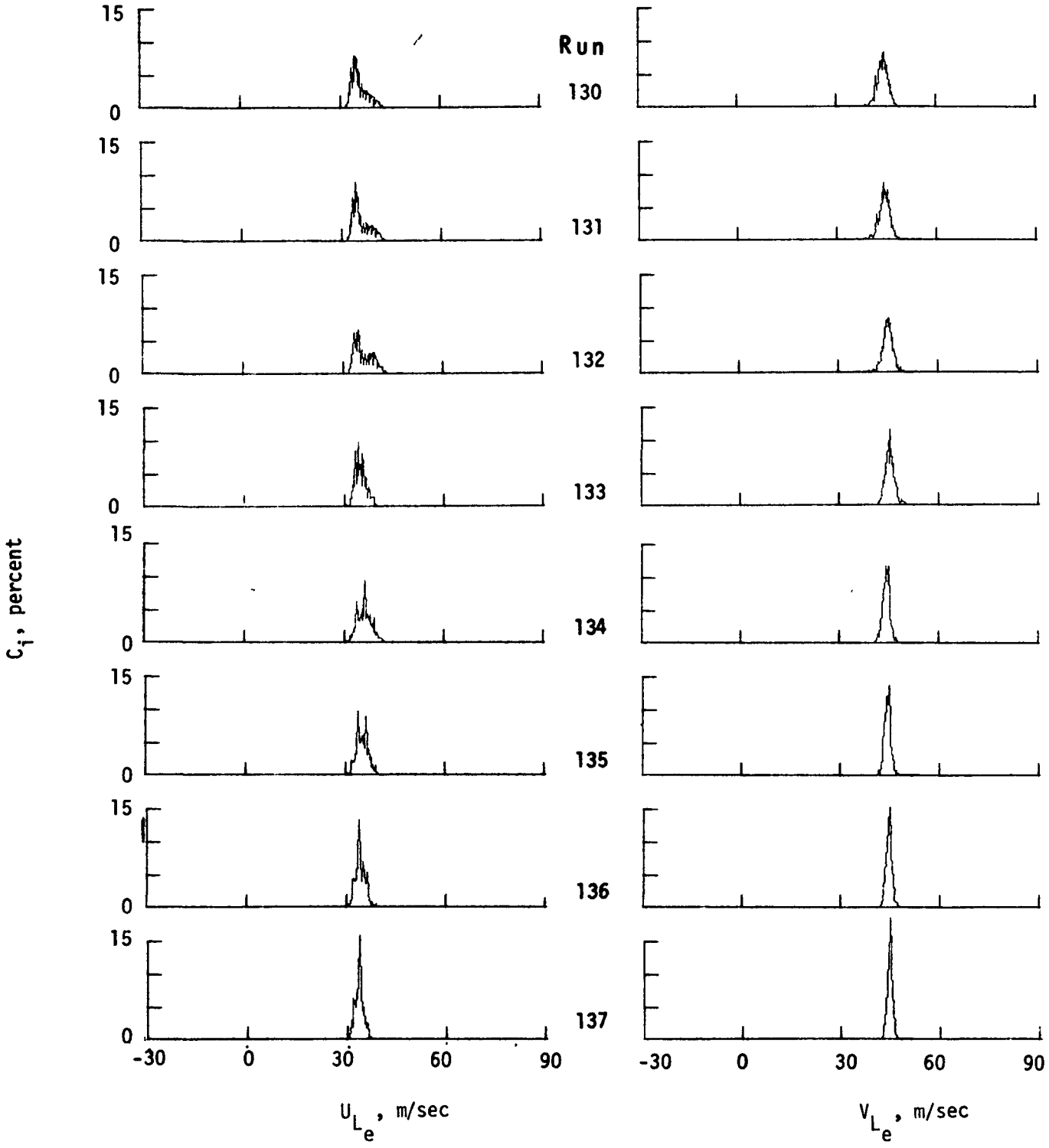

Figure B-11.-Concluded.

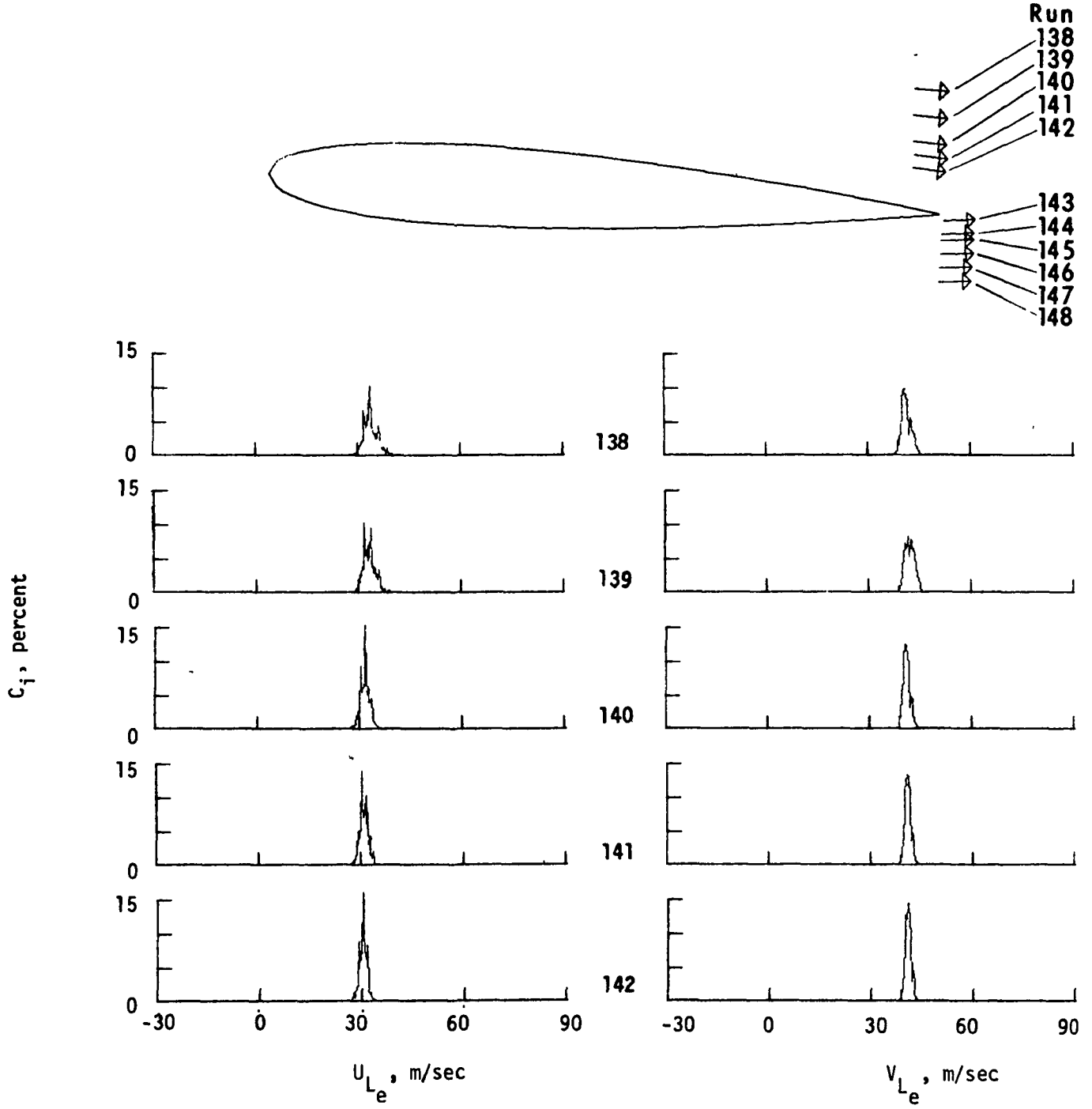

Figure B-12.- Histograms in scan at constant x_c/c = 0.96 and 1.01, α = 4.75°.

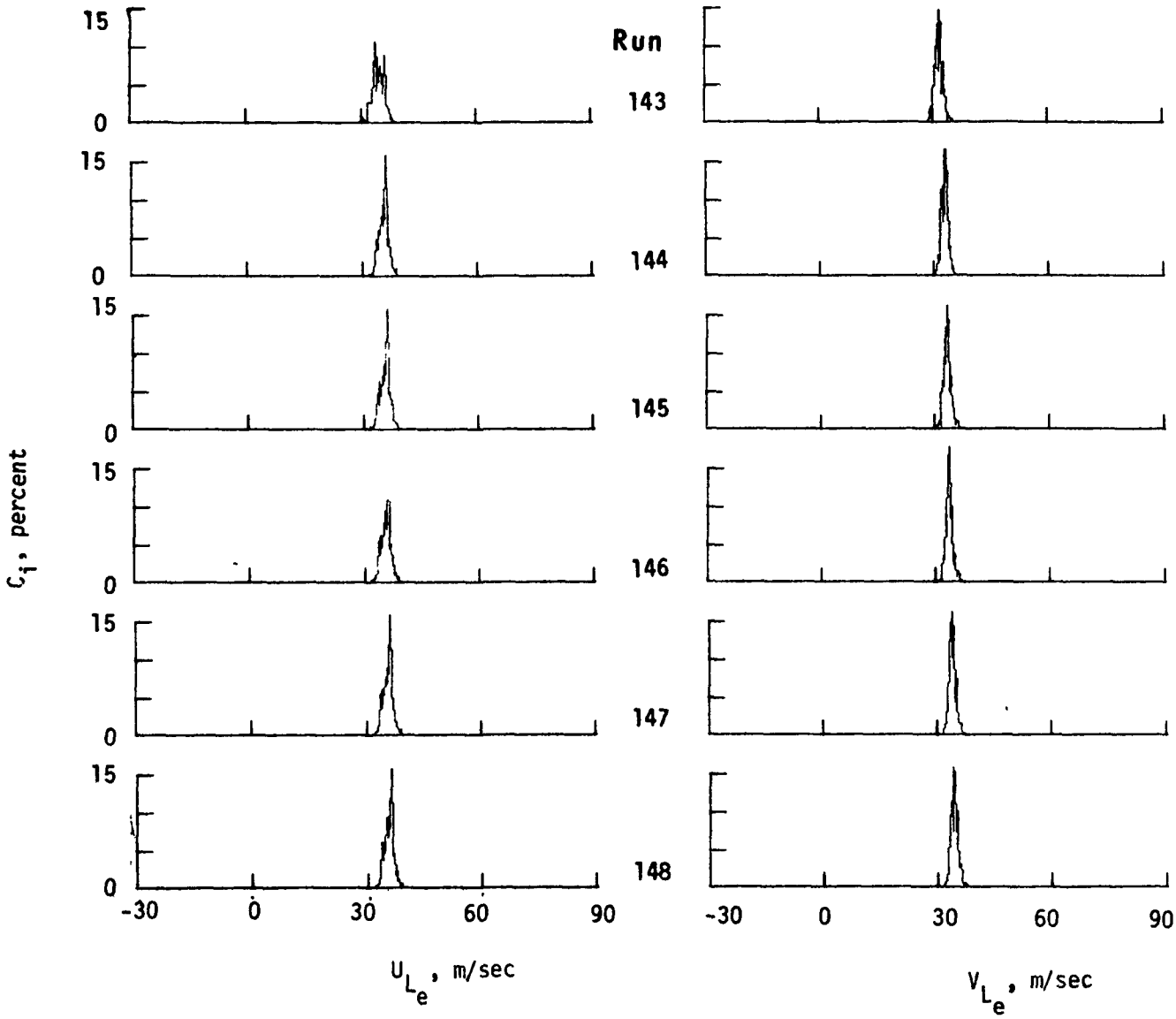

Figure B-12.- Concluded.

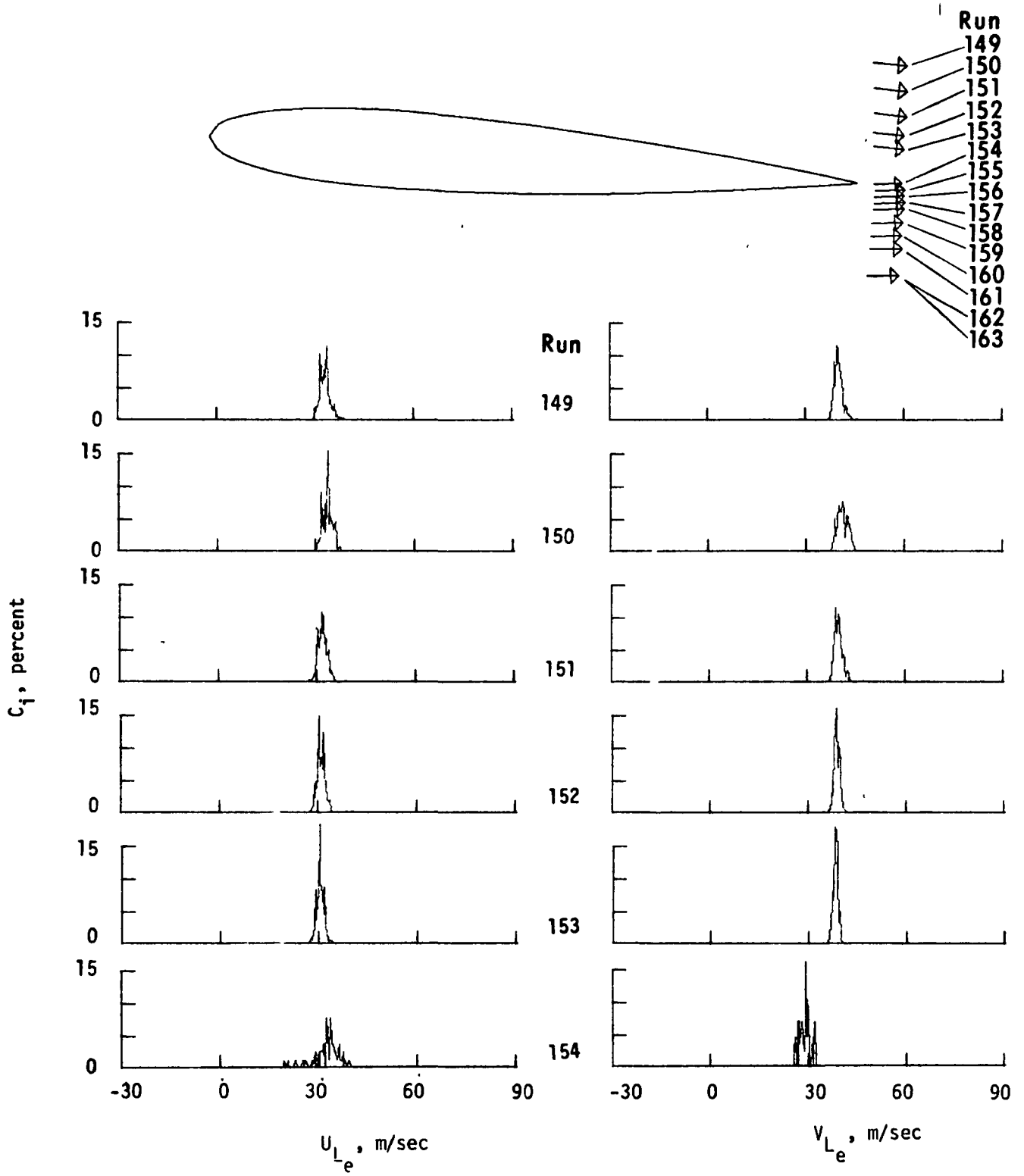

Figure B-13.- Histograms in scan at constant $x_c/c = 1.03$, $\alpha = 4.75^{o}$.

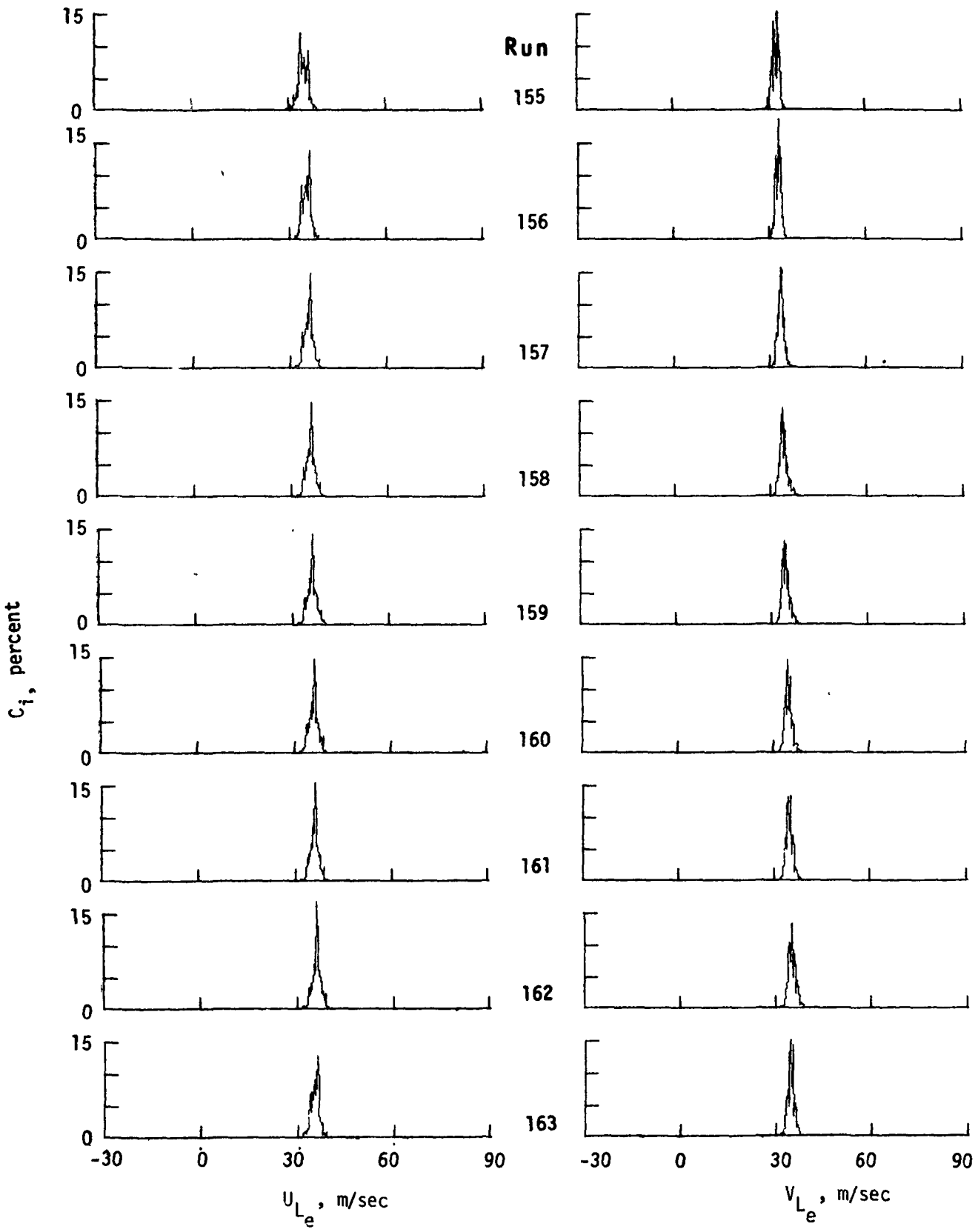

Figure B-13.- Concluded.

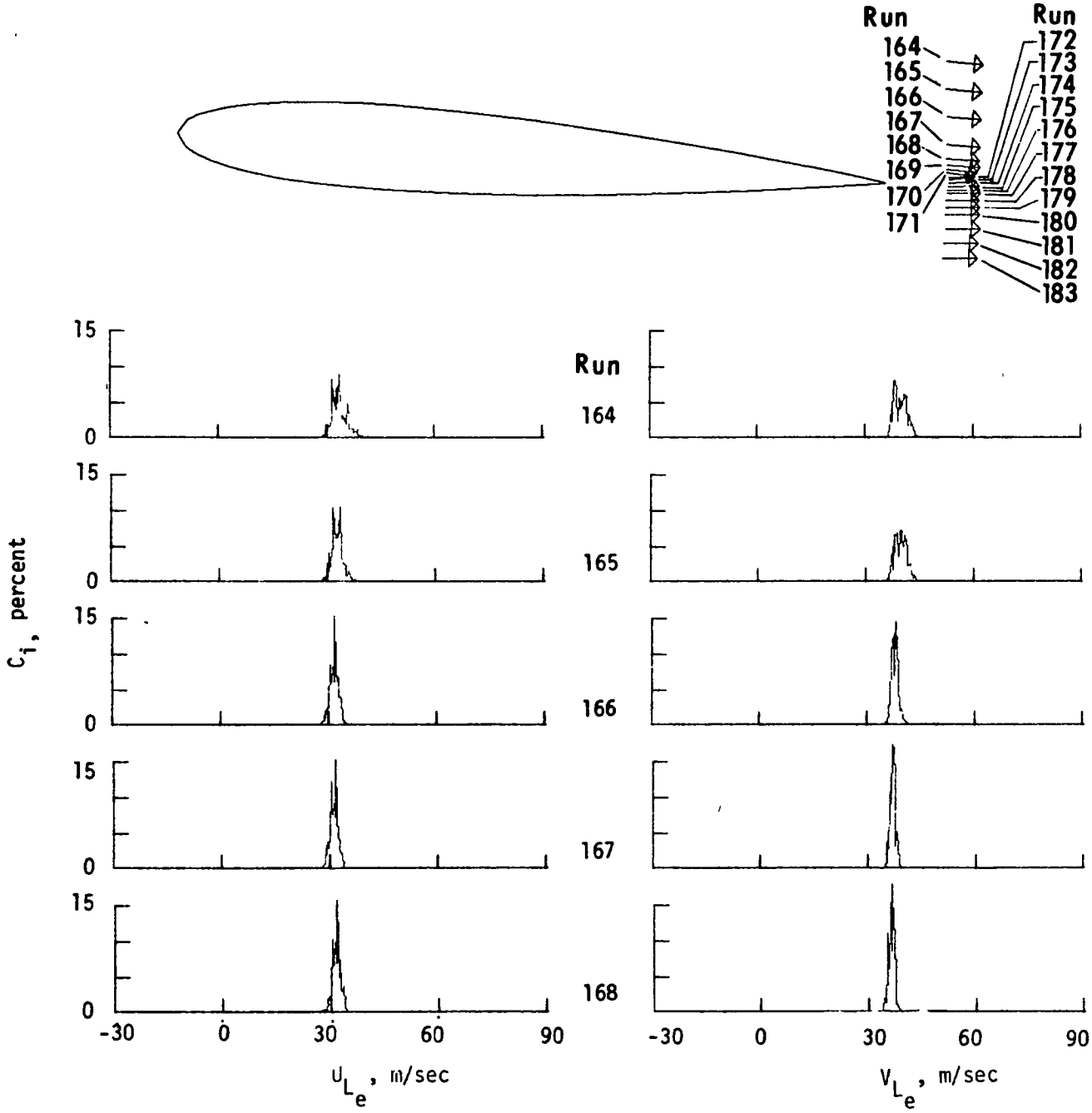

Figure B-14.- Histograms in scan at constant $x_c/c = 1.09$, $\alpha = 4.75^{o}$.

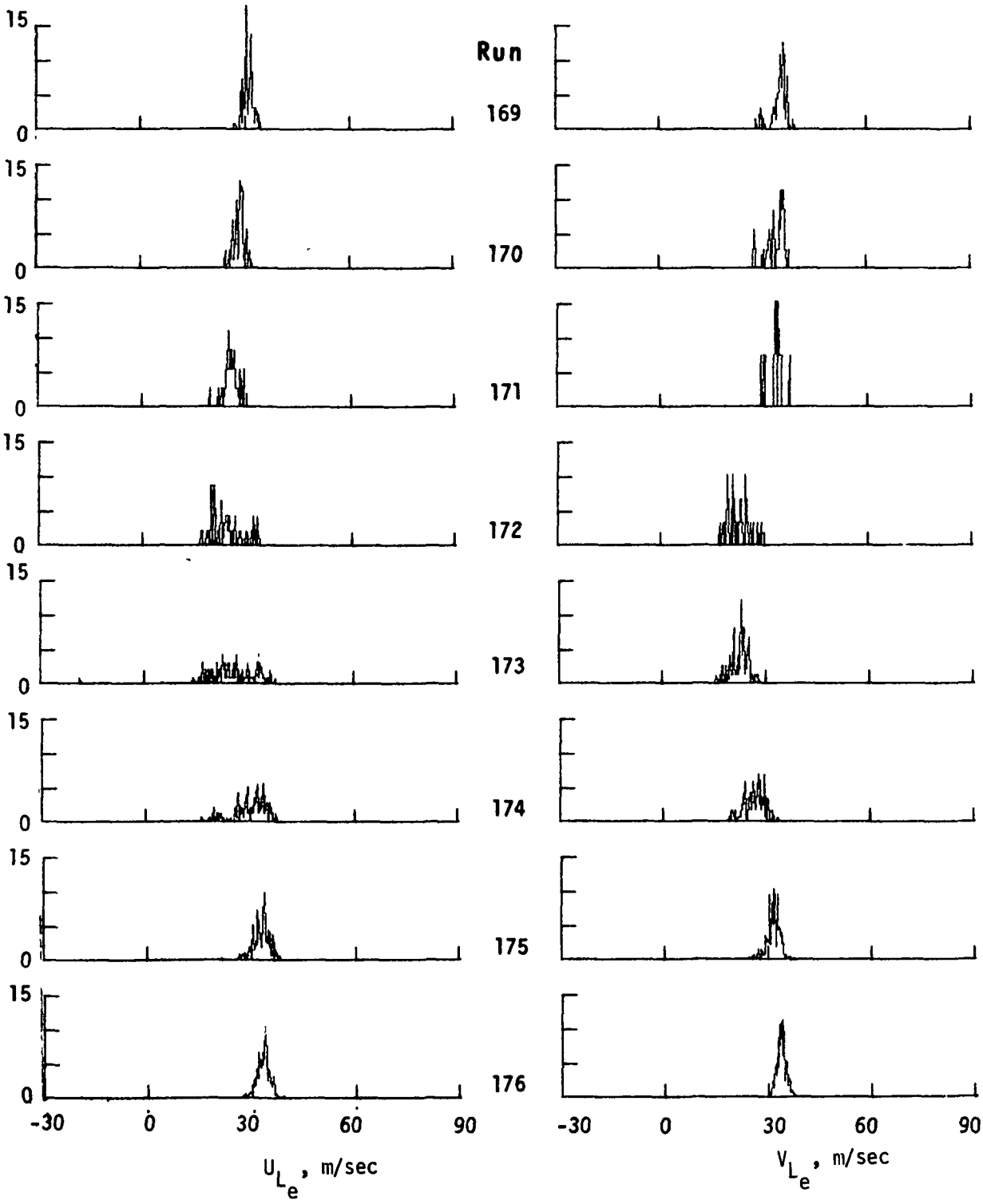

Figure B-14.- Continued.

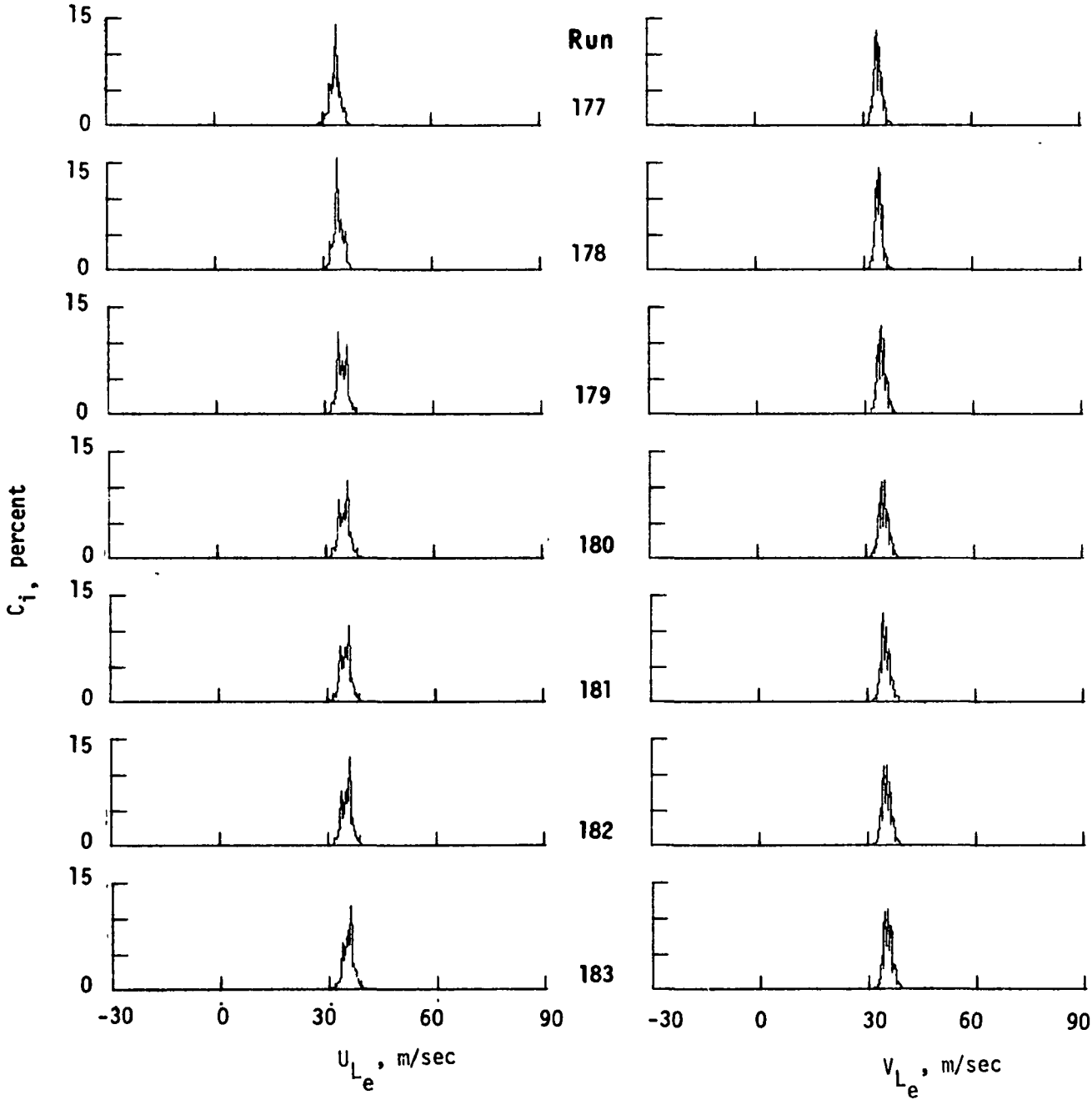

Figure B-14.- Concluded.

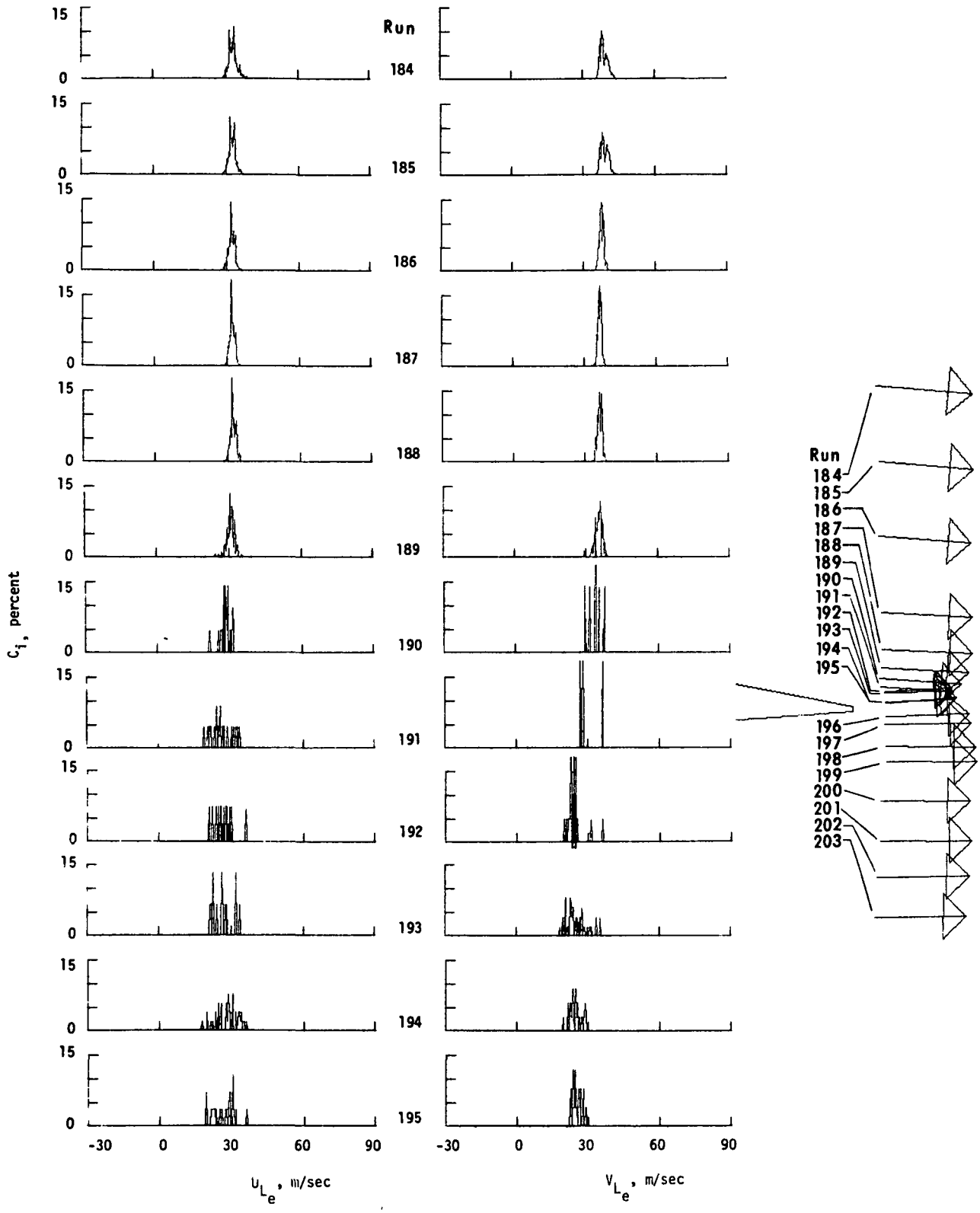

Figure B-15.- Histograms in scan at constant $x_c/c = 1.13$, $\alpha = 4.75^o$.

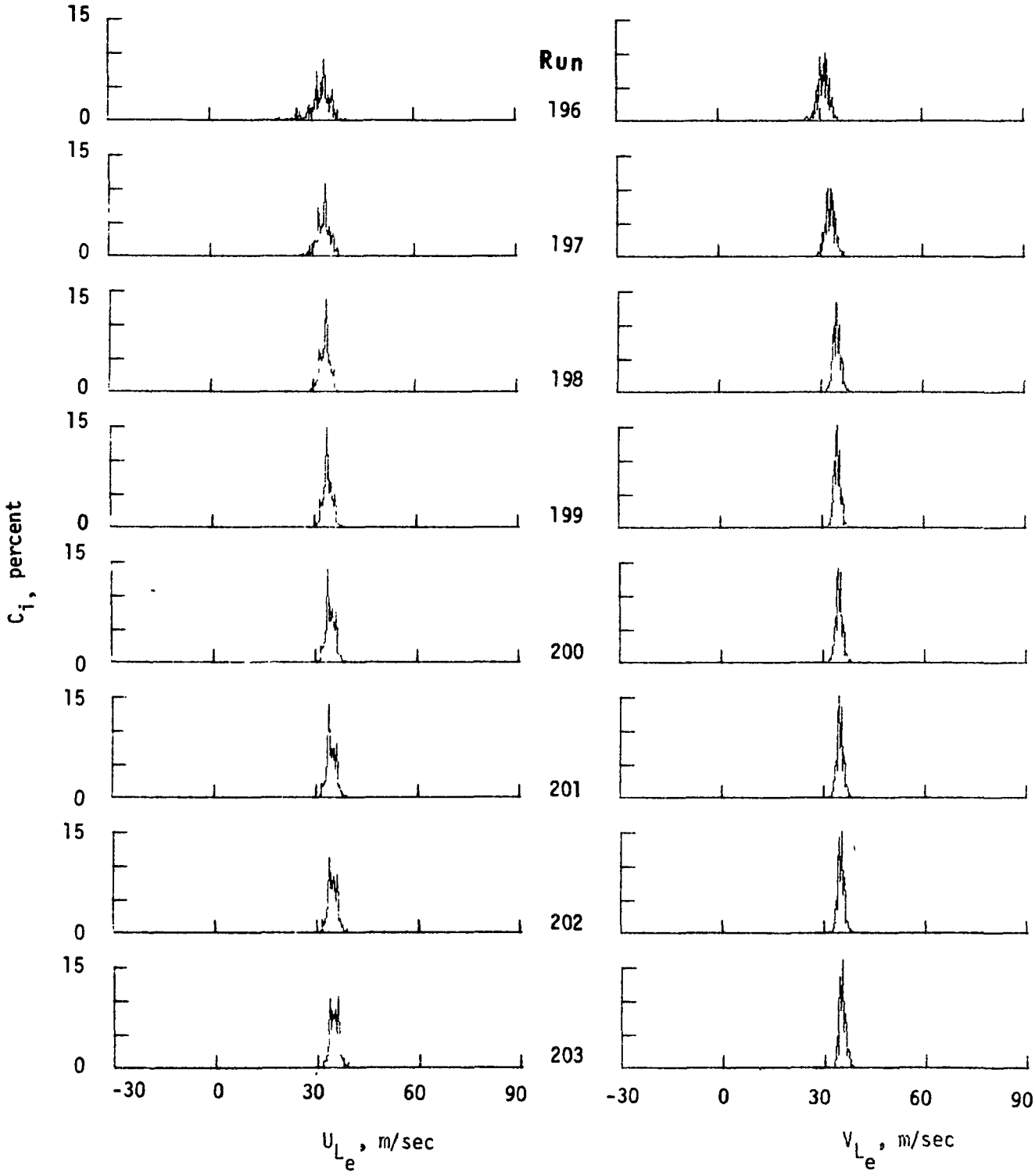

Figure B-15.- Concluded.

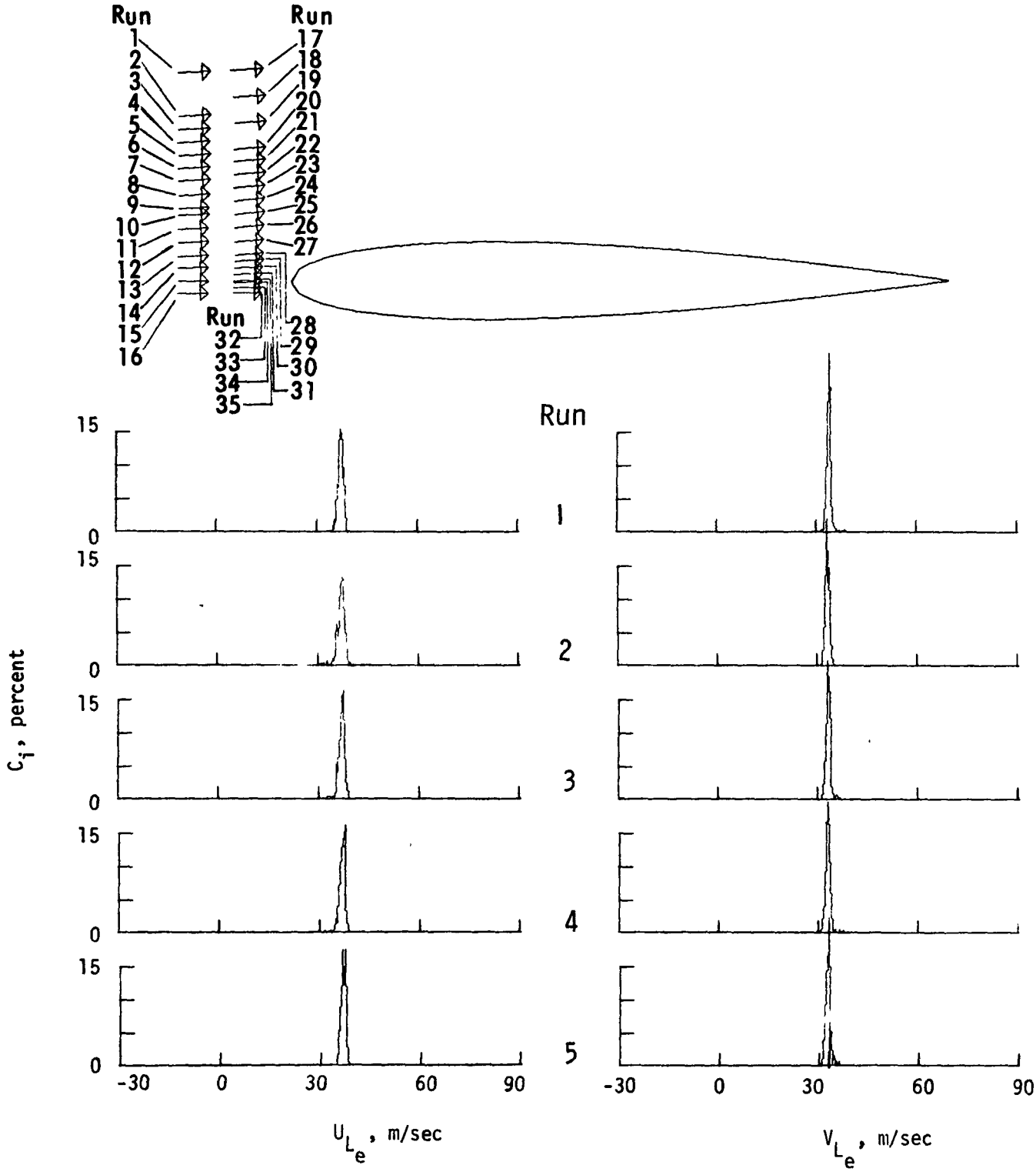

Figure B-16.- Histograms in scan at constant x_c/c = -0.17 and -0.09, $\alpha = 0.6^o$.

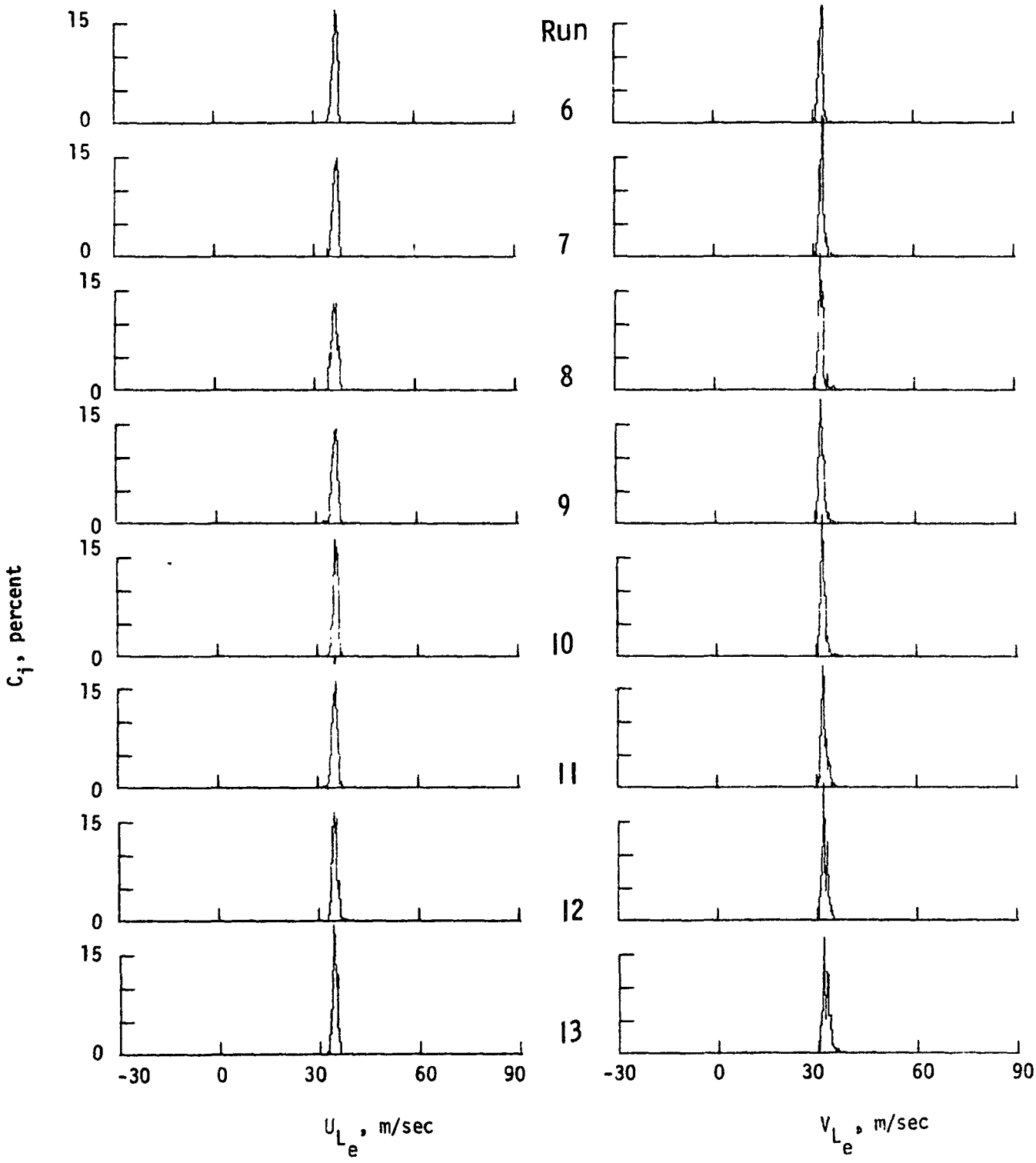

Figure B-16.- Continued.

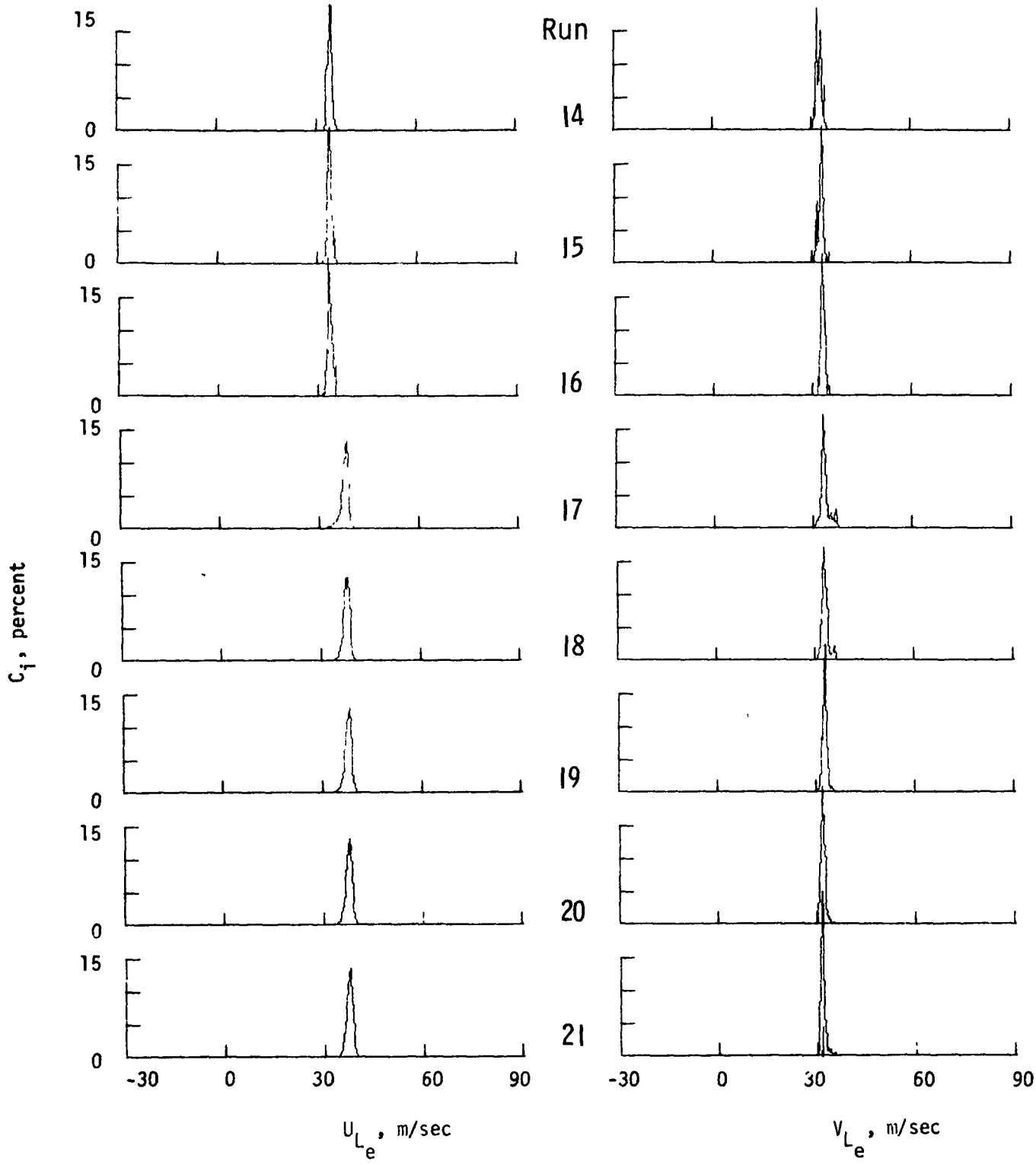

Figure B-16.- Continued.

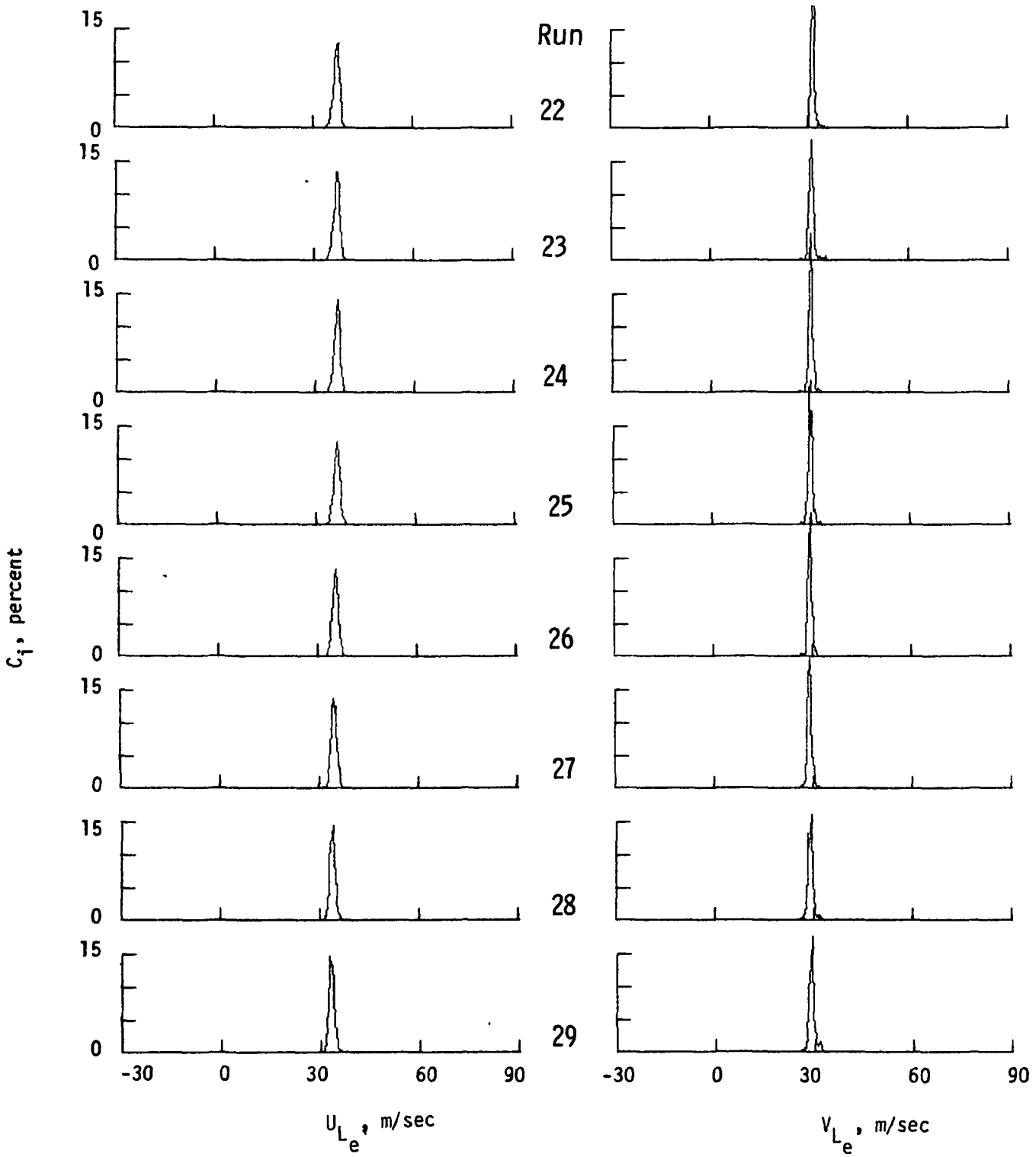

Figure B-16.- Continued.

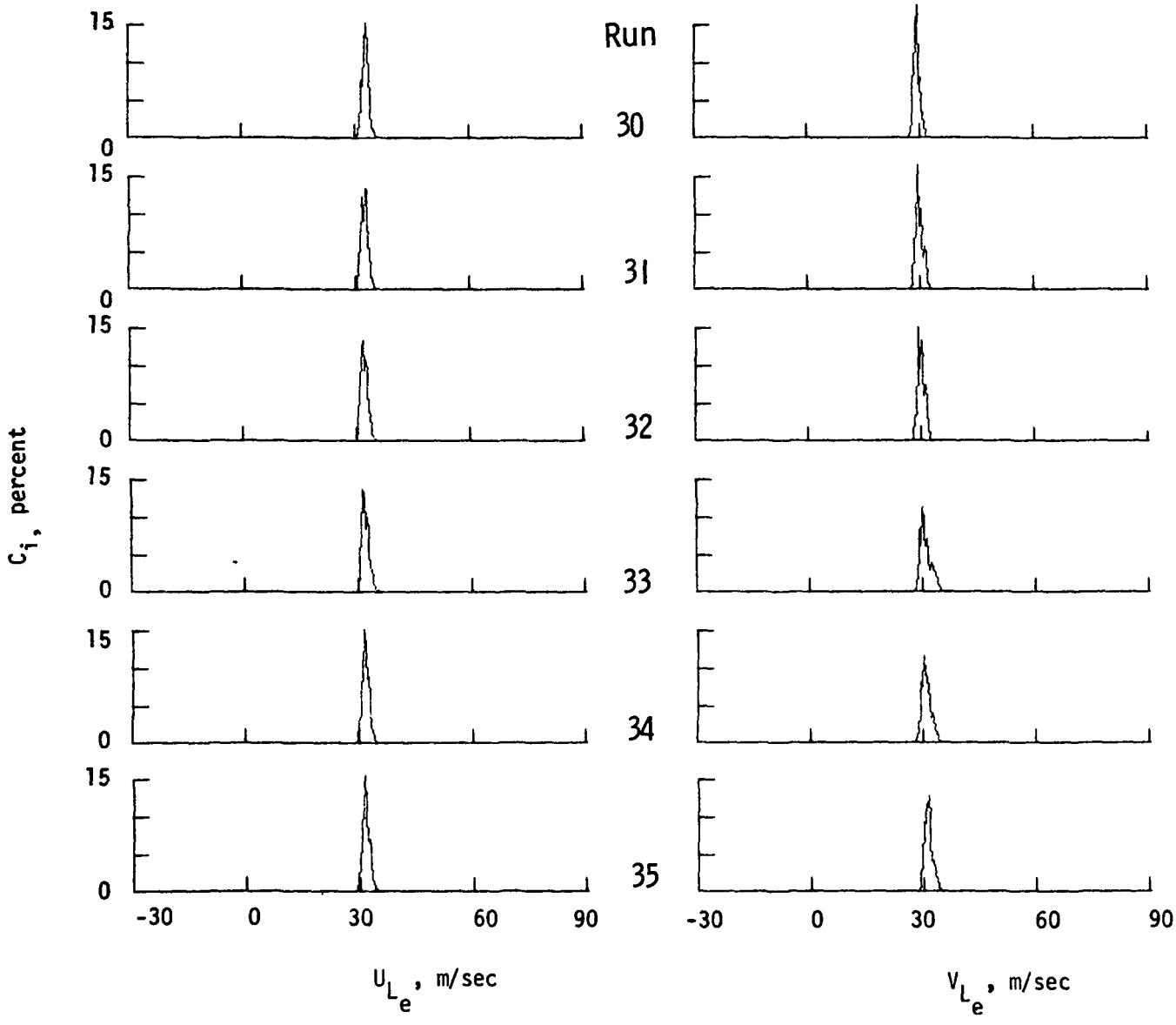

Figure B-16.- Concluded.

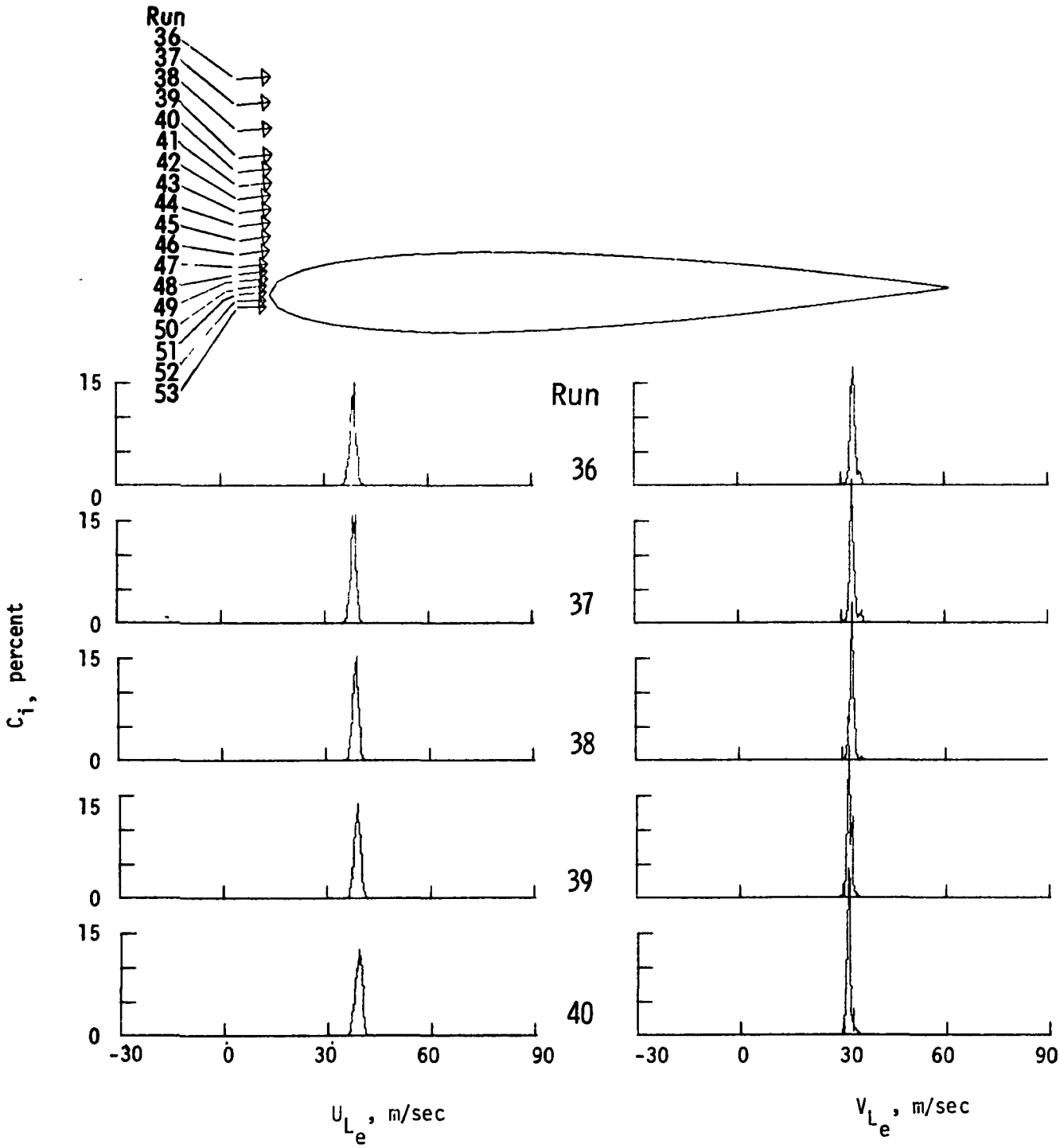

Figure B-17.- Histograms in scan at constant $x_c/c = -0.05$, $\alpha = 0.6^o$.

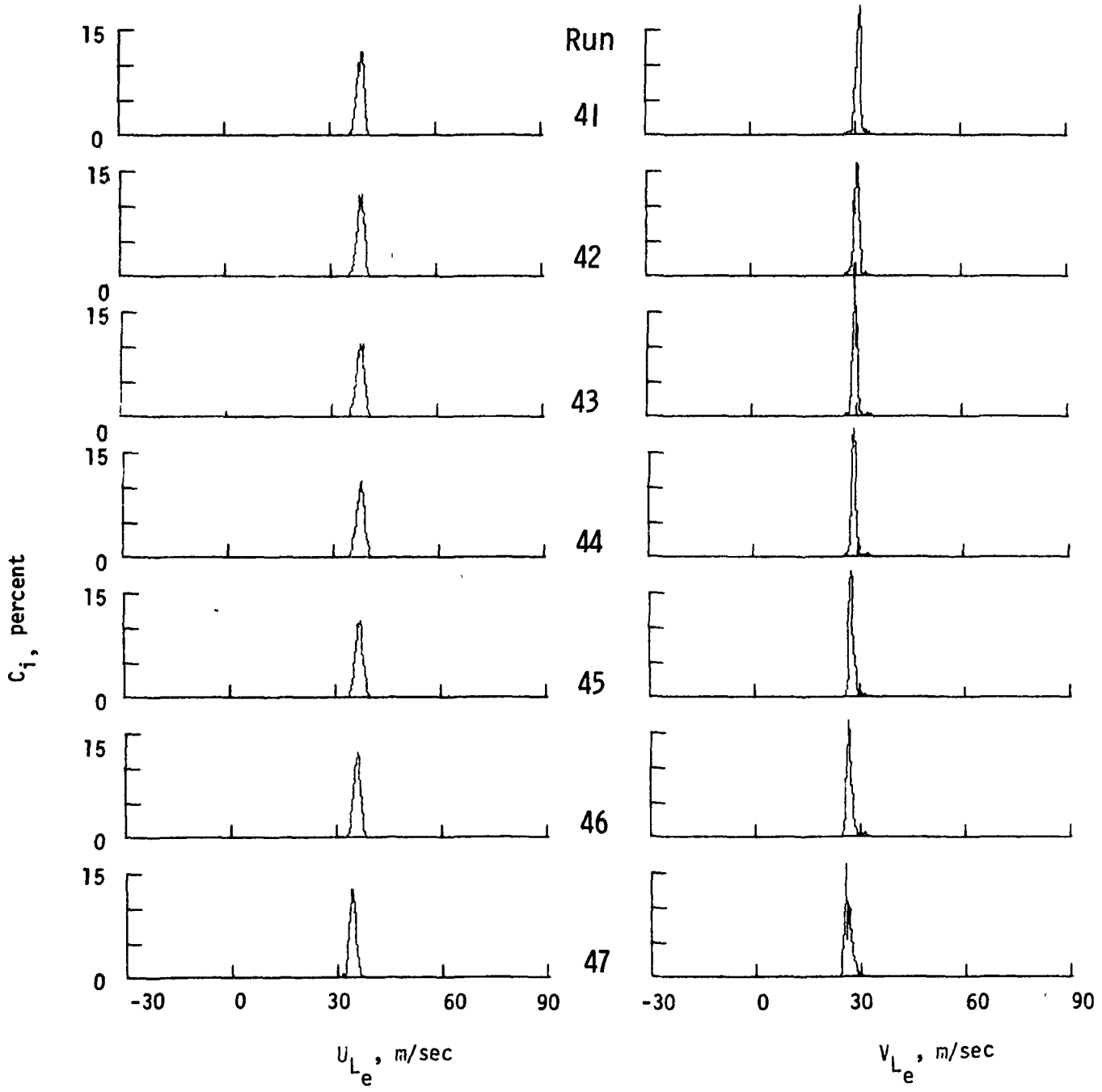

Figure B-17.- Continued.

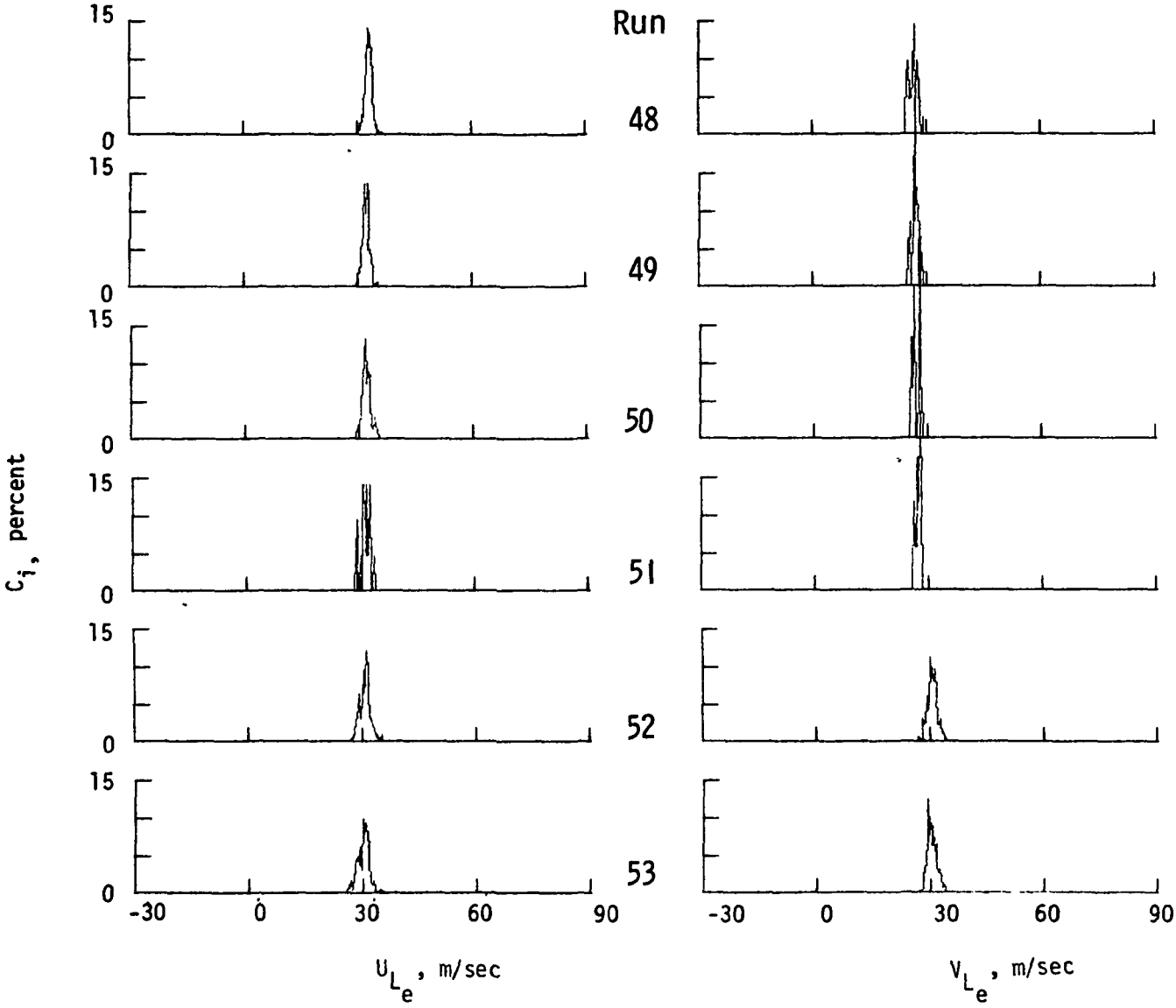

Figure B-17.- Concluded.

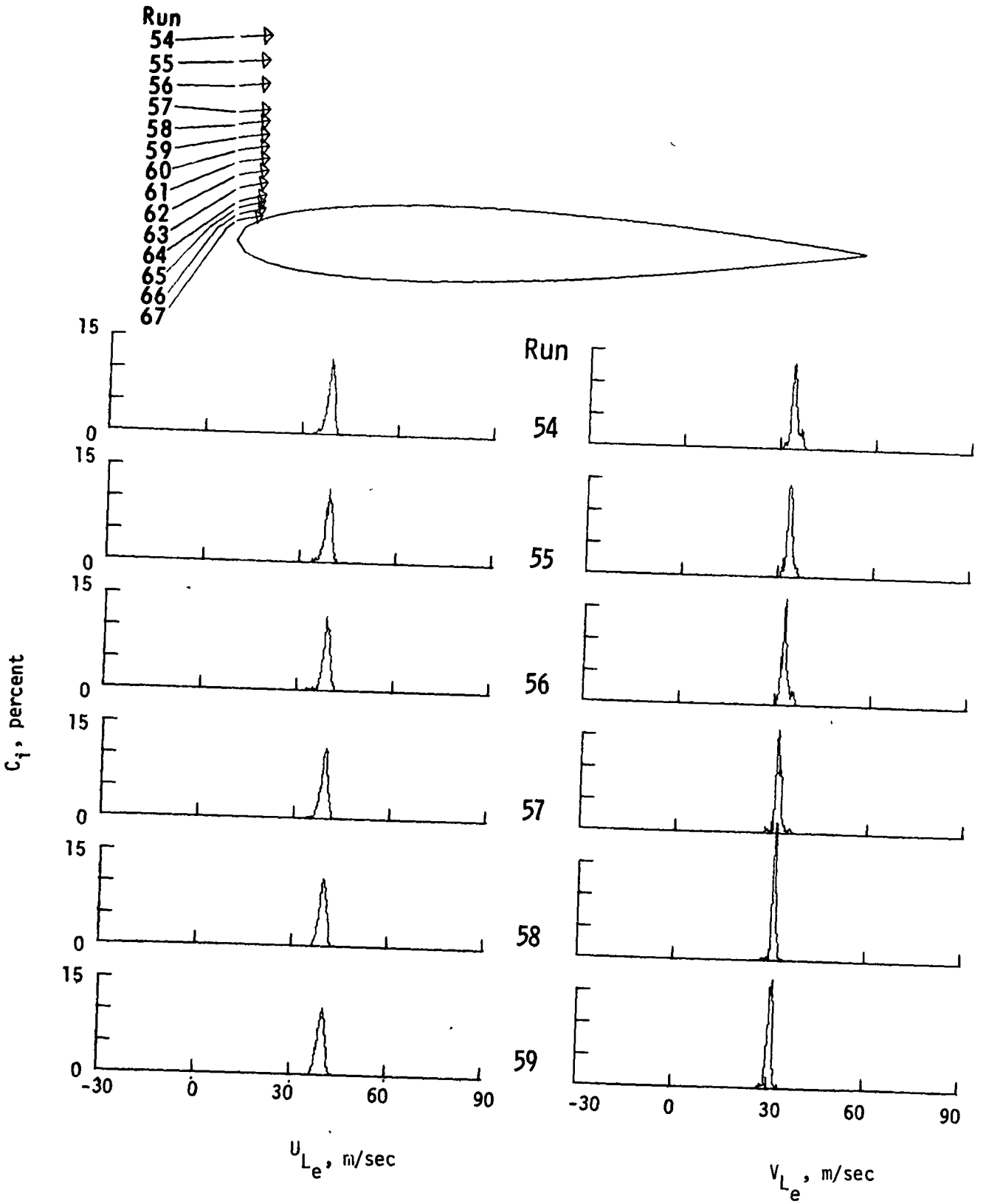

Figure B-18.- Histograms in scan at constant $x_c/c = 0$, $\alpha = 0.6^o$.

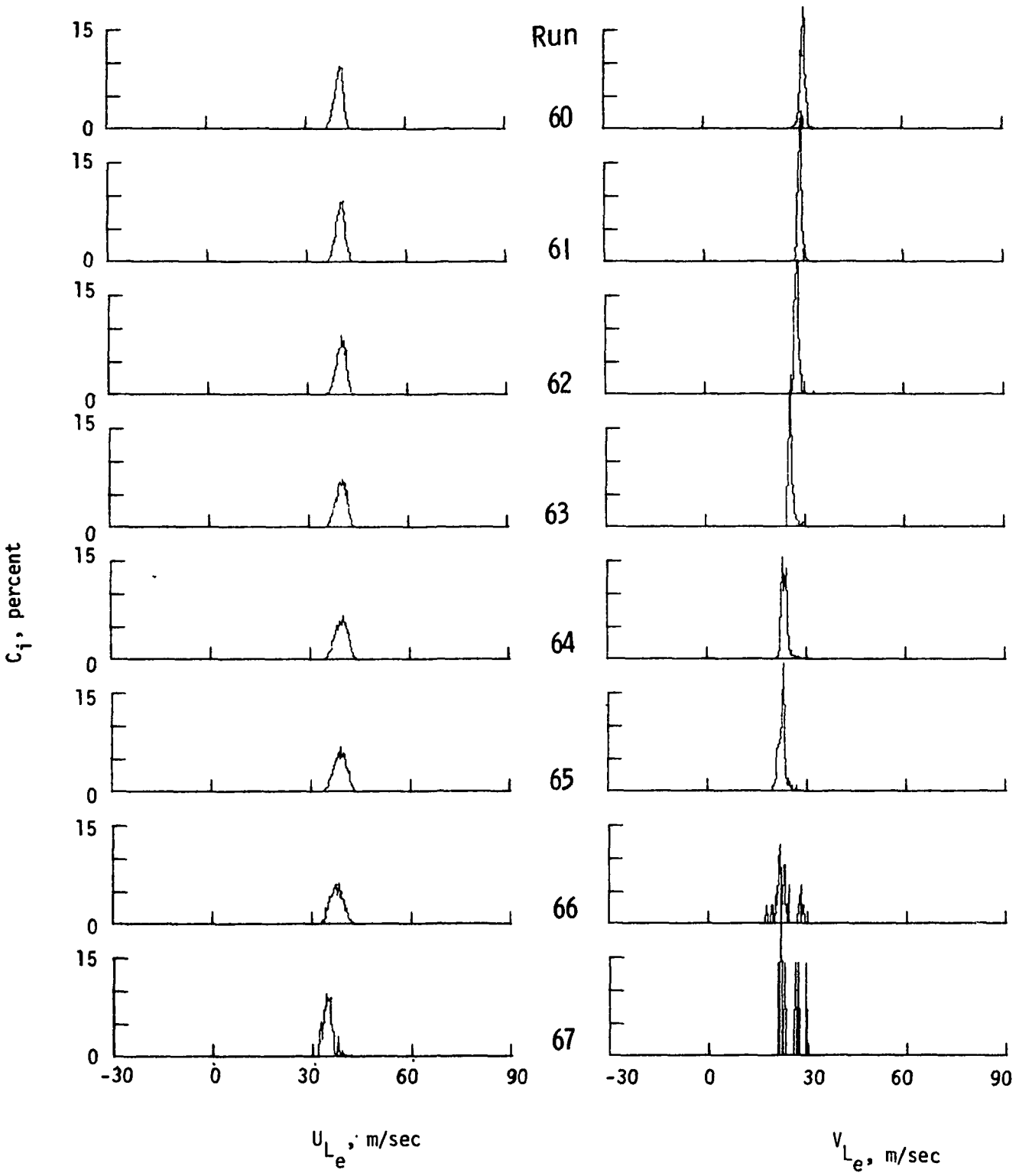

Figure B-18.- Concluded.

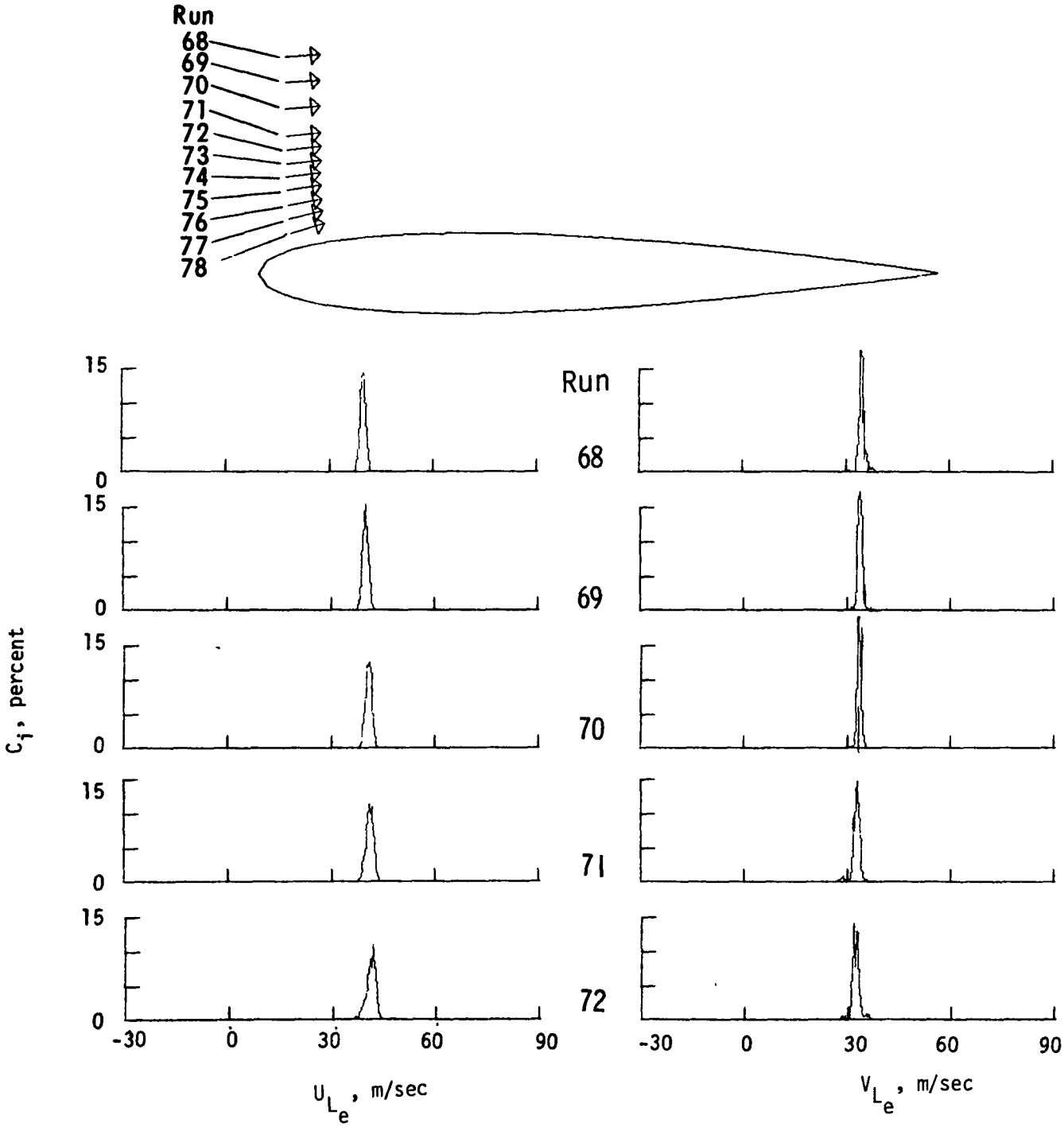

Figure B-19.- Histograms in scan at constant $x_c/c = 0.04$, $\alpha = 0.6^o$.

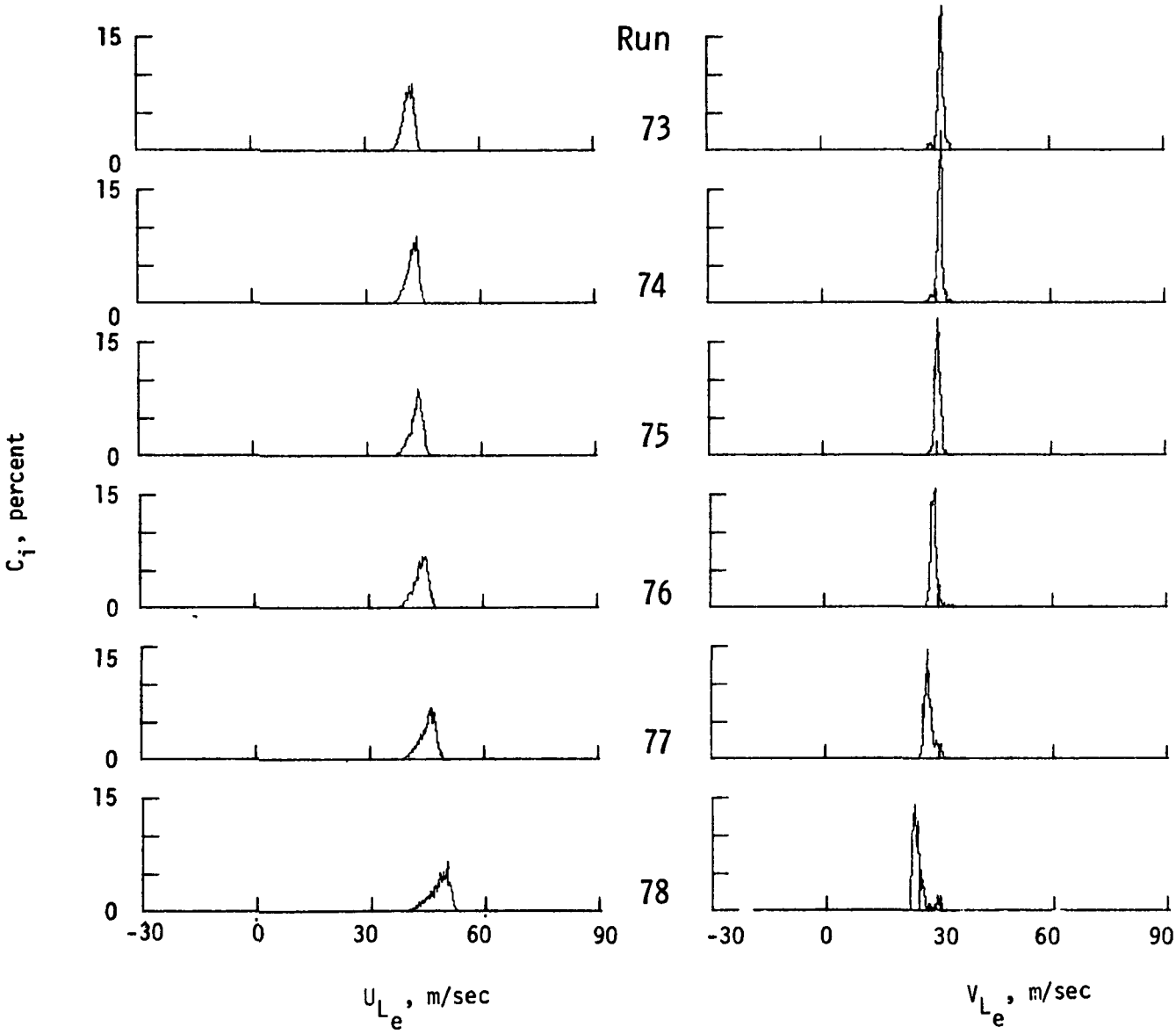

Figure B-19.- Concluded.

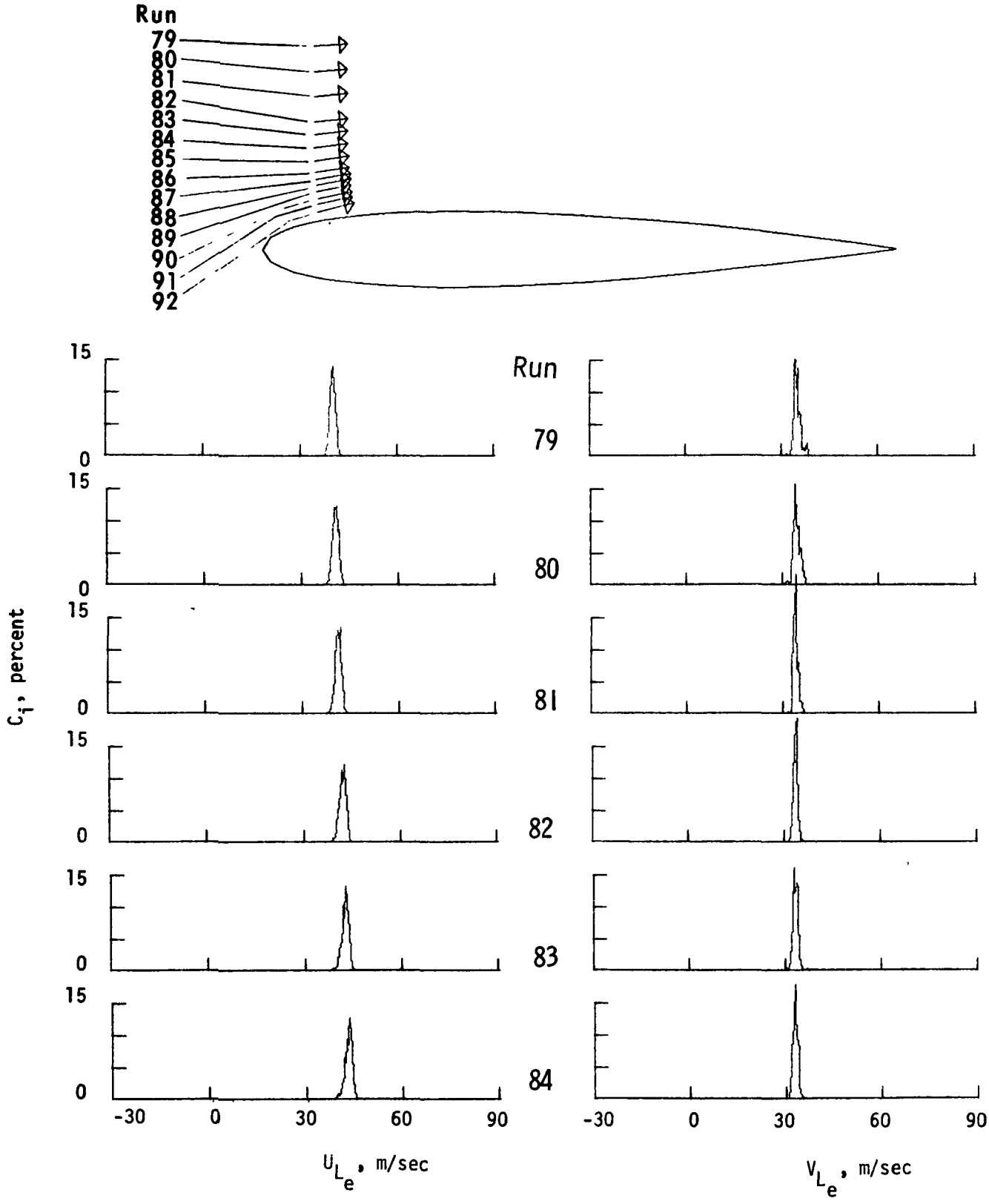

Figure B-20.- Histograms in scan at constant $x_c/c = 0.08$, $\alpha = 0.6^o$.

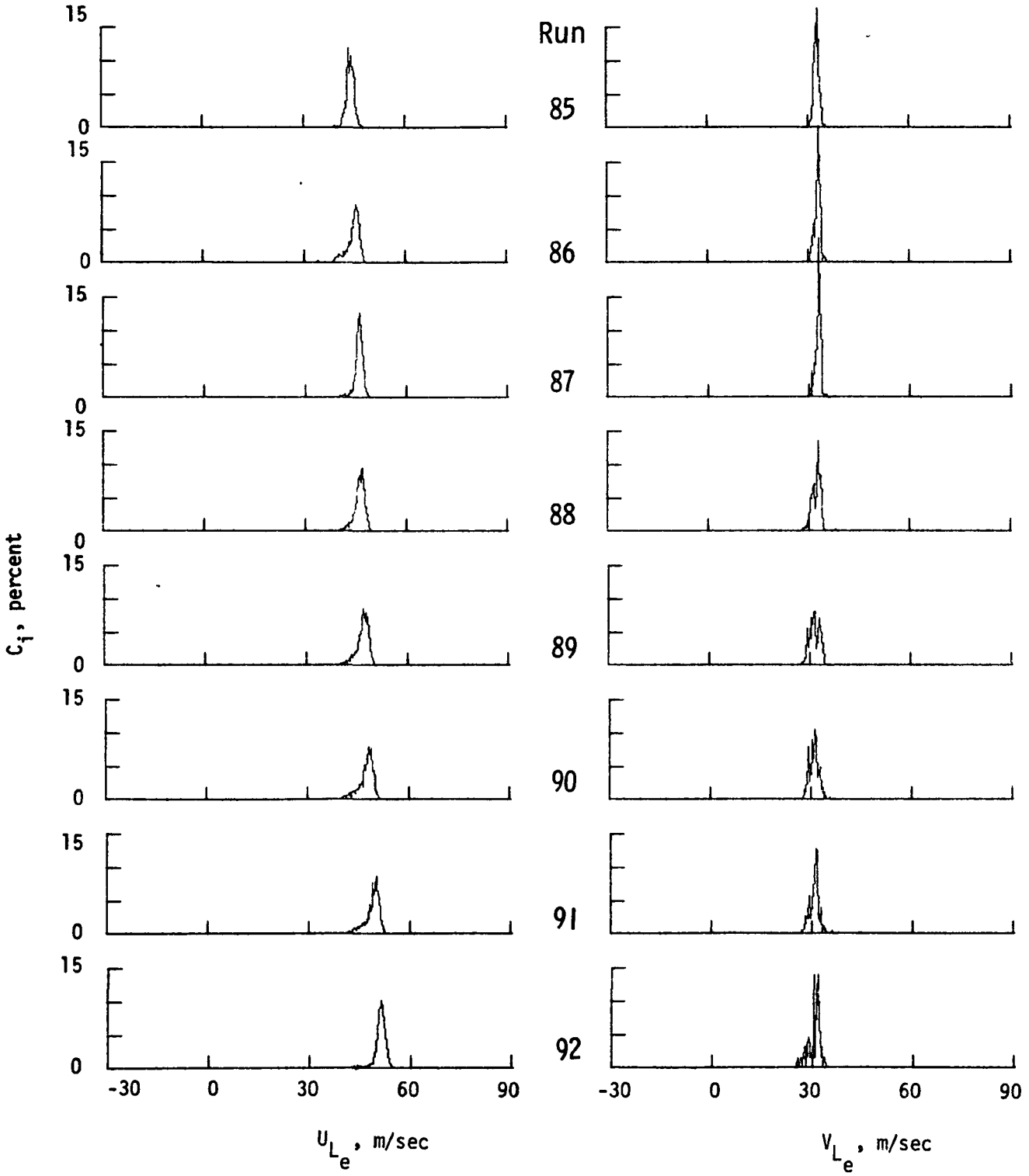

Figure B-20.- Concluded.

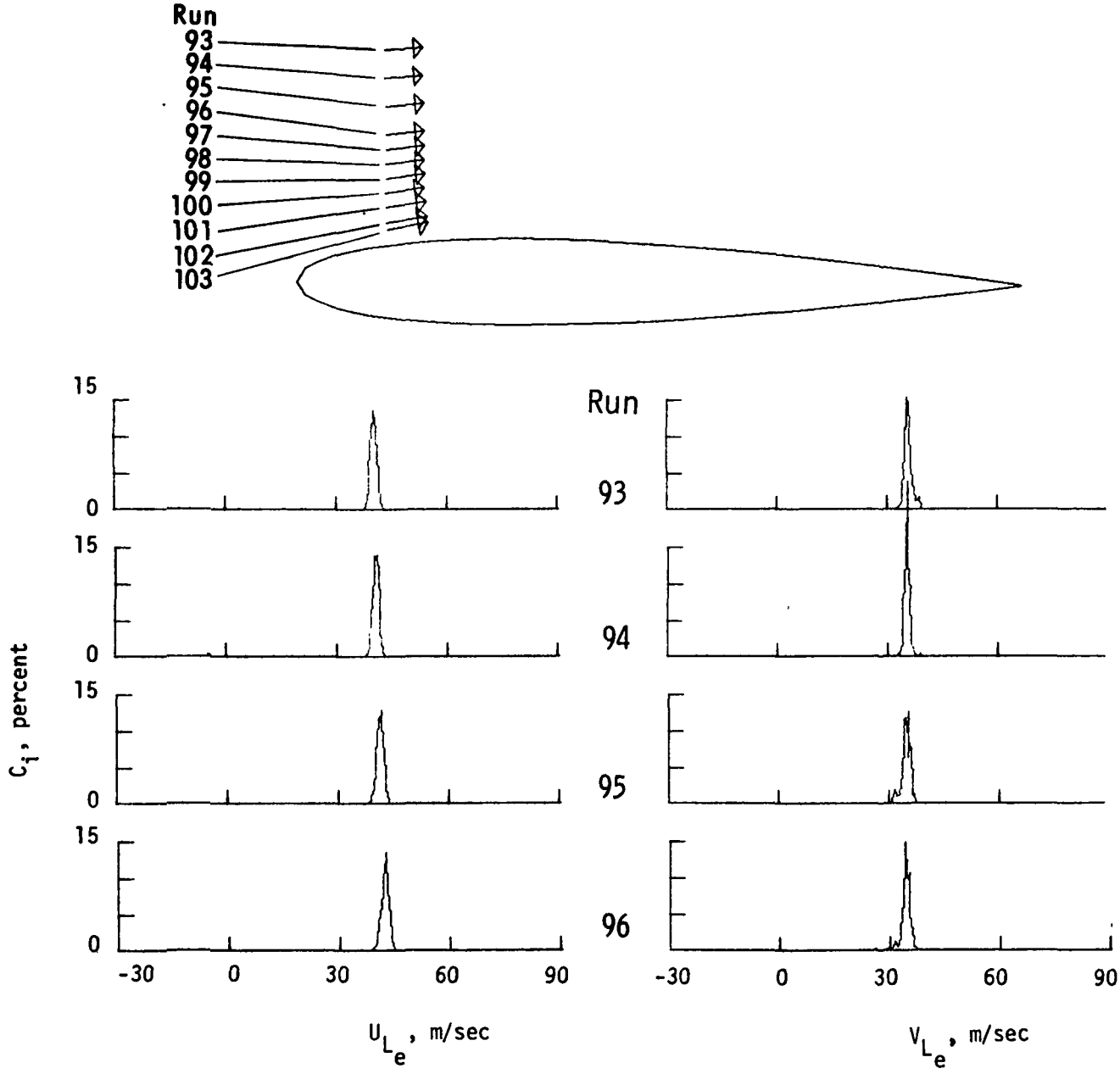

Figure B-21.- Histograms in scan at constant $x_c/c = 0.12$, $\alpha = 0.6^o$.

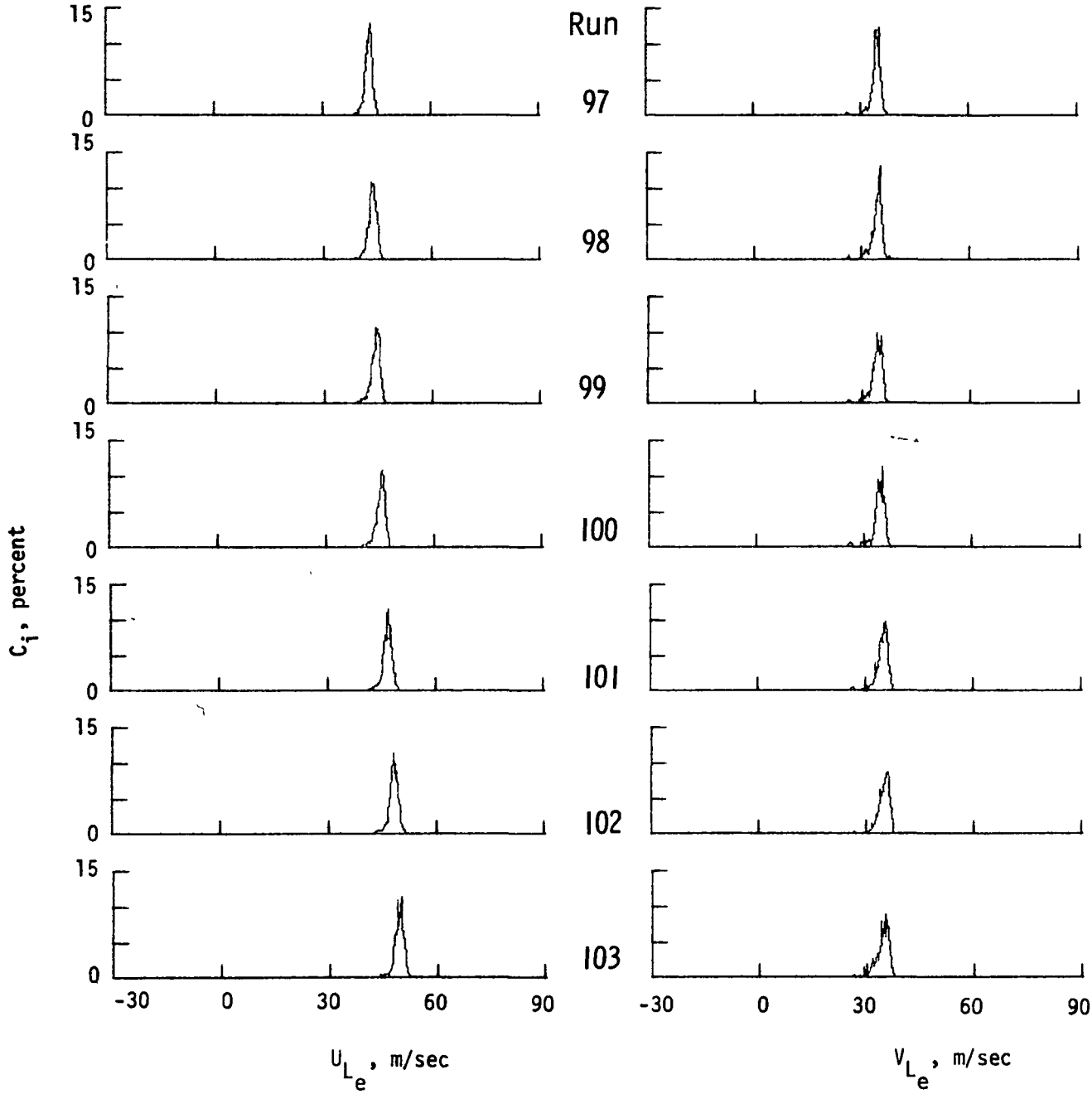

Figure B-21.- Concluded.

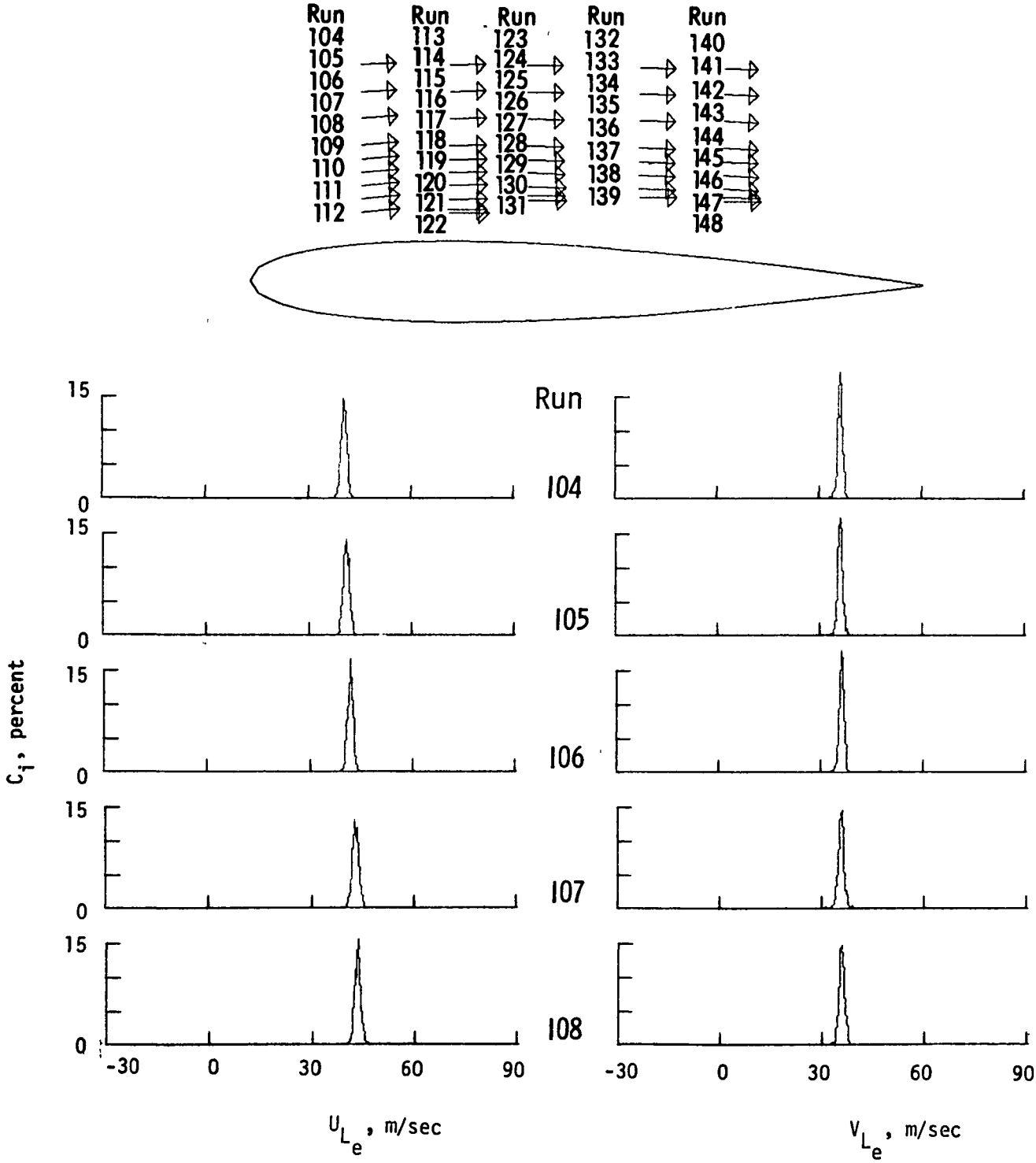

Figure B-22.- Histograms in scan at constant x_c/c = 0.16, 0.29, 0.41, 0.58, and 0.70, $\alpha = 0.6^{o}$.

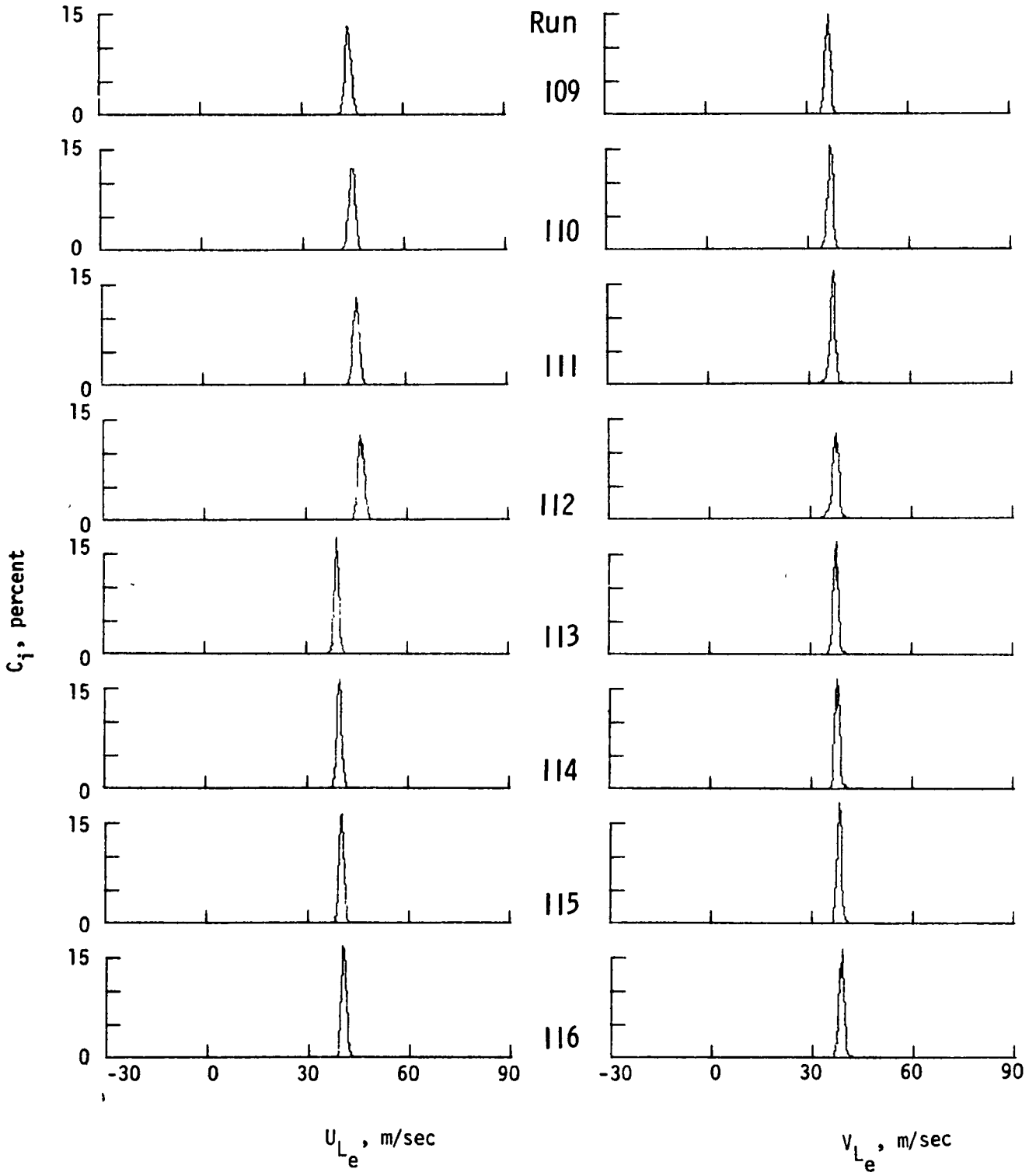

Figure B-22.- Continued.

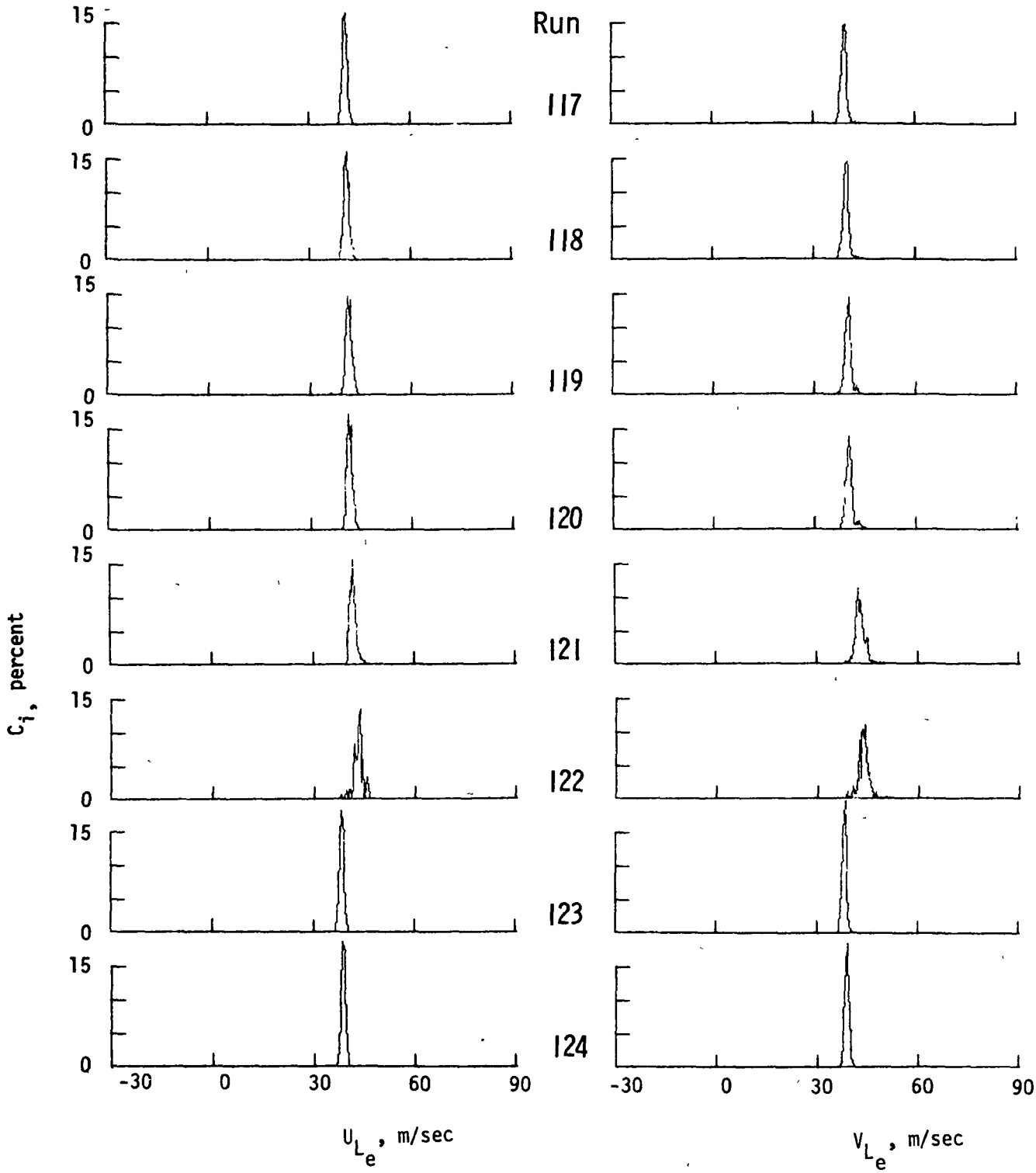

Figure B-22.- Continued.

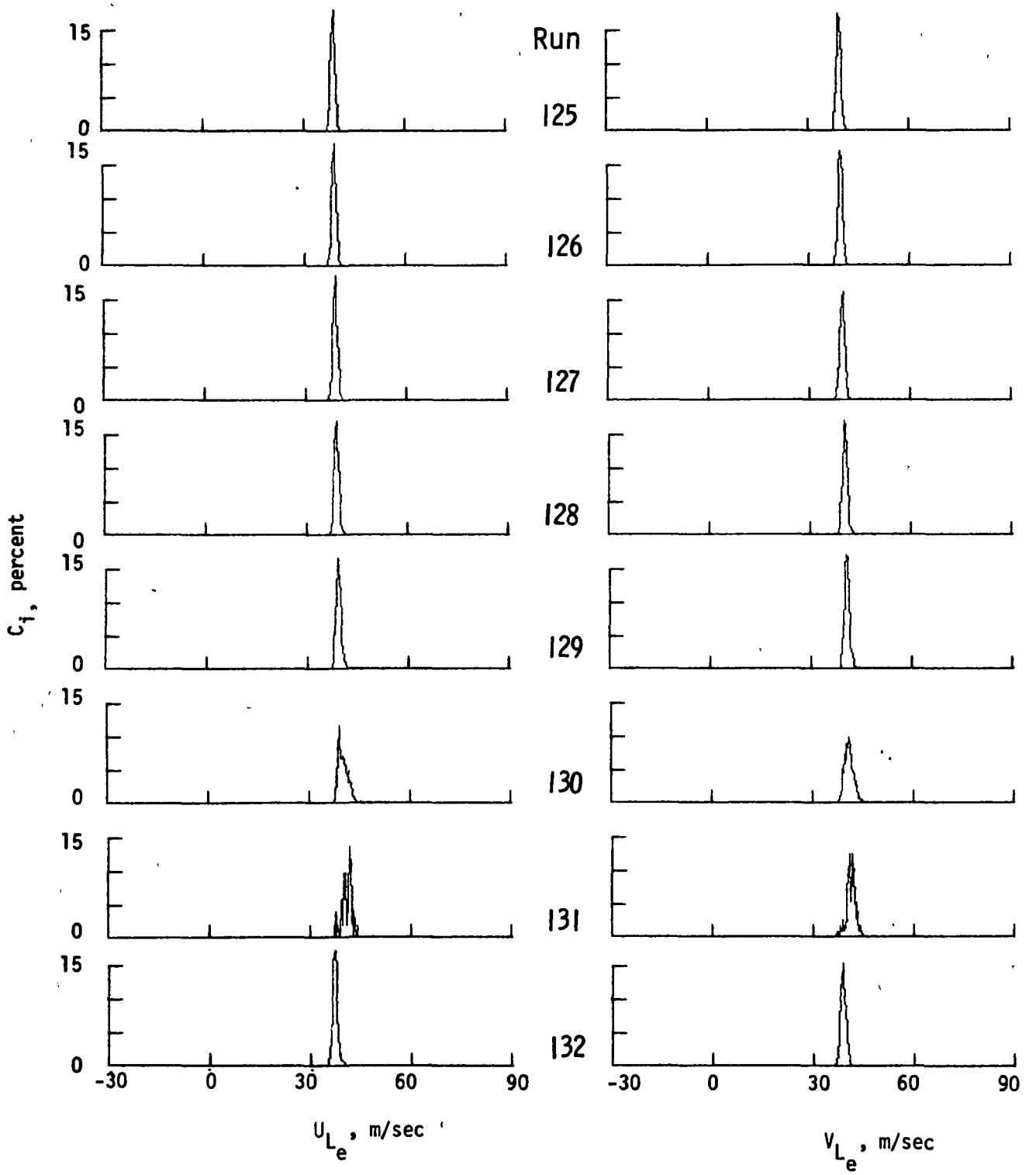

Figure B-22.- Continued.

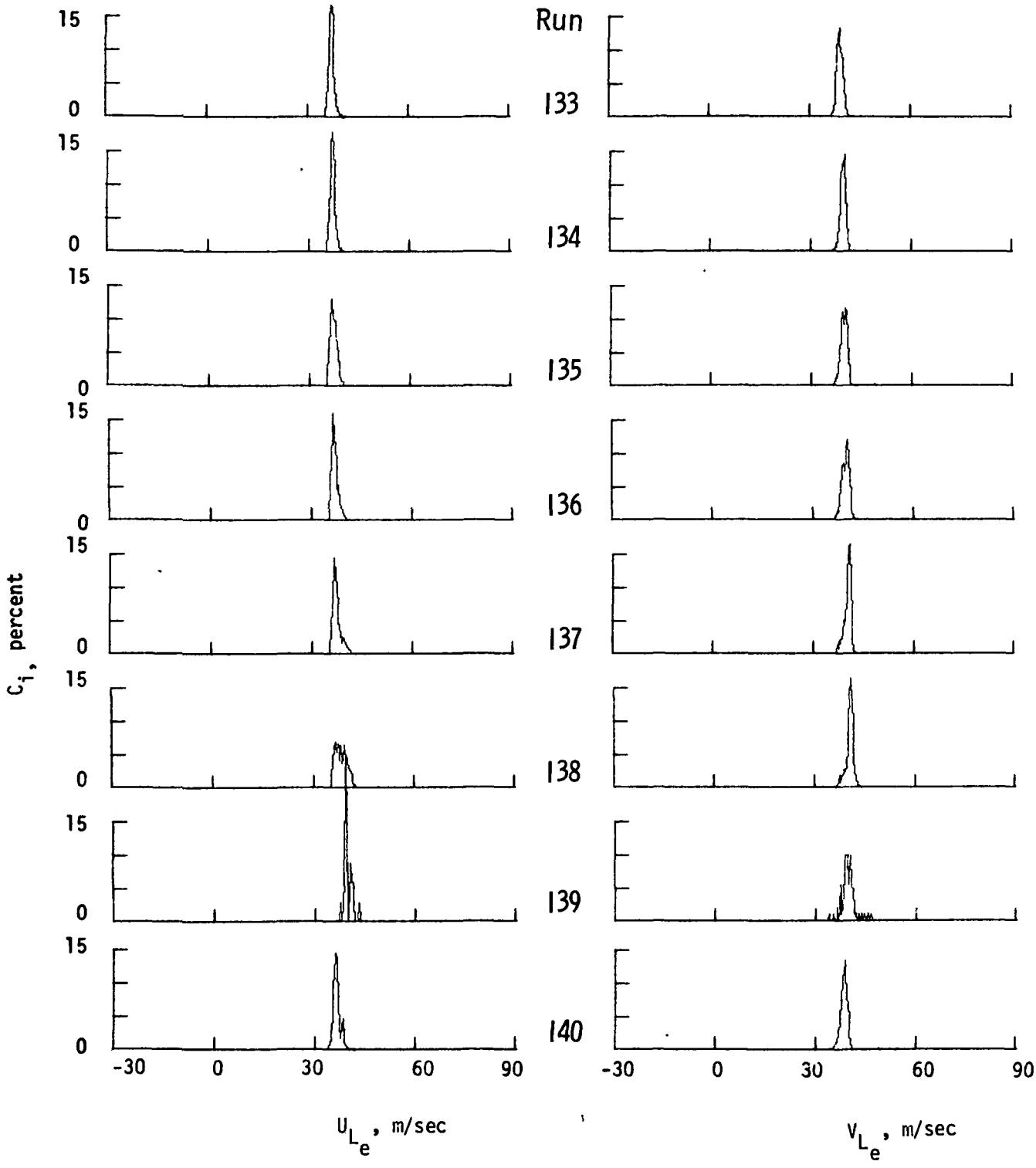

Figure B-22.- Continued.

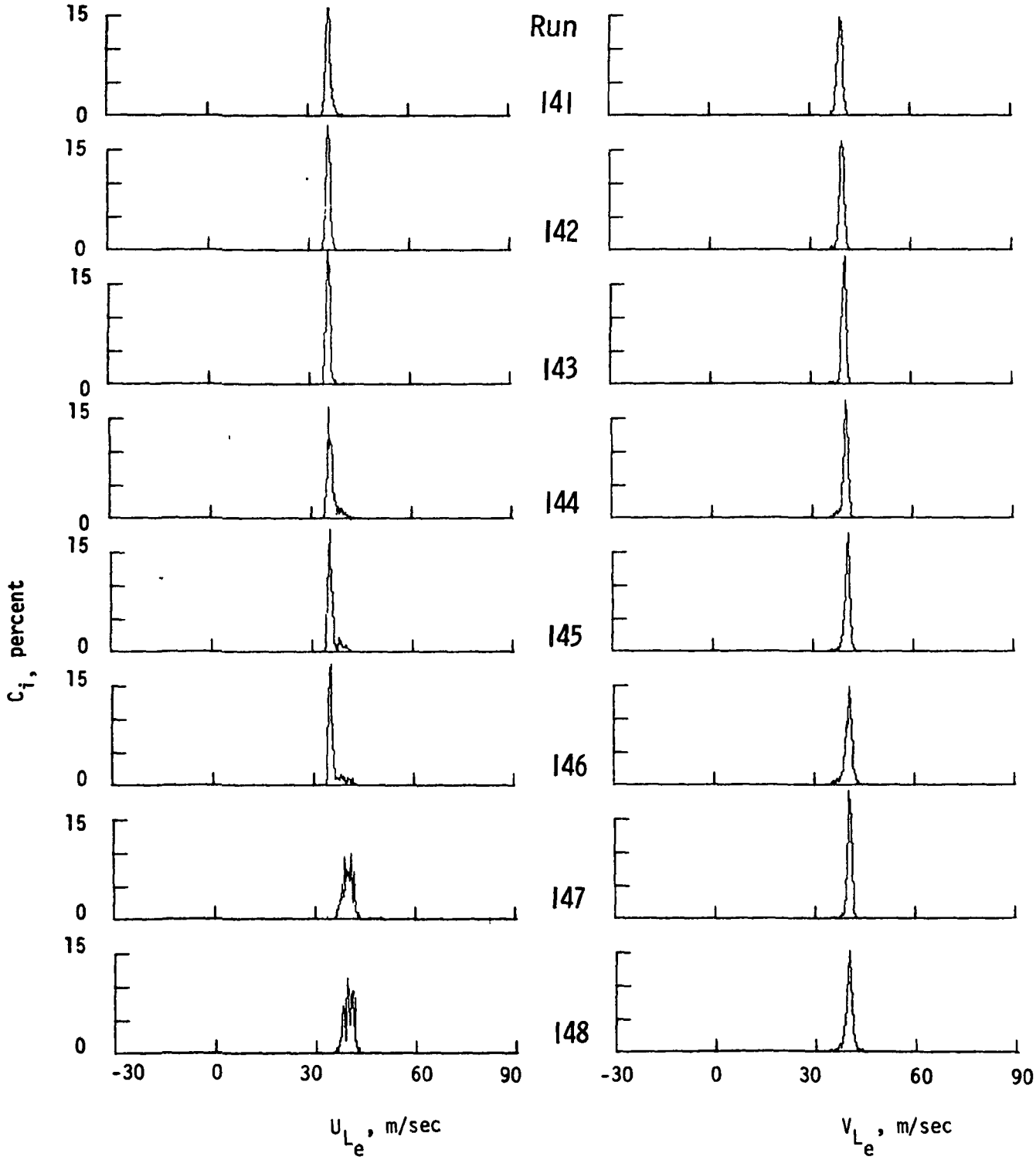

Figure B-22.- Concluded.

1. Report No.	2. Government Accession No	3 Recipient's Catalog No
TM 74040		

4 Title and Subtitle	5 Report Date
LASER VELOCIMETER SURVEY ABOUT A NACA 0012 WING AT LOW ANGLES OF ATTACK	January 1978
	6 Performing Organization Code
7 Author(s) Danny R. Hoad, James F. Meyers, Warren H. Young, Jr., and Timothy E. Hepner	8 Performing Organization Report No
	10 Work Unit No 505-10-23-05
9. Performing Organization Name and Address NASA Langley Research Center Hampton, VA 23665	11 Contract or Grant No
	13 Type of Report and Period Covered Technical Memorandum
12 Sponsoring Agency Name and Address National Aeronautics and Space Administration Washington, DC 20546 and Structures Laboratory, U.S. Army Res. and Tech. Labs (AVRADCOM)	14 Sponsoring Agency Code

15 Supplementary Notes

Hoad, Young, and Hepner - Structures Laboratory, U.S. Army Res. and Tech. Labs.
Meyers - NASA Langley Research Center

16 Abstract

An investigation has been conducted in the Langley V/STOL tunnel with a laser velocimeter to obtain measurements of airflow velocities around a wing at low angles of attack (0.6° and 4.75°). The applicability of the laser velocimeter technique for this purpose in the V/STOL tunnel was demonstrated in this investigation with measurement precision bias calculated at -1.33 percent to 0.91 percent and a random uncertainty calculated at ±0.47 percent. Free-stream measurements were obtained with this device and compared with velocity calculations from pitot-static probe data taken near the laser velocimeter measurement location. The two measurements were in agreement to within 1 percent. Velocity measurement results about the centerline at 0.6° angle of attack were typically those expected. At 4.75°, the velocity measurements indicated that a short laminar separation bubble existed near the leading with with an oscillating shear layer.

17 Key Words (Suggested by Author(s))	18 Distribution Statement
Laser velocimeter Aerodynamics Fluid dynamics NACA 0012 airfoil	Unclassified - Unlimited

19 Security Classif (of this report)	20 Security Classif (of this page)	21 No of Pages	22 Price*
Unclassified	Unclassified	151	$6.75

* For sale by the National Technical Information Service, Springfield Virginia 22161